Teija Laukala

CONTROLLING PARTICLE MORPHOLOGY IN THE IN-SITU FORMATION OF PRECIPITATED CALCIUM CARBONATE-FIBER COMPOSITES

ACTA UNIVERSITATIS LAPPEENRANTAENSIS 989

Teija Laukala

CONTROLLING PARTICLE MORPHOLOGY IN THE IN-SITU FORMATION OF PRECIPITATED CALCIUM CARBONATE-FIBER COMPOSITES

Dissertation for the degree of Doctor of Science (Technology) to be presented with due permission for public examination and criticism in the Auditorium 1314 at Lappeenranta-Lahti University of Technology LUT, Lappeenranta, Finland on the 12th of November, 2021, at noon.

Acta Universitatis
Lappeenrantaensis 989

Supervisor Adjunct Professor Kaj Backfolk
LUT School of Energy Systems
Lappeenranta-Lahti University of Technology LUT
Finland

Reviewers Professor Martin Hubbe
Department of Forest Biomaterials
North Carolina State University
United States

Professor Thad Maloney
Department of Bioproducts and Biosystems
Aalto University
Finland

Opponent PhD Hanna Koivula
Department of Food and Nutrition
University of Helsinki
Finland

ISBN 978-952-335-732-7
ISBN 978-952-335-733-4 (PDF)
ISSN-L 1456-4491
ISSN 1456-4491

Lappeenranta-Lahti University of Technology LUT
LUT University Press 2021

Abstract

Teija Laukala

Controlling particle morphology in the in-situ formation of precipitated calcium carbonate-fiber composites

Lappeenranta 2021
98 pages
Acta Universitatis Lappeenrantaensis 989
Diss. Lappeenranta-Lahti University of Technology LUT
ISBN 978-952-335-732-7, ISBN 978-952-335-733-4 (PDF), ISSN-L 1456-4491, ISSN 1456-4491

When precipitated or synthetized calcium carbonate (PCC) is prepared in the presence of cellulosic fibers, a large fraction of the PCC attaches partially onto and even into the fibers, forming a PCC-fiber composite. As the composite properties in, for example, a papermaking process are affected by the PCC morphology, the PCC-fiber composite properties can be engineered and optimized via PCC morphology control. This may be of special interest for micro- and nanofibrillated celluloses because when the composite is formed from these materials, it may be possible to deal with problems associated with the effects of filler on the mechanical properties of paper, filler retention, dewatering behavior and redispersion of micro- and nanofibrillated cellulose.

The aim of this study was to develop methods to control the morphology and growth of the mineral phase and the enrichment of PCC onto different fiber size fractions and onto different parts of the fiber. The PCC-fiber composite was prepared on different fibers (microcellulose, microfibrillated cellulose and bleached chemithermomechanical pulp) by carbonization of a suspension of lime (lime milk) in the presence of a fiber suspension in an open batch reactor with carbon dioxide (CO_2). PCC-chemithermomechanical pulp composite was fractionated in order to determine the affinity of the mineral enrichment in the various fractions and to further characterize the properties of the fractions and composite using e.g. laboratory handsheets.

The morphology of the precipitate was successfully controlled by altering CO_2 feed and fiber consistency, linked with the targeted (PCC) ash content of the composite material via the initial calcium hydroxide ($Ca(OH)_2$) concentration. The differences in morphology were ascribed to differences in the ratio of calcium to carbonate ions ($[Ca^{2+}]/[CO_3^{2-}]$). Although the PCC showed an affinity to all the fibers investigated, it was found to enrich onto the finer fiber fractions and onto cellulose-rich areas of individual fibers. The anionic surface charge of the fiber fraction before precipitation showed a good correlation with the ash content after precipitation. Whether or not this indicated that the fiber chemistry influences the PCC affinity is further discussed. In the laboratory handsheets, the nano-PCC on the fiber surfaces had a debonding effect, but refining the CTMP prior to the precipitation or strengthening agents could be used to restore the strength of the sheets.

Keywords: PCC, precipitated calcium carbonate, in-situ precipitation, composite filler, carbonization

Acknowledgements

This thesis is based on research carried out between 2013 and 2021 at the Lappeenranta-Lahti University of Technology LUT. The research was financially supported by Stora Enso Oyj, as well as by the Research Foundation of Lappeenranta University of Technology, and this is gratefully acknowledged.

I thank my supervisor Adjunct Professor Kaj Backfolk for his guidance, advice and patience during the course of this work, and I thank Lic. Tech. Isto Heiskanen, from whom I have received much good advice and ideas. Prof. Martin Hubbe and Prof. Thad Maloney are thanked for pre-examining the thesis manuscript. I also thank Dr. Anthony Bristow for valuable expert comments and for the linguistical review of the thesis and all the manuscripts.

During the years it took me to carry out this research, I had many interesting conversations (research-related and otherwise) with my colleagues, and I thank my colleagues, both current and former, for practical help and support in meeting various challenges.

Finally, I thank my parents, Heli and Esa Laukala, my partner Lauri Tuimala and all my friends for their emotional support.

Teija Laukala
September 2021
Lappeenranta, Finland

Contents

List of publications

This dissertation is based on the following papers. The rights have been granted by publishers to include the papers in dissertation.

I. Laukala, T., Kronlund, D., Heiskanen, I., Backfolk, K. (2017). The effect of polyacrylic acid and reaction conditions on nanocluster formation of precipitated calcium carbonate on microcellulose. *Cellulose*, 24(7), pp. 2813–2826.

II. Laukala, T., Backfolk, K., Heiskanen, I. (2021). Fractionation of pulp and precipitated $CaCO_3$–pulp composites: effects on sheet properties of selective $CaCO_3$ precipitation onto fiber size fractions. *Cellulose*, 28(9), pp. 5807–5826.

III. Laukala, T., Ovaska, S.-S., Kerttula, N., Backfolk, K. (2021). Three-dimensional thermomechanical converting of CTMP substrates: Effect of bio-based strengthening agents and new mineral filling concept. *Cellulose*, 28(15), pp. 9751–9768.

Author's contribution

The author is the principal and corresponding author of papers I to III.

I The author planned all the experiments, carried out the precipitation experiments, ash content measurements and scanning electron microscopy, but not the field-emission scanning electron microscopy, TGA and XRD analysis. The results were interpreted and the manuscript was written with the co-authors.

II The author planned and carried out all the experiments and the measurements. The results were interpreted and the manuscript was written with the co-authors.

III The author planned the experiments and carried out the precipitation experiments, fiber analysis measurements and scanning electron microscopy, excluding the field-emission scanning electron microscopy. The results were interpreted and the manuscript was written with the co-authors.

Supporting publications

1. Laukala, T., Lyytikäinen, J., Mielonen, K., Backfolk, K. (2020). Effect of PCC crystallization and morphology on flocculation with microfibrillated cellulose, on sheet densification and liquid absorption behavior. *Cellulose*, 27(17), pp. 10151–10166.

Nomenclature

In the present work, variables and constants are denoted using *slanted style* and abbreviations are denoted using regular style.

Latin alphabet

A	targeted weight of PCC ash	g
B	weight of the test specimen (e.g. PCC-fiber composite)	g
f_i	relative amount of component i	–
$k_{r,i}$	absorption coefficient of component i	m^2/kg
m	the weight of $Ca(OH)_2$ required to form a PCC-fiber composite with a chosen PCC content	g
$s_{r,i}$	light scattering coefficient of component i	m^2/kg

Abbreviations

$[Ca^{2+}]/[CO_3^{2-}]$	(ratio of) calcium cation concentration to carbonate anion concentration
ACC	amorphous calcium cabonate
AKD	alkyl ketene dimer
$AlO_3 \cdot 2\ SiO_3 \cdot 2H_2O$	aluminum silicate (clay)
A-PAM	anionic polyacrylamide
ASA	alkenyl succinic anhydride
Au	gold
Ba^{2+}	barium cation
BBK	bleached birch kraft (pulp)
BIB	broad ion beam
BSE-comp	backscatter electron imaging, compositional mode
$Ca(OH)_2$	calcium hydroxide
Ca^{2+}	calcium cation
$CaCl_2$	calcium chloride
$CaCO_3$	calcium carbonate
$CaCO_3 \cdot ½H_2O$	calcium carbonate hemihydrate
$CaCO_3 \cdot 6H_2O$	ikaite
$CaCO_3 \cdot H_2O$	monohydrocalcite
$CaSO_4 \cdot 2H_2O$	calcium sulfate (gypsum)
CBS	concentric back scatter (detector)

CMC	carboxymethylated cellulose
CNT	classical nucleation theory
CO_2	carbon dioxide
CO_3^{2-}	carbonate anion
C-PAM	cationic polyacrylamide
CS	cationic starch
CSF	Canadian standard freeness
CTMP	chemithermomechanical pulp
EC	electrical conductivity
ECF	elemental chlorine free (pulp)
ERIC	effective residual ink concentration
FE-SEM	field-emisson scanninc microscopy (or microscope)
GAD	gaseous analytical detector
GCC	ground calcium carbonate
H_2O	water
IS	in-situ
L-lys	L-lysine
MC	microcellulose
MFC	microfibrillated cellulose
Mg^{2+}	magnesium cation
$Mg_3{\cdot}Si_4{\cdot}O_{10}(OH)_2$	hydrous magnesium silicate (talc)
Mn^{2+}	manganese cation
MNFC	micro- and nanofibrillated cellulose
NaOH	sodium hydroxide
Na_2CO_3	sodium carbonate
Na-PAA	sodium salt of polyacrylic acid
NH_4HCO_3	ammonium bicarbonate
PAA	polyacrylic acid
PCC	precipitated calcium carbonate
Pd	palladium
PDADMAC	poly(diallyldimethylammonium chloride)
PES-Na	polyethene sodium sulfonate
PILP	polymer induced liquid precursor (of mineral)
RCF	recycled fiber (pulp)
RH	relative humidity
SEI	secondary electron imaging (mode)
SEM	scanning electron microscopy (or microscope)

TCF	totally chlorine free (pulp)
TiO_2	titanium dioxide
VP-SEM	variable pressure mode scanning electron microscopy

1 Introduction

1.1 Background

Most paper grades contain mineral fillers, which are typically white, inorganic materials added to the stock (Kirwan 2005). Fillers are used to reduce costs or adjust the end-product properties, or both (Hubbe 2004; Koivunen et al. 2009; Hubbe and Gill 2016). They are typically beneficial for brightness and opacity and for controlling the pore size and friction of the paper (Shen et al. 2009; Hubbe and Gill 2016), formation (Koivunen et al. 2009), dimensional stability, smoothness, and ink adsorption (Shen et al. 2009).

The typical method of using a mineral filler, such as calcium carbonate ($CaCO_3$), is to add a mineral slurry to the short circulation before the headbox, where the exact suitable locations for additions depend on the used retention aid system, for example (van de Ven 2005). The most commonly used fillers, according to Hubbe and Gill (2016), are $CaCO_3$ (as ground calcium carbonate, GCC, or as precipitated calcium carbonate, PCC), aluminum silicate ($AlO_3 \cdot 2\ SiO_3 \cdot 2H_2O$, as natural hydrous clay or precipitated aluminum silicate), titanium dioxide (TiO_2), hydrous magnesium silicate ($Mg_3 \cdot Si_4 \cdot O_{10}(OH)_2$, i.e. talc) and calcium sulfate ($CaSO_4 \cdot 2H_2O$, i.e. gypsum).

Although the commonly used fillers greatly differ from each other in terms of particle shape, for example, they share important characteristics such as inability to form bonds with fibers, which means that some of the sheet properties are negatively affected (Krogerus 2007). Besides strength loss, sheet bulk and first pass retention are typically reduced by the addition of a filler. Fillers also cause abrasion of production equipment, and the paper may dust excessively (Kumar et al. 2011; Hubbe and Gill 2016).

Over the years, strategies have been developed to overcome the negative effects of using mineral fillers, and the understanding of the reasons for the difficulties has increased. For example, the poor filler retention is usually explained by the fact that the filler particles are significantly smaller than the cellulosic fibers, as shown in Figure 1.1. The typical filler particle size is 0.1-10 µm (Hubbe and Gill 2016), while the typical fiber length is around 1 mm for hardwood and 3 mm for softwood pulps (Hakkila and Verkasalo 2009). The retention of fillers is commonly improved by the use of retention aid chemicals and systems (van de Ven 2005).

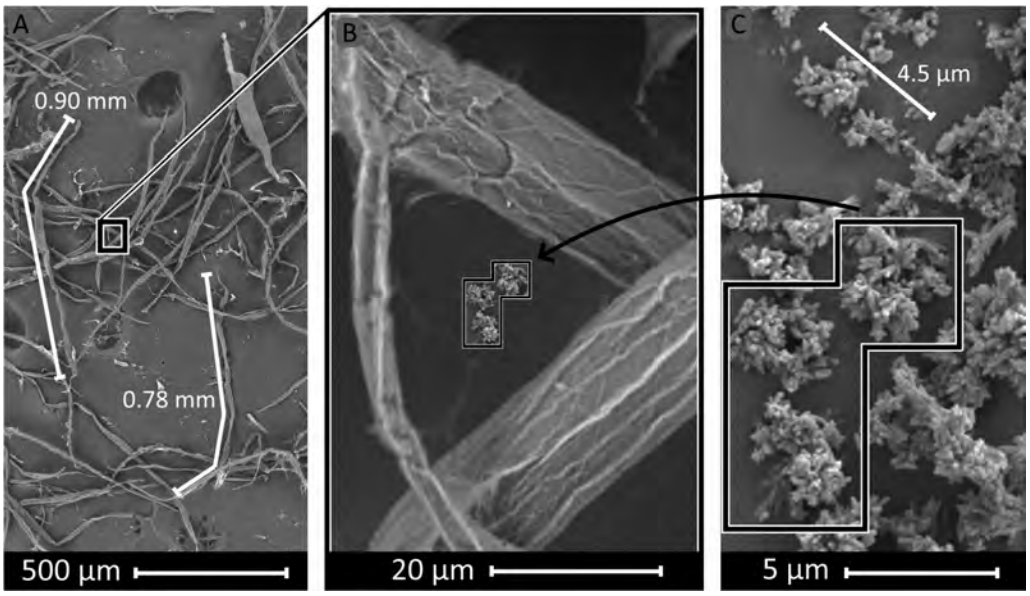

Figure 1.1: SEM micrographs of (A) bleached hardwood (birch) kraft pulp fibers and (C) rosette-like PCC filler. The image (B) shows the fibers and the PCC on the same scale. Images captured using secondary electron imaging (SEI), sputter coating (Au/Pd target) and 5 kV acceleration voltage

The paper bulk can be controlled by using fillers with an optimized particle size and shape, such as rosette-like scalenohedral PCC (Hubbe and Gill 2016) that also offers good light scattering (Hubbe 2004). The loss of strength caused by fillers can be reduced by increasing the degree of refining of the pulp, by using strengthening agents or by increasing the size of the filler particles (Hubbe and Gill 2016). Different fillers are often blended together to further improve the product performance (Koivunen et al. 2009).

Work is ongoing to develop high-performance fillers, i.e. materials able to positively affect the desired properties while limiting the negative effects, and various solutions have been proposed. For example, in the review paper by Shen et al. (2009), modified filler concepts such as acid-resistant $CaCO_3$ and the surface modification of fillers to give better bonding were discussed. Other examples of improved filler concepts include clay-starch composites (Yoon and Deng 2006) and enhanced filler concepts such as PCC-fiber composites, i.e. PCC attached onto, and possibly also into, the fibers or fines.

PCC-fiber composites appear to offer a way to reduce some of the negative effects of filling while simultaneously bolstering many of the good properties. The affinity of PCC (interaction) to cellulosic fibers also makes it possible to prepare the composite material by in-situ precipitation of the PCC in the presence of the fiber by carbonization of a lime suspension. PCC-fiber composites have been studied for several decades and are often presented in the literature with terminologies such as pigmented cellulosic pulp (Lutton

1952c), SuperFill (Silenius 2002) and in-line PCC (Matula et al. 2018). Despite their benefits, the PCC-fiber composite technologies have not however been commercially established, probably partially due to competing technologies such as sophisticated retention aid systems (Kumar et al. 2011).

Recent improvements in micro- and nanofibrillated cellulose (MNFC) technology and production have however brought attention to PCC-MNFC composites for e.g. their modified water-holding capabilities (Dimic-Misic et al. 2016; Rantanen 2016) and the re-dispersibility of MFC (Axrup et al. 2014), showing a potential for new products such as more sustainable substrates for printed electronics (Torvinen 2017). Simultaneously, the understanding of the mechanism of precipitation of $CaCO_3$ has improved, and the papermaking field has undergone changes such as an increased environmental awareness and a shift from printing papers to packaging materials and hygiene products. These changes justify a review of the potential of PCC-fiber composite in papermaking.

1.2 Objective of the study

The work was motivated by the knowledge that PCC can take different morphologies and particle sizes when a PCC-fiber composite is formed via the in-situ precipitation of a lime suspension. As shown by Subramanian (2008), the properties of PCC-fiber composites and their behavior in the papermaking are affected by the mineral phase morphology. If the mineral phase morphology in a PCC-fiber composite can be controlled, the engineering and optimization of the PCC-fiber composite becomes possible. Another feature of a PCC-fiber composite is that there is probably an uneven distribution of PCC into different fiber fractions of the pulp, as has been reported by Silenius (2002) who stated that the PCC showed a greater affinity towards finer fibers. This further intensifies the interest in PCC-MNFC composites.

The objective of the work was thus to investigate PCC-fiber composite preparation, and the distribution and affinity of the PCC for different fiber fractions when $Ca(OH)_2$-CO_2-H_2O carbonization was carried out in an open batch-precipitation reactor. The $Ca(OH)_2$-CO_2-H_2O carbonization reaction route for PCC precipitation was chosen to avoid the formation of large amounts of secondary salts. The work primarily focused on controlling the morphology via process conditions, i.e. without using additives such as morphology-altering chemicals. If such additives are not needed, washing steps otherwise needed to remove the residuals of the chemicals may be eliminated, and the additive-free carbonization reaction may also be used for in-line precipitation.

The main research targets were:

1) to control the morphology of the precipitate on fibers, and to be able to prepare nano-PCC-covered fibers and fines without using morphology-controlling additives
2) to confirm that the method of controlling the precipitate morphology can function satisfactorily with different fiber types, such as microcellulose, microfibrillated cellulose and chemithermomechanical pulp (MC, MFC and CTMP, respectively)
3) to investigate and clarify the affinity and enrichment of PCC onto different sized fractions and onto different parts of fibers (e.g. fibrillated areas, lumen walls) in nano-PCC-CTMP composites, and to assess the effect of precipitation onto the different fiber size fractions

For clarity the term “mineral-fiber composite” is used to refer to all materials in which the mineral or part of the mineral is firmly attached onto and possibly into the individual fibers, for example onto lumen walls. The term “mineral-fiber composite” is altered appropriately to specify the mineral (for example, PCC) or fiber (for example, MFC) used, or both.

The definition of a mineral-fiber composite includes different materials, such as mineral-fiber composite materials prepared via lumen loading and pre-flocculation. This thesis focuses however on PCC-fiber composites prepared by in-situ precipitation by carbonization of a lime suspension in the presence of fibers, and unless otherwise stated, the fibers referred to are wood-based, cellulosic and not chemically modified other than by pulping and bleaching.

1.3 Outline of the thesis

The thesis consists of a general introduction on the topic of PCC-fiber composites followed by a theoretical part and an experimental part. The theoretical part presents a brief historical review on the development and use of PCC-fiber composites in papermaking, and it summarizes the main progress made within the field of precipitation of PCC onto different fibers, focusing mainly on the $Ca(OH)_2$-CO_2-H_2O process.

The experimental part describes the methods and analytical procedures used in the work, and it summarizes the main results related to the morphological control of the precipitate on the PCC-fiber composite (Paper I and unpublished results), PCC enrichment onto fine fractions of the pulp (Paper II), and the effect of nano-PCC-CTMP on laboratory handsheet properties (Paper III). The precipitate morphology was characterized mainly by scanning electron microscopy, which was used to investigate the approximate size, shape and location of small precipitate particles when attached onto fibers of different types.

2 PCC-fiber composites: an overview

2.1 Historical review

In the 1960s, European paper mills started to use $CaCO_3$ as a filler (Burke 1993; Gane 2009; Hubbe and Gill 2016), not only to cut their production costs, but also because the product quality (such as slower deterioration of paper strength) could be improved due to the conversion of the papermaking conditions to alkaline or neutral, which was required when $CaCO_3$ was used (Burke 1993; Gane 2009; Hubbe and Gill 2016). The use of PCC followed slightly later, in the late 1970s and early 1980s in North America (Burke 1993; Gane 2009). Since then, PCC has become the dominant filler in papermaking (Hubbe and Gill 2016).

Ideas disclosed in patents filed before the commercialization and wide spread use of $CaCO_3$ as a filler and alkaline papermaking, however, describe what is essentially the formation of mineral-fiber composites via in-situ precipitation. Eide and Calbeck (1935) describe the preparation of "pigmented paper" by the precipitation of zinc sulfide in the presence of the fibers in order to improve opacity, and they mention that the precipitate strongly adheres to the fibers. Similarly, the lumen-loading concept, where the filler is placed in the lumen of fibers, and where the filler can participate in light scattering with little disturbance of the bonding, was discovered at an early stage (Haslam and Steele 1936). These two approaches have since remained as methods for preparing PCC-fiber composites (Kumar et al. 2011).

Although the details of the suggested processes have varied over the years, many of the key benefits and difficulties of the mineral-fiber composite concept were recognized many decades ago. Lutton (1952c) prepared a composite material which he called a "pigmented fibrous product" by precipitating pigments (including $CaCO_3$) onto, into and around cellulosic fibers. According to the patent (Lutton 1952c), the material "can advantageously be added as a fibrous pigment to refined paper pulp for paper manufacture", and the positive effect on filler retention was recognized.

Another patent (Lutton 1952b) describes the use of similarly produced pigmented pulp in multi-ply product liners. The patent mentions the white, printable surface of the product and warns against use the of alkaline salt in precipitation to avoid darkening of the stock. In yet another patent, Lutton (1952a) mentions that only a small amount of fiber should be pigmented, but heavily, in order to maintain the strength of the furnish and obtain sufficient strength properties on the sheet.

While the technical details, such as pulp consistency and chemicals used have been altered many times since Lutton's work, starting soon after his patent applications by e.g. Thomsen (1962), the early work outlined and essentially summarized the main motivation for the preparation of PCC-fiber composites. To this day, the improvement of the optical properties remains as one of the main motivations for PCC-fiber composite research. This

is illustrated in the list of the benefits of lumen-loaded mineral-filler composite in comparison with the traditional addition of fillers, presented by Kumar (2011):

1. *Easier white water management due to improved retention*
2. *Reduction in the dosages of expensive polymeric retention aids*
3. *Easier drying of paper, due to a higher mineral content at a given level of strength*
4. *Lower apparent density of the paper in cases where the treatment may inhibit the collapse of fiber voids during drying*
5. *Less abrasion damage to the forming fabric because the filler is inside the fiber*
6. *Less two-sidedness because the filler is retained within fibers during sheet formation*
7. *Less dusty paper than the conventionally filled paper, because the fine filler particles are firmly held inside the fiber*

Although the list is given in the context of lumen loading, much of it applies or may apply although slightly modified for other mineral-fiber composites. For example, in item 3 attention may be drawn to the improved water removal reported for PCC-MFC composites (Rantanen 2016).

For in-situ precipitation, an important development was the use of $Ca(OH)_2$ and CO_2. An early mention of this can be found in the Japanese patent 62-162098 granted to Yoshida et al. in 1987 (Matthew et al. 1997; Henricson 2006). The fast precipitation and lack of formation of secondary salt make possible an in-line PCC process: the in-situ precipitation of PCC in the papermaking line.

A further in-line PCC innovation and development by Imppola et al. (2013) mentions benefits such as equipment- and workforce-related savings related to the elimination of a PCC satellite plant and transportation costs. According to Matula et al. (2018), in-line precipitation can also be associated with a cleaning effect of especially white water. With the current trend to reduce the use of fresh water, the water loops are more closed than before and new methods to clean whitewater are therefore of interest.

Another fairly recent development is the co-grinding concept, where grinding rather than mixing of the mineral particles is used to facilitate energy transfer from moving parts to fiber material. This results in fibrillation and the formation of MFC blended with the $CaCO_3$ or other mineral (Svending 2014). This material (Svending 2014) and the PCC-MFC composite prepared via carbonization precipitation (Dimic-Misic et al. 2016; Rantanen 2016) have been linked with an improvement in the dewatering of a furnish that contains MFC. This is of interest since water retention by MFC is a major problem when processing the material (Dimic-Misic et al. 2016).

To summarize, decades of PCC-fiber composite research have identified various methods of obtaining properties and process-related benefits in the preparation of the composite (cf. Figure 2.2). The early motivation strongly related to sheet properties remains, but the changes in the paper and pulp industry and environmental awareness have brought new areas of interest into focus.

2.2 Calcium carbonate

$CaCO_3$ has three anhydrous crystalline polymorphs, listed from the most stable to the least stable these are: calcite, aragonite and vaterite (Naka and Chujo 2001). $CaCO_3$ is commonly said to have two hydrated crystalline forms: monohydrocalcite ($CaCO_3 \cdot H_2O$) and ikaite ($CaCO_3 \cdot 6H_2O$) (Jimoh et at 2018; Zou et al. 2019), but a third hydrated but metastable crystalline form, calcium carbonate hemihydrate ($CaCO_3 \cdot ½H_2O$), was recently reported by Zou et al. (2019). In addition to the crystalline forms, both metastable and unstable amorphous calcium carbonates (ACCs) have been detected. ACC is currently thought to play an important role in the precipitation of $CaCO_3$ (see 3.2 Precipitation of PCC).

$CaCO_3$ exists in numerous different morphologies, some of which differ from the simple geometrical shapes such as cubes or tetrahedrons typically associated with single crystals. For example, sea urchin spines are reported to be calcitic with a single crystal behavior in scattering experiments despite their curvature and complex, porous inner architecture (Su et al. 2000). These (Politi et al. 2004) and many other complex $CaCO_3$ structures found in the animal kingdom are associated with ACC-mediated biomineralization (Jin et al. 2018).

Biomimetic approach has been used to reproduce complex morphologies (Jin et al. 2018), but often simpler methods are applied. For example, Ajikumar et al. (2005) reported monodisperse spheres by self-assembly of magnesian calcite crystals at low temperature and high magnesium content, and simple methods for controlling the morphology in carbonization process exist (see 3.3 Morphology control of the precipitate in carbonization process).

In papermaking, $CaCO_3$ is usually used either as ground calcium carbonate (GCC) or as precipitated calcium carbonate (PCC). In contrast to synthetic PCC, GCC is obtained by grinding $CaCO_3$ rocks: chalk, limestone and marble (Gane 2009). Its purity (affecting color and brightness) and particle shape, size and size distribution are affected by the material source and processing. For example, chalk commonly contains remnants of micro-organisms, clearly visible in scanning electron microscopy (SEM), and is usually tinted with yellow due to the presence of iron impurities (Gane 2009).

PCC typically has narrower particle size distribution than GCC and contains less impurities (Imppola 2009). Common PCC morphologies include rosette shapes, blocky particles and needle-like shapes (Hubbe and Gill 2016), associated with scalenohedral calcite, rhombohedral calcite and acicular aragonite, respectively (Imppola 2009; Hubbe

and Gill 2016). Examples of different PCC and GCC morphologies are shown in Figure 2.1 together with calcinated kaolin and TiO_2. The effects of filler (or pigment) shape and size on the paper properties have been widely studied and they are summarized in reviews such as those by Hubbe (2004) and Hubbe and Gill (2016).

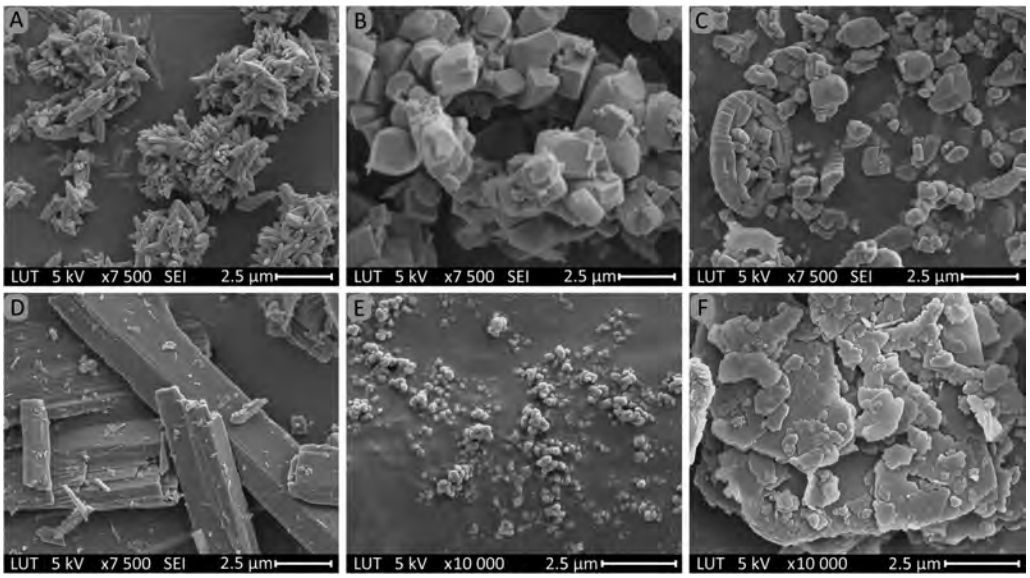

Figure 2.1: SEM micrographs showing examples of the morphology of different calcium carbonates and other mineral fillers or pigments used in papermaking. (A) rosette-like PCC, (B) cubical PCC, (C) GCC, coccolith at left of the image (D) wollastonite (E) TiO_2 and (F) calcinated kaolin. Images captured using secondary electron imaging (SEI) and sputter-coating of the sample (Au/Pd target)

An interesting property of $CaCO_3$ is its ability to readily form crystals on different substrates, including natural polymers such as chitosan (Zhang and Gonsalves 1998; Wada et al. 2004; Payne et al. 2007) and cellulose (e.g. Hosoda and Kato 2011; Ma et al. 2012). $CaCO_3$ also has been precipitated on synthetic polymers such as anionic polyamide (Lakshminarayanan et al. 2003) and essentially neutral polyvinyl alcohol fibers (Park et al. 2017).

The precipitate has often been guided onto the polymeric substrate using a polymeric additive, such as polyacrylic acid (PAA) (Hosoda and Kato 2001; Payne et al. 2007). Under suitable conditions PCC has been reported to form, for example, a thin film (Hosoda and Kato 2001). Additives are not however required to precipitate PCC onto a substrate.

In PCC-fiber composites, PCC has been reported to be both rhombohedral (cubical) (Subramanian et al. 2007; Ciobanu et al. 2010; Fortuna et al. 2013; Mohamadzadeh-

Saghavaz 2014) and scalenohedral, which however appeared almost ellipsoidal rather than rosette-like, based on SEM micrographs shared by the authors (Subramanian et al. 2007). Additionally, colloidal PCC nanoparticles aggregated to an ellipsoidal shape (Subramanian et al. 2007), spheroidal PCC (Vilela et al. 2010; Ma et al. 2012), and uniform or irregular PCC (Fuchise-Fukuoka et al. 2020b) has been reported.

No special efforts to control the morphology were usually reported, although Subramanian et al. (2007) mention that the precipitation route was controlled to obtain the different morphologies.

2.3 The main approaches for preparing PCC-fiber composites

Kumar et al. (2011) applied the term $CaCO_3$-cellulose fiber composite to "cases where mineral is precipitated or made to deposit onto and within the cell walls of cellulosic fibers". This definition includes PCC-fiber materials prepared using flocculation and fixation chemicals (Subramanian 2008; Othman et al. 2010) or by fixing the modified (cationic) $CaCO_3$ pigment onto the cellulosic fiber (Alince and Bednar 2003; Middleton et al. 2003).

The materials obtained using such methods are occasionally referred to as composites (He et al. 2016; Kang et al. 2020) but, for the purposes of this work, pre-flocculation was considered to be closer to the "traditional" PCC filling approaches and retention aid technology, and such materials have not been included in this work. Two main approaches for preparing PCC-fiber composites have therefore been recognized: co-mixing, targeting e.g. lumen loading (placing of mineral in the lumen), and co-precipitation or in-situ precipitation. See Figure 2.2.

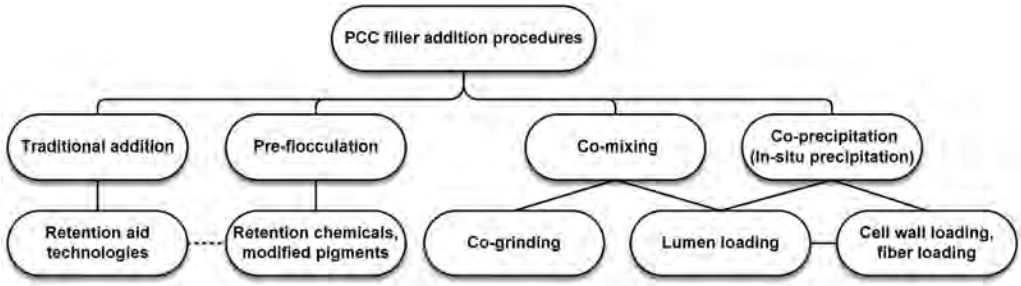

Figure 2.2: Approaches for using PCC as a filler

In the context of PCC-fiber composite preparation, in-situ precipitation can be defined as precipitation of PCC in the presence of fibers. There is therefore a significant overlap between the lumen-loading concept and in-situ precipitation. The mineral can be placed into the lumens either by co-mixing (Petlicki and van de Ven 1994; Kumar et al. 2009;

Othman et al. 2010) or, in the case of PCC, by precipitation in the presence of fiber by using soluble salts (Allan et al. 1998; Ciobanu et al. 2010; Fortuna et al. 2013).

To achieve lumen loading by in-situ precipitation, the precipitation must be guided not only to the fiber but also inside it. The in-situ precipitation procedure tends to precipitate the PCC excessively on the outer surfaces of the fibers, which has been said to be due to limited diffusion of the ionic species (Silenius 2002), but a better control of the precipitate placement has been attempted by intermediate filtration when using two soluble salts (Allan 1992). With $Ca(OH)_2$, placing the $Ca(OH)_2$ in the lumens have been attempted by slaking at high fiber concentration (Klungness et al. 1992). Technological difficulties in placing the mineral in the fiber and avoiding placing the mineral on the outer fiber surfaces and removal of excess mineral in the surfaces and the water nevertheless remain (Kumar 2011).

The methods for in-situ precipitation of PCC, targeting lumen loading or otherwise, are similar to those used for the industrial precipitation of PCC (see 3 Synthetizing PCC-fiber composite by in-situ precipitation).

The co-mixing method to achieve lumen loading operates through the mixing of ready-made mineral particles with fiber and applying shear forces that force the mineral into the fiber lumen through pit openings (Petlicki and van de Ven 1994; Othman et al. 2010). The deposition or higher affinity to the lumen is explained by electrostatic and hydrodynamic means, i.e. the electrostatic force that causes deposition of filler on the fiber surfaces is not sufficient to hold the filler particles on the outer surfaces due to hydrodynamic forces originating from agitation, whereas particles that are deposited or located in the lumen are, to a greater degree, protected from the hydrodynamic force (Petlicki and van de Ven 1994). Coflocculation of fiber and filler under flow conditions is, however, one of the mechanisms that attach the filler into the forming web, individual fibers and fibrils (Haslam and Steele 1936) and can be expected to function also when PCC-fiber composite is prepared using the precipitation route.

The agitation method requires conditions with a significant energy input (Middleton et al. 2003) and the processing times required can be long, typically of the order of one hour (Petlicki and van de Ven 1994). Lumen loading by in-situ precipitation or by mixing has not gained commercial success due to the competing technologies and technical challenges (Kumar 2011).

2.4 Role of the fiber source in the preparation of PCC-fiber composites

Papermakers are well aware of the fact that different pulps and different fiber fractions behave differently in papermaking both in terms of processing and in the generation of sheet properties. From the PCC-fiber composite point of view, the differences are of interest because the formation of the composite may be affected differently by different fiber types and fractions. Choosing or producing the optimal fiber for attachment of PCC

is not a trivial task, as the reason for the attachment is not well understood (see chapter 3.5 Nucleation and growth of PCC on a cellulosic substrate). Different PCC-fiber composites have also been reported to affect the sheet properties differently. Results from earlier reports are summarized in Table 2.1 (page 26).

Although this work focuses on wood-based cellulosic fibers, it is worth mentioning that composites can also be formed using non-cellulosic fibers (Lakshminarayanan et al. 2003; Park et al. 2017) and cellulosic non-fibers, and cellulose derivatives such as carboxymethylated cellulose (CMC) have been found to influence the PCC morphology (Mohamadzadeh-Saghavaz et al. 2013).

Table 2.1: Reported findings related to the development of sheet strength and optical properties when using PCC-fiber composites

Description	Strength	Optical	Ref
Precipitation on semichemical bleached bagasse pulp using "water-soluble, low-cost precursors". Final furnishes blends of bagasse and softwood.	Tensile and tear index improved compared with traditional filling	Loss of scattering and brightness compared with traditional filling	(1)
Precipitation using (A) $CaCl_2$, NaOH and CO_2, (B) $CaCl_2$ and Na_2CO_3 and (C) $Ca(OH)_2$ and CO_2. Precipitation was done on bleached chemical softwood pulp (30 SR). Handsheets prepared using washed and un-washed PCC-fiber composites.	Decrease in breaking length	Improvement in opacity	(2)
Precipitation done on bleached hardwood kraft pulp (softwood and hardwood) using carbonization with ultrafine bubbles. Pulp:$Ca(OH)_2$ was 1:1. Reference handsheet was prepared using laboratory-made PCC. Ash content above 40%.	Loss of tensile index, but the composite sample had a higher $CaCO_3$ content than the reference	Loss of brightness and scattering coefficient despite the composite sample having a higher $CaCO_3$ content than the reference	(3)
Precipitation using Na_2CO_3 and $Ca(OH)_2$. Precipitation on bleached pulps (never dried hardwood and bagasse). The composite was washed after precipitation. Ash content below 21%. Blended and unblended sheets. When blended, furnish mixtures of hardwood, bagasse and wheat straw (32 SR each).	Loss of tensile index and folding endurance. No clear change in tear index. Slight differences were obtained for different precipitate morphologies. Comparison by $CaCO_3$ content.	Improvement in light scattering, brightness and opacity. Comparison by $CaCO_3$ content.	(4)
Pilot trial (TCF pulp) and handsheet (TCF and ECF pulp) experiments. Carbonization precipitation on hardwood chemical pulp.		Loss of brightness in pilot testing, compared with traditional filling. Difference between TCF and ECF pulps in handsheet experiments.	(5)
Precipitation on bleached softwood chemical pulp (CSF 50 ml) using $CaCl_2$, and dimethyl carbonate. $CaCO_3$ contents of PCC-fiber composites 25-40%. Cationic polyacrylamide as a retention aid in reference sheets.	Improvement in tensile index and burst index. Tear index essentially unaffected. Comparison by $CaCO_3$ content (commercial scalenohedral reference).	Loss of opacity and brightness. Comparison by $CaCO_3$ content (commercial scalenohedral reference).	(6)
Carbonization precipitation on bleached chemical pulp fines. High $CaCO_3$ content in the PCC-fiber composite (50-85%). Furnish 30% bleached softwood (27 SR), 70% bleached hardwood (22 SR) chemical pulp	Improvement in tensile index, Scott bond, elastic modulus and bending stiffness compared with traditional filler. Comparison by ash content	Improvement in light scattering coefficient in comparison with traditional filler. Comparison by ash content	(7)
Carbonization precipitation on bleached softwood pulp fines. Precipitation conditions altered to produce different PCC morphologies (colloidal PCC, rhombohedral PCC and scalenohedral PCC). PCC:fines was 2:1 in the filler and base furnish 30:70 softwood(22 SR):hardwood(18 SR).	Increase in internal bond strength and tensile index. Slight difference between PCC-fiber types. Comparison by sheet filler content.	Slightly lower or similar light scattering. Comparison by sheet filler content.	(8)

(1) Allan et al. (1998)
(2) Ciobanu et al. (2010)
(3) Fuchise-Fukuoka et al. (2020b)
(4) Kumar (2002)
(5) Klungness et al. (1996)
(6) Mohamadzadeh-Saghavaz et al. (2013)
(7) Silenius (2002)
(8) Subramanian et al. (2007)

2.4.1 Mechanical and chemimechanical pulp

In comparison with kraft pulp, mechanical pulps have a high fines content, a high lignin content and a tendency to have a low strength but high light scattering properties (Lönnberg 2009). These factors together with poorer brightness stability of mechanical pulps in comparison with kraft pulps (Lönnberg 2009) make the mechanical pulps not the most obvious candidates for PCC-fiber composites in applications where sheet brightness is emphasized. As bleaching of mechanical pulps is lignin-retaining (Jäkärä et al. 2009) and phenolic compounds of lignin are prone to become colorized in alkaline conditions (Forsskåhl 2000), the high pH of $Ca(OH)_2$-CO_2-H_2O process is likely to result in brightness reversion.

CTMP is however often used in the middle layer of board to give bulk and stiffness, where it has the benefit of better strength properties and less odor and taste problems than other mechanical pulps (Vehniäinen et al. 2009). Both sheet bulk (Kumar 2011) and sheet stiffness (Silenius 2002) can be increased with the use of PCC-fiber composites. Mechanical pulps also tend to introduce contaminants into the paper mill water circulation (Manner et al. 2009).

2.4.2 Bleached chemical pulp

Bleached chemical (kraft) pulps have high brightness and good brightness stability (Chirat et al. 2011; Sharma et al. 2020), as well as softness (Sharma et al. 2020), and bleached kraft pulps are commonly used in paper and board grades that require these properties, such as paper for printing, tissue and absorbent products (Sharma et al. 2020). In the latter case, PCC-fiber composites have been investigated in connection with fluff pulps, where the target has been the opposite of that in printing papers, i.e. to reduce interfiber bonding and to reduce the energy needed during dry fibrillation (Xu et al. 2017).

PCC, especially nano-PCC, is thought to reduce the bonding while the fiber maintains its absorbing capabilities, whereas fibers treated, for example, with hydrophobic debonding agents tend to partially lose their absorption capacity (Xu et al. 2017). In case of nano-PCC, the loss of bonding is explained sterically (Xu et al. 2017): the mineral particles disrupt sheet structure and prevent interfiber contacts required to form hydrogen bonds (Krogerus 2007).

Maintaining sheet strength while increasing the brightness has been one of the main motivations for developing PCC-fiber composites. The two essentially opposite targets, the improved strength of filled paper and the debonding of fluff pulps may not rule each other out, as the morphology of the precipitate may alter the bonding of the PCC-fiber composite.

For the maintenance of brightness of paper containing a PCC-fiber composite, lignin and chromophoric groups are of special interest also on bleached kraft pulps. Bleached kraft pulps usually contain 0.1-0.5% lignin (Loureiro et al. 2012) and, although this amount is

low, lignin is assumed to be the main contributor of chromophoric groups in kraft pulp (Gellersted 1996), where an extremely low concentration of chromophoric groups can be sufficient to alter the brightness or color of the paper. The concentration of isolable chromophores in bleached pulp (kappa number less than 5) has been reported to be between 19 to 117 ppm, based on a chromophore release and identification method (Korntner et al. 2015).

The preparation of PCC-fiber composites by in-situ carbonization uses $Ca(OH)_2$ which, depending on process choices, may lead to a high pH during the process. High pH values may in turn result in the formation of chromophores in lignin (Forsskåhl 2000; Jäkärä et al. 2009). The use of alkali was rejected in the early patent literature (Lutton 1952b), and alkaline yellowing during PCC-fiber composite preparation was reported by Klungness et al. (1996), especially when a totally chlorine free (TCF) kraft pulp was used instead of an elemental chlorine free (ECF) pulp.

Another property of interest when PCC-fiber composites are prepared from bleached kraft pulp is the fiber charge. Charged groups on the substrate have been found to affect the precipitation of PCC onto the substrate, see 3.5 Nucleation and growth of PCC on a cellulosic substrate. For a great degree, the charge characteristics of bleached kraft pulps results from dissociated carboxylic groups in hemicelluloses, and is affected by the selected bleaching sequence (Laine 2007). Bleaching depolymerizes and oxidizes cellulose and hemicellulose (Chirat el al 2011) and creates or removes charged groups (Laine 2007). Reactions between hexenuronic acid and bleaching chemicals are especially important for the fiber charge (Laine 2007).

2.4.3 Micro- and nanofibrillated cellulose and fibrillar fines

Fines are usually defined as the material that passes the 200 mesh wire of a Bauer McNett classifier (Heinemann and Vehniäinen 2009), or sometimes as the material that passes the round holes (76 μm diameter) of a nominally 200 mesh screen of a drainage jar (TAPPI standard T 261 cm-94). The terms micro- and nanofibrillated celluloses (MNFC, or MFC and NFC, respectively) have been used somewhat loosely in the literature (Lavoine et al. 2012), although a standard (ISO/TS 20477:2017 Nanotechnologies - Standard terms and their definition for cellulose nanomaterial) has recently been published.

It is nevertheless fairly obvious that there is a significant overlap in MNFC and cellulosic fines in size and in terms of e.g. a large specific surface area, high water retention capacity and high aggregation tendency (Taipale 2010). Both MNFC and fines also offer excellent bonding ability and strengthen the sheet (Taipale 2010), and they may therefore be used to counter the negative effects on the strength caused by a filler.

Promising results in terms of strength and optical properties have been reported when a PCC-kraft fines composite was used (Silenius 2002). Later, Subramanian et al. (2007) reported similar results using fines (or MFC) obtained by Masuko grinding, where the first-pass retention, internal bonding strength and tensile index were improved compared

with a sheet comprising a reference PCC, while the light scattering remained at a similar level.

The large surface area, hydrophilic nature and high concentrations of hydroxyl groups available to form hydrogen bonds with water contribute to the dewatering and drying difficulties associated with MNFC (Sinquefield et al. 2020). High fibrillar swelling has been associated with the difficult dewatering of MNFC, as well as a sealing mechanism, i.e. the plugging of channels and inhibiting of water flow (Dimic-Misic et at 2013). Although a high water retention is of interest in some applications, it may lead to drying difficulties in a MNFC-containing paper web (Dimic-Misic et al. 2016).

The water-holding capability of MNFC has been reported to decrease when a PCC-MNFC composite is formed (Dimic-Misic et al. 2016; Rantanen 2016), due to a reduction in the total fiber and fibril surface area in the presence of PCC (Dimic-Misic et al. 2016). Subramanian et al. (2007) also reported differences in sheet properties and water removal depending on the PCC morphology: colloidal PCC was more detrimental for water removal in wet-pressing than scalenohedral or rhombohedral types, although the order changed with heavier filling (Subramanian et al. 2007).

2.4.4 Recycled fibers

Recovered paper and recycled fiber, RCF, are currently the most widely used raw materials in papermaking (Schabel 2010a), and numerous review articles can be found, for example by Hubbe et al. (2007). Many of the differences between recycled and virgin pulp can be expected to affect the forming of a PCC-fiber composite. For example, cell wall pore closure (Hubbe et al. 2007) and the subsequent loss of cell wall pore volume can be expected to decrease the ability of the fiber to take the PCC into the cell wall.

It is of interest to see whether a PCC-RCF composite can raise the papermaking potential of RCF. When present, residual ink affect the optical properties of a RCF sheet negatively and non-linearly: a small amount of ink particles result in a large drop in brightness, and fine ink particles are more prone than larger particles to cause a brightness loss (Schabel 2010a). Combined with the often hydrophobic nature of inks (Schabel 2010b) an improvement in recycled pulp quality and especially brightness can be expected when PCC-RCF composite is prepared, due to the PCC attaching on the ink particles and potentially partially covering the particles, altering their optical properties.

Such results have been reported by Kim et al. (2013) and Seo et al. (2014, 2017). Kim et al. (2013) precipitated PCC in-situ on recycled deinked printing paper (white ledger) both as a whole pulp and on separated fines fractions. In blends with virgin pulp, a decrease in the effective residual ink concentration (ERIC) and an increase in brightness and opacity were reported, and Seo et al. (2014, 2017) reported similar results for old newspaper, mentioning that they suspected that the colored impurities and macro stickies acted as initial nuclei for the precipitation. The removal of sticky material from deinked pulp by the IS-precipitation of PCC has also been reported by Klungness et al. (2002).

2.4.5 Non-wood natural fibers

Non-wood natural fibers are currently a marginal raw-material in the paper industry, amounting to only 3% of consumed pulp in the world (Liu et al. 2018), mainly in China and India (Ashori 2006; Liu et al. 2018), but the use of non-wood natural fiber from selected sources is partially in good agreement with current "green" trends.

The chemical compositions and fiber morphological characteristics (Marques et al. 2010; Liu et al. 2018) of non-wood fibers vary greatly. In general, however, non-wood fibers are short (2 mm or less) and the fines content is high (Saijonkari-Pahkala 2001; Liu et al. 2018), and some of the technical limitations, associated with the use of such pulps, could perhaps be alleviated by the formation of PCC-fiber composites.

Bagasse has gained some attention. Allan et al. (1998) and Kumar et al. (2009) have attempted to improve the modest optical properties by IS-precipitation of PCC. Both were able to improve the optical properties, and Kumar et al. (2009) reported light scattering similar to that of a filled hardwood sheet, although the strength properties were affected more. The excessive fines content of straw pulp is problematic because the fines impede water removal (Saijonkari-Pahkala 2001; Liu et al. 2018), and the improved water removal of PCC-fiber composite may be of interest in this context.

3 Synthetizing PCC-fiber composite by in-situ precipitation

3.1 Industrial methods of synthetizing PCC

$CaCO_3$ can be synthesized by numerous methods, including the use of supersaturated $CaCO_3$ solution obtained by the dissolution of $CaCO_3$ by bubbling with CO_2, (Hosoda and Kato 2001; Lakshminarayanan et al. 2003), a gas-liquid system using ammonium bicarbonate (NH_4HCO_3) and calcium chloride ($CaCl_2$) (Zheng et al. 2012), and the carbonization process. Industrially, two processes are mainly used: the calcium chloride process and the carbonization process, the latter of which is more common (Ciullo 1996; Teir et al. 2005; Ukrainczyk et al. 2007). These are also the main approaches used for in-situ PCC-fiber composite preparation.

The calcium chloride process, also known as the liquid-liquid-solid route of $CaCO_3$ precipitation (Ukrainczyk 2007), uses two soluble salts, $CaCl_2$ and sodium carbonate (Na_2CO_3) (Ciullo 1996; Teir et al. 2005). It is usually run in a satellite plant of a Solvay process (ammonia-soda process) because of the economic need for a low-cost source of $CaCl_2$ (Ciullo 1996; Teir et al. 2005). The reaction between the salts results in the formation of $CaCO_3$ with NaCl as a secondary salt (Teir et al. 2005). The most common crystal form obtained using the method is rhombohedral calcite (Ukrainczyk et al. 2007).

If this method is applied to PCC-fiber composite preparation, the secondary salt formed in the process may lead to difficulties, changing the wet end chemistry and retention aid performance which are sensitive to the electrolyte concentration (Stenius 2000; Laine 2007), which means it may be necessary to wash out the undesired salt.

The carbonization process (the solid-liquid-gas route of $CaCO_3$ precipitation (Jimoh 2018)) avoids the problem of a secondary salt since it uses $Ca(OH)_2$ and CO_2 or a CO_2-rich gas often obtained from a lime kiln or power plant and cooled and cleaned by scrubbing before use. Chemical additives may be used to alter the properties of the forming PCC (Jimoh 2018).

Precipitation by carbonization at an industrially justified concentration requires precipitation from a slurry due to the low solubility of $Ca(OH)_2$ in water (1.85 g/l at 0 °C or 0.71 g/l at 100 °C (Oates 1990)). This results in a three-phase system with a solid and gaseous reactant, a liquid reaction medium and a solid product. In terms of exact process variables, the three-phase system is more difficult to control than the liquid-liquid-solid route due to the need for CO_2 dissolution (Jimoh et al. 2018) and by the presence of the fiber when a PCC-fiber composite is prepared (see 3.4 Effect of fiber in PCC-fiber composite synthetization).

3.2 Precipitation of PCC

The driving force for crystallization from a solution is said to be supersaturation, where a system in a supersaturated state attempts to achieve thermodynamic equilibrium through crystallization (Mersmann et al. 2001; Karpinski and Wey 2002), but the understanding of the crystallization process itself has recently changed. The classical nucleation theory (CNT) has been challenged, with mounting evidence for non-classical or modern nucleation theory (Karthika et al. 2016; Cölfen 2020).

$CaCO_3$ is one of the substances that often do not follow the predictions of CNT. When PCC precipitates, stable clusters may be formed even in undersaturated solutions, and these clusters may eventually lose water and form a liquid phase, then an amorphous phase and finally a crystalline phase (Karthika et al. 2016; Cölfen 2020). Both liquid (Gower and Odom 2000; Dai et al. 2008; Schenk et al. 2012) and amorphous (Wang et al. 2012; Purgstaller et al. 2016; Tobler et al. 2016) precursor phases have been empirically detected in the case of $CaCO_3$, but it is also possible that the prenucleation clusters form critical nuclei, which thereafter grow by single-ion attachment (Karthika et al. 2016).

The precipitation mechanisms of $CaCO_3$ therefore are not thoroughly understood. The morphology of the precipitate can however be tailored by controlling the electrical conductivity (EC) in the carbonization process, maintaining the conductivity by the addition of $Ca(OH)_2$ into a bubbled semi-continuous batch process. Under a certain set of conditions, an uncontrolled, seemingly unexplained, increase in electrical conductivity can however occur (Garcia-Carmona 2003; Carmona et al. 2004; Ukrainczyk et al. 2007). Similarly, the electrical conductivity and pH at the beginning of the precipitation can decrease and thereafter recover unless the $Ca(OH)_2$ is not continuously added into the slurry (Yamada and Hara 1985; Subramanian 2008).

This has been associated with a precipitation route where $CaCO_3$ (usually thought to be an intermediate metastable ACC) begins to form on the solid $Ca(OH)_2$ particles in the slurry (Garcia-Carmona 2003; Carmona et al. 2004; Ukrainczyk et al. 2007; Subramanian 2008; Yamada and Hara 1984, 1985). This temporarily inhibits the dissolution of $Ca(OH)_2$ from the affected particles leading to a decrease in conductivity as the precipitation reaction continues. Thereafter, the $CaCO_3$ dissolves from the $Ca(OH)_2$ particles. The intermediate phase is then thought to lose (meta)stability, resulting in dissolution and a sudden increase of charged species in the reaction mixture, detected as an increase in conductivity. The dissolution of $Ca(OH)_2$ can continue, resulting in an increase in pH. The charged species (re)precipitate as crystalline $CaCO_3$.

Carmona et al. (2003) presented experimental data, including SEM micrographs, supporting this interpretation. They show and describe $Ca(OH)_2$ “coated by small, elongated particles”, which turn into “chain-like aggregates” that grow in size and detach from the $Ca(OH)_2$ surfaces. Only after the $Ca(OH)_2$ disappears can the final calcite morphology be formed (Carmona et al. 2003).

This precipitation route is especially interesting for PCC-fiber precipitation because the electrical conductivity and pH have been reported to develop as indicated when fiber is present (Subramanian 2008). The route stresses the importance of having solid, non-$CaCO_3$ surfaces in the reaction mixture. Carmona et al. (2003) discuss the possibility of ACC stabilization (affected by the negative net charge) at the interface of $Ca(OH)_2$ particles. This brings the typically anionic cellulosic fiber surfaces interest as well.

3.3 Morphology control of the precipitate in carbonization process

SEM microcraphs of the PCC-fiber composites show that the precipitate morphology often differs from the rosette-shaped aggregate associated with the scalenohedral primary particles typically obtained in a carbonization process (Ukrainczyk et al. 2007). It has also been reported that the morphology of the precipitated PCC is affected by the substrate (Yamanaka et al. 2009), and cellulosic fibrils have been reported to disrupt the growth of scalenohedral calcite (Subramanian 2008).

The methods used to control PCC morphology in the absence of fiber cannot therefore be expected to yield identical results when a PCC-fiber composite is being prepared, although the methods used to control PCC morphology in the absence of fiber have been successfully utilized to alter the precipitate morphology of PCC-fiber by e.g. Subramanian et al. (2007).

In industrial applications, supersaturation and therefore crystallization are controlled by controlling the material and energy flows in the crystallizer and thus the nucleation and growth of the crystals (Mersmann 2001). Although the general principles of crystallization such as nucleation and crystal growth due to supersaturation apply to precipitation crystallization (Karpinski and Wey 2002), the practicalities may be slightly altered. For PCC, the possibility that the precipitation may occur by non-classical routes may further complicate the situation (see 3.2 Precipitation of PCC).

If the reactant concentration is high (as is the case for PCC) combined with a fast reaction and low solubility of the reaction product, the situation may lead to high local supersaturation, primary nucleation and a large amount of small particles (Mersmann 1999; Karpinski and Wey 2002). The high concentration of particles and high degree of supersaturation, however, result in an aggregation of particles (Schubert and Mersmann 2000) and other secondary processes such as Ostwald ripening (Karpinski and Wey 2002). Such processes affect not only the size and shape of the particles but also their growth rate in precipitation (Schubert and Mersmann 2000; Karpinski and Wey 2002).

Further complexity but also opportunities for crystal design arise due to polymorphism and different possible crystallization pathways. Ostwald's rule of stages states that when a transformation takes place from one state to another, the newly formed state is not the thermodynamically most stable but the one closest to the stability of the original state (Mersmann 2001; Threlfall 2003). This is the least stable state available (Threlfall 2003), the formation of which is explained kinetically (Mersmann 2001; Threlfall 2003). The

rule is not however a universal law. Exceptions are known (Threlfall 2003), some of which may be related to complex crystallization pathways (Hedges and Whitelam 2011).

Such factors create some difficulty in controlling or reliably predicting the PCC morphology obtained under a given process and process conditions, even when no fiber is present. Therefore, an empirical approach is often chosen.

The **temperature** and **conductivity** have been identified as important factors determining the PCC morphology in a carbonization process but it is important to realize that the source of conductivity may differ. It may originate from (super)saturation with respect to $CaCO_3$, from the presence of a different salt or whether, for example, there is an excess of CO_2 and a $Ca(OH)_2$ solution is slowly fed into the process.

Ukrainczyk et al. (2007) used the conductivity as a measure of supersaturation, and they found that increasing the conductivity changed the calcite morphology from rhombohedral to truncated prismatic to scalenohedral at elevated reaction temperatures (35 and 50 °C), but that the change was from rhombohedral to nano-sized spheroidal particles that organized into "chains" at room temperature (20 °C). García-Carmona et al. (2003) reported similar results, with rhombo-scalenohedral shapes occurring between the rhombohedral and scalenohedral morphologies.

The **ratio of $[Ca^{2+}]/[CO_3^{2-}]$** is commonly thought to affect the morphology in a manner where a ratio close to the stoichiometric ratio yields rhombohedral calcite (García-Carmona et al. 2003) and a higher ratio results in the scalenohedral type (García-Carmona et al. 2003). This has been associated with the stabilization of crystal faces due to a crystal face-Ca^{2+} interaction (Cizer et al. 2012).

In the case of in-situ precipitation, a similar but not identical result has been reported by Matthew et al. (1995). They used a sequence of CO_2 additions, which allowed control of $CO_2/Ca(OH)_2$ ratio in each pass, while using ratios greater than and less than 1. Matthew et al. (1995) mentioned that the use of lower ratios produced a smaller and rounder precipitate, whereas the higher ratios resulted in a larger and less round precipitate on fibers.

Fuchise-Fukuoka et al. (2020b) also reported that the CO_2 feed affected the precipitate size and morphology on the cellulosic fiber when the gas was added as ultrafine (<100 μm) bubbles. Counter-intuitively from the classical crystallization point of view, Fuchise-Fukuoka et al. (2020b) reported an increase in PCC particle size on fibers with increasing CO_2 flow rate, which they explained as being due to the $[Ca^{2+}]/[CO_3^{2-}]$ ratio (decreasing with increasing CO_2 feed) rather than to high degree of supersaturation and resulting heavy nucleation.

García-Carmona et al. (2003) reported that the increase in conductivity in a PCC precipitation study was associated with an increase in the amount of Ca^{2+} in the reaction mixture, and that a change towards a scalenohedral precipitate with increased

conductivity was associated with an increase in the $[Ca^{2+}]/[CO_3^{2-}]$ ratio. Ukrainczyk et al. (2007) however precipitated scalenohedral calcite with a low $Ca(OH)_2$ concentration in the reaction mixture. They explained that this was due to a lack of accumulated solid $Ca(OH)_2$ and to a dissolution of $Ca(OH)_2$ faster than the formation of PCC, the increase in conductivity being due to the large amount of dissolved CO_2.

The $[Ca^{2+}]/[CO_3^{2-}]$ ratio has also been reported to affect the polymorphism. Chakraborty and Bhatia (1996) reported that a high $[Ca^{2+}]/[CO_3^{2-}]$ ratio resulted in "stable" vaterite, and that a low ratio resulted in the nucleation of vaterite that however transformed to calcite.

The reports regarding the effects of **stirring** and **CO_2 feed** vary. It has been reported that stirring does not affect the morphology or particle size (Ukrainczyk et al. 2007), but that it may be of importance in determining them (Chakraborty and Bhatia 1996).

Similarly, CO_2 feed has been reported by Ukrainczyk et al. (2007) not to affect, and by Wen et al. (2003) to affect the morphology and particle size. This is probably due to the indirect and also interconnected effect these parameters have on the process, where stirring affects the material transfer, including the gas (CO_2) dispersion in the process. Stirring and CO_2 feed are thus connected to the $[Ca^{2+}]/[CO_3^{2-}]$ ratio and to supersaturation and conductivity. A change may or may not therefore result in a change in precipitation that affects the precipitate. **Reaction vessel geometry**, **gas bubble size** and **CO_2 concentration in the feed gas** can be expected to have similar indirect effects.

The presence of **undissolved $Ca(OH)_2$** has also been reported to affect the precipitate (García-Carmona et al. 2003; Ukrainczyk et al. 2007). This has been associated with the route by which the precipitation proceeds; whether it proceeds by a surface route (precipitation on the $Ca(OH)_2$ surface) or if the $Ca(OH)_2$ dissolves prior to precipitation (García-Carmona et al. 2003; Ukrainczyk et al. 2007). Interestingly, from a PCC-fiber composite preparation point of view, solid $Ca(OH)_2$ in the system has been reported to reduce the tendency for nano-sized PCC particles to aggregate (García-Carmona et al. 2003).

Other chemical substances, both organic and inorganic, can be used to control the morphology of the precipitate, as well as polymorphism and other properties such as surface charge (El-Sheikh et al. 2013). Examples of the effects of different additives on the PCC morphology and polymorphism are presented by Jimoh et al. (2018). Negatively charged organic additives have usually been reported to be more effective than positively charged organic additives, which have had only a slight effect on PCC in most studies according to Cantaert et al. (2012). Inorganic cations such as bivalent magnesium, barium and manganese ions (Mg^{2+}, Ba^{2+} and Mn^{2+}) have however often been effective (Chen et al. 2006). The mechanism typically suggested for the effect of other chemical substances is that they adsorb on crystal faces where they may alter the kinetics of the crystal face growth and therefore the morphology of the growing crystals (Mersmann et al. 2001).

3.4 Effect of fiber in PCC-fiber composite synthetization

Different fiber substrates differ in their tendency to form flocks and affect the viscosity of the fiber slurry, and these factors can be expected to affect the material transfer within the precipitation process. In a bubbled batch system, an increase in viscosity may increase the time which the CO_2 gas bubbles take to escape from the system, increasing the CO_2-reaction slurry contact area unless the bubble size is simultaneously affected. Floc-forming and breaking may affect the material transfer and the concentrations of ions, and densely formed flocs may trap $Ca(OH)_2$ or other particles and affect the local conditions of precipitation.

The specific surface area of the fiber may be of importance in heterogeneous nucleation and lead to a situation where the surface area of fiber per volume of the reaction mixture is altered although the reaction consistency with respect to the fiber is fixed. Similarly, fixing the specific surface area of the fiber will probably result in a different fiber volume in a given volume of fiber mixture, which is related to slurry viscosity and crowding of the reaction mixture.

The PCC-fiber composite must be prepared to a defined PCC content. The weight of $Ca(OH)_2$ (m) required to form a PCC-fiber composite with a chosen PCC content is calculated using the equation (3.1), derived from TAPPI standard T 211 om-02 relating to ash definition:

$$m_{Ca(OH)_2} = \frac{Ash,\% \cdot (B - A)}{100 - Ash,\%} \cdot 0.7402 \qquad (3.1)$$

where A is the targeted weight of PCC ash, assuming 100% conversion, B is the weight of the test specimen and B-A is therefore the weight of oven-dry fiber. The factor 0.7402 is the ratio of the molar mass of $Ca(OH)_2$ and that of $CaCO_3$.

When the targeted PCC content of the composite is fixed, increasing the fiber surface area per reaction mixture volume by increasing the fiber consistency and therefore the $Ca(OH)_2$ concentration will probably affect the ratio of ionic species due to material transfer and dissolution kinetics. If the fiber surface area per reaction mixture volume is instead controlled by altering the fiber specific surface area, e.g. by refining, in order to maintain $Ca(OH)_2$ concentration, the mixture rheology and the tendency of the fiber to flocculate will be affected.

3.5 Nucleation and growth of PCC on a cellulosic substrate

The tendency for PCC and other minerals to attach onto fibers has been known for years but the mechanism is not fully understood. The situation is complicated by the different possible routes of $CaCO_3$ crystal forming, and various explanations of $CaCO_3$ precipitation on a solid substrate have been suggested.

From the theoretical point of view, the explanation offered e.g. by Silenius (2002) where the PCC nucleates and precipitates on the cellulosic substrate as predicted by the classical nucleation theory is fairly straight-forward.

This approach emphasizes the surface area of the fiber or the fiber fractions in the pulp. Silenius (2002) reported that PCC precipitated in larger amounts on cellulosic fines than on the larger fibers. PCC enrichment in fines has also been reported by Seo et al. (2017). This finding is in good agreement with the heterogeneous nucleation explanation, but the fines also contain more carboxyl groups, more metal ions and are more negatively charged than the bulk of the fiber (Odabas et al. 2016), so that PCC enrichment onto fines is in good agreement with other suggested explanations of PCC attachment as well.

Dalas et al. (2000) have suggested that the precipitation is steered onto the cellulose because of the presence of functional groups such as hydroxyl groups that are capable of binding metal ions to form subcritical $CaCO_3$ nuclei on the cellulosic substrate with subsequent nucleation.

In some cases, precipitation on the substrate has been associated with an interaction between the additive chemical and charged groups in the substrate (Hosoda and Kato 2001; Xu et al. 2005). Interesting results were reported especially by Hosoda and Kato (2001), who precipitated thin films of $CaCO_3$ on cellulose, chitosan and chitin with PAA present in the solution (inhibiting bulk nucleation), but also the crystallization on substrate polymer was inhibited when the substrate was derivatized to protect its proton-donating groups (hydroxyl and amine).

Hosoda and Kato (2001) also reported rhombohedral calcite crystal precipitation on both derivatized and non-derivatized templates when the crystallization was carried out without PAA, demonstrating that although proton-donating groups are important under certain conditions, they are not required under other conditions.

When the precipitation is carried out under conditions in which ACC can be expected to form, as is often the case, the presence of ACC means that the “simple” classical heterogeneous nucleation explanation cannot suffice. If the precipitation process advances via an ACC precursor, the precipitation onto cellulosic surface may be linked to inter-particle interactions due to polarization of the particles (Subramanian 2008).

In the case of non-cellulosic substrates, PCC precipitation onto the substrates has been linked with surface wetting properties and the interaction between the ACC and the substrate. Xu et al. (2005) were able to show ACC hemisphere and film deposition onto substrates, followed by crystallization of ACC when it came into contact with moist air. They noted that the hemispheres resembled droplets of liquid on the surface as seen in solid-liquid-gas system, and that the angle of contact with the substrate was approximately constant. PCC precipitation onto the surface was associated with both adhesive (ACC-fiber) and cohesive (ACC-ACC) forces, and the ACC stabilizing and

film-forming effect of PAA was explained as being due to the change in ACC zeta potential, resulting in reduced cohesive forces.

For non-cellulosic substrates, Chevalier (2014) used glass, silanized glass and polyethylene with controlled wettability and found that the degree of nucleation (indicated as crystals/mm^2) decreased with increasing hydrophilicity of the substrate, resulting in a situation where precipitation on the surface was energetically less beneficial than on a hydrophobic surface. Similarly, Yamanaka et al. (2009) investigated surfaces of similar roughness but different surface energies (mica and highly oriented pyrolytic graphite) and were able to detect different ACC contact angles on the substrates. They reported that a low contact angle between the substrate and ACC resulted in a large number of crystals.

Much of the research related to ACC and PCC crystallization onto substrates has been done using a process different from the carbonization, so that the precipitation route may differ from that in carbonization precipitation.

3.6 Water cleaning effect and potential alteration of PCC

The trend in papermaking towards a more closed water system leads to the enrichment of substances in the paper mill waters, including wood components, anionic and cationic polymers such as retention aids, chemicals used in coating, fixing agents, strengthening agents and sizing agents, anionic and cationic polyacrylamide (A-PAM and C-PAM), carboxymethylated cellulose (CMC), and cationic starch (CS), and inorganic salts such as sulphates from cooking, surfactants, and dispersed solids such as alkenyl succinic anhydride (ASA), alkyl ketene dimer (AKD) and latices (Hubbe 2007a; Laine 2007; Manner et al. 2009).

These impurities may result in difficulties such as poor strength due to increased salt concentration, poor first pass retention and increased retention chemical demand due to the excessive accumulation of negatively charged polyelectrolytes and colloidal material (Hubbe 2007a; Laine 2007; Stenius 2000). Various “kidney technologies” to clean the white water include membrane filtration, enzyme treatment and chemical coagulation (Hubbe 2007b).

Precipitating PCC is capable of sorbing ions and macromolecules (Naka and Chujo 2001), and this suggests that when a PCC-fiber composite is prepared in-line or when process water is used as a medium for PCC precipitation, the precipitation process may also perform a kidney function. Results supporting this suggestion have been reported by Matula et al. (2018).

Although the water-cleaning effect may be beneficial and of interest when contaminant-rich pulps such as RCF are used, these contaminants may at the same time alter the properties of the precipitated PCC. The change in $CaCO_3$ morphology has been demonstrated in biomimetic systems by polymers (Naka and Chujo 2001) and in simpler

precipitation processes by e.g. sulfate ions (Tang et al. 2012). It has been reported that in-line PCC ash has a different color because of incorporated iron (Matula et al. 2018).

Although the concentration of a single substance in PCC-fiber composite preparation may be low and below the concentration at which it alone would significantly affect the precipitation, the net effect of different substances may be much greater. Many morphology-altering substances are anionic organic materials (Cantaert et al. 2012) and the papermaking waters contain many substances perhaps capable of altering the PCC morphology.

4 Materials and methods

The PCC-fiber composites or PCC were prepared in open batch reactors using precipitation of $CaCO_3$ by the reaction of $Ca(OH)_2$ with CO_2 gas in aqueous media in the presence of dispersed fibers. The $Ca(OH)_2$ was prepared either in the laboratory by slaking CaO or used as obtained (see Table 4.1).

The carbonization led to the neutralization of $Ca(OH)_2$, which was detected as a decrease in the pH which was used to indicate the end point of the reaction, typically at a pH between 6 and 8, i.e. neutral. A slight variation in the end point pH was associated with different reaction conditions affecting the ionic balance.

The reaction between $Ca(OH)_2$ and CO_2 is exothermic, and the reaction was performed under non-isothermal conditions. The temperature before precipitation was approximately 20 °C unless otherwise stated. Most of the experiments were carried out without morphology-controlling chemicals, but as indicated in the text, the morphology-controlling chemicals L-lysine (L-lys) and the sodium salt of polyacrylic acid (Na-PAA) were sometimes used.

After preparation, the composites were characterized in the wet condition by pulp fractionation, fiber analysis and surface charge density, and in the dry condition by ash content and scanning electron microscopy. Some of the composites and pulps were used to prepare laboratory handsheets to study the effect of the PCC-fiber composite on sheet properties. In some of the handsheets, MFC or cationic starch (CS) was used as a strengthening agent as indicated in the text.

The materials used to prepare the samples are listed in Table 4.1.

Table 4.1: Materials used for preparing the samples and their pre-treatment

	Source and preparation	Used for
Fibers		
BBK	Air dry bleached kraft (birch) pulp sheets (Stora Enso, Kaukopää mill Imatra, Finland), disintegrated according to ISO 5263-1 using tap water	Precipitation experiments with Reactor II (unpublished results)
CTMP	Air dry hardwood (birch) pulp sheets (Stora Enso, Kaukopää mill Imatra, Finland), disintegrated and refined using Valley beater (standard ISO 5264-1:1979)(1)	PCC-CTMP composite preparation, preparation of laboratory handsheets (Paper II and Paper III)
MFC	Laboratory prepared by mechanical refining (Microfluidizer M-110EH-30, Microfluidics Corp.) from hardwood kraft pulp (2x 400/200 + 1x 200/100 µm chambers, using pressures of 1100 bar and 1500 bar)	PCC-MC composite preparation (Unpublished results)
MC	Commercial grade (JRS, Arbocel UFC100). The dry powder and was dispersed in water using strong mixing (Diaf dissolver type FFBH 30) without dispersing aids. The mean particle size according to the supplier was 8 µm	PCC-MC composite preparation (Paper I, Unpublished results)
$Ca(OH)_2$		
Lime A	Provided by Stora Enso Oyj (Varkaus Mill). Dry matter content 8.5-10.4%. Used as obtained or diluted with tap water when necessary.	PCC-MC and PCC-MFC composite preparation (Paper I, Unpublished results)
Lime B	Prepared from CaO (Honeywell, reagent grade) by slaking for 4 h using CaO-to-H_2O ratio 1-to-9 and an initial reaction temperature of 40 °C, which was allowed to change freely	PCC-MFC and PCC-CTMP composite preparation, precipitation of reference PCC (Paper II, Paper III, Unpublished results)
Gases		
CO_2 A	Commercial gas (AGA, purity 99.7%)	Precipitation experiments with Reactor I and Reactor II (Paper I, Unpublished results)
CO_2 B	Commercial gas (AGA, purity ≥99.8%)	Precipitation experiments with Reactor III (Papers II and III)
Additive chemicals		
CS	Commercial cationic starch (Chemigate, Raisamyl 50021). Cationized potato starch with DS 0.035. Mixed in 60 °C water, heated to 95-98 °C and cooked for 30 minutes while stirring. Stored at 65 °C, used within 24 hours of cooking	Strengthening agent in handsheets (Paper III)
L-lys	Commercial L-lysine grade (Aldrich Chemistry, purity ≥ 98.0%). Used as 5.0 wt-% solution.	PCC morphology control (Unpublished results)
MFC	Commercial wood-based grade (Daicel FineChem Ltd, Celish KY100S) obtained at high solids, dispersed and diluted using strong mixing (Diaf dissolver type FFBH 30) without dispersion aids	Strengthening agent in handsheets (Paper III)
Na-PAA	Commercial grade of sodium salt of polyacrylic acid (Sigma-Aldrich, M ~1800 g/mol), dissolved in water (2, 5 and 8 wt-%)	PCC morphology control (Paper I, Unpublished results)

(1) For pulp pre-treatment details, see 4.1.2 PCC-CTMP

4.1 Preparation of PCC-fiber composites

4.1.1 PCC-MC, PCC-MFC and PCC-BBK

PCC-MC, PCC-MFC and PCC-BBK composites were prepared under various precipitation conditions (fiber consistency, $Ca(OH)_2$ concentration, CO_2 feed and bubble size) with and without morphology-controlling additives (Na-PAA and L-lys). The conditions used in each experiment are clarified in the text in connection with the results. The precipitation was done using 2000 g batches (before precipitation) in Reactor I and Reactor II, see Figure 4.1 for equipment details. The batches were prepared by mixing water, additives (when used), $Ca(OH)_2$ and fibers in this order.

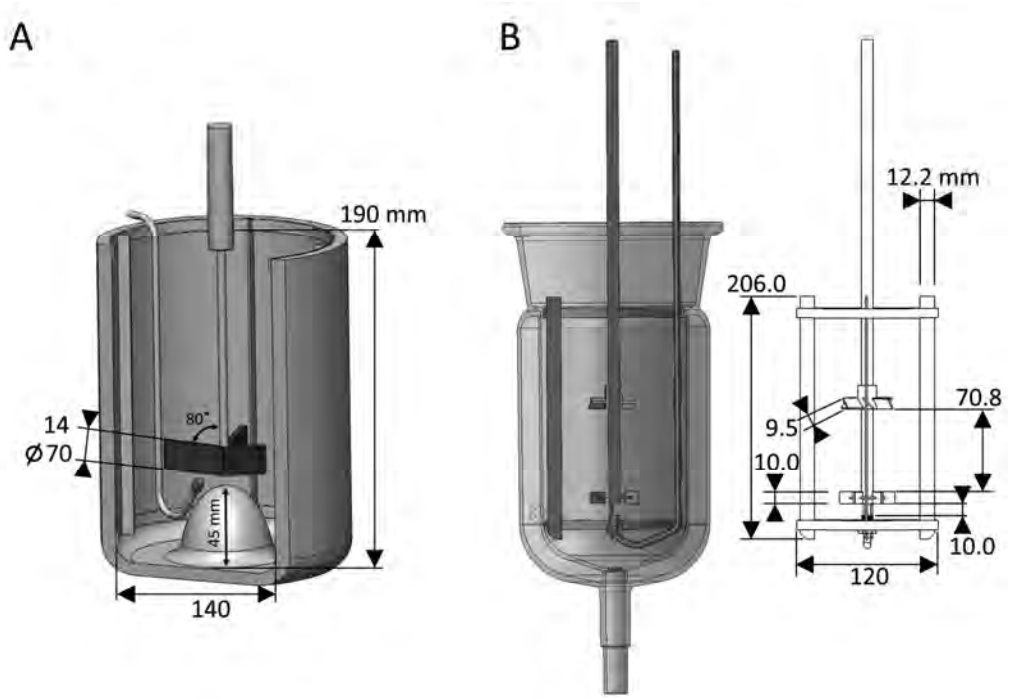

Figure 4.1: (A) Reactor I and (B) Reactor II. Both reactors were equipped with a cooling or heating jacket (not shown in Reactor I image). Both reactors were designed for 2 L batches and Reactor I was insulated. The size of the CO_2 bubbles in each reactor was controlled by using sintered metal filters with different opening sizes as gas spargers. The experiments with Reactor I were all performed using a sparger with 40 µm opening. Most of the experiments with Reactor II were carried out without a gas sparger, i.e. the CO_2 was fed in directly from the piping (inner diameter 5 mm), otherwise $CaCO_3$ would precipitate in the sparger and clogg the openings, resulting in a constant need for cleaning and, especially in longer experiments, difficulties in maintaining the CO_2 feed.

4.1.2 PCC-CTMP

PCC-CTMP was prepared using various sets of conditions (fiber consistency, $Ca(OH)_2$ concentration and CO_2 feed) to study the precipitate morphology, and using fixed conditions to prepare materials for further analysis (fractionation and the preparation of laboratory handsheets). The conditions used in each experiment are clarified in the text together with the results

Reactor III was used for precipitation experiments, see Figure 4.2 for equipment details. The batch size was 9.5 liters. The batches were prepared mixing water, fibers and $Ca(OH)_2$ in this order; the order of $Ca(OH)_2$ and fibers being the opposite of that adopted in Reactors I and II because the batch was mixed in the reactor and adding the large volume of fiber slurry as the final component often resulted in splashing.

Figure 4.2: Reactor III. The reactor was equipped with a cooling or heating jacket. The stirring element was attached to a motor (Elma Troyan 1.5 kW, 2.0 hp) for powerful stirring. The reactor was designed for 10 L batches but a slightly smaller batch size was used as stirring and the presence of the gaseous phase required additional space.

The pulps used for fractionation (Paper II) had freenesses of 23, 42 and 58 SR and were refined for 0, 30 and 60 min, respectively (Valley beater, standard ISO 5264-1). For the fractionation experiments, the conditions for PCC-CTMP composite preparation were chosen to yield nano-PCC evenly distributed on the fiber.

The pulp used for the 190 g/m^2 handsheets (Paper III) was not refined. Instead, it had undergone a washing procedure to reduce the amount of fines at the beater consistency (15.7 g/L) by stirring ca. 8 L of CTMP slurry on a 200 mesh metal wire (measured diagonal hole size 0.10 mm) while allowing the water and fines to drain through the wire. Tap water was added to maintain the pulp volume. In each case, there were eight washing batches washed using ca. 16 L of water. The precipitation conditions were the same as those used to make the PCC-CTMP for composites fractionation.

4.2 Preparation of PCC

A laboratory-prepared PCC, free from fibers and chemical additives such as dispersion aids, was used as a reference filler in 190 g/m^2 handsheets (Paper III), as a reference for PCC-BBK composite morphology, and to test the effect of a morphology-controlling chemical (L-lys) on the morphology of the PCC precipitate in the absence of fibers. PCC was synthesized in a similar manner with PCC-fiber composites, but without the presence of fiber. Reactor II was used. The conditions of each precipitation are indicated in more detail in the text.

In order to control the particle morphology and agglomeration when PCC was prepared for laboratory handsheets, the reaction was carried out at a temperature of 77±3 °C using a $Ca(OH)_2$ concentration of 22 wt-%.

4.3 Characterization of wet PCC and PCC-fiber samples

4.3.1 Pulp fractionation

The CTMP and PCC-CTMP composites were fractionated using a Bauer-McNett classifier according to the SCAN-M 6:96 standard, with the exception of the dosed pulp weight (10 g according to the standard) and wires.

In the case of PCC-CTMP, 20 g of oven-dry solids, i.e. PCC and CTMP combined, was used. As the PCC content of the PCC-CTMPs was close to 50%, the CTMP dose was close to the 10 g. In the fractionation of the corresponding CTMP alone, the amount of fiber dosed was equal to the amount of CTMP in the PCC-CTMP.

The 30, 100 and 200 mesh wires of the ASTM series were used, and to collect some of the fines, the fourth wire used was a non-standard 400 mesh wire with a measured opening of 25 μm.

In the case of the PCC-CTMP (but not the CTMP), a significant amount of material was found to pass the 400 mesh wire. This material was partially collected by retaining the waste water from the point when the waste water became cloudy to the point when it became clear. The water was left for two days to allow sedimentation before the excess

water was siphoned off. This fraction was labelled ‘pass’. The fractionation experiments and sample labelling are shown in Figure 4.3.

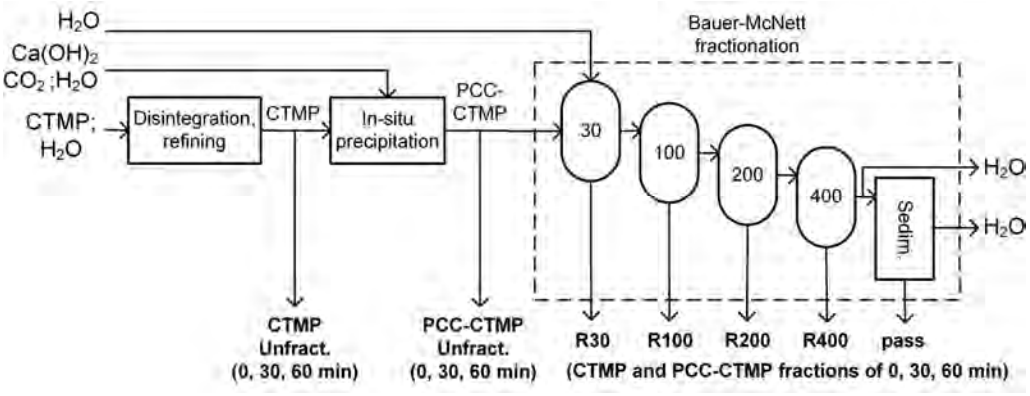

Figure 4.3: Scheme of the fractionation experiments. The Bauer-McNett fractionation values indicate the wire meshes used (ASTM series and a non-standard 400 mesh wire). The R30, R100, R200, and R400 fractions were collected after the fractionation. An additional sedimentation phase (‘sedim.’) was added after the fractionation, and this yielded the ‘pass’ fraction. The bold text indicates the samples taken for further analysis.

At least seven fractionations were carried out for each CTMP and PCC-CTMP. The material from at least five fractionations was collected and combined for use in further analysis and handsheet preparation. The fraction name refers to the wire from which the fraction was collected, i.e. the RX sample was collected from the X mesh wire.

Two fractionations were done in order to weigh the fractions as instructed in the SCAN-M 6:96 standard. The ash contents (TAPPI standards T 211 om-02 and T 413 om-11 in combination) were determined on fractions collected on ashless filter paper (Macherey-Nagel MN 640 m) and dried in an oven (105 °C) prior to the ash content measurement.

4.3.2 Fiber analysis

The fiber morphology was characterized according to the ISO 16065-2:2007 standard using the L&W Fiber Tester (Lorentzen & Wettre). The PCC-CTMP and CTMP were diluted to approximately 0.1 g fiber in 100 ml water, as instructed by the equipment manufacturer. The fiber morphology results are weigthed based on fiber length.

When the PCC-CTMP composite was fractionated (Paper II), the three PCC-CTMPs, the corresponding CTMPs, and the collected fractions (R30, R100, R200, R400, pass) were analyzed. Three parallel measurements were run for each sample. The results are given as the average of the three measurements. Raw fiber data were recorded in order to create

distributions of the recorded parameters (fiber length, fiber width, shape factor, amount of fines and kink index).

When 190 g/m^2 handsheets (Paper III) were prepared, the CTMP, the PCC-CTMP composite filler, the laboratory-made reference PCC, the MFC and all the furnishes used for the handsheet preparation were characterized. The machine pixel size was roughly 10 x 10 µm and particles recognized as (fine) fibers were 4 times as long as wide, i.e. the minimum size was approximately 10 µm wide and 40 µm long. This sets a limitation for the reliable characterization of the PCC and MFC, but the PCC and MFC samples were measured in order to understand how the free MFC and PCC would probably affect the result for the handsheet furnishes. Each sample was run once. An example of a partial optical analyzer image is shown in Figure 4.4.

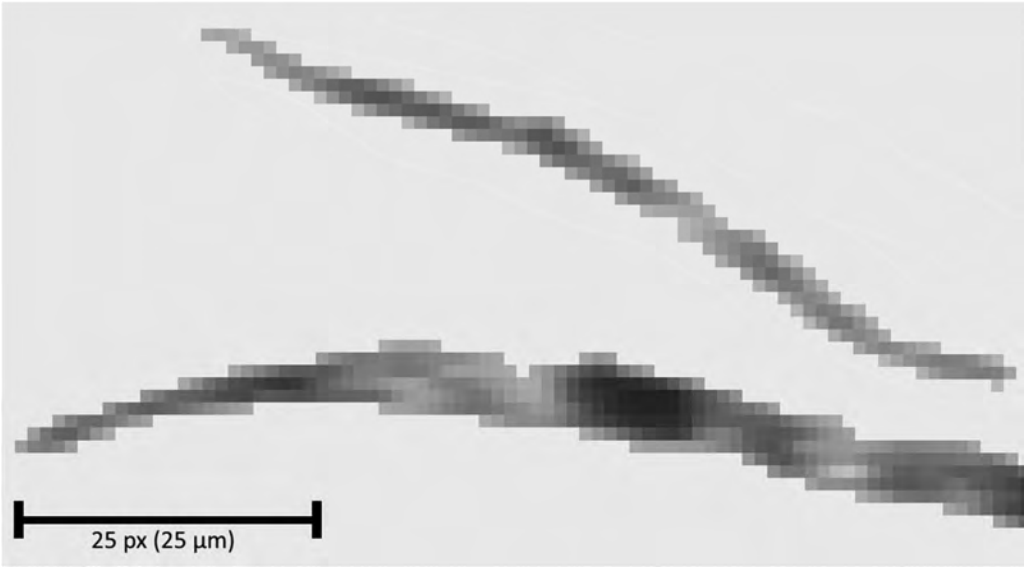

Figure 4.4: A partial optical analyser image showing a fine fibrillar particle (above) and part of a fiber (below). The background color was solidified for viewing. The sample was R200 unrefined CTMP.

4.3.3 Surface charge density

The surface charge density (cationic demand) of the PCC-CTMPs and CTMPs used in fractionation experiments and of their fractions was measured using cationic demand titration (PCD 02, BTG Mütek GmbH and Mettler DL25, GWB for titrant dosing). The measurements were made using a back-titration procedure as recommended by the manufacturer, although the targeted amount of fiber was reduced to 0.2 g. After the titrations, the fiber was dried overnight at 105 °C to determine the fiber weight and this weight was used in the surface charge density calculation.

The desired amount of fiber slurry was filtered on a polycarbonate membrane (GE Water & Process technologies, 3.0 µm) and the resulting cake was rinsed into a decanter using deionized water to obtain a 5.0 g sample. 20 g poly(diallyldimethylammonium chloride) (PDADMAC, 1.0 mN, M=107000 g/mol, BTG) was then added. After a reaction time of at least 4 hours, the fibers were removed from the residual PDADMAC solution by centrifugation (Hermle Z200A, 6400 g). Titration was done using polyethene sodium sulfonate (PES-Na, 1.0 mN, M=19100 g/mol, BTG). The results are given as averages of 3 to 4 titrations.

4.4 Characterization of dry PCC and PCC-fiber samples

4.4.1 Drying the samples

MC and PCC-MC were oven-dried (overnight, 105 °C) before analysis. The PCC-MC was powder-like and, when dried, it readily formed a loose powder.

When dried in the same way, the other fibers and PCC-fiber composites formed cakes which were difficult to break without damaging the material. Oven-drying was used when ash content was measured, but for scanning electron microscopy, the samples were either freeze-dried or vacuum-dried. The method used is indicated in the text.

Freeze drying was performed by diluting the sample to approximately 0.1 wt-% with deionized water. The samples were frozen at -18 °C, at least overnight and then transferred to the freeze-drier (Christ Alpha 2-4 LDplus) for drying. The procedure resulted dry material resembling an extremely loose cotton pad.

When samples were vacuum-dried, they were first diluted to a consistency of approximately 0.1 wt-% and stirred to homogenize them. A small amount of sample was pipetted and spread onto conductive tape (Electron Microscopy Sciences, Conductive Double Sided Carbon Tape 8 mm) to immobilize the dried sample. The water was evaporated under a partial vacuum in the sputter coating unit. The vacuum drying method was chosen because it has previously been found suitable for pulp, conserving the fibrillar structure at the fiber surfaces better than in the freeze-drying of a pulp sample frozen in water (Kiuru 2018).

4.4.2 Ash content

Ash contents of PCC-fiber composites and handsheets were measured at 525±25 °C and 900±25 °C using the TAPPI T 211 om-02 and T 413 om-11 standards, respectively. The standards were used in combination when the conversion of $Ca(OH)_2$ to $CaCO_3$ was assessed.

4.4.3 Scanning electron microscopy

Scanning electron microscopy (SEM) was used to visually asses the size and morphology of the precipitates, and whether or not the precipitate was located on fibers. Two SEM systems were used to produce the micrographs shown in this thesis. The more commonly used system was the Hitachi SU3500 equipped with a tungsten filament. The SEM was used in secondary electron imaging mode (SEI) or backscatter electron imaging in compositional mode (BSE-comp). The less often used microscope was the JEOL JMS-5800, which was used only in the SEI mode.

SE imaging was carried out using an acceleration voltage from 5 to 15 kV. The samples were sputter-coated (Au or Au/Pd target, Edwards Scancoat Six Sputter Coater). BSE-comp mode was applied on PCC-CTMP, CTMP, their fractions and the reference PCC (Paper II and Paper III). BSE-comp imaging was done using the variable pressure (VP-SEM) mode with 60 Pa and 15 kV acceleration voltage.

In addition to the micrographs captured using these methods, high resolution images were obtained from selected PCC-MC composite samples by field-emission scanning electron microscopy (FE-SEM) using a FEI Nova NanoSEM 450 instrument equipped with a Schottky-type field emitter using 10.0 kV accelerating voltage, 8 mm working distance and a retractable concentric back scatter detector (CBS). When this equipment was used, it is indicated in the text.

Cross-section images of 190 g/m^2 handsheets were obtained using the FE-SEM (low vacuum mode, a gaseous analytical detector (GAD) and the field-free final lens mode, detected signals backscattered electrons. The chamber pressure was 70 Pa, using water vapor from a built-in reservoir. The set working distance was 5.0 mm and the acceleration voltage 5.0 kV. On some images, the individual FE-SEM micrographs were mapped and stitched (FEI MAPS 2.0).

The cross-section samples of the 190 g/m^2 handsheets were prepared using a broad ion beam (BIB) cross section cutter (Hitachi IM4000, beam current 120 μA, 3 kV acceleration voltage, 1.5 kV discharge voltage, 400 μA discharge current, argon (Ar) gas flow).

4.5 Preparation and testing of laboratory handsheets

4.5.1 60 g/m^2 handsheets (Paper II)

Laboratory handsheets were prepared from CTMP, PCC-CTMP and the fractions according to the ISO 5269-1:2005 standard with the following exceptions: use of auxiliary wire (90 g/m^2 polyester satin, thread width approximately 300 μm, on top of the sheet mould wire), sheet pressing (4 minutes at 0.4 MPa), and drying (drum-drying for 4 hours, including the time to heat the drum to a surface temperature of ca. 60 °C). The auxiliary wire was removed after wet-pressing.

The fractions and pulps were used in handsheet preparation diluted with tap water but otherwise unaltered.

4.5.2 190 g/m^2 handsheets (Paper III)

Handsheets were prepared according to the ISO 5269-1:2005 standard with the following exceptions: grammage (190 g/m^2), sheet pressing (4 minutes using 0.4 MPa), and drying (drum-drying for 4 hours, including the time to heat the drum to a surface temperature of ca. 60 °C).

The furnishes containing PCC-CTMP were prepared by mixing the CTMP and PCC-CTMP in the desired ratio to reach the targeted PCC content. The CS was dosed assuming 100% retention. The MFC dose was controlled gravimetrically to compensate for retention losses. The PCC content, when PCC was used, was also controlled gravimetrically.

4.5.3 Handsheet testing (Paper II and Paper III)

The physical properties of the handsheets were tested according to the ISO 536:1995 (grammage), ISO 534:2005 (density and thickness) and ISO 1924-3:2005 (tensile strength, tensile stiffness, and elastic modulus) standards. Grammage was measured using all the test pieces available, i.e. usually four. Bulking thickness and apparent bulk density were used, except for the 190 g/m^2 handsheets for which the single sheet thickness and apparent sheet density were determined due to the greater thickness of the samples. For bulking thickness, the number of test pieces was 4 and the test piece size was 140 mm x 70 mm.

Brightness and opacity were measured using Elrepho (L&W) according to the ISO 2470-1:2009 (brightness) and ISO 9416:2009 (light scattering coefficient (s_r), light absorption coefficient (k_r) and calculated opacity for 65 g/m^2 sheet) standards, with the exception that 4 test pieces were used instead of 10.

The physical and optical properties were measured on conditioned handsheets (23 °C and 50% relative humidity (RH)). Ash contents at 525±25 °C and 900±25 °C were measured using the TAPPI T 211 om-02 and T 413 om-11 standards, respectively.

5 Results and Discussion

5.1 Tailoring the precipitate morphology on PCC-fiber by controlling the precipitation conditions

The preferred PCC morphology in papermaking is the rosette-like (scalenohedral) PCC due to its bulking ability and porous structure that provides light scattering, but the PCC in PCC-fiber composite is often cubical and methods to control the morphology are not well-known.

5.1.1 The effect of electrical conductivity (unpublished results)

The electrical conductivity (EC) has previously been used to control the PCC morphology in additive-free semi-continuous precipitation without fiber (García-Carmona et al. 2003; Ukrainczyk et al. 2007), and a similar approach was tested in the present work for the batch process with and without the fiber.

The initial EC of the batch before the CO_2 feed was started was due mainly to the $Ca(OH)_2$ addition, but when the CO_2 feed was started, the EC initially decreased and thereafter partially recovered. The pH of the suspension showed a similar behavior, as shown in Figure 5.1. The EC and pH development were therefore in agreement with precipitation route described under 3.2 Precipitation of PCC.

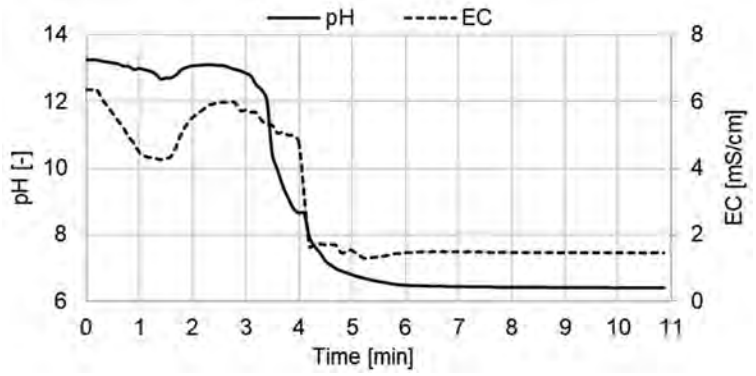

Figure 5.1: The development of pH and EC during the precipitation of PCC in the absence of fiber. The initial $Ca(OH)_2$ concentration was 1.9 g/l, corresponding to 5 g $CaCO_3$ in the batch. The CO_2 feed (0.5 L/min) was started at t=0 min and stopped at t=5.5 min. The data were acquired using the Reactor II and the time interval between recorded values was 6 seconds.

When PCC was precipitated at 35 °C with $Ca(OH)_2$ at a concentration of 0.4 g/l (dosing corresponding to EC=2 mS/cm at room temperature), the precipitate morphology was cubical (Figure 5.2A), but with a $Ca(OH)_2$ concentration of 2.5 g/l (dosing corresponding to EC=7 mS/cm at room temperature), the precipitate consisted of cigar-shaped or

"spiky" particles and aggregates of these, resulting in the formation of rosette-like PCC (Figure 5.2B).

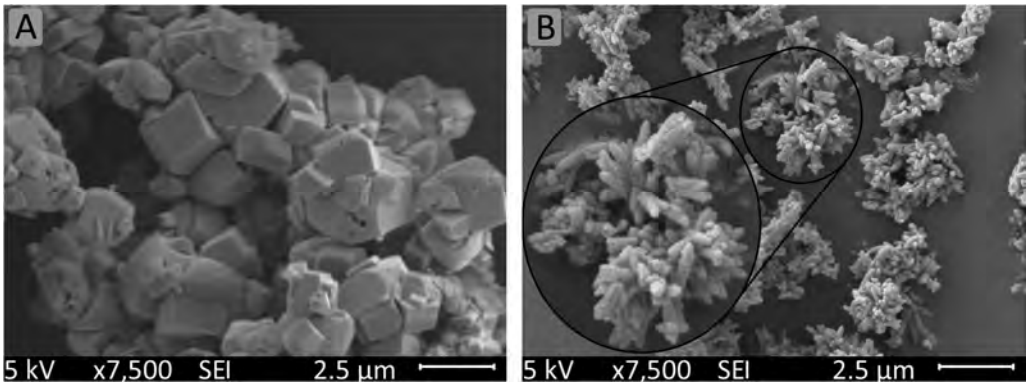

Figure 5.2: SEM micrographs showing PCC made without fiber at a temperature of 35 °C and a $Ca(OH)_2$ concentration of (A) 0.4 g/l and (B) 2.5 g/l. The experiments were carried out using Reactor II and the CO_2 feed was 0.5 L/min. The samples were oven-dried and sputter-coated (Au/Pd target) before SEM imaging.

When the two experiments were repeated in the presence of 1 wt-% BBK, the precipitate morphology was again affected by the $Ca(OH)_2$ concentration, but the PCC morphology with fiber differed from that of the precipitate made without fiber. The cubical crystals were more round and the rosette-like particles were replaced with nano-sized particles, as shown in Figure 5.3.

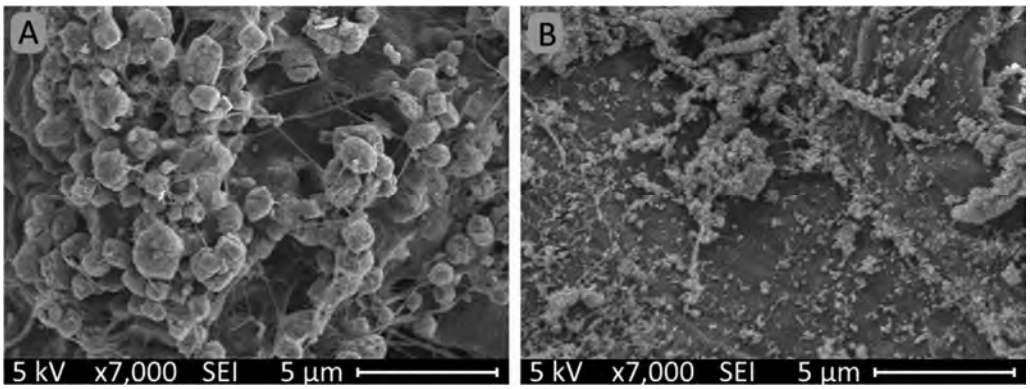

Figure 5.3: SEM micrographs showing PCC precipitated onto BBK fiber at a temperature of 35 °C and at a $Ca(OH)_2$ concentration resulting in (A) 5% targeted PCC content (0.4 g/l) and (B) 25% targeted PCC content (2.5 g/l). The experiments were carried out using Reactor II. The samples were freeze-dried and sputter-coated (Au target) before SEM imaging.

Since the $Ca(OH)_2$ concentration differed between the two experiments in Figure 5.3 while the fiber consistency remained constant, the PCC contents of the PCC-fiber composites differed. $Ca(OH)_2$ concentrations of 0.4 g/l and 2.5 g/l corresponded to calculated PCC contents of 5 and 25%, respectively. Figure 5.4A shows the EC (before starting the CO_2 feed) versus the targeted PCC content in the PCC-fiber composites, when the PCC content is calculated based on $Ca(OH)_2$ concentration in the batch, and Figure 5.4B shows the relationship between the targeted PCC content and the $Ca(OH)_2$ concentration at different fiber consistencies.

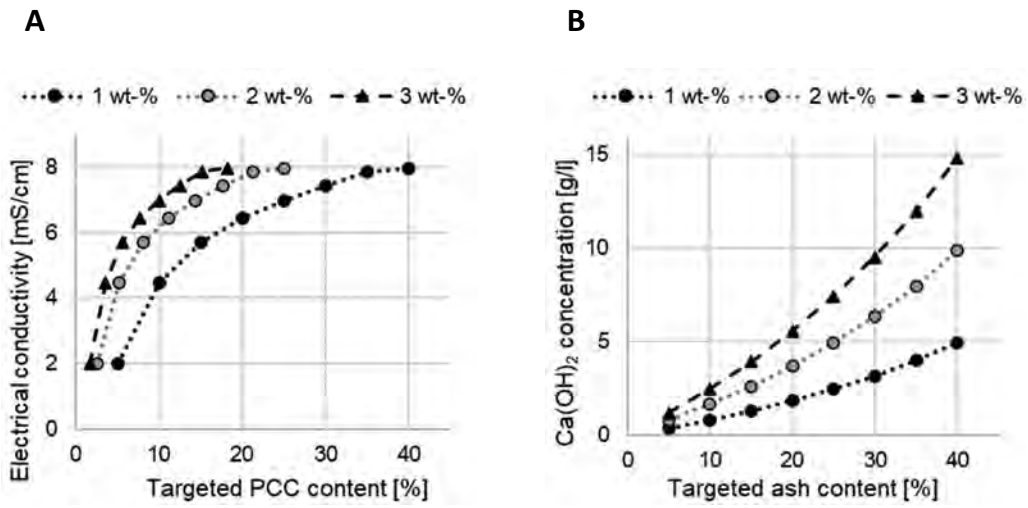

Figure 5.4: (A) Electrical conductivity (at the beginning of precipitation, originating mainly from $Ca(OH)_2$) versus targeted PCC content of the PCC-fiber composite, with fiber concentrations of 1, 2 and 3 wt-%. (B) The $Ca(OH)_2$ concentration required to reach a targeted PCC content when the fiber concentration used was 1, 2 or 3 wt-%. The electrical conductivity was measured at room temperature, without fiber at present and after ca. 15 minutes of stirring.

The differences in morphology show that the system was sensitive to the $Ca(OH)_2$ concentration whether or not fiber was present. Without fiber, the morphology corresponded well with that reported by García-Carmona et al. (2003) and by Ukrainczyk et al. (2007). When fiber was present, the PCC on fiber shifted slightly from cubical to a more round morphology. It was suspected that this was due to dissolved material entering into the process with the pulp, but this was not confirmed.

In the case of the samples with a high initial EC, the loss of rosette shape when fiber was introduced into the process could be due to dissolved substances or an enhanced heterogeneous nucleation. The enhanced heterogeneous nucleation perhaps consumed the calcium cation (Ca^{2+}) and carbonate anion (CO_3^{2-}) available for PCC crystal growth, resulting in reduced particle growth and aggregation, or to a change in the self-aggregation of an amorphous intermediate phase. A similar result regarding the disruption of crystal growth of scalenohedral calcite in the presence of cellulosic fiber has been reported by Subramanian (2008).

Figure 5.4 reveals that there is an important link between fiber concentration and PCC content and their effect on precipitate morphology, showing that the ability to control the precipitate morphology using EC originating from $Ca(OH)_2$ is limited because the amount of added $Ca(OH)_2$ is dictated by the PCC content and fiber concentration in the batch. A semicontinuous process with controlled $Ca(OH)_2$ addition could however be used,

especially if a low EC, high fiber concentration, high PCC content or a combination of these are targeted.

5.1.2 Material transfer: the effect of carbon dioxide feed from the gas phase (unpublished results)

The temperature of the reaction mixture increased during the precipitation process due to the exothermic reaction. The rate of temperature change in the batch was therefore used as a rough indication of the reaction rate. The temperature increase was found to be 0.14±0.01 °C for each gram of $Ca(OH)_2$ in the batch when the precipitation was carried out in Reactor I. Examples of the temperature change versus time are given in Figure 5.5.

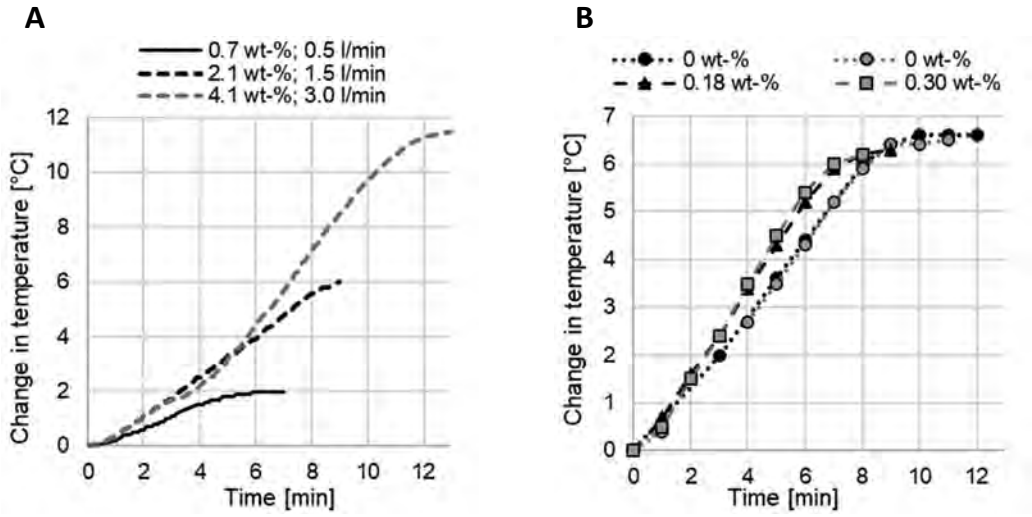

Figure 5.5: (A) Temperature change in batches free from Na-PAA. The legend indicates the initial $Ca(OH)_2$ concentration in the batch and the CO_2 feed. The fiber concentrations (up to down) were 1, 3, and 6 wt-%. (B) Temperature change in batches containing Na-PAA. The legend indicates concentration of Na-PAA in the batch (before precipitation), when the fiber concentration was 3 wt-%, the $Ca(OH)_2$ concentration 2.1 wt-% (before precipitation) and the CO_2 feed 1.5 L/min. The reactions were carried out in Reactor I.

At the lower CO_2 feeds, increasing the CO_2 feed increased the reaction rate, but when the CO_2 was further increased, the reaction rate did not increase correspondingly. Bubbling of the batch was visible when the high CO_2 feed (3 L/min and above) was used in both Reactor I and II. The addition of Na-PAA increased the rate of increase of the batch temperature, indicating an increase in reaction rate.

The effect of bubble size on the precipitate morphology on fiber was further studied using gas spargers with different pore sizes with the high CO_2 feed in Reactor II. A change in morphology from cubical to cigar-shaped (Figure 5.6) was detected under otherwise

identical conditions when a sparger with a larger pore size was used. The time to complete the reaction was also shorter when a sparger with smaller pore size was used.

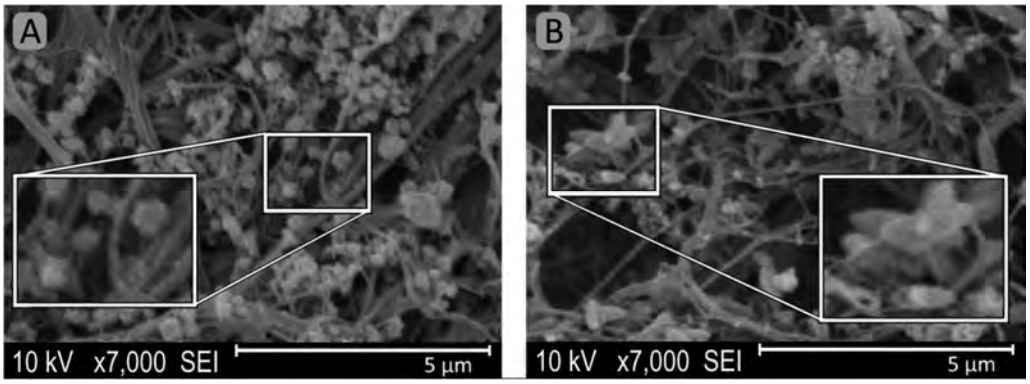

Figure 5.6: SEM micrographs showing the change in morphology of the PCC-MFC precipitate, caused by altering the bubble size with a sparger (sintered filter) with pore size of (A) 15 µm and (B) 60 µm, other parameters being held constant: MFC concentration 1 wt-%, CO_2 feed 3 L/min and temperature before precipitation 20.0±0.5 °C, after precipitation 21.0±0.5 °C. The targeted PCC content was 48.2% and the batch temperature increase was the same (1.6 °C) in both cases. Precipitation in Reactor II. The samples were freeze-dried and sputter-coated (Au target) before SEM imaging.

The increase in temperature development and in reaction rate were primarily associated with material transfer from the gaseous to the liquid phase. In the system used, increasing the CO_2 feed above 3 L/min was found to have only a minor beneficial effect on the reaction due to loss of CO_2 gas into the atmosphere. Material transfer can however be expected to change with, for example, a different reactor type or geometry or if more efficient mixing is applied.

The temperature development suggests that the $[Ca^{2+}]/[CO_3^{2-}]$ ratio could be expected to decrease with increasing CO_2 feed due to an increase of CO_3^{2-}, with the other parameters remaining unchanged. The $[Ca^{2+}]/[CO_3^{2-}]$ ratio is probably not linear however with respect to the gas feed and due to the rate of dissolution of $Ca(OH)_2$, although the $Ca(OH)_2$ concentration and thus the total surface area of the particles can also be expected to have increased in many experiments, including those shown in Figure 5.5.

The change in morphology resulting from the change in the CO_2 bubble size was also associated with a change in the $[Ca^{2+}]/[CO_3^{2-}]$ ratio, which decreased due to more rapid material transport from the smaller bubbles to the reaction mixture. This conclusion is supported by the shorter time to complete the reaction and the faster temperature increase.

The cubical shapes of PCC on fiber (Figure 5.6A) were in agreement with the literature stating that a low $[Ca^{2+}]/[CO_3^{2-}]$ ratio tends to produce rhombohedral calcite (García-Carmona et al. 2003; Ukrainczyk et al. 2007). The higher $[Ca^{2+}]/[CO_3^{2-}]$ ratio at 20 °C has however been reported to produce nano-sized spheroidal particles rather than scalenohedral particles (García-Carmona et al. 2003; Ukrainczyk et al. 2007). The cigar-shaped PCC similar to that in Figure 5.6B has however been reported only at slightly elevated temperatures (25 °C) when the conductivity due to the presence of Ca^{2+} has only slightly increased (Ukrainczyk et al. 2007).

5.1.3 Preparation of PCC-fiber composite with surface covered with nano-PCC (Paper I, unpublished results)

To prepare nano-PCC on MC in order to achieve a high fiber coverage by the nanoparticles, different PCC-MC composites were prepared to a targeted PCC content of 48.2% by altering the CO_2 feed and fiber consistency. The $Ca(OH)_2$ concentration therefore depended linearly on the fiber consistency.

The most typical morphology was nano-sized particles, either as aggregates (Figure 5.7A) or distributed more evenly over the surface of the fiber (Figure 5.7B). Stacked cubical PCC was also seen at low fiber and $Ca(OH)_2$ concentrations. At higher fiber consistencies, the PCC formed aggregates of nanoparticles. A lower CO_2 feed resulted in more aggregation of nano-PCC than a higher CO_2 feed, although at the highest CO_2 feeds, aggregation again increased. The effect of fiber consistency (and thus $Ca(OH)_2$ concentration) and CO_2 feed on the morphology of the PCC-fiber composite is summarized in Figure 5.8 (see page 60-61).

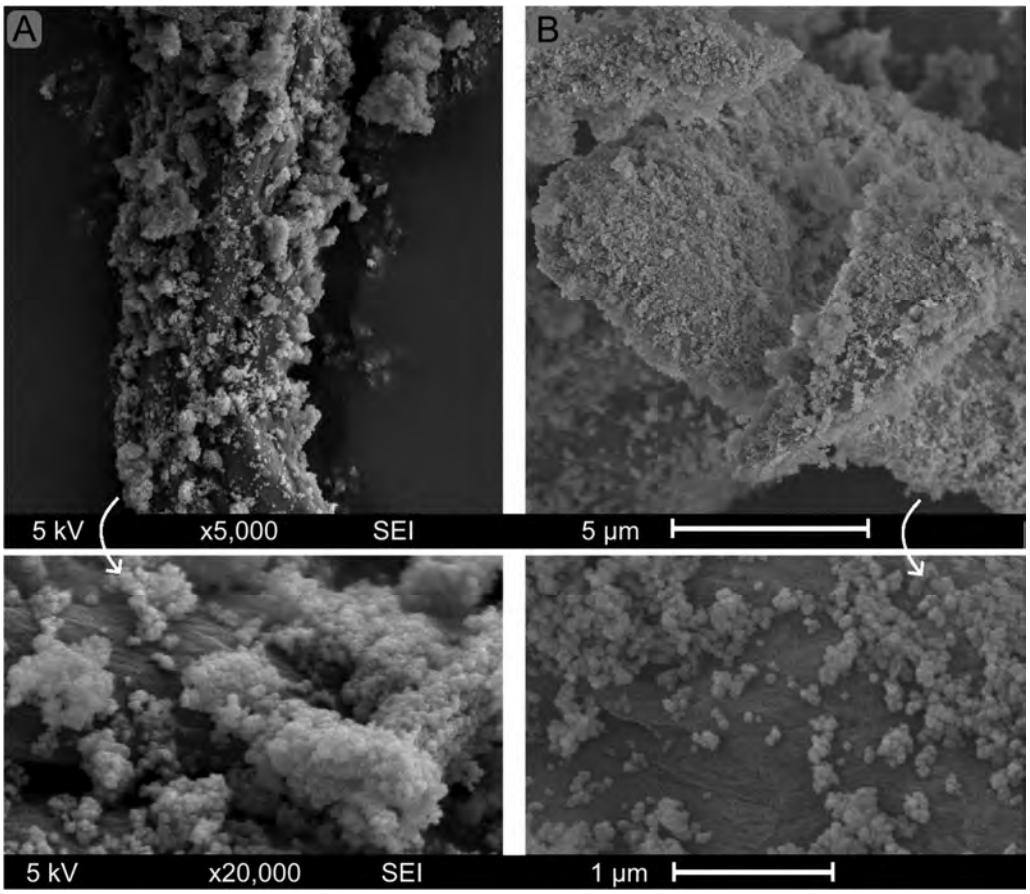

Figure 5.7: FE-SEM micrographs showing (A) aggregation and (B) a more uniform distribution of nano-PCC on an MC surface. Image (A) was taken on a sample precipitated using 1 wt-% MC consistency and a CO_2 feed of 0.5 L/min, and image (B) on a sample precipitated using 3 wt-% MC consistency and a CO_2 feed of 1.5 L/min. The targeted PCC content was 48.2% for both samples. Precipitation was carried out in Reactor I

Intentionally blank page

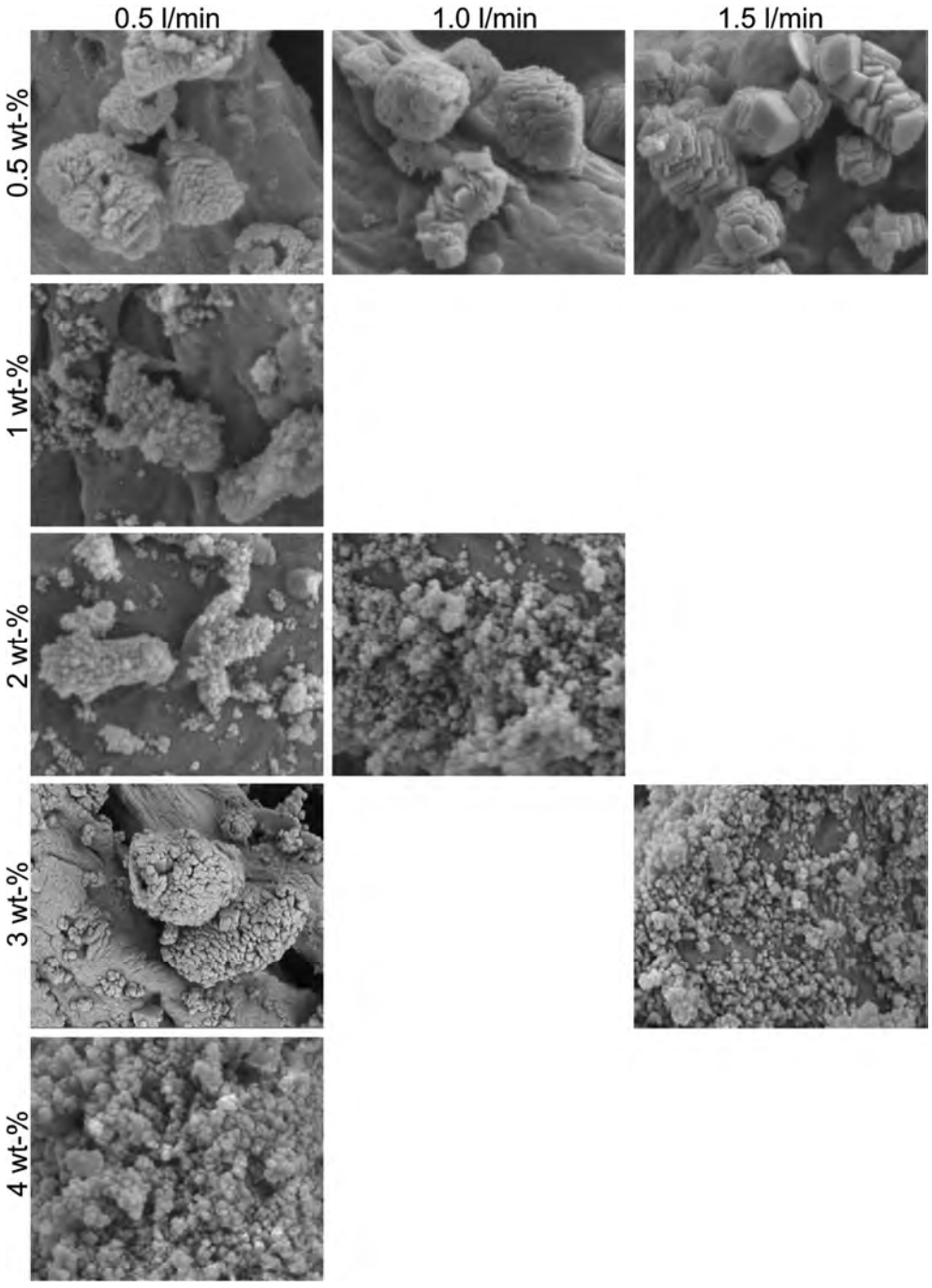

Figure 5.8: SEM micrographs showing PCC morphology on MC when the MC concentration out in Reactor I. Imaged in SEI mode, sputter coated (Au or Au/Pd target) before imaging.

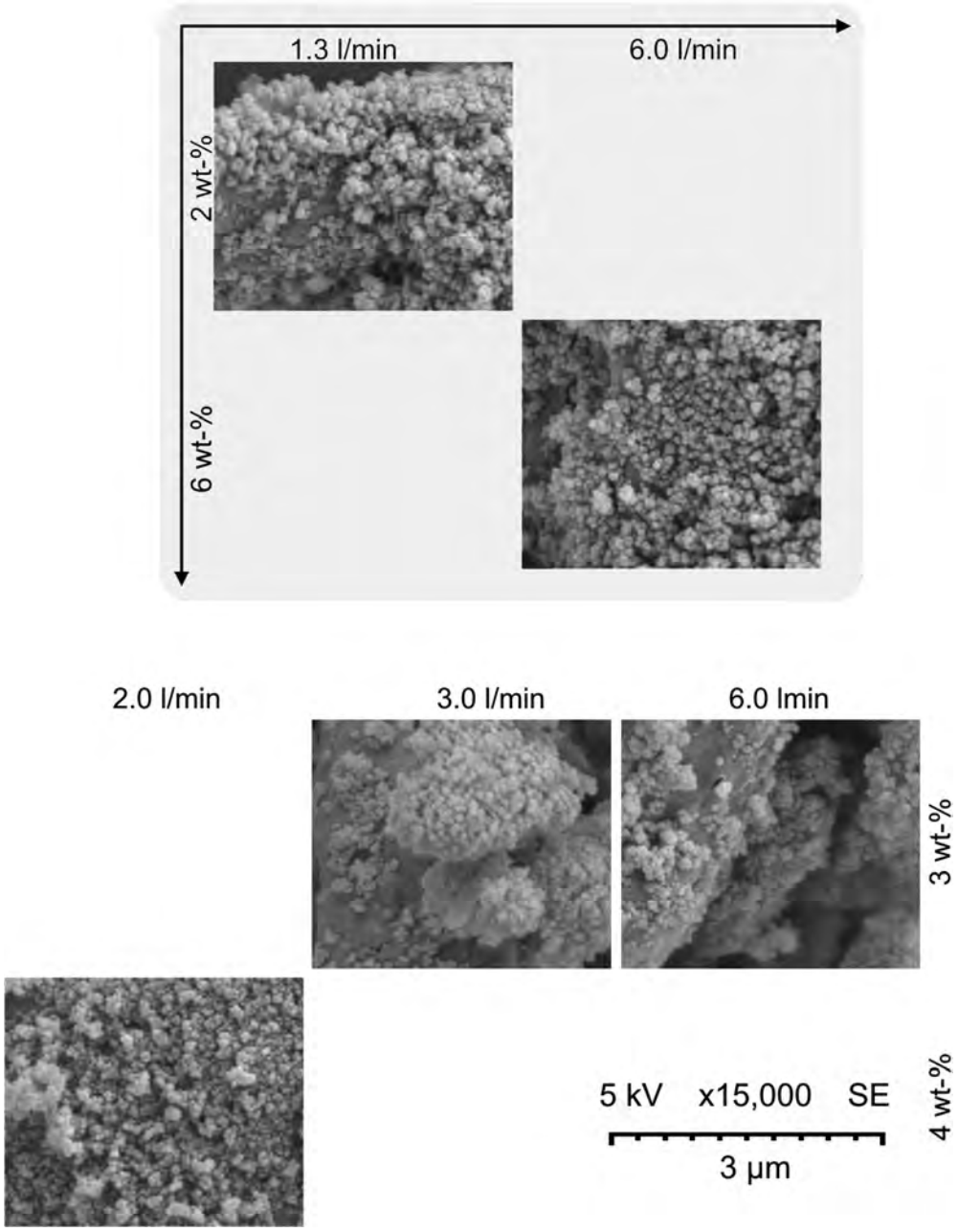

and CO_2 feed were varied. The targeted PCC content was 48.2%. The experiments were carried

The formation of nanosized particles in carbonization process has previously been described in the literature both without fiber (Carmona et al. 2004; García-Carmona et al. 2003; Ukrainczyk et al. 2007) and with fiber (Subramanian 2008). Subramanian (2008) presented results with nano-PCC aggregated in an ellipsoidal form on cellulose microfibrils, but a uniform distribution of the nano-PCC onto the fiber was achieved in the present work, where the formation of nanoparticles was probably explained by high $[Ca^{2+}]/[CO_3^{2-}]$ ratio and the low precipitation temperature (ca. 20 °C at the beginning of the precipitation), while the stacked cubical morphology was probably due to the lower $[Ca^{2+}]/[CO_3^{2-}]$ ratio.

The initial EC value of 7 mS/cm previously found to result in a non-cubical morphology and nanoparticles did not always do so in this case, probably because of the different reactor and a difference in the material transfer from CO_2 gas to the reaction mixture (more effective due to the use of sparger) resulting in a too low $[Ca^{2+}]/[CO_3^{2-}]$ ratio for nanoparticle formation. The use of MC instead of the BBK used in the EC tests may also have affected the material transfer efficiency from the gaseous phase by altering the rheological properties of the reaction mixture.

An increase in fiber concentration resulted in the use of a higher $Ca(OH)_2$ concentration that probably gave a sufficiently high Ca^{2+} concentration for the creation of nanoparticles even at the higher CO_2 feeds. When the nanoparticles were formed, their tendency to adhere to the fiber surface rather than to aggregate explained why the PCC particle size decreased with decreasing fiber-to-CO_2 ratio and increasing fiber concentration so that a uniform covering of the MC fiber with nano-PCC was obtained. The $[Ca^{2+}]/[CO_3^{2-}]$ ratio did not however solely explain the degree of aggregation of nano-PCC, as a high level of aggregation was seen at both extremes of the CO_2 feed range used.

The fiber concentration at which the aggregation decreased and the precipitate became more evenly distributed on the fiber also depended on the fiber type, suggesting that the aggregation of the nano-PCC was perhaps partially determined by, for example, flow or crowding conditions in the batch, or the surfaces properties of the fiber. The fiber type probably also affects the gas bubbles and may therefore alter the material transfer from the gas to the reaction mixture.

5.1.4 pH development during CO_2 feed and effect of time of dosing of the morphology-controlling chemical (Paper I, unpublished results)

The pH was recorded as a function of time during the precipitation process in experiments conducted with and without the use of PCC-morphology-altering chemical aids dosed either before the CO_2 feed was started with fiber present (Na-PAA) or during the CO_2 feed without fiber present (L-lys). The experiments with L-lys were done in order to further investigate how an intermediate drop in pH affected the PCC morphology. These experiments were carried out at room temperature.

When no morphology-controlling chemicals were used and fiber consistency was less than 6 wt-%, while targeting a PCC-fiber composite with an ash content of 48.2%, the pH dropped rapidly at the beginning of the experiment and then recovered until another sudden decrease occurred at the end of the experiment. An example of the pH behavior for samples with and without the Na-PAA is shown in Figure 5.9, accompanied by micrographs of precipitates when the batch was sampled during precipitation. The samples were quickly dried using pre-heated (220 °C) crucibles and small sample volumes, which resulted in a rapid temperature increase in the samples.

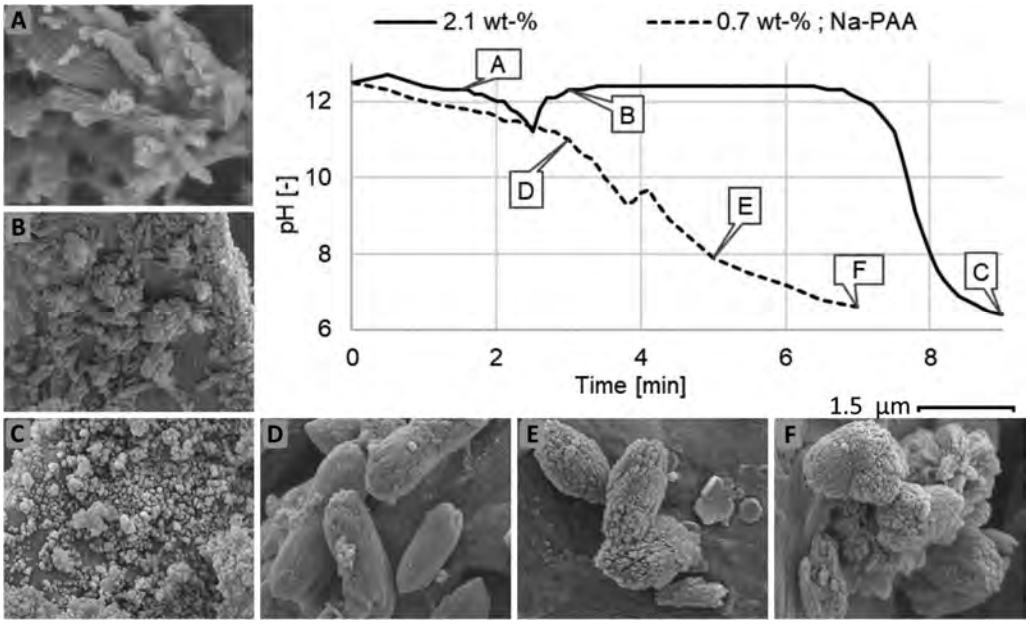

Figure 5.9: pH and morphology development during precipitation with MC, and SEM micrographs showing the morphology of quickly dried samples. The legend indicates $Ca(OH)_2$ concentration and the presence of Na-PAA, and the scale bar applies to all the SEM micrographs. The 2.1 wt-% $Ca(OH)_2$ batches contained 3 wt-% fiber and the CO_2 feed was 1.5 L/min (images A to C). The 0.7 wt-% $Ca(OH)_2$ batch contained 1 wt-% fiber and the CO_2 feed was 0.5 L/min (images D to F). The Na-PAA concentration was 3 wt-% of the $Ca(OH)_2$ before precipitation, and the contact time between Na-PAA, the $Ca(OH)_2$ and the fiber was 20 h before the precipitation. The data were obtained using Reactor I. SEM micrographs made using SEI, acceleration voltage 5 kV and sputter-coating (Au/Pd target).

The local minimum pH and its location in time depended on the $Ca(OH)_2$ concentration, on the CO_2 feed and on the use of Na-PAA. When Na-PAA was used, the local minimum pH was reached later than when the batch was free from Na-PAA, and the minimum value was typically lower.

Although the morphology of the dried intermediate samples likely did not fully agree with the morphology in the reactor, the mineral phase morphologies of the mid-precipitation samples showed that the final morphology did not develop immediately. Essentially no morphology matching the final morphology of the precipitate was observed when a sample was taken before the local pH minimum.

When morphology-altering chemical L-lys was added at 4.5 min, i.e. after the observed local pH minimum the precipitate morphology was only slightly affected, but when L-lys was added after 2 min, i.e. before the local pH minimum, the particle morphology was greatly affected and the local pH minimum disappeared and the pH continued to decrease. The morphologies and pH development are shown in Figure 5.10.

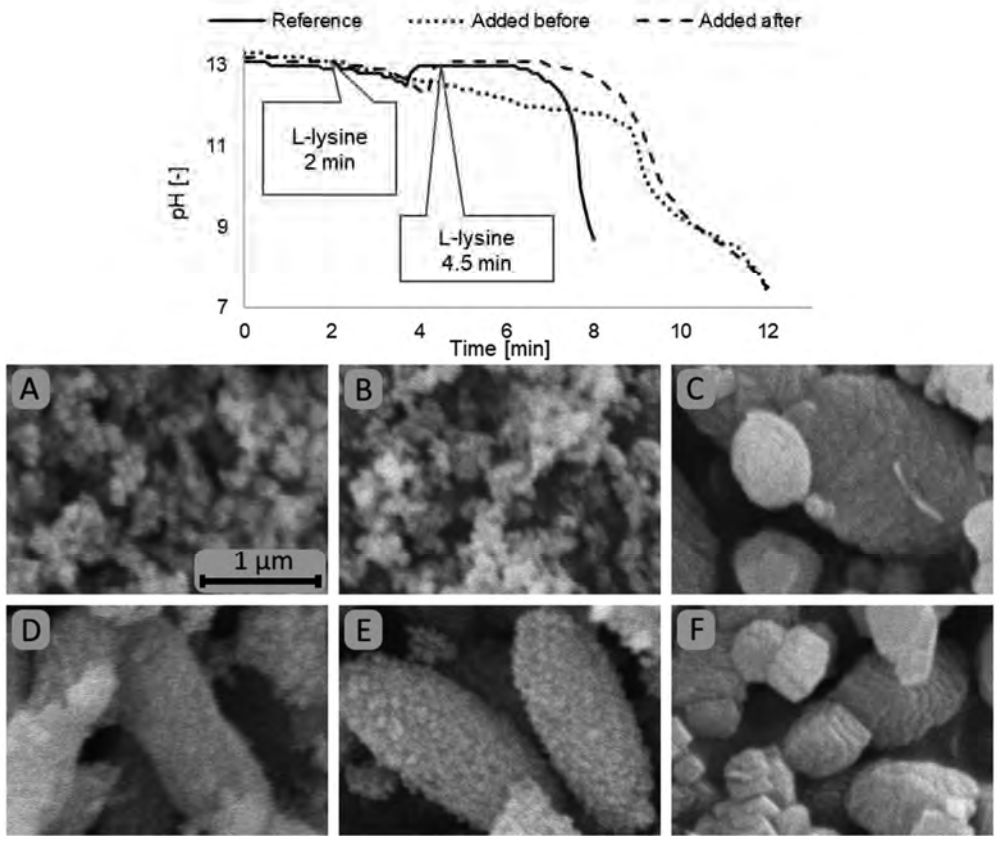

Figure 5.10: pH development and SEM micrographs showing the precipitate morphology when L-lys (0.4 wt-% of initial batch) was added during precipitation. A: Reference (0.5 L/min), B: L-lys added after, and C: before the local pH minimum with 0.5 L/min CO_2 feed. D: Reference (3 L/min), E: L-lys added after, and F: before the local pH minimum with 0.5 L/min CO_2 feed. The data were obtained using Reactor I. Imaged using SEI mode, sputter coated (Au target) before imaging.

The decrease in pH at the end of the process was caused by depletion of $Ca(OH)_2$, but the reason for the intermediate pH drop was less obvious. In most experiments, a large amount of solid $Ca(OH)_2$ should have been present at this stage of the process, as indicated by the $Ca(OH)_2$ solubility, batch temperature and remaining reaction time. The pH development was associated with the reaction involving ACC on $Ca(OH)_2$ particles, as described in 3.2 Precipitation of PCC.

Further information about the precipitation mechanism was gained by sampling the materials before and after the pH drop, and adding a morphology-altering additive to the mixture. Lack of the final morphology in the samples taken during the process shows that the final morphology probably formed via an intermediate phase, and intermediate morphologies similar to those described by Carmona et al. (2004) were imaged on the fiber (Figure 5.9A and B), but with a larger particle size.

Whether the intermediate phase was amorphous or for example vaterite, or whether both amorphous and crystalline intermediate phases were at present is not however clear. From this point of view, the pH development of the Na-PAA-containing samples was of interest because the local pH minimum occurred at a later point in time, even though the Na-PAA increased the reaction rate, as indicated in Figure 5.5B.

Na-PAA is known to stabilize ACC and to induce the formation of polymer induced liquid precursors (PILPs) (Kim et al. 2007), hypothesized to form when the polymer sequesters and concentrates the ions while delaying nucleation (Gower and Odom 2000). The pH development in presence of Na-PAA therefore probably supports the hypothesis that a non-crystalline precursor is present and that the intermediate pH drop is related to its dissolution.

The same or a similar mechanism involving an intermediate, probably amorphous phase breaking at the pH minimum can also explain the development of the morphology when L-lysine was added during the precipitation. The drastic alteration in the PCC morphology when the L-lysine was added before the immediate pH drop, and the lack of any such change when the L-lysine was added after the pH drop, further supports the hypothesis that the pH drop marks a stage in process where the precipitation of PCC allows a morphology-controlling additive to affect the resultant morphology.

5.2 The effect of fiber in the precipitation of PCC-fiber composite

Four different fiber types were used in the precipitation experiments, viz: MC, MFC, BBK, and CTMP (refined and unrefined). After the route to control the morphology of the precipitate in the PCC-MC composite had been developed, the method and conditions were tested with MFC and CTMP.

5.2.1 Effect of fiber type on precipitate morphology (Paper II, Paper III, unpublished results)

The fiber consistency and the $Ca(OH)_2$ concentration in the precipitation experiments were varied in order to confirm that the morphology of the PCC in PCC-CTMP and PCC-MFC composites could be affected, and that a nano-PCC-fiber composite with a high level of fiber coverage by PCC could be produced using precipitation conditions similar to those used with MC.

For the MFC, 1 wt-% consistency was found to be sufficiently high to give a good PCC distribution on the fibrils. A higher consistency could not be used due to the limited mixing capability of the Reactor II and the high viscosity of the MFC. The precipitate morphology of the PCC-MFC composite was therefore primarily investigated by altering the ash content.

The effect of increasing the ash content of the PCC-MFC composite prepared using 1 wt-% fiber concentration is shown in Figure 5.11. At low ash contents, the PCC morphology was cubical but with increasing ash content it developed through a mixture of cubical stacked particles and aggregated nano-PCC to a uniformly distributed nano-PCC. Above an ash content of ca. 60% the degree of aggregation of the PCC again increased.

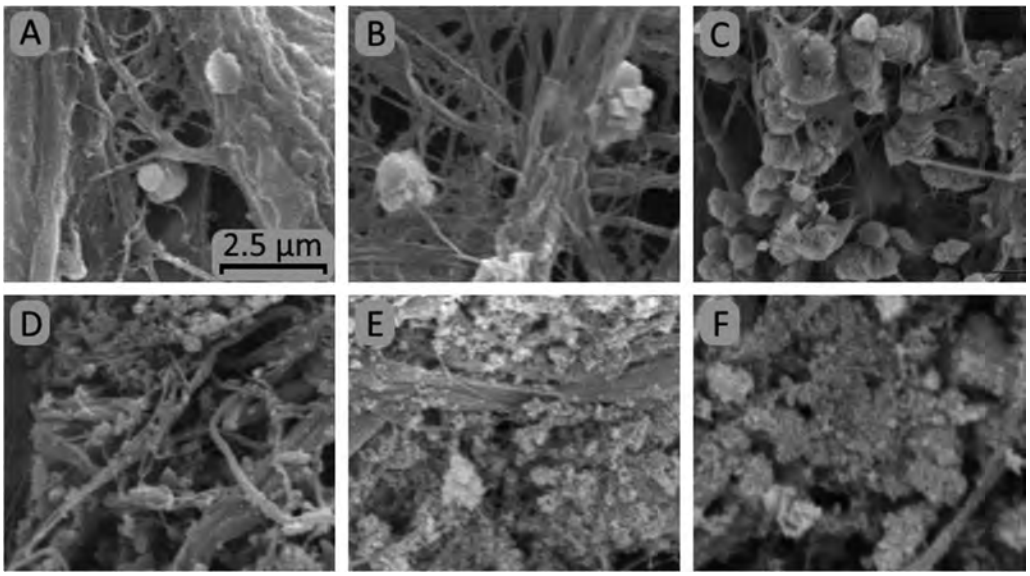

Figure 5.11: SEM micrographs showing PCC morphology development on MFC with increasing ash content from (A) to (F). The fiber consistency was 1 wt-% from (A) to (D) and 0.7 wt-% from (E) to (F). The CO_2 feed was 1.5 L/min, except for (D) 1 L/min. The ash contents from (A) to (F) were 4.8; 11.0; ca. 30; 44.2; 60.4 and 79.4%. The experiments were carried out in Reactor II. Freeze-dried samples, SEM micrographs made using SEI, 10 kV acceleration voltage and sputter coating (Au target)

In the case of the CTMP and Reactor III, a larger range of fiber consistencies could be used, so the experiments were carried out altering the fiber consistency and CO_2 feed. At a fiber consistency of 0.1 wt-% and low CO_2 feed (0.5 L/min), only a few nanosized particles were observed. The precipitate morphology was mainly cubical, as shown in Figure 5.12A and B, but with a higher fiber consistency and CO_2 feed (5 L/min) a fairly uniform distribution of nano-PCC was obtained on the CTMP surface (Figure 5.12C and D).

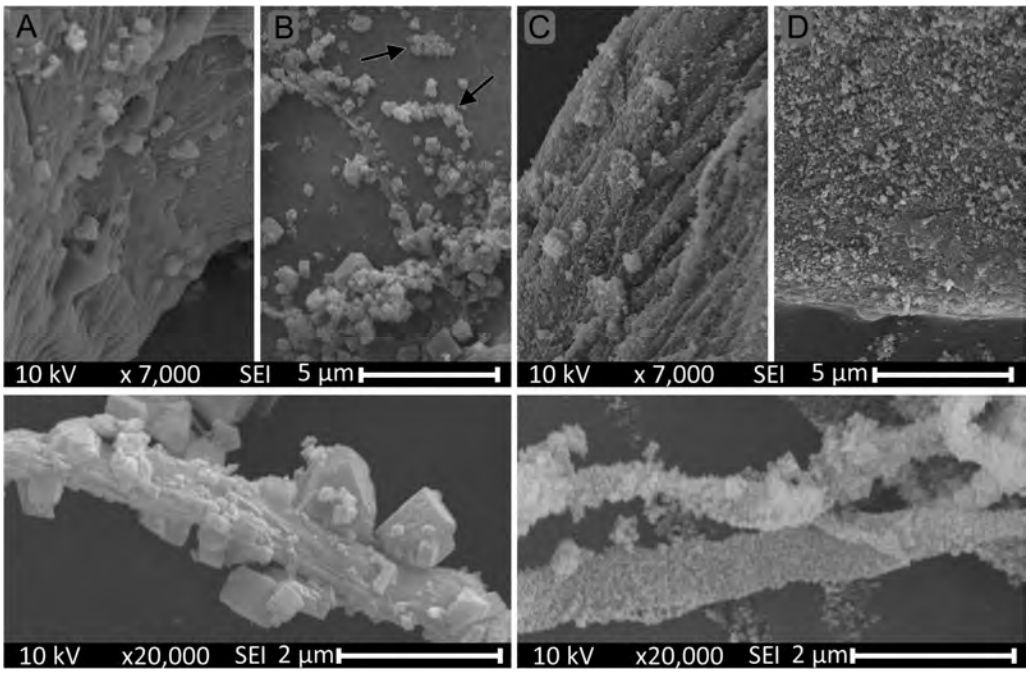

Figure 5.12: SEM micrographs showing PCC morphology on CTMP fiber (upper row) and fines (lower row). The targeted PCC content was 45%. In (A) and (B) both, the fiber consistency was 0.1 wt-%. The CO_2 feed was 0.5 L/min in (A) and 5 L/min in (B). The arrows in (B) indicate aggregates of nano-sized particles. In (C) and (D) both, the fiber consistency was 3 wt-% and the CO_2 feed was 0.5 L/min in (C) and 5 L/min in (D). The precipitation was carried out in Reactor III. The samples were vacuum-dried and imaged using SEI, 10 kV acceleration voltage and sputter coating (Au/Pd target)

The method for controlling the PCC morphology and the level of nanoparticle aggregation on the fiber gave qualitatively the same results as with MC, although the conditions (fiber concentration, CO_2 feed and $Ca(OH)_2$ concentration) under which the nano-PCC was distributed evenly on the fiber differed slightly. This was ascribed to the reactor geometry and the properties of the reaction slurry, both of which may alter the CO_2 transfer from the gaseous phase to the reaction slurry, and perhaps to a difference in the affinity of precursor state of PCC for the different fibers.

5.2.2 Enrichment of PCC onto smaller fiber fractions (Paper II)

The distribution of PCC in PCC-CTMP composite size fractions and the attachment of PCC on different areas of fibers was investigated by the precipitation of $CaCO_3$ onto CTMP at three different freeness levels, the precipitation conditions being chosen to promote a PCC-CTMP composite with high fiber coverage by nano-PCC. The PCC-

CTMP composite and the CTMP pulps were then fractionated using a Bauer-McNett classifier.

The ash content in the PCC-CTMP composite fractions increased in the order: R30 < R100 < R200 < R400 < 'pass'. The results are shown in Figure 5.13 and the values are tabulated in Paper II. The ash contents of all the CTMP fractions were between 0.8 and 1.6%, and the PCC-CTMP composite ash content was therefore not equal to but fairly close to the PCC content.

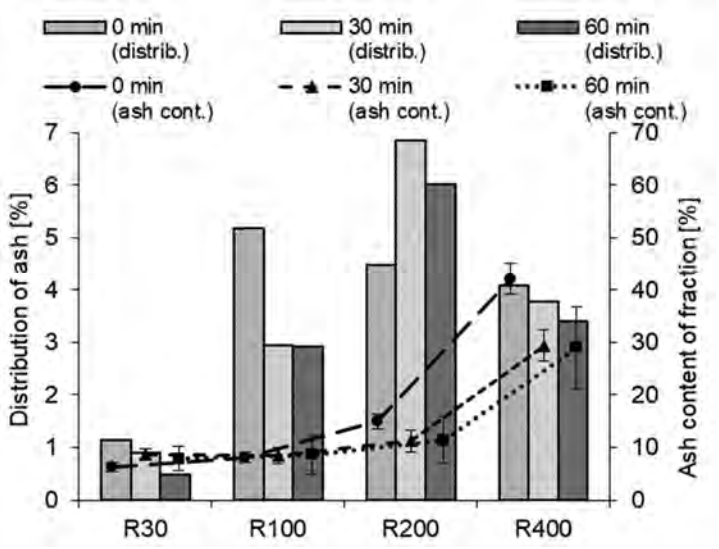

Figure 5.13: Ash (525±25 °C) distribution in the fiber fractions. The bars (indicated on the left-hand ordinate, 'Distribution of ash') show the distribution of the total ash between the fractions. The lines (indicated on the right-hand ordinate, 'ash content of fraction') show the ash content in each fraction.

The ash content of the PCC-CTMP fractions was found to correlate positively with the measured anionic surface charge of the corresponding CTMP fraction. The R^2 of liner fit of ash content versus CTMP surface charge was 0.85, although the significance of the value is diminished by a gap in the data, see the fit in Paper II.

SEM micrographs showed that PCC was located on the fiber regimes where the outer layer of fibers was removed (Figure 5.14A) or where the fiber was damaged or fibrillated (Figure 5.14B). Such material was present especially in the fines, which were also especially rich in PCC (Figure 5.14C). Split fibers instead had PCC deposits in the lumen, where the PCC was attached to the lumen wall, while the outer surface appeared to be essentially free from PCC (Figure 5.14D).

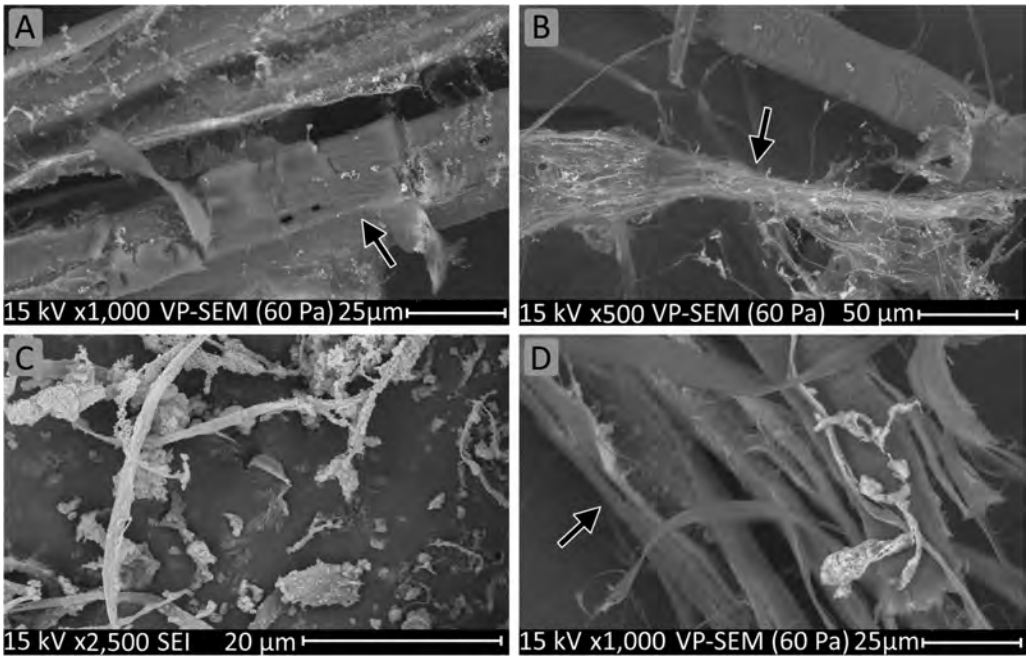

Figure 5.14: SEM micrographs showing the fractionated PCC-CTMP samples and the location of PCC on the fibers. (A) R200, 30 min refined CTMP: a band of outer fiber layers essentially free from PCC (indicated by the arrow), surrounded by more PCC rich areas. (B) R200, unrefined CTMP: heavily fibrillated fiber with high content of PCC, indicated by the arrow, and more intact fiber with substantially no PCC. (C) 'pass' fraction, unfractionated CTMP: fibrillar and other fines extremely rich in PCC. (D) R200, 60 min refined CTMP: split or cleaved fiber with PCC deposited in the lumen and with the outer layer essentially free from PCC, indicated by the arrow. Note the different magnifications of the micrographs. The precipitation was carried out in Reactor III. Vacuum-dried, uncoated sample for VP-SEM and sputter-coated for SEI (Au/Pd target)

The enrichment of PCC on the fines is in good agreement with results previously reported by Silenius (2002) and by Fuchise-Fukuoka et al. (2020a). In the past, this enrichment has been associated with the greater specific surface area (in m^2/g) of the fine material (Silenius 2002).

The literature describing the precipitation on fiber suggests however that PCC nucleation on the substrate is affected by the charged sites on the substrate surface, and an increased precipitation onto the surfaces has also been associated with an increase in hydrophobicity. The correlation between the ash content and the surface charge was in good agreement with the fact that PCC shows a high affinity to substrates with a high anionic surface charge, although the surface charge (in µekv/g) of the CTMP fraction was

probably dominated by the surface area accessible to the polyelectrolyte. The correlation may therefore support the importance of the fiber surface area of the sample as well as the direct effect of charge.

The SEM micrographs, in contrast, revealed that the PCC was prone to precipitate on the cellulosic fibrils and lumen wall, i.e. areas typically associated with a lower charge and higher hydrophilicity than the primary wall, which is known to be richer in charged species (such as lignin) than the inner layers of the fibers, in turn richer in less charged cellulose (Hubbe 2006).

The previous appears to be in conflict with the possible role of the substrate surface charge, but it may be explained, for example, by hydroxyl groups of the cellulose undergoing metal-ion-facilitated deprotonation, which occurs especially at high pH (Al-Sogair et al. 2011). This could be expected to enhance the bonding between $CaCO_3$ and the substrate, and this would decrease the interfacial free energy between the substrate and PCC and make the surface more receptive to PCC precipitation, as explained by Chevalier (2014). The fiber regimes rich in PCC were, however, also those more protected from hydrodynamic forces that may wash particles from the fiber surfaces, i.e. lumens (Petlicki and van de Ven 1994) or reported to collect filler more readily than fiber surface under flow conditions (Haslam and Steele 1936).

Nevertheless, the enrichment of PCC onto the smaller fibers, and especially onto the fines fraction was confirmed for PCC-CTMP composite when the composite was prepared via carbonization precipitation. Due to the uneven precipitation of PCC onto the different fractions, the properties including the bonding ability of the different fiber fractions can be expected to change unevenly. This emphasizes the importance of controlling the PCC precipitation onto the desired fiber fractions in order to tailor the PCC-fiber composite properties e.g. to optimize the PCC-fiber for papermaking purposes.

5.2.3 Effect of the IS-precipitation on fiber morphology of PCC-CTMP (Paper II, Paper III)

The fiber morphology of 4 unfractionated CTMP and PCC-CTMP samples refined to different freeness levels, and of the Bauer-McNett fractions of the CTMP and PCC-CTMP was studied, the precipitation conditions for PCC-CTMP being chosen so that nano-PCC distributed fairly evenly on the surfaces of the fibers as shown in Figure 5.12C and D.

The fiber morphology of the unfractionated fibers (Table 5.1) showed only minor changes but the mean kink index was systematically lower in the PCC-CTMP than in the CTMP. A slight systematic increase in shape factor was also seen. The fiber width and fines content were slightly higher in the PCC-CTMP than in the corresponding CTMP.

Table 5.1: Mean fiber morphology values for CTMP and PCC-CTMP samples (unfractionated), weighted by fiber length. When available, the 95% confidence limit based on three measurements are indicated in the table.

Pre-treatment of fiber	Material	Length [mm]	Width [µm]	Shape factor [%]	Fines [%]	Mean kink index [-]
None	CTMP	1.49	39.3	90.8	10.9	0.46
	PCC-CTMP	1.50	40.4	91.1	13.7	0.38
	Change	0.01	1.10	0.30	2.80	-0.08
Refining, 30 min	CTMP	1.26	38.2	91.0	14.5	0.33
	PCC-CTMP	1.31±0.09	40.6±0.7	91.7±0.6	16.3±1.4	0.31±0.04
	Change	0.05	2.40	0.70	1.80	-0.02
Refining, 60 min	CTMP	1.15	38.2	91.1	15.3	0.30
	PCC-CTMP	1.12±0.05	40.3±0.4	92.1±0.4	17.2±0.8	0.24±0.06
	Change	-0.03	2.10	1.00	1.90	-0.06
Washing	CTMP	1.57	41.4	89.5	10.2	0.42
	PCC-CTMP	1.53	41.7	90.7	13.5	0.41
	Change	-0.04	0.30	1.20	3.30	-0.01

PCC-CTMP and CTMP fraction morphology results are shown in Figure 5.15 and the values are tabulated in Paper II. In comparison with CTMP, the CTMP-PCC R30 fraction consisted of slightly longer fibers, but the lengths of the other fractions were not affected in any great degree. Instead, the fiber width increased in all the fractions. The fines contents of the CTMP-PCC fractions were lower than or similar to those of the CTMP fractions, despite the fact that the unfractionated CTMP-PCC contained more fines than the unfractionated CTMP.

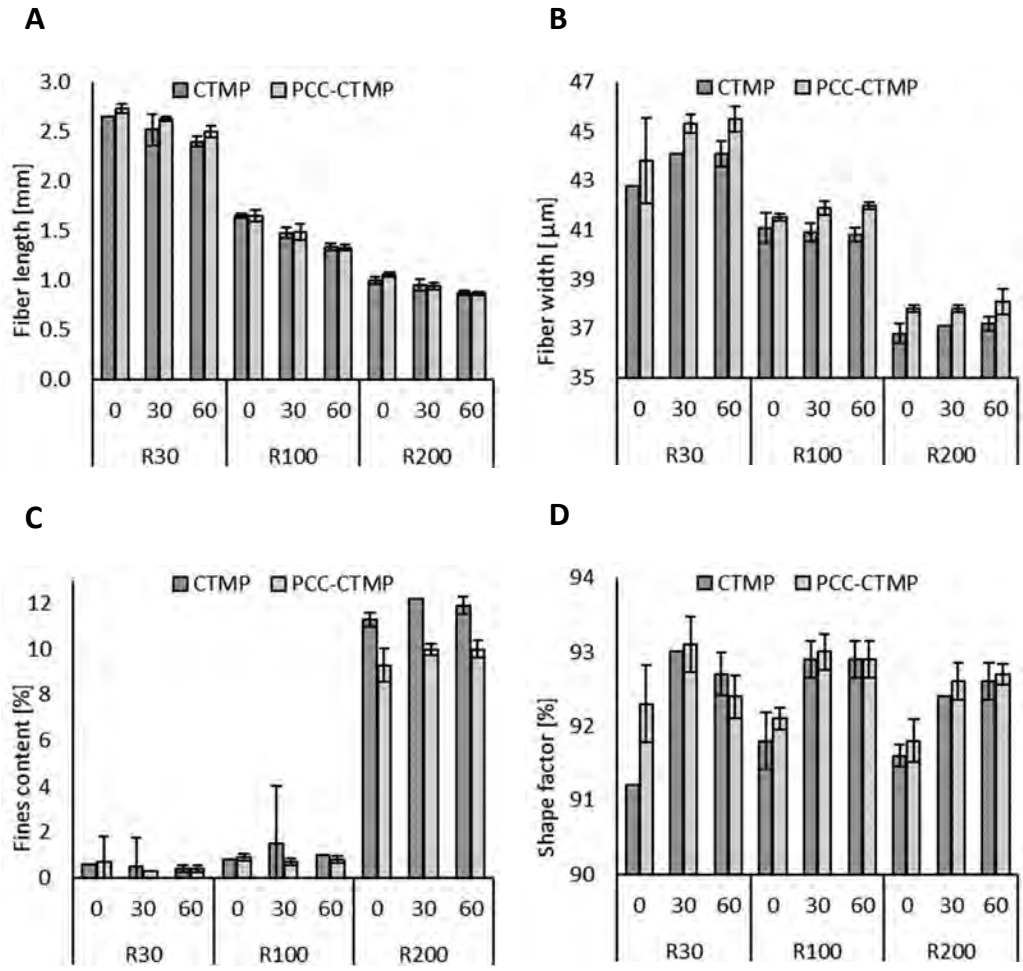

Figure 5.15: Data for PCC-CTMP fractions: (A) fiber length, (B) fiber width, (C) fines content and (D) shape factor of fibers. The bars are 95% confidence values based on three measurements. The upper x-axis refers to the refining time. Note that the y axes often do not start from zero. The precipitations were carried out in Reactor III.

Although some large PCC aggregates may have been registered as fines, the free particles of PCC were usually too small to be detected as fines in the fiber analyzer. An increase in fines content was associated with two factors: an increase in size of the fines where some of the smallest fines became visible for the analyzer, and a reduced tendency for the fines to attach onto other particles, so that they were detected and counted separately.

The increase in size of the fine was supported by SEM micrographs (e.g. Figure 5.14C), and the reduced tendency to aggregate was supported by the morphology data of the fiber fractions. The decrease in fines content suggests that a large amount of fines was lost

through the wires during the fractionation process. When the fractionation was being carried out, the refined CTMPs especially tended to clog the 400 mesh wire and form a slimy mat on it, but the clogging and sliminess was significantly less with the PCC-CTMP.

The PCC attached to the fines thus appeared to reduce interfiber interaction. Similar results were reported by Klungness et al. (1996) relating to first-pass retention. They reported that in-situ precipitation increased the filler retention on both a pilot and a laboratory scale, but the total first-pass retention was found to be lower with IS-precipitated material than with the traditionally filled material.

The increase in fiber width observed in the present work was primarily associated with PCC precipitation onto the external surfaces of fibers, but the SEM micrographs suggest that PCC was also precipitated inside the fibers, sometimes heavily (see Figure 5.17). The filler in fiber lumens has been associated with less fiber collapse (Kumar 2011), and this may have affected the mean width.

The images of the separate fiber fractions (Figure 5.15) suggest that the increase in width also took place in the coarsest R30 fiber fraction. According to the SEM micrographs (Figure 5.14 and those shown in Paper II), this fraction did not contain as much PCC on the outer surfaces of the fibers as the smaller fractions. This supports the hypothesis that there was less fiber collapse and that PCC was present inside the fiber, but behavior of the material during the fractionation with an apparently greater tendency to pass the wires may have affected the result. The gain in width was also small enough not to be obvious in the fiber width distributions. Examples of the width and length distributions are shown in Paper II.

The essentially unaffected fiber morphology suggests that the changes accompanying the use of PCC-CTMP as a filler were associated with the presence and distribution of the mineral phase on the fiber surface and within the sheets.

5.3 Handsheet results (Paper II, Paper III)

When the precipitation was done on CTMP, the PCC became enriched in the smaller fiber fractions. This meant that the fiber fractions were expected to behave differently after PCC precipitation, leading to differences in the physical, chemical and optical properties of the handsheets.

5.3.1 The effect of in-situ precipitation on sheet physical properties

Handsheets were prepared to clarify the effect of PCC-CTMP composite on sheet properties, either from fractions of PCC-CTMP and CTMP (the reference), or using PCC-CTMP as a filler in CTMP sheets together with either CS or MCF as a strengthening agent. PCC-filled CTMP sheets were used as a reference in the latter case.

The PCC-CTMP composite for these experiments was prepared under conditions that resulted in nano-sized particles which were fairly evenly spread on the fiber surfaces. See Paper III for a more detailed description of the precipitation process.

PCC-CTMP filled CTMP handsheets

When a PCC-CTMP composite was used as a filler in handsheets, the sheet density increased and the strength decreased with increasing ash content, the same effects as those obtained when using a traditional filler.

Cationic starch and MFC affected both the density and the sheet strength of PCC-CTMP sheets, see Figure 5.16. The sheet density was increased by the MFC and appeared to be decreased by the cationic starch, but the decrease in density with CS was probably an artifact caused by rougher sheets, as indicated by the cross-section SEM micrographs of the sheets (shown in Paper III).

The strength properties of the sheets (bending stiffness index, tensile index and tensile stiffness index) were affected to different degrees by the MFC and CS when the type of PCC was changed, i.e. whether the filling was with PCC-CTMP or PCC. The MFC had a more positive effect on the PCC-filled sheets than on the PCC-CTMP-filled sheets. With CS, the situation was the opposite, as shown in Figure 5.16B to D. The probable reason was the small particle size of the PCC in PCC-CTMP and the synergy reported in some cases with small mineral particles when cationic starch was used as a strengthening agent (Lindström et al. 2005).

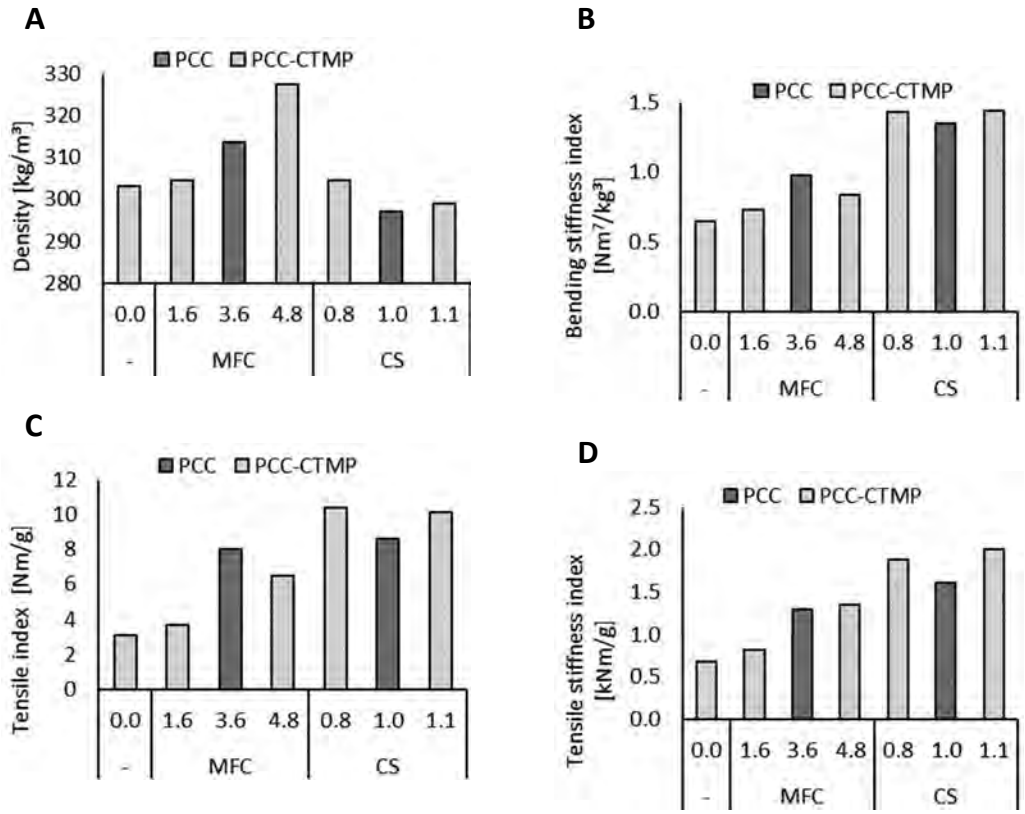

Figure 5.16: (A) Apparent sheet density, measured using a single sheet, (B) bending stiffness index, (C) tensile index and (D) tensile stiffness index of PCC-CTMP sheets filled with CTMP or PCC when using CS or MFC as a strengthening agent. For clarity, the results are interpolated to an ash content of 12%. The precipitation was carried out in Reactor III.

An indication of the position of the mineral in the sheet is shown in Figure 5.17. Figure 5.17A shows that in the reference sheets filled with PCC, PCC-free fiber surfaces and especially PCC-free fibril surfaces remained, whereas essentially no PCC-free fiber or fibril surface was seen in the PCC-CTMP filled sheets, except in the cross-cut region of the fiber (Figure 5.17B and C), even though none of the MFC used and only a part of the CTMP used were present during the IS-precipitation. The lack of a PCC-free surface was also seen on other SEM micrographs of PCC-CTMP-containing sheets (Paper III). Figure 5.17B and C also show the precipitate in the fiber lumens.

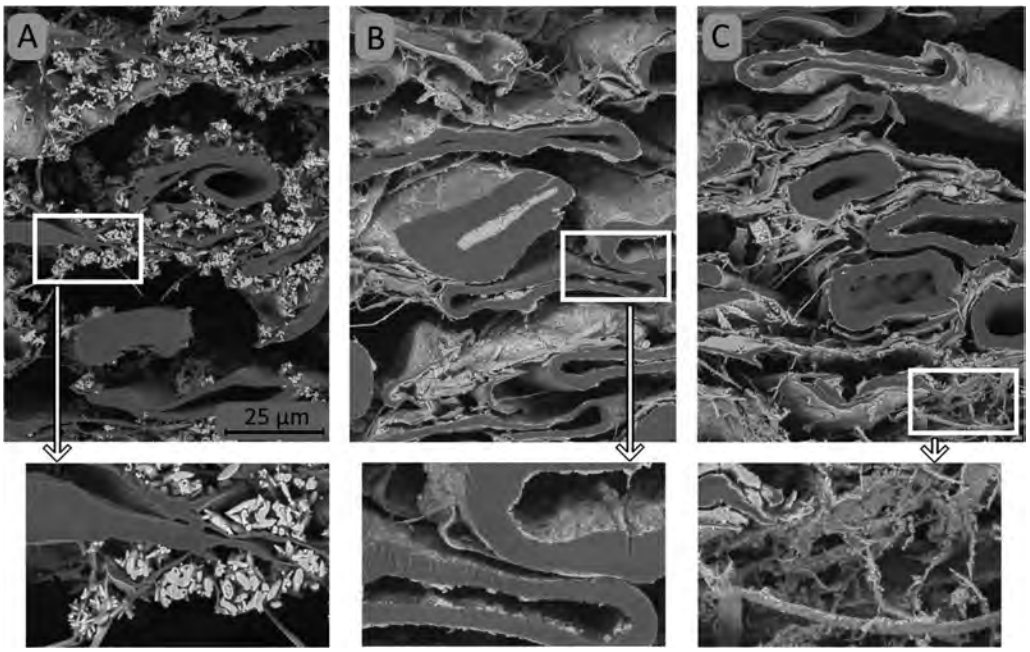

Figure 5.17: FE-SEM micrographs of cross-sections of handsheets. (A) 1.2 wt-% CS-reinforced handsheet filled with PCC. The close-up shows PCC attached to fibrils, but also PCC-free fiber and fibril regions. (B) PCC-CTMP-filled handsheet without strengthening agents. The higher magnification shows PCC precipitated in fiber lumens. (C) 13 wt-% MFC reinforced PCC-CTMP handsheet. The higher magnification images show fibrillar fines (probably MFC) covered with PCC. In all the images, the wire side is upwards. The ash content of the sheets was ca. 15% and the grammage ca. 190 g/m^2.

PCC-CTMP handsheets

The tensile strength index can in many cases give an indication of the bonding potential of a pulp (TAPPI standard T 494 om-01) whereas tensile stiffness indicates sheet stiffness and the response to mechanical converting (TAPPI standard T 494 om-01) and is related to other paper and board properties such as elastic modulus and bending stiffness (Kajanto 1998). Special interest was therefore focused on the development of these properties in the different size fractions of the pulps when PCC-CTMP was produced by IS-precipitation. The fiber-weight-based index (i.e. the index calculated using grammage from which ash weight was subtracted) was used to limit the effect of an uneven distribution of PCC between the fractions.

The non-fines fractions of PCC-CTMP sheets were of either a similar or a lower density than the CTMP sheets made using the corresponding fraction. There was however a difference between the fine (R400) fractions, where the PCC-CTMP fines sheets were denser than the CTMP fines sheets. The non-fractionated PCC-CTMP sheets were also

denser than the corresponding CTMP sheets. The densities of the sheets are shown in Figure 5.18.

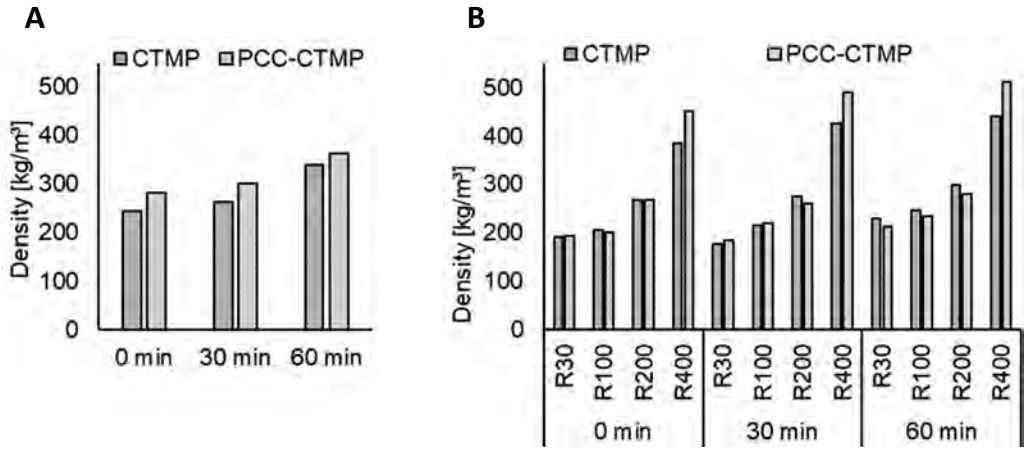

Figure 5.18: (A) Density of CTMP and PCC-CTMP sheets made using non-fractionated materials and (B) density of CTMP and PCC-CTMP sheets made using the fractions. The upper x-axis refers to refining time. The pulps were prepared using Reactor III and fractionated with a Bauer-McNett classifier. The handsheets were prepared using an auxiliary wire to improve the retention.

The strength properties were generally lower for PCC-CTMP than for CTMP, whether or not the comparison was made for sheets made using fractions, but fiber-weight-based tensile index was more affected by the level of refining than by the IS-precipitation. Tensile stiffness and tensile strength indices using fiber-weight-based grammage are given in Figure 5.19 (see Paper II for tabulated values).

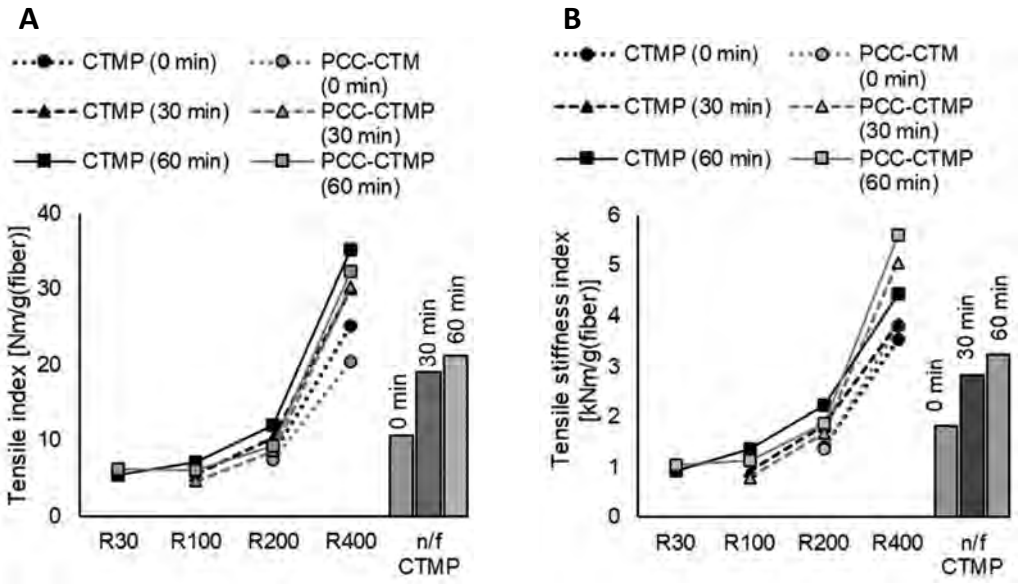

Figure 5.19: (A) Fiber-weight-based tensile index and (B) fiber-weight-based tensile stiffness index of CTMP and PCC-CTMP handsheets. n/f = non-fractionated pulp, and the times refer to the refining time of the pulp. All the PCC-CTMP sheets prepared using non-fractionated pulp had a tensile strength below the detection limit of the equipment. The composites were prepared using Reactor III and fractionation was done with a Bauer-McNett classifier.

The fiber-weight-based tensile index of the fractions suggested that, although the bonding potential of PCC-CTMP was affected by the presence of in-situ precipitated PCC, the change was fairly minor. The loss in fiber-weight-based tensile and tensile stiffness index could both be overcome by refining the CTMP on which the PCC was precipitated. This resulted, however, in an increase in sheet density.

The improvement in sheet stiffness by in-situ precipitation of PCC, reported by Silenius (2002), was not observed except for the R400 fraction. This may be partly due to the initial stiffness of the CTMP fiber, which results in a situation where the PCC can improve the CTMP fiber stiffness proportionally less than a more flexible fiber, as Silenius (2002) suggested that the possible reason for the sheet stiffness increase could have been increased fiber stiffness due to mineral in the fiber structure.

The increase in tensile stiffness of the CTMP sheet has also been linked to an increase in the amount of fines and to an increase in density (Motamedian et al. 2019). In the present case, the tensile stiffness index (whether sheet-weight-based or fiber-weight-based) correlated linearly with the density, as did the tensile index (shown in Figure 5.20A and B). In the case of the tensile stiffness index, however, the linear fits for CTMP and PCC-CTMP were essentially identical. This could be related to the finding that the tensile stiffness may not be affected solely by the bond strength (Motamedian et al. 2019).

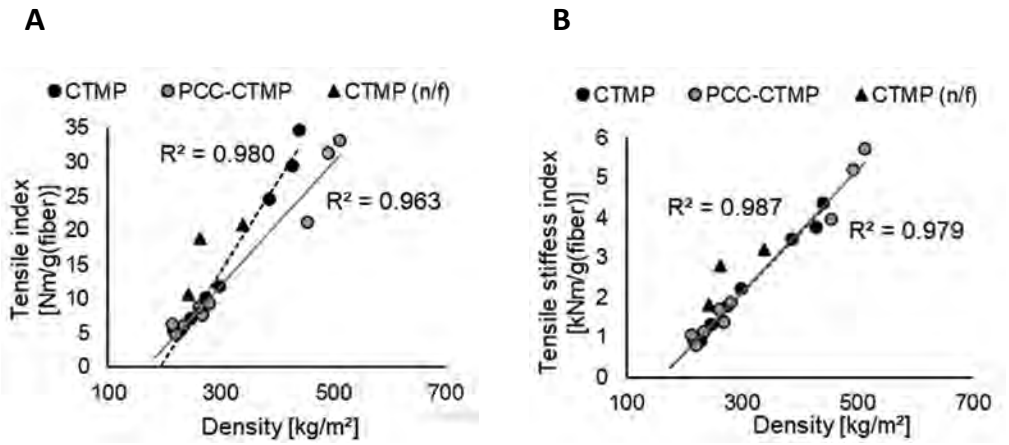

Figure 5.20: (A) Fiber-weight-based tensile index and (B) tensile stiffness index plotted against the density of the sheets. The composites were prepared using Reactor III and fractionation was done with a Bauer-McNett classifier.

5.3.2 Optical properties of PCC-CTMP fraction handsheets (Paper II)

One of the main motivations for making PCC-fiber composites has been to improve the optical properties of paper. In the present case, the optical properties (brightness, opacity, light scattering coefficient (s_r) and absorption coefficient (k_r)) were determined for sheets prepared from fiber fractions of PCC-CTMP and CTMP, and the s_r and k_r values of the fractions were compared with respect to tensile index and used in a Kubelka-Munk calculation.

The opacity values calculated for 65 g/m^2 sheets and the brightness values are shown in Figure 5.21. The tabulated values can be found in Paper II.

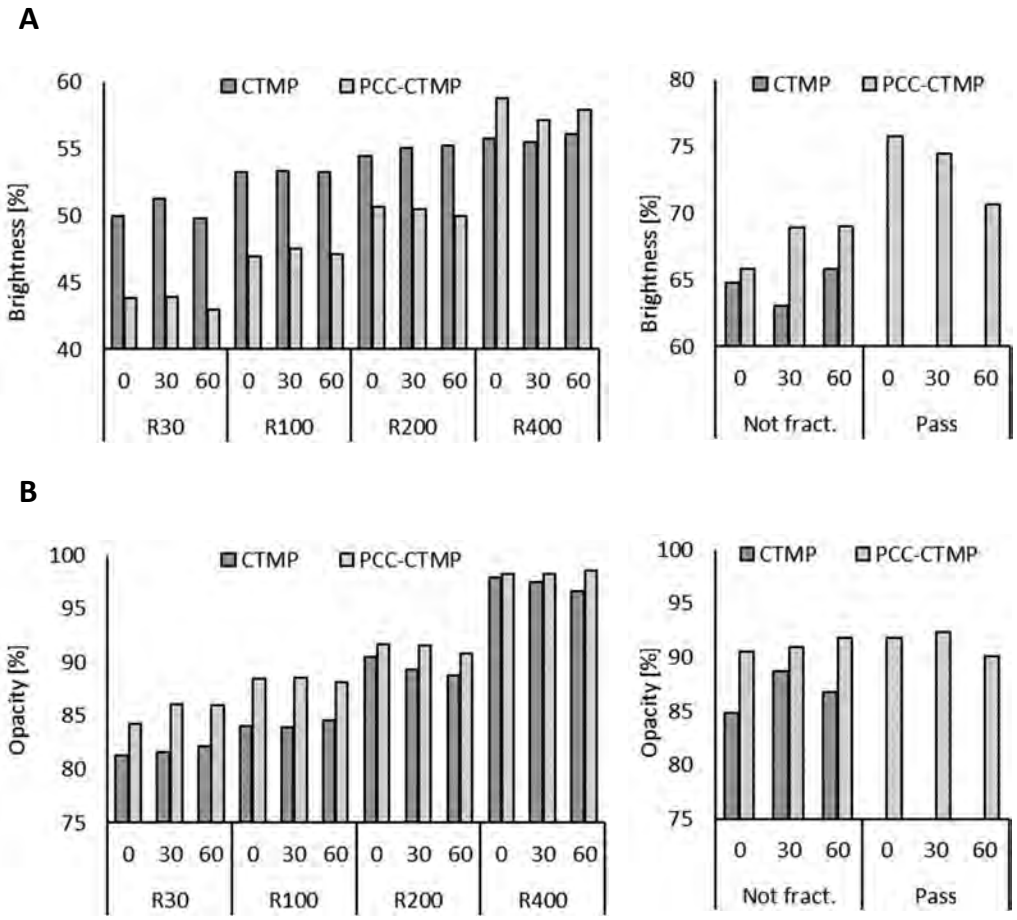

Figure 5.21: (A) Brightness and (B) opacity of handsheets prepared from CTMP and PCC-CTMP fiber fractions and from the unfractionated pulps. The upper x-axis refers to refining time. Note the different y-axes for the brightness data. The composites were prepared using Reactor III and fractionation was done with a Bauer-McNett classifier.

The PCC-CTMP sheets made using unfractionated material had a higher brightness than those made using unfractionated CTMP pulp. The brightness of both CTMP and PCC-CTMP fractions increased with decreasing fiber size. Increasing refining resulted in a decrease in the brightness of the PCC-CTMP sheets.

In all cases except for the fines (R400) fraction, the PCC-CTMP fractions had a lower brightness than the CTMP fractions. The difference between the brightness values of the corresponding PCC-CTMP and CTMP fractions, both in percentage points and as a percentage, was greater for the coarser fractions and less for the finer fiber fractions.

The opacity values showed a similar pattern, with the opacity increasing with decreasing fiber size. The opacity of PCC-CTMP fractions was systematically greater than the opacity of the CTMP sheets.

The scattering and absorption coefficients plotted against the fiber-weightbased tensile index (in Figure 5.22) reveals that, although refining of CTMP increased the fiber-weight-based tensile index, the s_r and k_r of the PCC-CTMP fractions were only slightly affected, with the exception of the R400 fractions.

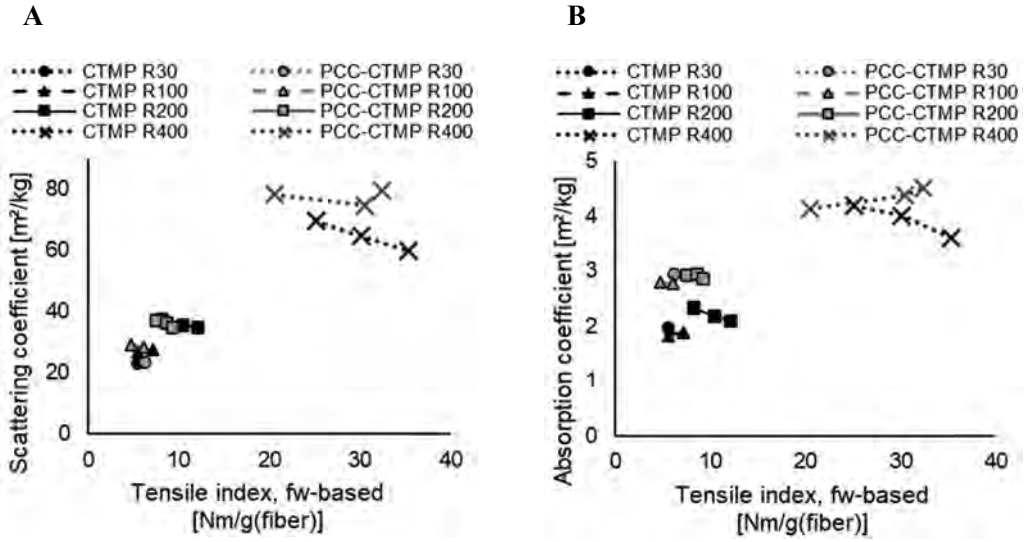

Figure 5.22: (A) Scattering and (B) absorption coefficients of sheets prepared using Bauer-McNett wire residuals of materials of different freeness levels. The value in labels refers to ASTM series wire from which the fiber fraction was collected. The fiber-weight based (i.e. non 525±25 °C ash) grammage was used in tensile index calculation due to different PCC contents of the fractions. The composites were prepared using Reactor III and fractionation was done with Bauer-McNett classifier.

The Kubelka-Munk calculation of pulp mixture typically assumes linear additivity for pulp mixtures (Leskelä 1998), i.e.

$$s_r = \sum_{i=0}^{n} f_i s_{r,i} \tag{5.1}$$

$$k_r = \sum_{i=0}^{n} f_i k_{r,i} \tag{5.2}$$

in which f_i refers to the relative amount of component i in the mixture. However, the assumption of additivity for the s_r is often incorrect due to changes in paper structure that result in changes in the scattering surfaces of the particles (Hubbe et al. 2008). In the present case, the densities of the sheets were clearly affected by the fractionation, signaling a change in packing of particles and a probable change in the scattering area.

When the s_r and k_r values for the pulp fractions were used to calculate the brightness of unfractionated pulp, the calculation predicted a brightness value for PCC-CTMP 5 to 7 percentage points higher than that for CTMP, which was slightly more than the measured difference of 1 to 6 percentage points.

The calculation underestimated the brightness of the unfractionated sheets by on average 9 percentage points for CTMP and 7 percentage points for PCC-CTMP. The poor agreement between the calculated and the measured brightness of the unfractionated sheets was indicative of a change in scattering area in the furnish, and the CTMP data especially can be expected to be affected by the fines loss during fractionation. As no sedimentation was included to catch the CTMP 'pass' fraction (6.7-8.4 wt-% of pulp), the brightness was calculated by combining the 'pass' and R400 values and assuming the s_r and k_r values measured for R400.

Qualitatively, however, the approximate linear additivity suggests that the increase in brightness of the unfractionated PCC-CTMP sheets was mostly due to the fines fractions (R400 and pass), while the other fractions were affected negatively. The negative effect was strongly associated with alkaline yellowing, to which the CTMP is prone due to its high lignin content (Jäkärä et al. 2009). The positive effect instead was mainly associated with the increased scattering due to the increasing ash content with decreasing fiber size, and especially, in the case of the unfractionated pulp handsheets, with an increase in the optically active surface due to debonding.

Although yellowing can be expected to be less problematic in the case of bleached kraft pulps, the results stress the importance of controlling the PCC precipitation into the different fractions. Methods to affect the PCC affinity for fibers of different sizes might include a carefully executed refining of the pulp prior to precipitation to control external fibrillation, or the use of a pre-treatment such as a bleaching sequence to control the pulp surface charge if a link between pre-precipitation surface charge and post-precipitation ash content could be further established. Refining is also able to improve bonding, important for recovering the strength potential lost by the addition of a filler

6 Conclusions

The objective of the work was to investigate PCC-fiber composite preparation and the PCC distribution and affinity for the different fiber fractions. The work focused mainly on controlling the precipitate morphology, and especially the preparation of fibers and fines with a high surface coverage of nano-PCC without the use of morphology-controlling aids.

The PCC-fiber composite was prepared via in-situ precipitation using $Ca(OH)_2$-CO_2-H_2O carbonization at room temperature. The morphology of the precipitate on the fibers was controlled by altering the CO_2 feed, by material transfer from the gas into the reaction solution and by the fiber consistency, which is linked to the targeted PCC content of the composite material via the initial $Ca(OH)_2$ concentration in the batch. The PCC morphologies created included cubical particles, cubical rounded particles and nanoparticles either aggregated in ellipsoidal shapes or distributed uniformly on the fiber surfaces to give fibers with a high surface coverage of evenly distributed nano-PCC.

To form a PCC-fiber composite with a high fiber coverage of nano-PCC, the degree of mineral phase aggregation on the fiber surfaces was altered by changing the CO_2 feed and fiber consistency in the reaction mixture. An evenly distributed PCC, instead of nano-PCC aggregated into micron-sized particles, was formed when a moderate CO_2 feed was combined with a high fiber concentration.

The method for controlling the precipitate morphology by altering the precipitation conditions was applied to three different fiber types: microcellulose, microfibrillated cellulose and chemithermomechanical pulp. The conditions under which a PCC-fiber composite with a high surface coverage with nano-PCC was formed differed slightly for the different fibers, due perhaps to surface-related effects, or to differences in reaction mixture properties such as viscosity, which may have altered the $[Ca^{2+}]/[CO_3^{2-}]$ ratio.

When precipitation was done on CTMP, the PCC was found to be enriched in the finer fiber fractions, especially on the fines, and on regions where the outer layer of the fibers had been removed and where the fiber was damaged or fibrillated. A correlation was found between the anionic surface charge of the CTMP before IS-precipitation of PCC and the ash content of the PCC-CTMP fraction after the precipitation, although the role of fiber surface area could not be excluded. PCC was more prone to precipitate onto cellulose-rich regions and onto regions of lower charge.

The uneven PCC distribution within the fractions resulted in differences to different degrees in the properties of the laboratory handsheets prepared from the fractions. The PCC disturbed bonding, which resulted in a loss of strength when fiber-weight-based indices were considered. Refining CTMP prior to precipitation could however be used to recover the strength of the fiber fractions, and MFC or cationic starch could also be used to increase the sheet strength when PCC-CTMP was used as a filler. The cationic starch

was especially effective, which was assumed to be due to the small particle size of the mineral phase in the PCC-CTMP type used.

The fractionation of PCC-fiber composite and handsheet results emphasize the importance of developing methods for a more controlled precipitation of PCC onto the fiber. A method of controlling the precipitate morphology without the need for morphology-controlling chemicals was successfully demonstrated for a batch process.

References

Ajikumar, P.K., Wong, L.G., Subramanyam, G., Lakshminarayanan, R., Valiyaveettil, S. (2005). Synthesis and characterization of monodispersed spheres of amorphous calcium carbonate and calcite spherules. *Crystal Growth & Design*, 5(3), pp.1129-1134.

Al-Sogair, F., Operschall, B.P., Sigel, A., Sigel, H., Schnabl, J., Sigel, R.K.O. (2011). Probing the metal-ion-binding strength of the hydroxyl group. *Chemical Reviews*, 111, pp. 4964-5003.

Allan, G.G. (1992). *Cell wall loading of never-dried pulp fibers*. US5096539A.

Allan, G.G., Carroll, J.P., Jimenez, G., Negri, A.R. (1998). Enhancement of the optical properties of a bagasse newsprint furnish by fiber-wall -filler. *Cellulose Chemistry and Technology*, 32, pp. 339-347.

Alince, B., Bednar, F. (2003). Role of cationic polyacrylamide in fiber-$CaCO_3$ pigment interactions. *Journal of Applied Polymer Science*, 88, pp. 2409-2415.

Ashori, A. (2006). Nonwood fibers – a potential source of raw material in papermaking. *Polymer-Plastics Technology and Engineering*, 45, pp. 1133-1136.

Axrup, L., Saxell, H., Jokela, V., Kastinen, H., Kauppi, A., Backfolk, K., Ruohoniemi, N., Laitinen, R., Heiskanen, I., Laukala, T. (2014). *Method for forming a subsequently drying a composite comprising a nanofibrillated polysaccharide*. US9562328B2.

Burke, D.J. (1993). Calcium carbonate and the evolution of alkaline papermaking in North America. *Tappi Journal*, 76(4), pp. 40A-40E.

Cantaert, B., Kim, Y.-Y., Ludwig, H., Nudelman, F., Sommerdijk, N.A.J.M., Meldrum, F.C. (2012). *Think positive: phase separation enables a positively charged additive to induce dramatic changes in calcium carbonate morphology.* Advanced Functional Materials, 22(5), pp. 907-915.

Carmona, J.G., Morales, J.G., Sáinz, J.F., Loste, E., Clemente, R.R. (2004). The mechanism of precipitation of chain-like calcite. *Journal of Crystal Growth*, 262, pp. 479-489.

Chakraborty, D., Bhatia, S.K. (1996). Formation and aggregation of polymorphs in continuous precipitation. 2. Kinetics of $CaCO_3$ precipitation. *Industrial & Engineering Chemistry Research*, 35, pp. 1995-2006.

Chen, T., Neville, A., Yuan, M. (2006). Influence of Mg^{2+} on $CaCO_3$ formation – bulk precipitation and surface deposition. *Chemical Engineering Science*, 61(16), pp. 5318-5327.

Chevalier, N.R. (2014). Do surface wetting properties affect calcium carbonate heterogeneous nucleation and adhesion?. *The Journal of Physical Chemistry C*, 188, pp. 17600-17607.

Chirat, C., Hostachy, J.-C., Paloniemi, J., Pelin, K., Pohjanvesi, S., Nordén, S., Vesala, R., Wennerström, M. (2011). Bleaching. In: P. Faradim, ed., *Papermaking science and technology. Book 6, Chemical pulping. Part 1, Fibre chemistry and technology*, 2nd ed. Helsinki: Fapet Oy, pp. 460-599.

Ciobanu, M., Bobu, E., Ciolacu, F. (2010). In-situ cellulose fibres loading with calcium carbonate precipitated by different methods. *Cellulose Chemistry and Technology*, 44(9), pp. 379-387.

Ciullo, P.A. (1996). The industrial minerals. In: P.A. Ciullo, ed., *Industrial Minerals and Their Uses: A Handbook and Formulary*, 1st ed. Westwood: Noyes Publications, pp. 17-82.

Cizer, Ö., Rodriguez-Navarro, C., Ruiz-Agudo, E., Elsen, J., Van Gemert, D., Van Balen, K. (2012). Phase and morphology evolution of calcium carbonate precipitated by carbonation of hydrated lime. *Journal of Materials Science,* 47, pp. 6151-6165.

Cölfen, H. (2020). Nonclassical nucleation and crystallization. *Crystals* [online]. 10(2). [7.5.2021]. Available from: doi: 10.3390/cryst10020061

Dalas, E., Klepetsanis, P.G., Koutsoukos, P.G. (2000). Calcium carbonate deposition on cellulose. *Journal of Colloid and Interface Science*, 224, pp. 56-62.

Dai, L., Douglas, E.P., Gower, L.B. (2008). Compositional analysis of a polymer-induced liquid-precursor (PILP) amorphous $CaCO_3$ phase. *Journal of Non-Crystalline Solids*, 354(17), pp. 1845-1854.

Dimic-Misic, K., Rantanen, J., Maloney, T.C., Gane, P.A.C. (2016). Gel structure phase behavior in micro nanofibrillated cellulose containing in situ precipitated calcium carbonate. *Journal of Applied Polymer Science* [online]. 133(22) [7.5.2021]. Available from: doi: 10.1002/app.43486

Eide, A.C., Calbeck, J.H. (1935). *Method of making pigmented paper*. US 2,006,016A.

El-Sheikh, S.M., El-Sherbiny, S., Barhoum, A., Deng, Y. (2013). Effects of cationic surfactant during the precipitation of calcium carbonate nano-particles on their size, morphology, and other characteristics. *Colloids and Surfaces A: Physicochemical and Engineering Aspects,* 422, pp. 44-49.

Forsskåhl, I. (2000). Brightness reverson. In: P. Stenius, ed., *Papermaking science and technology. Book 3, Forest products chemistry,* 1st ed. Helsinki: Fapet Oy, pp. 279-332.

Fortuna, M.E., Harja, M., Bucur, D., Cimpeanu, S.M. (2013). Obtaining and utilizing cellulose fibers with in-situ loading as an additive for printing paper. *Materials*, 6, pp. 4532-4544.

Fuchise-Fukuoka, M., Goto, S., Isogai, A. (2020a). Structural analysis of $CaCO_3$ nanoparticle/pulp fiber composites by tube flow fractionation. *BioResources*, 15(3), pp. 7048-7057.

Fuchise-Fukuoka, M., Oishi, M., Goto, S., Isogai, A. (2020b). Preparation of $CaCO_3$ nanoparticle/pulp fiber composites using ultrafine bubbles. *Nordic Pulp & Paper Research Journal,* 35(2), pp. 279-287.

Gane, P.A.C. (2009). Pigments. In: J. Paltakari, ed., *Papermaking science and technology. Book 11, Pigment coating and surface sizing of paper*, 2nd ed. Helsinki: Fapet Oy, pp. 98-109.

García-Carmona, J., Morales, J., Clemente, R. (2003). Morphological control of precipitated calcite obtained by adjusting the electrical conductivity in the $Ca(OH)_2$–H_2O–CO_2 system. *Journal of Crystal Growth,* 249, pp. 561-571.

Gellersted (1996). Chemical structure of pulp components. In: C.W. Dence, D.V. Reeve, eds., *Pulp Bleaching: Principles and Practice*, 1st ed. Atlanta: Tappi Press, pp. 91-111.

Gower, L.B., Odom, D.J. (2000). Deposition of calcium carbonate films by a polymer-induced liquid-precursor (PILP) process. *Journal of Crystal Growth,* 210(4), pp. 719-734.

Hakkila, P., Verkasalo, E. (2009). Structure and properties of wood and woody biomass. In: S. Kellomäki, ed., *Papermaking science and technology. Book 2, Forest resources and sustainable management*, 2nd ed. Helsinki: Fapet Oy, pp. 134-215.

Haslam, J.H., Steele, F.A. (1936). The retention of pigments in paper. *Technical Association Papers*, 19, pp. 249-252.

He, M., Cho, B.U., Won, J.M. (2016). Effect of precipitated calcium carbonate – cellulose nanofibrils composite filler on paper properties. *Carbohydrate Polymers*, 136, pp. 820-825.

Hedges, L.O., Whitelam, S. (2011). Limit of validity of Ostwald's rule of stages in a statistical mechanical model of crystallization. *The journal of chemical physics* [online]. 135(16). [7.5.2021]. Available from: doi: 10.1063/1.3655358

Henricson, K. (2006). *Method and apparatus for treating pulp with filler*. US7070677B2.

Heinemann, S., Vehniäinen, A. (2009). The character and properties of mechanical pulps. In: R. Alén, ed., *Papermaking science and technology. Book 4, Papermaking chemistry,* 2nd ed. Helsinki: Fapet Oy, pp. 458-514.

Hosoda, N., Kato, T. (2001). Thin-film formation of calcium carbonate crystals: effects of functional groups of matrix polymers. *Chemistry of Materials*, 13, pp. 688-693.

Hubbe, M.A. (2004). Filler particle shape vs. paper properties - A review. In: *TAPPI Paper Summit - Spring Technical and International Environmental Conference*. Atlanta: Tappi Press. Paper 7-3, pp.1–10.

Hubbe, M.A. (2006). Sensing the electrokinetic potential of cellulosic fiber surfaces. *BioResources*, 1(1), pp. 116-119.

Hubbe, M.A. (2007a). Water and papermaking 2. White water components. *Paper Technology*, 48, pp. 31-40.

Hubbe, M.A. (2007b). Water and papermaking 3. Measures to clean up process water. *Paper Technology*, 483(3), pp. 23-30.

Hubbe, M.A., Pawlak, J.J., Koukoulas, A.A. (2008). Paper's appearance: a review. *BioResources,* 3(2), pp. 627-665.

Hubbe, M.A., Gill, R.A. (2016). Fillers for papermaking: a review of their properties, usage practices, and their mechanistic role. *BioResources,* 11(1), pp. 2886-2963.

Hubbe, M.A., Venditti, R.A., Rojas, O.J. (2007). What happens to cellulosic fibers during papermaking and recycling? A review. *BioResources,* 2(4), pp. 739-788.

Imppola, O., (2009). Pigments. In: J. Paltakari, ed., *Papermaking science and technology. Book 11, Pigment coating and surface sizing of paper*, 2nd ed. Helsinki: Fapet Oy, pp. 134-145.

Imppola, O., Kukkamaki, E., Matula, J., Solismaa, P. (2013). *Method and apparatus for in-line production of milk of lime into an in-line production process of PCC arranged in connection with a fibrous web machine*. US2013216468A1.

Jimoh, O.A., Ariffin, K.S., Hussin, H.B., Temitope, A.E. (2017). Synthesis of precipitated calcium carbonate: a review. *Carbonates and Evaporites,* 33, pp. 331-346.

Jin, W., Jiang, S., Pan, H., Tang, R. (2018). Amorphous phase mediated crystallization: fundamentals of biomineralization. *Crystals*, 8(1), 48.

Jäkärä, J., Persson, M., Mårtens, H., Lindholm, C.A. (2009). Bleaching of mechanical pulps. In: B. Lönnberg, ed., *Papermaking science and technology. Book 5, Mechanical pulping,* 2nd ed. Helsinki: Fapet Oy, pp. 362-398.

Kang, H., Myoung, M., Byounk-uk, C. (2020). Composite filler by pre-flocculation of fiber fines and PCC and its effect on paper properties. *Nordic Pulp & Paper Research Journal*, 35(2), pp. 251-60.

Kajanto, I. (1998). Structural mechanics of paper and board. In: K. Niskanen, ed., *Papermaking science and technology. Book 16, Paper physics*, 1st ed., Helsinki: Fapet Oy, pp. 193-221.

Karthika, S., Radhakrishnan, T.K., Kalaichelvi, P. (2016). A review of classical and nonclassical nucleation theories. *Crystal Growth & Design,* 16, pp. 6663-6681.

Karpinski, P.H, Wey, J.S. (2002). Precipitation processes. In: A.S. Myerson, ed., *Handbook of Industrial Crystallization*, 2nd ed. Woburn: Butterworth-Heinemann, pp. 141-160.

Naka, K., Chujo, Y. (2001). Control of crystal nucleation and growth of calcium carbonate by synthetic substrates. *Chemistry of Materials*, 13(10), pp. 3245-3259.

Kim, J.J., Ahn, J.W., Lee, M.W., Kim, Y.W., Lee, J.K., Seo, Y.B. (2013). Improving recycled fibres in printing paper by application of an in-situ $CaCO_3$ formation method 2. Paper properties. *Appita,* 66(1), pp. 54-58.

Kim, Y.-Y., Douglas, E.P., Gower, L.B. (2007). Patterning inorganic ($CaCO_3$) thin films via a polymer-induced liquid-precursor process. *Langmuir,* 23, pp. 4862-4870.

Kirwan M.J. (2005). Paper and paperboard – raw materials, processing and properties. In: M.J. Kirwan, ed., *Paper and paperboard packaging technology*. Oxford: Blackwell Publishing Ltd, pp. 1-49.

Kiuru, A. (2018). Esikäsittelymenetelmien vertaileminen prosessoidun puukuidun morfologisten ominaisuuksien tutkimista varten valo- ja pyyhkäisyelektronimikroskoopilla. BCs (Tech.), Lappeenranta University of Technology.

Klungness, J.H., Caulfield, D.F., Sachs, I.B., Sykes, M.S., Tan, F., Shilts, R.W. (1992). *A method for fiber loading a chemical compound*. WO92/15754.

Klungness, J.H., Gleisner, R.L., Sykes, M.S. (2002). Pacification of stickies by fibre loading. *7th Recycling Technology Conference*. Brussels, Belgium, 14-15th of February 2002. Leatherhead, U.K. : Pira International, 2002.

Klungness, J.H., Sykes, M.S., Tan, F., Abubakr, S., Eisenwasser, J.D. (1996). Effect of fiber loading on paper properties. *Tappi Journal*, 79(3), pp. 297-301.

Koivunen, K., Niskanen, I., Peiponen, K.-E., Paulapuro, H. (2009). Novel nanostructured PCC fillers. *Journal of Materials Science,* 44, p. 477-482.

Korntner, P., Hosoya, T., Dietz, T., Eibinger, K., Reiter, H., Spitzbart, M., Röder, T., Borgards, A., Kreiner, W., Mahler, A.K., Winter, H., Groiss, Y., French, A.D., Henniges, U., Potthast, A., Rosenau, T. (2015). Chromophores in lignin-free cellulosic materials

belong to three compound classes. Chromophores in cellulosics, XII. *Cellulose,* 22 pp. 1053-1062.

Krogerus, B. (2007). Papermaking additives. In: R. Alén, ed., *Papermaking science and technology. Book 4, Papermaking chemistry,* 2nd ed. Helsinki: Fapet Oy, pp. 56–126.

Kumar, P., Gautam, S.K., Kumar, V., Singh, S.P. (2009). Enhancement of optical properties of bagasse pulp by in-situ filler precipitation. *BioResources*, 4(4), pp. 1635-1646.

Kumar, P., Negi, Y.S., Singh, S.P. (2011). Filler loading in the lumen or/and cell wall of fibers - A literature review. *BioResources*, 6(3), pp. 3526-3546.

Laine, J. (2007). General aspects of papermaking chemistry. In: R. Alén, ed., *Papermaking science and technology. Book 4, Papermaking chemistry,* 2nd ed. Helsinki: Fapet Oy, pp. 28-51.

Lakshminarayanan, R., Valiyaveettil, S., Loy, G.L. (2003). Selective nucleation of calcium carbonate polymorphs: role of surface functionalization and poly(vinyl alcohol) additive. *Crystal Growth and Design,* 3(6), pp. 953-958.

Lavoine, N., Desloges, I., Dufresne, A., Bras, J. (2012). Microfibrillated cellulose – Its barrier properties and applications in cellulosic materials: a review. *Carbohydrate Polymers*, 90, pp. 735-764.

Lindström, T., Wågberg L., Larsson T. (2005). On the nature of joint strength in paper – A review of dry and wet strength resins used in paper manufacturing. In: S.J. I'Anson, ed., *Advances in Paper Science and Technology, Trans. of the XIIIth Fund. Res. Symp.*, Manchester: FRC, pp 457–562

Liu, Z., Wang, H., Hui, L. (2018). Pulping and papermaking of non-wood fibers. In: S.N. Kazi, ed., *Pulp and Paper Processing*, 1st ed. pp. 3-32.

Loureiro, P.E.G., Domingues, M.R.M., Fernandes, A.J.S., Carvalho, M.G.V.S., Evtuguin, D.V. (2012). Discriminating the brightness stability of cellulosic pulp in relation to the final bleaching stage. *Carbohydrate Polymers*, 88, pp. 726-733.

Lutton, C.W. (1952a). *Forming pigment in cellulose fiber and paper containing the pigmented fiber*, US2599091A.

Lutton, C.W. (1952b). *Multiple layer paper containing pigmented pulp and method of making*. US2599092A.

Lutton, C.W. (1952c). *Production of pigmented cellulosic pulp*. US Patent US2583548A.

Lönnberg, B. (2009). Idea of mechanical pulping. In: B. Lönnberg, ed., *Papermaking science and technology. Book 5, Mechanical pulping,* 2nd ed. Helsinki: Fapet Oy, pp. 18-22

Ma, M.-G., Fu, L.-H., Sun, R.-C., Jia, N. (2012). Compared study on the cellulose/$CaCO_3$ composites via microwave-assisted method using different cellulose types. *Carbohydrate Polymers*, 90(1), pp. 303-315.

Manner, H., Reponen, P., Holmbom, B., Pajula, T. (2009). Future outlook. In: B. Lönnberg, ed., *Papermaking science and technology. Book 5, Mechanical pulping,* 2nd ed. Helsinki: Fapet Oy, pp. 432-455.

Marques, G., Rencoret, J., Gutiérrez, A., del Río, J.C. (2010). Evaluation of the chemical composition of different non-woody plant fibers used for pulp and paper manufacturing. *The Open Agriculture Journal*, 4, pp. 93-101.

Matula, J., Räsänen, J., Tahkola, K. (2018). In-line PCC technology cleans up circulation water from dissolved materials, metals and bio based microorganisms resulting to clean process and high runnability. In: *2018 PAPERCON Conference Proceedings*. Charlotte: Tappi Press.

Matthew, M.C., Patnaik, S., Hart, P., Amidon, T. (1997). Process for enhanced deposition and retention of particulate filler on papermaking fibers, US 5,679,220.

Mersmann, A. (1999). Crystallization and precipitation. *Chemical Engineering and Processing,* 38, pp. 345-353.

Mersmann, A. (2001). Physical and chemical properties of crystalline systems. In: A. Mersmann, ed., *Crystallization technology handbook*, 2nd ed. New York: Dekker, pp. 1-44

Mersmann, A. Eble, A., Heyer, C. (2001). Crystal growth. In: A. Mersmann, ed., *Crystallization technology handbook*, 2nd ed. New York: Dekker, pp. 81-143

Middleton, S.R., Desmeules, J., Scallan, A.M. (2003). Lumen loading with calcium carbonate fillers. *Journal of Pulp and Paper Science*, 29(7) pp. 241-246.

Mohamadzadeh-Saghavaz, K., Resalati, H., Ghasemian, A. (2014). Cellulose-precipitated calcium carbonate composites and their effect on paper properties. *Chemical Papers,* 68(6), pp. 774–781.

Mohamadzadeh-Saghavaz, K., Resalati, H., Mehrabi, E. (2013). Characterization of cellulose–PCC composite filler synthesized from CMC and BSKP fibrils by hydrolysis of ammonium carbonate. *Powder Technology*, 246, pp. 93-97.

Motamedian, H.R., Halilovic, A.E., Kulachenko, A. (2019). Mechanisms of strength and stiffness improvement of paper after PFI refining with a focus on the effect of fines. *Cellulose*, 26, pp. 4099-4124.

Oates, T. (1990). Lime and Limestone. In: B. Elvers, S. Hawkins, G. Schultz, eds., *Ullman's encyclopedia of industrial chemistry vol. A15,* 5th ed. Weinheim: VHH, pp. 317-345

Odabas, N., Henniges, U., Potthast, A., Rosenau, T. (2016). Cellulosic fines: Properties and effects. *Progress in Materials Science*, 83, pp. 574-594.

Othman, R., Zakaria, S., Chia, C.-H., Zuriyati, A., Isa, N. (2010). Mechanical and optical properties of $CaCO_3$ lumen-loaded paper: effect of polyethylenimine and alum. *Sains Malaysiana*, 39(3), pp. 435-439.

Park, Y., Rawat, P., Ford, E. (2017). Role of polymerized micelles on the calcium carbonate mineralization of nanofibers. *Industrial & Engineering Chemistry Research*, 56, pp. 8241-8250.

Payne, S.R., Heppenstall-Butler, M., Butler, M.F. (2007). Formation of thin calcium carbonate films on chitosan biopolymer substrates. *Crystal Growth & Design,* 7(7), pp. 1262–1276.

Petlicki, J., van de Ven, T.G.M. (1994). Kinetics of lumen loading. *Journal of Pulp and Paper Science,* 20(12) pp. 375-382.

Politi, Y., Arad, T., Klein, E., Weiner, S., Addidi, L. (2004). Sea urchin spine calcite forms via a transient amorphous calcium carbonate phase. *Science*, 306(5699), pp. 1161-1164.

Purgstaller, B., Mavromatis, V., Immenhauser, A., Dietzel, M. (2016). Transformation of Mg-bearing amorphous calcium carbonate to Mg-calcite – In situ monitoring. *Geochimica et Cosmochimica Acta*, 174, pp. 180-195.

Rantanen, J. (2016). *The manufacturing potential of micro and nanofibrillated cellulose composite papers*. PhD. Dissertation (Tech.). Aalto University.

Saijonkari-Pahkala, K. (2001). *Non-wood plants as raw material for pulp and paper*. Ph.D. Dissertation (Tech.). University of Helsinki.

Schabel, S. (2010a). Papermaking potential of recycled fiber. In: L. Göttsching, H. Pakarinen, eds., *Papermaking science and technology. Book 7, Recycled fiber and deinking,* 2nd ed. Helsinki: Fapet Oy, pp. 436-517.

Schabel, S. (2010b). Unit operations and equipment in recycled fibre processing. In: L. Göttsching, H. Pakarinen, eds., *Papermaking science and technology. Book 7, Recycled fiber and deinking,* 2nd ed. Helsinki: Fapet Oy, pp. 126-278.

Seo, Y.B., Ahn, J.H., Lee, H.L. (2017). Upgrading waste paper by in-situ calcium carbonate formation. *Journal of Cleaner Production*, 155, pp. 212-217.

Seo, Y.B., Lee, Y.H., Chung, J.K. (2014). The improvement of recycled newsprint properties by in-situ $CaCO_3$ loading. *BioResources,* 9(4), pp. 6254-6266.

Sharma, N., Bhardwaj, N.K., Singh, R.B.P. (2020). Environmental issues of pulp bleaching and prospects of peracetic acid pulp bleaching: A review. *Journal of cleaner production* [online]. 265. [7.5.2021]. Available from: doi: 10.1016/j.jclepro.2020.120338

Shen, J., Song, Z., Qian, X., Liu, W. (2009). Modification of papermaking grade fillers: a brief review. *BioResources*, 4(3), pp. 1190-1209.

Schenk, A.S., Zope, H., Kim, Y.Y., Kros, A., Sommerdijk, N.A.J.M., Meldrum, F.C. (2012). Polymer-induced liquid precursor (PILP) phases of calcium carbonate formed in the presence of synthetic acidic polypeptides-relevance to biomineralization. *Faraday Discussions*, 159, pp. 327-344.

Schubert, H., Mersmann, A. (2000). How aggregation process affect experimentally detected nucleation rates. In: B. Sen Gupta, S. Ibrahim, eds., *Mixing and crystallization*, 1st ed. Dordrecht: Springer, pp. 105-112.

Silenius, P. (2002). *Improving the combinations of critical properties and process parameters of printing and writing papers and paperboards by new paper-filling methods*. PhD. Dissertation (Tech.), Helsinki University of Technology.

Sinquefield, S., Ciesielski, P.N., Li, K., Gardner, D.J., Ozcan S. (2020). Nanocellulose dewatering and drying: current state and future perspectives. *ACS Sustainable Chemistry & Engineering*, 8, pp. 9601-9615.

Stenius, P. (2000). Macromolecular, surface, and colloid chemistry. In: P. Stenius, ed., *Papermaking science and technology. Book 3, Forest products chemistry*, 2nd ed. Helsinki: Fapet Oy, pp. 173-276.

Su, X., Kamat, S., Heuer, A.H. (2000). The structure of sea urchin spines, large biogenic single crystals of calcite. *Journal of Materials Science,* 35, pp. 5545-5551.

Subramanian, R. (2008). *Engineering fine paper by utilising the structural elements of the raw materials*. PhD. Dissertation (Tech.), Åbo Akademi University.

Subramanian, R., Fordsmand, H., Paulapuro, H. (2007). Precipitated calcium carbonate (PCC)-cellulose composite fillers; effect of PCC particle structure on the production and properties of uncoated fine paper. *BioResources*, 2(1), 91-105.

Svending, P. (2014). Commercial break-through in MFC processing. In: *2014 TAPPI International Conference on Nanotechnology for Renewable Materials*. Vancouver: Tappi Press.

TAPPI T 261 cm-94, *Fines fraction of paper stock by wet screening, TAPPI* provisional method

TAPPI T 494 om-01, *Tensile properties of paper and paperboard (using constant rate of elongation apparatus),* TAPPI Standard

TAPPI 261 cm-94, *Fines fraction of paper stock by wet screening,* T 261 cm-94, TAPPI Standard

Taipale, T. (2010). *Interactions of microfibrillated cellulose and cellulosic fines with cationic polyelectrolytes*. PhD. Dissertation (Tech.), Aalto University.

Tang, Y., Zhang, F., Cao, Z., Jing, W., Chen, Y. (2012). Crystallization of $CaCO_3$ in the presence of sulfate and additives: Experimental and molecular dynamics simulation studies. *Journal of Colloid and Interface Science,* 337(1), pp. 430-437.

Teir, S., Eloneva, S., Zevenhoven, R. (2005). Production of precipitated calcium carbonate from calcium silicates and carbon dioxide. *Energy Conversion and Management*, 46(18-19), pp. 2954-2979.

Threlfall, T. (2003). Structural and Thermodynamic Explanations of Ostwald's Rule. *Organic Process Research & Development,* 7(6), pp. 1017-1027.

Thomsen, A.M. (1962). *Method of increasing the opacity of cellulose fibers*. US3029181.

Tobler, D.J., Rodriguez-Blanco, J.D., Sørensen, H.O., Stipp, S.L.S., Dideriksen, K. (2016). Effect of pH on amorphous calcium carbonate structure and transformation. *Crystal Growth and Design*, 16(8), pp. 4500-4508.

Torvinen, K. (2017). *Flexible pigment-cellulose nanofibril composites for printed electronics applications*. PhD. Dissertation (Tech.), Helsinki University of Technology.

Ukrainczyk, M., Kontrec, J., Babić-Ivančić, V., Brečević, L., Kralj, D. (2007). Experimental design approach to calcium carbonate precipitation in a semicontinuous process. *Powder Technology*, 171, pp. 192-199.

van de Ven, T.G.M. (2005). Filler and fines retention in papermaking. In: *Advances in Paper Science and Technology Trans. XIIIth Fund. Res. Symp. Cambridge, 2005*. Manchester: FRC, pp. 1193-1224.

Vehniäinen, A., Haikkala, P., Suhonen, T. (2009). Future outlook. In: S. Kellomäki, ed., *Papermaking science and technology. Book 2, Forest resources and sustainable management*, 2nd ed. Helsinki: Fapet Oy, pp. 516-532.

Vilela, C., Freire, C.S.R., Marques, P.A.A.P., Trindade, T., Neto, C.P., Fardim, P. (2010). Synthesis and characterization of new $CaCO_3$/cellulose nanocomposites prepared by controlled hydrolysis of dimethylcarbonate. *Carbohydrate Polymers*, 79, pp. 1150–1156.

Wada, N., Suda, S., Kanamura, K., Umegaki, T. (2004). Formation of thin calcium carbonate films with aragonite and vaterite forms coexisting with polyacrylic acids and chitosan membranes. *Journal of Colloid and Interface Science*, 1(1), p. 167-174.

Wang, Y.-W., Kim, Y.-Y., Stephens, C.J., Meldrum, F.C., Christenson, H.K. (2012). In situ study of the precipitation and crystallization of amorphous calcium carbonate (ACC). *Crystal Growth and Design,* 12(3), pp. 1212-1217.

Wen, Y., Xiang, L., Jin, Y. (2003). Synthesis of plate-like calcium carbonate via carbonation route. *Materials letters*, 57(16-17), pp. 2565-2671.

Xu, X., Han, J.T., Cho, K. (2005). Deposition of amorphous calcium carbonate hemispheres on substrates. Langmuir, 21, pp. 4801-4804.

Xu, Y., Jiang, C., Duan, C., Zhang, W. (2017). In-situ preparation of nano-calcium carbonate/cellulose fiber composite and its application in fluff pulp. *Journal of Engineered Fibers and Fabrics,* 12(3), pp. 48-53.

Yamada, H., Hara, N. (1984). Formation process of colloidal calcium carbonate in the reaction of the system $Ca(OH)_2$-H_2O-CO_2. *Gypsum&Lime*, 194, pp 3-12.

Yamada, H., Hara, N. (1985). Synthesis of basic $CaCO_3$ from the reaction of the system $Ca(OH)_2$-H_2O-CO_2. *Gypsum&Lime*, 196, pp 130-140.

Yamanaka, S., Ito, N., Shimosaka, A., Shirakawa, Y., Hidaka, J. (2009). AFM investigation for the initial growth processes of calcium carbonate on hydrophilic and hydrophobic substrate. *Crystal Growth and Design,* 9(7), pp. 3245-3250.

Yoon, S.-Y., Deng, Y. (2006). Clay-starch composites and their application in papermaking. *Journal of Applied Polymer Science*, 100, pp. 1032–1038.

Zhang, S., Gonsalves, K.E. (1998). Influence of the chitosan surface profile on the nucleation and growth of calcium carbonate films. *Langmuir*, 14(23), p. 6761-6766.

Zheng, L., Hu, Y., Ma, Y., Zhou, Y., Nie, F., Liu, X., Pei, C. (2012). Egg-white-mediated crystallization of calcium carbonate. *Journal of Crystal Growth,* 361, pp 217-224.

Zou, Z., Habraken, W.J.E.M., Matveeva, G., Jensen, A.C.S., Bertinetti, L., Hood, M.A., Sun, C., Gilbert, P.U.P.A., Polishchuk, I., Pokroy, B., Mahamid, J., Politi, Y., Weiner, S., Werner, P., Bette, S., Dinnebier, R., Kolb, U., Zolotoyabko, E., Fratzl, P (2019). A hydrated crystalline calcium carbonate phase: Calcium carbonate hemihydrate. *Science,* 363, pp. 396-400

Publication I

Laukala, T., Kronlund, D., Heiskanen, I., and Backfolk, K.
The effect of polyacrylic acid and reaction conditions on nanocluster formation of precipitated calcium carbonate on microcellulose

Cellulose
Vol. 24(7), pp. 2813-2826, 2017

The final publication is available at Springer via
http://dx.doi.org/10.1007/s10570-017-1296-8

The effect of polyacrylic acid and reaction conditions on nanocluster formation of precipitated calcium carbonate on microcellulose

Laukala Teija, Kronlund Dennis, Heiskanen Isto, Backfolk Kaj

The precipitation of micro- and nanoparticles of calcium carbonate onto lignocellulosic microfibers was investigated at different microfiber concentrations with and without polyacrylic acid (PAA), i.e. a polymer commonly used to form polymer-induced liquid precursors of $CaCO_3$. Concentrations of PAA, $Ca(OH)_2$, CO_2 and microfiber were varied in order to study the impact of reaction conditions on PCC formation in a batch reactor operated at ambient temperature. High resolution scanning electron micrographs of the samples show that both microfiber concentration and PAA dosage affected the nucleation and crystal growth of PCC filler on cellulosic fiber. Interestingly, at higher microfiber concentrations, larger amount of nanosized spherical crystals were formed on the microfibers. A higher dosage of PAA, on the other hand, resulted in less nucleation on the microfiber, suggesting a preferential bulk nucleation mechanism. A higher concentration of PAA during the precipitation also led to the formation and stabilization of amorphous $CaCO_3$, which was supported by SEM images and XRD analysis (lack of characteristic crystal structure)

Keywords: In-situ precipitation ; Calcium compounds ; Substrates ; Nanostructures ; Morphology control

1. Introduction

Minerals can be fixed onto lignocellulose by various methods: using modified pigments (Alince and Bednar 2003; Shen et al. 2009), by co-mixing with flocculation or fixation chemicals (Burgess et al. 2000; Shen et al. 2009), or by using in situ precipitation, i.e. precipitating the mineral in presence of the lignocellulosic material. When calcium carbonate ($CaCO_3$) is precipitated in situ onto cellulose fibers, e.g. during paper manufacturing, a unique composite material of engineerable properties is obtained.

From papermaking point of view, the composite has high filler content (Ciobanu et al. 2010), high filler retention (Ciobanu et al. 2010; Klungness et al. 1997; Silenius 1996) and a more uniform distribution of filler material within the paper sheet (Silenius 1996; Mohamadzadeh-Saghavaz et al. 2014). These benefits can result to improved optical properties without pronounced loss of strength (Ciobanu et al. 2010; Mohamadzadeh-Saghavaz et al. 2014; Klungness et al. 2000). The literature, however, also reports decreased optical and strength properties (Klungness et al. 1994, 2000; Mohamadzadeh-Saghavaz et al. 2014). Some of these contradictory results have been linked to the different materials used in the experiments (Klungness et al. 1996, 2000; Kumar et al. 2009) including the calcium carbonates: commercial precipitated calcium carbonates (PCCs) have been optimized for light scattering by tuning their crystal morphology and particle size, whereas calcium carbonate precipitated in situ has not been similarly controlled and optimized (Klungness et al. 1994). This difference may

offer a possibility to improve properties of in situ precipitated fiber-$CaCO_3$ by controlling and optimizing the $CaCO_3$ properties during in situ precipitation.

Due to possible improvements from papermaking point of view, in situ precipitation of calcium carbonate has gained interest in the paper industry for high filler content papers, but also for improving water retention properties of micro and nano cellulose containing furnishes (Rantanen et al. 2015), although full-scale implementation of the concept still poses challenges in view of product quality and technology. The papermaking industry is the most widely studied application of fibers with in situ precipitated $CaCO_3$, which has been reviewed by Kumar et al. (2011) and demonstrated in doctoral theses by Silenius and Subramanian (Silenius 2002; Subramanian 2008). Other fields of use for cellulose fiber and $CaCO_3$ composite materials include substrates for printed electronics (Penttilä et al. 2012; Torvinen et al. 2012) and transparent cellulose film (Gebauer et al. 2011).

The methods commonly used for $CaCO_3$ precipitation onto fiber surfaces are carbonization of calcium hydroxide, $Ca(OH)_2$, in the presence of fibers (Ciobanu et al. 2010; Klungness et al. 1994, 1996; Subramanian et al. 2007) or by reactions between electrolytes that contain calcium and carbonate (Ciobanu et al. 2010; Mohamadzadeh-Saghavaz et al. 2014; Kumar et al. 2009), both of which have advantages and disadvantages.

In the absence of lignocellulosic fibers, significantly higher amount of options have been presented in the literature to controlling PCC morphology and particle size. The methods include controlling the ratio of carbonate to calcium ions (Kitamura et al. 2002), the use of crystallization-controlling agents such as polymers (Butler et al. 2006; Hardikar and Matijević 2001; Kumar et al. 2011; Matahwa et al. 2008; Nielsen et al. 2012; Jada et al. 2007), organic acids (Vdović and Kralj 2000), surfactants (Wei et al. 2005) and inorganic compounds (Hu and Deng 2004; Park et al. 2008; Kellermeier et al. 2010). It is currently usually claimed that $CaCO_3$ precipitation proceeds via nonclassical crystallization pathways, often including amorphous calcium carbonate (ACC) nanoparticles or liquid precursor stages (polymer-induced liquid precursors, PILPs). Polyelectrolytes (Cölfen and Antonietti 2008), especially atactic low molecular weight polyacrylic acid (PAA) (Volkmer et al. 2005), have been used to achieve liquid $CaCO_3$ precursors. It is suggested that the polymers sequester calcium ions, thus creating locally high calcium concentrations while inhibiting crystallization (Gower and Odom 2000). As a result, PILP droplets are formed and may aggregate on solid surfaces before crystallizing or forming ACC (Cölfen and Antonietti 2008).

Also for fiber–$Ca(OH)_2$–CO_2 precipitation process, precipitation of $CaCO_3$ onto fiber is often thought to proceed via ACC that initially forms on $Ca(OH)_2$ particles (Subramanian 2008). After this, ACC is thought to aggregate on fiber surface on which it converts to crystalline $CaCO_3$ (Subramanian et al. 2007; Subramanian 2008), although ACC is sometimes thought to dissolve, at least partly, and then precipitate as a crystalline polymorph (Xu et al. 2004; Zhang et al. 2012). If viewed from a more classical crystallization theory point of view, nucleation can be thought as heterogeneous on the fibers (Silenius 2002). Significantly, both views consider surface of the cellulosic fiber (template material) as an area of interest for precipitation process.

An interesting property of some crystallization controlling agents is they may interact with functional groups of the template material, such as cellulose. When $CaCO_3$ is precipitated onto cellulose fibers, this interaction is of particular interest. While the effect of polymeric additives in a modified precursor system is not well understood in the cellulosic fiber–$Ca(OH)_2$–CO_2 precipitation, the mentioned interaction and effects on crystal formation may provide tools to control and optimize in situ precipitated $CaCO_3$ on fiber. In a setting different from fiber-

$Ca(OH)_2$–CO_2 precipitation, the interaction has been utilized by Hosoda and Kato (2001) who obtained a continuous, thin calcite film on the cellulosic surface

In this work, the aim was to clarify the role of Sodium Polyacrylic acid (Na-PAA), a known PILP-inducing polymer, in a cellulosic fiber–$Ca(OH)_2$–CO_2 batch precipitation when controlling the PCC particle and its crystal size and shape. The use of Na-PAA to control $CaCO_3$ crystal morphology has been previously demonstrated (Yu et al. 2004; Huang et al. 2007; Ouhenia et al. 2008), and also when $CaCO_3$ crystals were deposited on a cellulosic substrate (Matahwa et al. 2008; Hosoda and Kato 2001), but, to our knowledge, effect of PAA in a cellulosic fiber-$Ca(OH)_2$–CO_2 system has not been investigated before. The precipitation conditions needed to create submicron particles and nanocrystal aggregates on the cellulose microfibers were of particular interest.

2. Materials and methods

Experiments with Sodium Polyacrylic acid (Na-PAA, denoted PAA in the text) were made using three different fiber concentrations, *viz.* 1.0, 3.0 and 6.0 wt%, with a fixed ratio of fiber to CO_2 of 0.5. The effects of Na-PAA and $Ca(OH)_2$ concentration were thus varied in order to determine their impact on the complexes obtained. For $CaCO_3$ precipitated onto microfibers without polymeric additives, 5 different fiber concentrations (from 0.5 to 6.0 wt%) were used in addition to different carbon dioxide feeds (from 0.5 to 6.0 l/min).

The calcium carbonate was precipitated at ambient temperature (20-23 °C) using $Ca(OH)_2$ as lime milk, - and CO_2 (AGA, purity 99.7%). A dry cellulosic microfiber (Arbocel UFC100, JRS), with a mean particle size of 8 µm according to the manufacturer was dispersed in water with strong mixing. Sodium polyacrylic acid, Na-PAA (Sigma-Aldrich, M ~ 1800 g/mol) was dissolved in water (2, 5 and 8 wt%, stock solutions, using a concentration as low as possible to reach the targeted concentration in the reaction batch) and diluted with water immediately prior use.

The batches were prepared by mixing water, PAA solution (if used), $Ca(OH)_2$ and fibers, in this order. The contents of the solutions and suspensions were determined gravimetrically with an error margin of ±0.5 g. The precipitation was performed in an open batch reactor equipped with mixer and inlet for CO_2, as shown in Fig. 1. The stirring speed was set to a constant 800 rpm and the initial batch temperature was ca. 20 °C. Changes in temperature and pH were monitored during the experiments, and the experiments were terminated when the pH began to stabilize at a low level, usually at ca. pH 6.5.

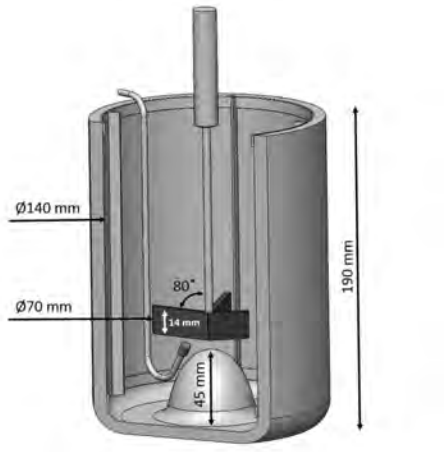

Fig. 1 Drawing of the reactor used in the experiments

The morphology of the cellulose microfiber-PCC agglomerates and the size of PCC crystals and agglomerates on the cellulose were determined from the SEM images. The $CaCO_3$ and cellulose polymorphs were characterized using x-ray diffraction (XRD measurements on a Bruker Discover D8 diffractometer (Karlsruhe, Germany) using Cu(Ka) radiation (k = 1.54184 nm). The XRD diffractograms were collected in the 2h range of 13°–48°. The X-ray tube was operated at

40 kV and 40 mA. For phase identification, a PDF-2 database (2012) was used.

The variables relevant for the precipitating nanoclusters and crystals on the microfibers are listed and explained in Table 1. Although the fiber appears to be a non-reactive component in the precipitation reaction, it plays an important but indirect role in the supersaturation of the solution, in addition to its ability to assist nucleation. This is explained as follows. The $Ca(OH)_2$/fiber ratio at a given ash content and a given amount of fiber is decided by the targeted filler (PCC) content of the fiber-PCC composite material according to the following equation, derived from the T 211 om-02 ash definition in TAPPI.

$$m_{Ca(OH)_2} = \frac{Ash,\% \cdot (B-A)}{100 - Ash,\%} \cdot 0.7402 \qquad \textit{(eq. 1)}$$

where A is the weight of targeted PCC ash, and B is the weight of the test specimen so that B - A is the weight of fiber. The constant 0.7402 is the ratio of the molar masses of $Ca(OH)_2$ and $CaCO_3$, to translate the targeted weight of PCC ash to the weight of $Ca(OH)_2$.

In the batch system used, increasing fiber concentration increases $Ca(OH)_2$ concentration when the targeted ash content is kept at constant. An increase in $Ca(OH)_2$ concentration can in turn affect the degree of supersaturation and supersaturation profile of precipitating $CaCO_3$ and the ratio of ionic species in reaction by providing reactive (dissolved) material for the reaction in higher concentration due to e.g. increased dissolution via increase in $Ca(OH)_2$ surface area per volume unit.

An important consequence is that when the "same" batch process is used for different targeted PCC ash contents by simply changing the amount of added $Ca(OH)_2$ and perhaps the CO_2 feed, the PCC properties and thus the fiber furnish properties may change. Even if all the process parameters were changed so that the ratios were truly fixed, the precipitation process would still change with a change in the amount of $Ca(OH)_2$ added, as the driving force for precipitation is supersaturation that under given conditions depends on the concentration of the precipitating species. Changing the fiber concentration in order to fix the $Ca(OH)_2$ concentration would, instead, change the surface area of fiber per volume unit. This change can potentially be significant, since it has been shown that the specific surface area of fiber might affect $CaCO_3$ precipitation on the fiber (Silenius 2002).

Table 1: Variables investigated and units used. Ratios are calculated using the units given in the table

Variable	Clarification
$Ca(OH)_2$ concentration	Calcium hydroxide concentration in reaction mixture wt%, of batch before precipitation; 0.7–4.1
Microfiber concentration	Microfiber concentration in reaction mixture wt%, of batch before precipitation; 0.5–6.0
CO_2 feed	Carbon dioxide feed l/min, at 20 °C; 0.5–6.0
PAA concentration	Concentration of additive Na-PAA wt%, of fiber; 0–100
$Ca(OH)_2/CO_2$	Ratio of calcium hydroxide concentration to carbon dioxide feed wt%/l/min; 0.1–8.2
$Ca(OH)_2$/fiber	Ratio of calcium hydroxide concentration and fiber concentration, wt%/wt%; 1.45–3.31
PAA/$Ca(OH)_2$	Ratio of additive concentration to calcium hydroxide concentration (wt%/wt%)

3. Results and discussion

3.1 Effect of microfiber concentration and CO_2 feed

$CaCO_3$ was precipitated onto microfibers without polymeric additives at 5 different fiber concentrations, *viz*. 0.5, 1.0, 2.0, 3.0 and 6.0 wt%. The targeted $Ca(OH)_2$ concentration was 69 wt% based on ovendry fiber, giving 48.2% mineral filler content for the material if fully reacted. The precipitation gave on average 46.3 wt% ash (mineral filler) content measured on unfiltered samples. In this case, mineral filler content and ash content are synonymous, since microfiber gave less than 0.0% ash. The obtained ash from the PCC containing samples gave a 91 mol% conversion efficiency of $Ca(OH)_2$, based on weight loss (TAPPI standards T 211 om-02 and T 413 om-11 in conjunction), assuming that the lime milk was essentially free from impurities or reaction products such as $CaCO_3$.

The size of the PCC particles deposited onto fiber surfaces was found to decrease with decreasing ratio of fiber (wt%) to carbon dioxide (l/min), and with increasing fiber concentration when the fiber-tocarbon dioxide was kept as constant. The difference was most obvious when investigating the agglomerates of PCC deposited on the surface of fiber seen as ellipsoidal particles or less systematically aggregated/ agglomerated particles covering fiber surfaces, seen in Fig. 2. Figure 2a, b show samples with the same CO_2 feed but prepared at different fiber concentrations (i.e. $Ca(OH)_2/CO_2$ was changed, as the target PCC ash content was fixed). Ellipsoidal PCC structures were found in both samples but for sample shown in Fig. 2b, it appears that the fiber surface was not as well covered and that the ellipsoidal particles were larger compared to samples shown in Fig. 2a. Figure 2b, c, on the other hand, were prepared with same fiber concentration, but for sample shown in Fig. 2c, CO_2 feed was increased in such a way to attain same $Ca(OH)_2/CO_2$ ratio as for sample shown in Fig. 2b. The ellipsoidal PCC structures formed in sample shown in Fig. 2c were clearly smaller than those obtained for sample shown in Fig. 2b. In addition, the fiber surface was more evenly covered, although locally the deposited PCC on fiber surface indication

agglomerates forming irregularly shaped PCC particles. This change was presumably caused by an increase in fiber surface area per unit volume, and higher degree of supersaturation in the system.

Notably much of the difference in observed PCC particle sizes was due to aggregation and agglomeration of nano-sized crystals that form ellipsoidal particles at low microfiber concentrations, rather than to the size of individual crystals (see magnifications in Fig. 2). When the fiber concentration was increased from 1.0 to 3.0 wt% at a constant CO_2 feed (0.5 l/ min), the morphology of the PCC particles was slightly altered and many of the particles precipitated onto the microfibers were larger (similar with the ones in Fig. 2b), which is attributed to more intensive agglomeration of the nano-size particles, which, again, was in line with results presented by Subramanian et al. (2007), who denoted similar structures as colloidal PCC (c-PCC). Moreover, increasing the CO_2 feed from 0.5 to 6.0 l/min for the suspension containing 0.5 or 1.0 wt% microfiber did not lead to any detectable change in the morphology of the PCC particles. Instead, when the CO_2 feed was increased in batches containing 3.0 wt% or more fiber, the particle size decreased as can be seen in Fig. 2b, c. Therefore, the changes in aggregation and agglomeration resulted in a more even PCC distribution on the fiber surface and a better coverage of the fiber, decreasing the amount of ellipsoidal PCC structures. Both increased fiber concentration and sufficiently high CO_2 feed were required to obtain these effects.

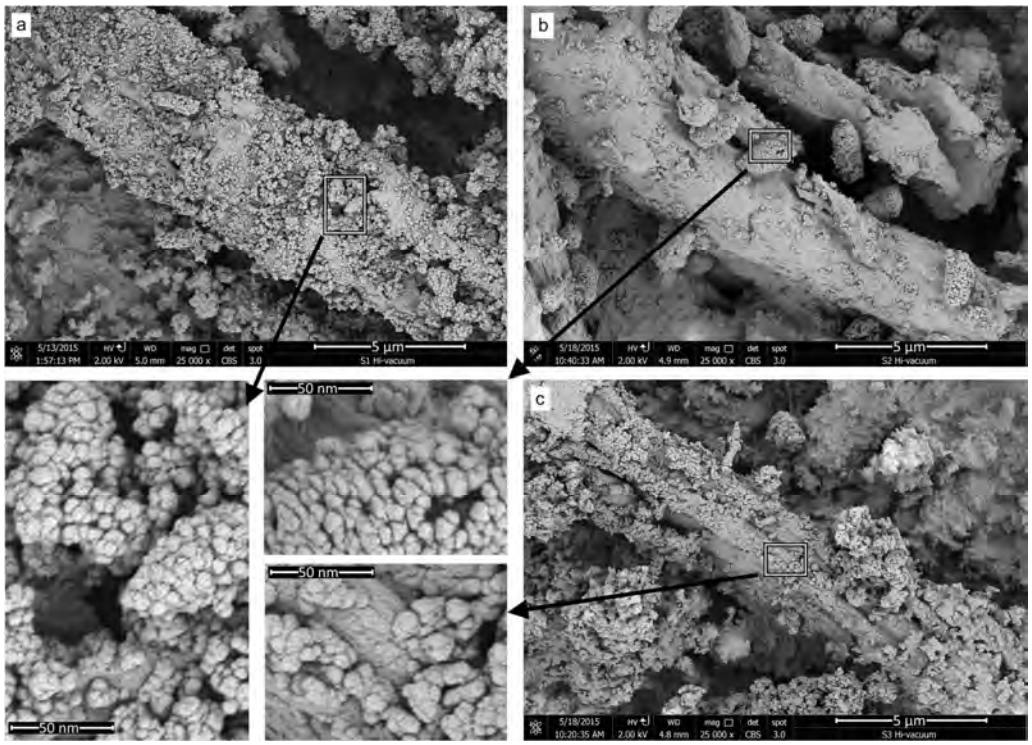

Fig. 2 $CaCO_3$ precipitated on microfiber with targeted ash of 48.2% using a 1.0 wt% fiber concentration and 0.5 l/min CO_2 feed, b 3.0 wt% fiber concentration and 0.5 l/min CO_2 feed, c 3.0 wt% fiber concentration and 1.5 l/min CO_2 feed

Figure 3 shows SEM micrographs of the ash obtained from the microfiber-PCC–PAA samples combusted at 525 ± 25 °C. At low PAA/$Ca(OH)_2$ ratios, PCC particles were uniform in size with a symmetrical, spherical or ellipsoid morphology similar with the morphology obtained without PAA. With increasing PAA/$Ca(OH)_2$ ratio, the particles became non-uniform, developing a "molten" appearance linked with liquid precursors of $CaCO_3$ (Gower and Odom 2000). Especially at 50 and 100 wt% PAA concentrations, the particles formed large polycrystalline aggregates with curved shapes, also linked with the formation of crystals via PILPs and ACC (Gower and Odom 2000). Because of low ash content, these "molten" appearances were most clearly seen in SEM micrographs of the ash, such as Fig. 3, but the development can also be seen when PCC locates on fiber (see Figs. 2, 5).

When, at a PAA concentration of 3.0 wt%, the addition of $Ca(OH)_2$ was increased from 32 to 69 wt%, no obvious differences were seen in the PCC particles on the microfibers. The morphology of the particles determined after combustion, on the other hand, showed an increase in particle regularity with increasing $Ca(OH)_2$ concentration above 41 wt%. The particle irregularity increased when the PAA/$Ca(OH)_2$ ratio increased, which agrees with results presented by e.g. Yu et al. (2004) who concluded that PAA/$CaCO_3$ ratio has a more pronounced effect on the $CaCO_3$ morphology than on the concentration of the $CaCO_3$ formed.

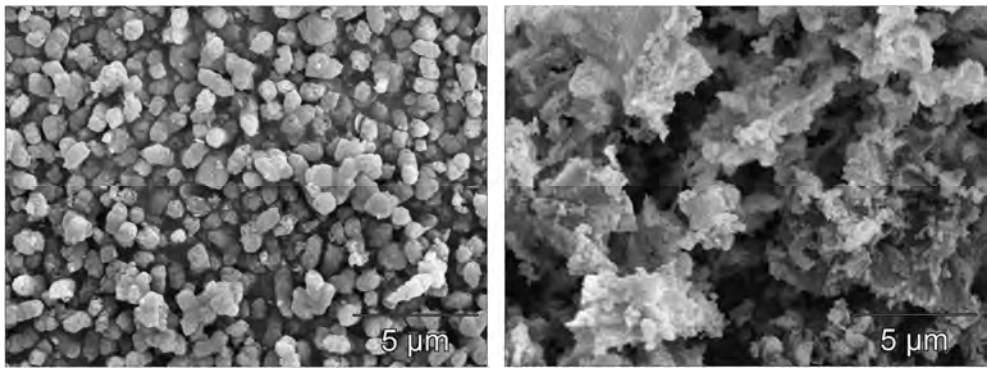

Fig. 3 SEM micrographs of the ash (PCC), precipitated in presence of PAA. PAA/$Ca(OH)_2$ was 1.4 (at left) and 72.5 (at right). PAA additions corresponding to 1 and 50 wt% of fiber, respectively

Figure 4 shows pH of the suspension as function of time upon CO_2 dosage and subsequent carbonation and its dependence on the fiber concentrations. At low fiber concentrations, pH dropped quite rapidly at constant CO_2 feed, especially at the beginning of the experiment, followed by an increase in the pH value. When increasing the fiber concentration (at constant ash content target), the inflection point occurred later. The behavior was attributed to the heterogeneous nucleation meachanism as suggested by Subramanian (2008), according to which the $Ca(OH)_2$ particles are initially covered with an intermediate ACC phase, resulting to inhibited dissolution of $Ca(OH)_2$ that is responsible for the observed drop in pH. Thereafter, following the same mechanism of nucleation and crystal growth, the ACC particles are thought to leave the $Ca(OH)_2$ surfaces, opening them for further

dissolution and resulting an increase in pH. The ACC leaving the surface was thought to aggregate in line-like structures that lead to the ellipsoidal c-PCC particles as described and obtained by Subramanian (2008), which also were seen in this study, or distributed more evenly on fiber surfaces. The change in PCC distribution on fiber surfaces was thought to result from the increasing fiber concentration and increasing available surface area of fiber, which resulted in the interaction between the microfiber particles and the formded ACC. This was suspected to disturb the ACC chain formation. Therefore, when ACC transformed to a crystalline polymorph, the morphology of the precipitate was altered to follow the modified ACC distribution, or the ACC crystallized after forming smaller particles or shorter chains.

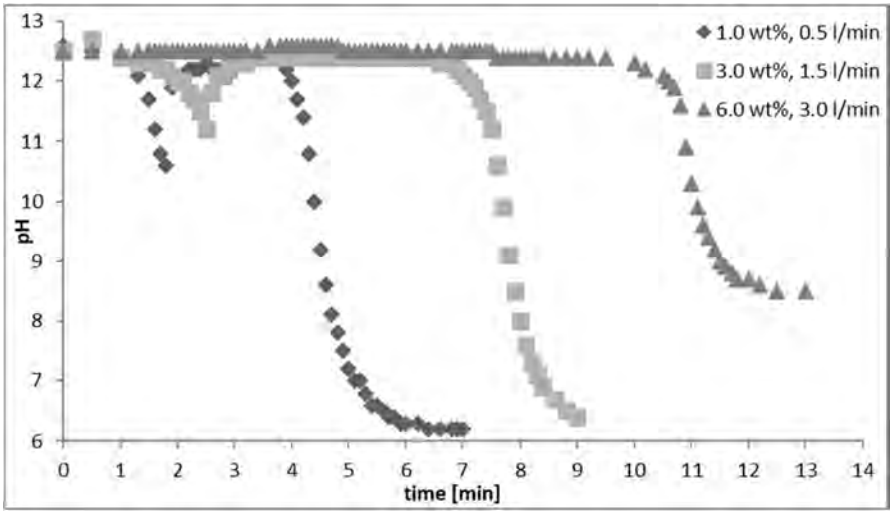

Fig. 4 pH as a function of time during carbonation of samples having different fiber concentrations

3.2 The effect of Sodium Polyacrylic Acid (PAA) as precursor stabilizer

The results from fiber-PCC samples made in presence of PAA are summarized in Table 2 and Fig. 5. The results show that at a microfiber concentration of 1.0 wt% and a $Ca(OH)_2$ concentration of 69 wt%, an increase in PAA concentration initially resulted in an increase in PCC particle size. The SEM images (Fig. 5) show that this was due to increased agglomeration and nanoparticle cluster formation. The ability of PAA to inhibit nucleation in bulk solution may have contributed to this process by supporting aggregate growth. The PCC particles formed were elongated and had a rice-like shape (PAA concentration 0.5 wt%), similar to those seen in Fig. 5c, but slightly larger. At PAA concentrations 1.0 and 3.0 wt%, the PCC crystals were rounder, see Fig. 5b. The difference was probably caused by temporary ACC stabilization by PAA, but this was not confirmed. Matahwa et al. (2008) obtained similar $CaCO_3$ particles when precipitating in presence of PAA, and these were ascribed to an ACC-PAA gel similar to that obtained by Ulčinas et al. (2007). They describe the formation of a viscous ACC gel temporarily stabilized by PAA, which precipitates into more stable polymorphs after losing its stability.

Surprisingly, the effect of PAA at a microfiber concentration of 3.0 wt% was opposite to that at 1.0 wt%. With increasing

dosage of PAA from 0.3 to 3.3 wt%, the PCC crystal size increased, and crystals became elongated. The crystals retained their elongated shape but the crystal size increased when the PAA concentration was increased further. At very low and fixed PAA concentrations (0.06 wt%) and a microfiber concentration of 3.0 wt% an increase in $Ca(OH)_2$ from 32 to 69 wt% led to a significant decrease in the PCC crystal particle size. A clear region of morphology transition was seen at a $Ca(OH)_2$ concentration between 51 and 69 wt%, where the particle morphology changed from approximately 1 micron roundish crystals to more elongated PCC crystals with a greater aspect ratio (length ca. 1 µm and width 0.2 µm). At 32 wt% $Ca(OH)_2$ addition, the crystals were more elongated at a microfiber concentration of 6.0 wt% that at 3.0 wt%. An Increase in microfiber concentration from 3.0 to 6.0 wt% resulted in a morphology transition between 32 and 51 wt% of $Ca(OH)_2$ addition.

However, when the concentration of PAA was increased to 10.0 wt%, it was found that the particle size and amounts of large PCC crystals and clustered PCC agglomerates deposited on the microfibers decreased significantly, but that a few individual nano-sized PCC crystal particles were still formed and present on the microfiber surface (not shown here). Figure 5a shows that when the PAA concentration was increased further to 100.0 wt%, crystal formation of PCC on the surface of the microfiber was inhibited, which was confirmed by a lower ash content in samples rinsed before drying.

The ash contents of some of microfiber–PAA–$CaCO_3$ complexes (rinsed before drying) were clearly lower than unreacted $Ca(OH)_2$ should yield. This can only be explained by the removal of soluble compounds or nanocrystals in bulk solution during filtering of the samples through the 0.6 µm membrane and subsequent rinsing. A pronounced loss of crystalline material during filtration should mean that an increased dose of PAA would facilitate bulk solution precipitation, instead of decreasing it as stated frequently in the literature (Hosoda and Kato 2001; Huang et al. 2007; Watamura et al. 2014). A possible alternative is heterogeneous nucleation in bulk solution, improved by PAA addition in a manner similar to that in which the addition of PAA can improve crystallization on cellulosic fibers, i.e. via electrostatic interaction between calcium ions and anionic groups of the polyelectolyte (PAA) and foreign particles. Bulk solution precipitation is not, however, supported by the filtrate collected in these experiments, since the filtrate was transparent, which suggests an absence of crystalline material and the presence of amorphous transparent ACC as reported in the literature (Gower and Odom 2000; Mohamadzadeh-Saghavaz et al. 2013), or a complex. The formation of an electrostatic complex between carboxyl groups and calcium ions is frequently described in the literature (Hosoda and Kato 2001; Huang et al. 2007; Ouhenia et al. 2008; Ulcˇinas et al. 2007; Watamura et al. 2014) and ascribed to the formation of an ACC-containing gel (Matahwa et al. 2008; Ulčinas et al. 2007) suggesting that role of the PAA in the system is the stabilization of ACC or the formation of a precursor or complex, or both.

At low PAA concentration, the mechanism of nucleation was thought to follow the one seen in experiments made without PAA. This was supported by the similar morphologies of the precipitate obtained for c-PCC (see Figs. 2, 5b, c for comparison), and and by the similar but not the excact same pH development trends obtained during experiments. With PAA, the intermediate increase of pH, attributed to ACC dissolution or removal from $Ca(OH)_2$, was delayed. Interestingly, ellipsoidal or roundish morphologies could be achieved at higher fiber concentrations compared to corresponding sample free from PAA. In particular, the pH development measured during carbonation indicate ACC stabilization or formation of PILP and a subsequent conversion to a crystalline polymorph onto fiber surface,

which could be interpreted as heterogeneous nucleation.

Table 2: Results of the PCC-PAA-Microfiber experiments. PAA concentration is given as wt-% of the fiber content.

Microfiber concentration [wt-%]	$Ca(OH)_2$ addition [wt-%]	PAA concentration [wt-%]	PCC morphology and size	
			Low PAA conc.	High PAA conc.
1	69	0.1; 0.5; 1.0; 3.0; 10.0; 50.0; 100.0	Elongated	Round, irregular Reduced particle size
	32; 41; 51; 60; 69	3.0	Elongated	Elongated-irregular
3	69	0.3; 1.0; 2.0; 3.3	Round	Elongated Increased particle size
	32; 51; 69	6.0	Slightly elongated	Elongated Reduced particle size
6	32; 51	1.0	Elongated	Reduced particle size

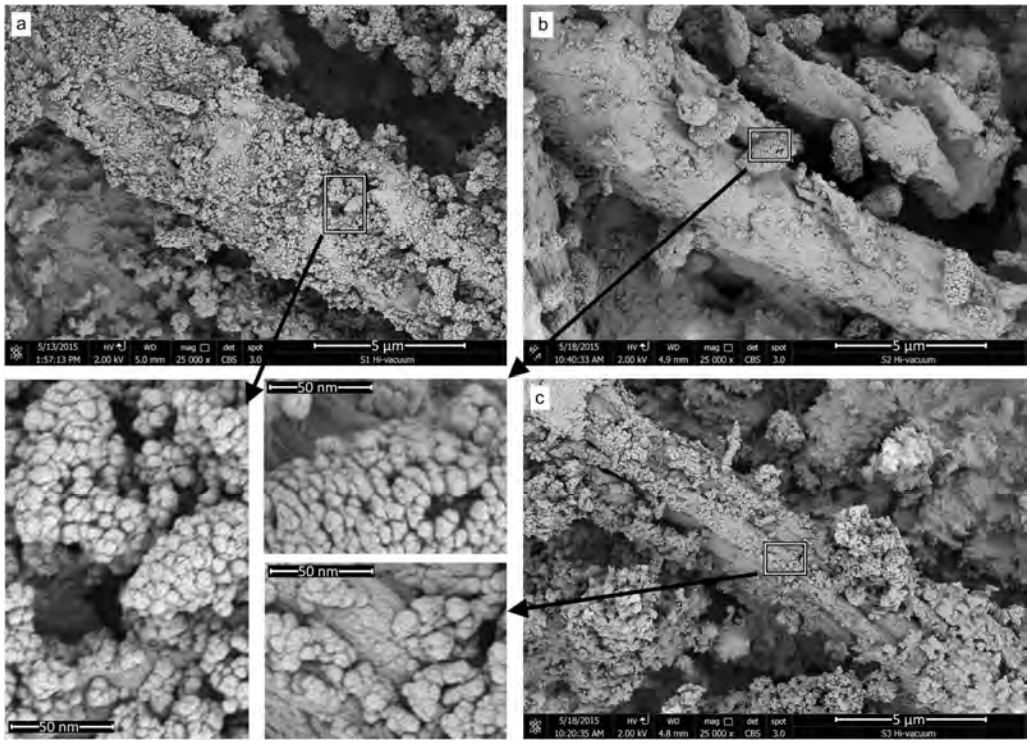

Fig. 5 $CaCO_3$ precipitated on microfiber in presence of PAA concentration: a) 100.0 wt-% b) 3.0 wt-% and c) 1.0 wt-%. The microfiber concentration was 1.0 wt-% (A), 1.0 wt-% (B), and 3.0 wt-% (C), respectively. Note that PAA concentration is given as wt-% of fiber addition

3.3 XRD and TGA

Ten microfiber-PCC samples, with and without precipitated calcium carbonate, were characterized using XRD. Diffractograms were collected in the 2h range of 13°–48°. XRD patterns are shown in Fig. 6 and summarized in Table 3.

Figure 6 shows different crystalline forms of cellulose, with slight peak shifts between some of them. The main peak for cellulose, located at 20°–22° (Haleem et al. 2014; Obi Reddy et al. 2014; Tibolla et al. 2014), was found in samples 0, 5 and 6, where it is quite sharp, but the calcite peak located at the same angle makes it difficult to reliably determine the presence of crystalline cellulose in the samples. However, a smaller peak originating from cellulose at 34.6° was clearly observed in all the diffractograms except those for samples 1 and 3. The presence of cellulose I_α in these two samples was therefore considered as possible. In the case of the fiber reference sample, the co-existence of cellulose I_α and cellulose I_β was suspected.

The only $CaCO_3$ polymorph observed in the samples was calcite, although some PAA with different molecular weights have been linked with the formation of aragonite in the literature (Ouhenia et al. 2008; Watamura et al. 2014). Calcite peaks (Kim et al. 2013; Kirboga et al. 2014; Lo´pez-Periago et al. 2010) were observed in all samples except for the 0 (the fiber reference) and 5 and 6 ($Ca(OH)_2$ 69 wt%, CO_2 feed 0.5 l/min and PAA concentrations 50.0 and 100.0 wt%). The ash contents (525 ± 25 °C) for samples 5 and 6were 8.2 and 4.0%, respectively, confirming that samples 5 and 6 clearly contained sufficient ash to be detectable in the XRD measurement.

For sample 5 and 6, the absence of both crystalline $Ca(OH)_2$ and crystalline $CaCO_3$ suggests that the high PAA concentration in the samples led to the formation and stabilization of amorphous $CaCO_3$. The unstable character of amorphous ACC is well known, but no phase transition to a crystalline material detectable with XRD as observed, despite the long delay time between the precipitation experiments and the XRD measurements, even though particulate matter residing on the fibers was observed with SEM and the ash content of the samples showed that the concentration of inorganics was detectable with XRD, if crystalline. Huang et al. (2008) suggested that PAA might inhibit the formation of crystalline particle, leading to PCC agglomerates formed through a spherulitic growth mechanism. They also suggested that the increase in the stability of ACC was due to a polyelectrolyte complexation with the calcium ion, causing a more disordered structure within an intermediate range ordering.

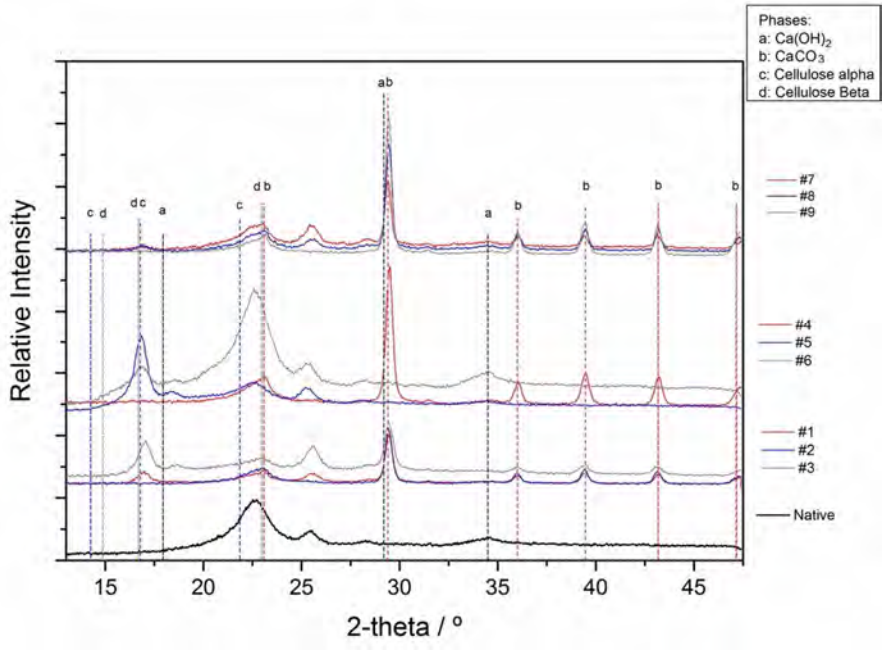

Fig. 6 XRD patterns for the samples. Sample description and pattern interpretations are listed in Table 3

Table 3: XRD results.

Sample number and description		Cellulose I	PCC
Fiber reference	0 - Microfiber, untreated	α, β	-
No PAA	1 - fiber 1 wt-% CO_2 feed 0.5 l/min	β (possible)	Calcite
	2 - fiber 3 wt-% CO_2 feed 0.5 l/min	β	Calcite
	3 - fiber 3 wt-% CO_2 feed 1.5 l/min	β (possible)	Calcite
$Ca(OH)_2$ 69 wt-% CO_2 feed 0.5 l/min	4 - PAA 1.0 wt-%	β	Calcite
	5 - PAA 50.0 wt-%	β	-
	6 - PAA 100.0 wt-%	β	-
PAA 3.3 wt-% CO_2 feed 0.5 l/min	7 - $Ca(OH)_2$ 32 wt-%	β	Calcite
	8 - $Ca(OH)_2$ 51 wt-%	β	Calcite
	9 - $Ca(OH)_2$ 69 wt-%	β	Calcite

Table 4 shows the results of the thermogravimetric measurements. The data (550 and 925 °C) were used to estimate the conversion yield and possible residual $Ca(OH)_2$. The results indicate that all the samples contained unreacted $Ca(OH)_2$, the

amount of $Ca(OH)_2$ in the samples being typically ca. 5 wt% of the inorganic species, with the notable exception of sample 5 which was formed in the presence of a high PAA concentration of 50 wt%. The result is approximately in line with the conversion estimate from the TAPPI ash content measurements. The remaining $Ca(OH)_2$ was not, however, identified in the XRD analysis, suggesting either that the material was not crystalline or that it resided in $CaCO_3$ particles or microfibers, too far from the particle surfaces to be determined by the method. On the other hand, the TGA resultsmay also interfere with the release of physisorbed water at 525 °C and at higher temperature the possible dihydroxylation of $Ca(OH)_2$ (Renaudin et al. 2008).

Table 4 TGA results of samples. Sample numbering follows that of Table 3. For samples 10 and 11, see the footnotes.

Property	**Method/basis**	**Unit**	**1**[a]	**2**	**3**	**5**	**6**	**10**[b]	**11**[c]
Dry matter (105 °C)	TGA (105 °C)	%	98.2	97.72	97.97	94.87	97.48	98.02	98.06
Ash content (550 °C)	TGA (550 °C)	%, dry basis	44.2	30.5	45.5	7.8	36.9	44.8	45.6
Ash content (925 °C)	TGA (925 °C)	%, dry basis	26.4	17.7	26.4	4.9	21.0	25.9	26.4
[$CaCO_3$]	Theoretical (TGA 550 and 925 °C)	%, dry basis	40.6	29.0	43.4	6.6	36.0	43.0	43.8
[$Ca(OH)_2$]	Theoretical (TGA 550 and 925 °C)	%, dry basis	4.8	1.9	2.7	1.5	1.2	2.3	2.4
[$Ca(OH)_2$]	Theoretical	%, inorganic species	10.6	6.2	5.9	18.7	3.1	5.1	5.2

[a] Not taken at the end of the process and therefore holds a larger proportion of $Ca(OH)_2$

[b] Microfiber concentration 3 wt-%, PAA concentration 1.0 wt-%

[c] Microfiber concentration 3 wt-%, PAA concentration 0.3 wt-%

4. Conclusions

In the papermaking field, PCC morphology and particle size are important factors governing filler performance. Morphology control is therefore an important factor in in situ precipitation, but, to our knowledge, little effort has been made to improve PCC morphology control in cellulosic fiber-$Ca(OH)_2$–CO_2 systems, and the effect of PAA for this or another purpose has not been investigated. In this work, in situ precipitation of PCC onto cellulosic microfiber in the presence of PAA was performed using a batch reactor. The reaction between carbon dioxide and calcium hydroxide was varied to give different PCC morphologies depending on the concentrations of microfiber and PAA. It was demonstrated that the morphology of the PCC

particles formed on the microfiber can be altered by changing the process parameters and the concentrations of calcium hydroxide and PAA

surface with and without PAA depended on process conditions. The effect of the precipitation conditions on the PCC crystal size and size distribution was not clear since PCC nanocrystals had a strong tendency to agglomerate. The fiber concentration in the reactor was found to be very critical, wether PAA was used or not. This was partly ascribed to the degree of supersaturation during precipitation, and to aggregation and agglomeration of $CaCO_3$ that were clearly affected by changes in fiber concentration. The concentrations of $Ca(OH)_2$ and PAA and the ratio of the species were also important, while their effect was not fully distinguishable from the effects of fiber concentration, due to implications of Eq. 1 (discussed under "Materials and methods"). The same applies for CO_2 feed and its effect on the precipitate.

The presence of an unstable ACC phase at beginning of the precipitation was suspected based on the behavior of the pH and on reports in the literature. The use of high concentration of PAA revealed the probable formation of an ACC compound stable for a time of many months, which was supported by a combination of SEM imaging and XRD analysis.

5. Acknowledgements

Stora Enso Oyj is acknowledged for financial support of the project. Dr Anthony Bristow is thanked for linguistic revision of the work. Senior specialist Kimmo Velling is acknowledged for providing SEM images and for the TGA analysis.

6. References

Alince B, Bednar F (2003) Role of cationic polyacrylamide in fiber-$CaCO_3$ pigment interactions. J Appl Polym Sci 88:2409–2415

Burgess MS, Philipps JS, Xiao H (2000) Flocculation of PCC induced by polymer/microparticle systems: floc characteristics. Nordic Pulp Paper Res J 15(5):572–578

Butler M, Glaser N, Weaver A, Kirkland M, Heppenstall-Butler M(2006) Calcium carbonate crystallization in the presence of biopolymers. Cryst Growth Des 6(3):781–794

Ciobanu M, Bobu E, Ciolacu F (2010) In-situ cellulose fibres loading with calcium carbonate precipitated by different methods. Cellul Chem Technol 44(9):379–387

Cölfen H, Antonietti M (2008) Mesocrystals and nonclassical crystallization. Wiley, Chichester

Gebauer D, Oliynyk V, Salajkova M, Sort J, Zhou Q, Bergström L, Salazar-Alvarez G (2011) A transparent hybrid nanocrystalline cellulose and amorphous calcium carbonate nanoparticles. Nanoscale 3:3563–3566

Gower L, Odom D(2000) Deposition of calcium carbonate films by a polymer-induced liquid-precursor (PILP) process. J Cryst Growth 210:719–734

Haleem N, Arshad M, Shahid M, Tahir M (2014) Synthesis of carboxymethyl cellulose from waste of cotton ginning industry. Carbohydr Polym 113:249–255

Hardikar V, Matijevic´ E (2001) Influence of ionic and nonionic dextrans on the formation of calcium hydroxide and calcium carbonate particles. Colloids Surf A 186:23–31

Hosoda N, Kato T (2001) Thin-film formation of calcium carbonate crystals: effects of functional groups of matrix polymers. Chem Mater 3:688–693

Hu Z, Deng Y (2004) Synthesis of needle-like aragonite from calcium chloride and sparingly soluble magnesium carbonate. Powder Technol 140:10–16

Huang S-C, Naka K, Chujo YA (2007) Carbonate controlledaddition method for amorphous calcium carbonate spheres stabilized by poly(acrylic acid)s. Langmuir 23:12086–12095

Huang S-C, Naka K, Chujo Y (2008) Effect of molecular weights of poly(acrylic acid) on crystallization of calcium carbonate by the delayed addition method. Polym J 40(2):154–162

Jada A, Ait Akbour R, Jacquemet C, Suau J, Guerret O (2007) Effect of sodium polyacrylate molecular weight on the crystallogenesis of calcium carbonate. J Cryst Growth 306:373–382

Kellermeier M, Melero-García E, Glaab F, Klein R, Drechsler M, Rachel R, García-Ruiz J, Kunz W (2010) Stabilization of amorphous calcium carbonate in inorganic silica-rich environments. J Am Chem Soc 132:17859–17866

Kim H, Park S, Han J, Lee H (2013) Microbially mediated calcium carbonate precipitation on normal and lightweight concrete. Constr Build Mater 38:1073–1082

Kirboga S, Oner M, Akoyl E (2014) The effect of ultrasonication on calcium carbonate crystallization in the presence of biopolymer. J Cryst Growth 401:266–270

Kitamura M, Konno H, Yasui A, Masuoka H (2002) Controlling factors and mechanism of reactive crystallization of calcium carbonate polymorphs from calcium hydroxide suspensions. J Cryst Growth 236:323–332

Klungness J, Caulfield D, Sachs I, Tan F, Sykes M, Shilts R (1994) Fiber-loading: a progress report. In: Proceedings of the 1994 TAPPI recycling symposium. TAPPI, Boston, pp 283–290

Klungness J, Sykes M, Tan F, Abubakr S, Eisenwasser J (1996) Effect of fiber loading on paper properties. Tappi J 79(3):297–301

Klungness J, Tan F, Aziz S, Sykes M (1997) Retention of calcium carbonate during recycling: direct loading versus fiber loading. In: Environmental conference and exhibit book 1. TAPPI, Atlanta, pp 497–503

Klungness J, Ahmed A, Ross-Sutherla N, AbuBakr S (2000) Lightweight, high-opacity paper by fiber loading: filler comparison. Nord Pulp Pap Res J 15(5):345–350

Kumar P, Gautam S, Kumar V, Singh S (2009) Enhancement of optical properties of bagasse pulp by in situ filler precipitation. BioResources 4(4):1635–1646

Kumar P, Negi Y, Singh S (2011) Filler loading in the lumen or/ and cell wall of fibers—a literature review. BioResources 6(3):3526–3546

López-Periago A, Pacciani R, Cracı´a-Gonza´lez C, Vega L, Domingo CA (2010) Breakthrough technique for the preparation of high-yield precipitated calcium carbonate. J Supercrit Fluids 52:298–305

Matahwa H, Ramiah V, Sanderson R (2008) Calcium carbonate crystallization in the presence of modified polysaccharides and linear polymeric additives. J Cryst Growth 310:4561–4569

Mohamadzadeh-Saghavaz K, Resalati H, Mehrabi E (2013) Characterization of cellulose–PCC composite filler synthesized from CMC and BSKP fibrils by hydrolysis of ammonium carbonate. Powder Technol 246:93–97

Mohamadzadeh-Saghavaz K, Resalati H, Ghasemian A (2014) Cellulose-precipitated calcium carbonate composites and their effect on paper properties. Chem Pap 68(6):774–778. doi:10.2478/s11696-013-0513-7

Nielsen J, Sand K, Pedersen C, Lakshtanov L, Winther J, Willemoës M, Stipp S (2012) Polysaccharide effects on calcite growth: the influence of composition and branching. Cryst Growth Des 12:4906–4910

Obi Reddy K, Zhang J, Zhang J, Varada Rajulu A (2014) Preparation and properties of self-reinforced cellulose composite films from Agave microfibrils using an ionic liquid. Carbohydr Polym 144:537–545

Ouhenia S, Chateigner D, Blekhir M, Guilmeau E, Krauss C (2008) Synthesis of calcium carbonate polymorhs in the presence of polyacrylic acid. J Cryst Growth 310:2832–2841

Park W, Ko S-J, Lee S, Cho K-H, Ahn J-W, Han C (2008) Effects of magnesium chloride and organic additives on the synthesis of aragonite precipitated calcium carbonate. J Cryst Growth 310:2593–2601

Penttilä A, Sievänen J, Torvinen K, Ojanpera¨ K, Ketoja JA (2012) Filler-nanocellulose substrate for printed electronics: experiments and model approach to structure and conductivity. Cellulose 19:821–829

Rantanen J, Dimic-Misic K, Kuusisto J, Maloney TC (2015) The effect of micro and nanofibrillated cellulose water uptake on high filler content composite paper properties and furnish dewatering. Cellulose 22:4003–4015

Renaudin G, Bertrand A, Dubois M, Gomes S, Chevalier P, Labrosse P (2008) A study of water releases in ground (GCC) and precipitated (PCC) calcium carbonates. J Phys Chem Solids 69:1603–1614

Shen J, Song Z, Qian X, Liu W (2009) Modification of papermaking grade fillers: a brief review. BioResources 4(3):1190–1209

Silenius P (1996) Preparation of filler containing papermaking materials by precipitating calcium carbonate in situ in the presence of cellulosic materials. Lic.Sc.(Tech.) Thesis, Lappeenranta university of technology

Silenius P (2002) Improving the combinations of critical properties and process parameters of printing and writing papers and paperboards by new paper-filling methods. Ph.D. Dissertation (Tech.), Helsinki University of Technology

Subramanian R (2008) Engineering fine paper by utilising the structural elements of the raw materials. Ph.D. Dissertation (Tech.), Helsinki University of Technology

Subramanian R, Fordsmand H, Paulapuro H (2007) Precipitated calcium carbonate (PCC)-cellulose composite fillers; effect of PCC particle structure on the production and properties of uncoated fine paper. BioResources 2(1):91–105

Tibolla H, Pelissari F, Menegalli F (2014) Cellulose nanofibers produced from banana peel by chemical and enzymatic treatment. LWT Food Sci Technol 59:1311–1318

Torvinen K, Sieva¨nen J, Hjelt T, Helle´n E (2012) Smooth and flexible filler-nanocellulose composite structure for printed electronics applications. Cellulose 19:821–829

Ulčinas A, Butler M, Heppenstall-Butler M, Singleton S, Miles M(2007) Direct observation of spherulitic growth stages of$CaCO_3$ in a poly(acrylic acid)–chitosan system: in situ SPM study. J Cryst Growth 307:378–385

Vdovič N, Kralj D (2000) Electrokinetic properties of spontaneously precipitated calcium carbonate polymorphs: the influence of organic substances. Colloids Surf A 161:499–505

Volkmer D, Harms M, Gower L, Ziegler A (2005) Morphosynthesis of nacre-type laminated $CaCO_3$ thin films and coatings. Angew Chem Int Ed 44:639–644. doi:10.1002/ anie.200461386

Watamura H, Sonobe Y, Hirasawa I (2014) Polyacrylic acidassisted crystallization phenomena of carbonate crystals. Chem Eng Technol 37(8):1422–1426. doi:10.1002/ceat. 201400017

Wei H, Shen Q, Zhao Y, Zhou Y, Wang D, Xu D (2005) On the crystallization of calciumcarbonate modulated by anionic surfactants. J Cryst Growth 279:439–446

Xu X, Han JK, Cho K (2004) Formation of amorphous calcium carbonate thin films and their role in biomineralization. Chem Mater 16:1740–1746

Yu J, Lei M, Cheng B, Zhao X (2004) Effects of PAA additive and temperature on morphology of calcium carbonate particles. J Solid State Chem 177:681–689

Zhang Z, Xie Y, Xu X, Pah H, Tang R (2012) Transformation of amorphous calcium carbonate into aragonite. J Cryst Growth 343:62–67

Publication II

Laukala, T., Backfolk, K., and Heiskanen, I.

Fractionation of pulp and precipitated $CaCO_3$–pulp composites: effects on sheet properties of selective $CaCO_3$ precipitation onto fiber size fractions

Reprinted with permission from
Cellulose
Vol. 28(9), pp. 5807–5826, 2021

The final publication is available at Springer via
http://dx.doi.org/10.1007/s10570-021-03856-0

Cellulose
https://doi.org/10.1007/s10570-021-03856-0

ORIGINAL RESEARCH

Fractionation of pulp and precipitated $CaCO_3$–pulp composites: effects on sheet properties of selective $CaCO_3$ precipitation onto fiber size fractions

Teija Laukala · Kaj Backfolk · Isto Heiskanen

Received: 22 December 2020 / Accepted: 29 March 2021

Abstract $CaCO_3$-pulp composite was prepared via precipitation of calcium hydroxide in the presence of pulp. In order to investigate the precipitation selectivity and mechanism, the substrate pulps and the obtained composites were fractionated (R30, R100, R200, R400 and a sedimented fraction that passed the 400 mesh wire) using a Bauer-McNett unit. The main fractionation criterion was therefore fiber length. The pulp used was CTMP (chemithermomechanical pulp), yielding a precipitated calcium carbonate-chemithermomechanical pulp (PCC-CTMP) composite with a targeted PCC-to-CTMP ratio of 1:1. The PCC consisted primarily of nano-sized primary particles which formed aggregates and clusters on the fibers. When the fiber morphology, zeta potential and surface charge density of the fractions were determined, a correlation was found between the surface charge density of the CTMP and the ash content of the corresponding PCC-CTMP fractions. This supports the hypothesis that the precipitation on the CTMP fiber is driven by the charge interparticle interaction. The use of refined CTMP furnishes and fractionation of the PCC-CTMP furnishes demonstrates that PCC is preferably fixed on fines and fibrils since it appears at a higher content in the fines fractions. Fiber activation via fiber split, removal of primary wall and surface defibrillation enhanced the affinity of the PCC for the fibrils. The laboratory handsheets prepared from the material demonstrated the importance of controlling the substrate fiber properties for the mineral-fiber composite, e.g. via refining, as differences between the refining levels and fractions were found to lead to differences in both optical properties and bonding.

T. Laukala (✉)
Lappeenranta-Lahti University of Technology Packaging technology of LUT School of Energy Systems, P.O. Box 20, 53850 Lappeenranta, Finland
e-mail: teija.laukala@lut.fi

K. Backfolk · I. Heiskanen
Stora Enso OyjResearch Center Imatra, 55800 Imatra, Finland

Published online: 11 May 2021

Graphic abstract

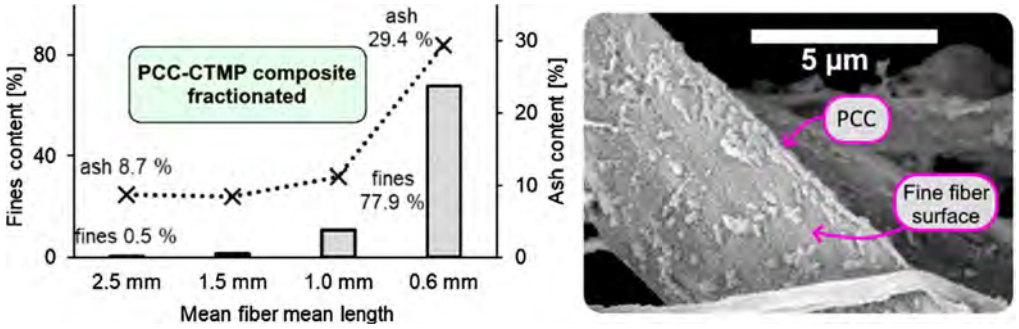

Keywords PCC · Precipitated calcium carbonate · CTMP · Improved filler · Composite filler · In-situ precipitation

Introduction

Calcium carbonate, $CaCO_3$, is a commonly used filler or pigment in many industrial applications including ceramics, composites, paints, plastics and paper. While the effects of typical fillers and filling mechanisms on paper properties are fairly well understood and widely discussed in the literature, e.g. by Hubbe and Gill (2016), work on different filler dosing concepts and modified fillers is still in progress and requires more attention. In a review paper by Shen et al. (2009), different approaches for filler modification were explored and discussed, for example the use of inorganic substances to improve acid tolerance, the use of organic polymers to enhance filler-fiber bonding, and filler modification with cellulose and cellulose derivatives. The traditional way of adding fillers has its limitations, and alternative concepts such as in-situ precipitation onto fibers or in-line precipitation have therefore recently gained interest.

One approach where $CaCO_3$ is used as a filler is through in-situ precipitation (IS-precipitation), i.e. the synthesis and precipitation of calcium carbonate (PCC) in the presence of the cellulosic fiber, where the conditions of precipitation can be controlled and adjusted so that the PCC is precipitates directly onto cellulosic material (Rantanen 2016; Silenius 2002; Subramanian 2008) or into the lumen and cell wall pores (Ciobanu et al. 2010; Fortuna et al. 2003). Mechanisms have been proposed to explain the PCC attachment onto the cellulose, but results and theories are controversial and there is still a lack of understanding of the fixation and adhesion mechanism. Subramanian (2008) suggested that the precipitation proceeds via an amorphous calcium carbonate (ACC) precursor which forms line-like aggregates on the cellulosic particles due to inter-particle interactions (due to polarization of the ACC particles), and is subsequently precipitated as calcite. Silenius (2002), on the other hand, suggested a heterogeneous nucleation based on classical crystallization theory. The crystallization on cellulose has been associated with the functional groups capable of binding metal ions (including Ca^{2+}), which is thought to lead to subcritical nuclei being formed on the cellulosic substrate, and subsequent nucleation (Dalas et al. 2000).

Silenius (2002) pointed out that the PCC precipitates mainly on the cellulosic fines due to the large surface area of the fines in comparison to that of the larger fibers. 'Fines' is usually defined as the material that passes the 200 mesh wire of Bauer McNett classifier (Heinemann and Vehniäinen 2009). Silenius' (2002) result has been supported by Seo et al. (2017). Wood pulp fines also contain more carboxyl groups, metal ions and negative charges than the larger fibers (Odabas et al. 2016). This suggests that the preferential precipitation of PCC onto fines may be partially due to the charged, metal-binding groups. The importance of functional groups has also been observed with synthetic polymers. For example, Lakshminarayanan et al. (2003) precipitated PCC in-situ onto both untreated and chemically treated

synthetic polyamide fibers (Nylon 66 and Kevlar 29) and reported that the nucleation density was greater on the treated fibers, confirming the importance of charged sites. On the other hand, recent findings have demonstrated that PCC can also be precipitated on essentially uncharged fibers such as bacterial nanocellulose (Stoica-Guzun et al. 2012) or polyvinyl alcohol fiber (Park et al. 2017).

The formation of the PCC-fiber composite makes it possible to create a novel platform of engineered fillers which may provide new features for the papermaking process and end products. The surface morphology and chemistry of the fibers are altered by the mineral precipitation process, which can be used to enhance the material property space and to control optical properties, fiber-fiber contacts and bonding in sheets. The effects on sheet properties have often been contradictory when filling is done using IS-precipitated $CaCO_3$. For example, sheet opacity has been reported to increase by Ciobanu et al. (2010), and to decrease by Klungness et al. (2000) and Kumar et al. (2009). The brightness has been reported to increase by Mohamadzadeh-Saghavaz et al. (2014) and to decrease by Klungness et al. (2000). Similarly, the tensile index has been reported to increase by Silenius (2002) and to decrease by Mohamadzadeh-Saghavaz et al. (2014).

One possible reason for the contradictory findings and statements is the use of different raw materials. A thorough review of the role of fiber source and particularly of the dependence on size fractions and fiber size in the precipitation mechanism and nucleation is lacking. Also identically performed IS-precipitation has been found to result in different PCC-fiber properties depending on the fiber source (Klungness et al. 2000).

In general, the presence of fines increases inter-fiber bonding in sheets. Fines affect many strength properties and especially the tensile strength (Odabas et al. 2016), although the strength-enhancing effect is greater with kraft fines than with mechanical fines (Retulainen et al. 1998). Light scattering, important for optical development of sheets, is instead increased by the presence of mechanical fines, while kraft fines tend to reduce it (Odabas et al. 2016). This is explained by the non-bonded surface of the mechanical fines (Leskelä 1998). The assumed preferential precipitation of PCC onto fines can be expected to alter the properties of the fines fraction more than those of the coarser fiber fractions. The preferential precipitation might reduce the strength-enhancing properties of the fines fraction, although the optical properties would be positively affected.

In the present work, PCC was precipitated onto refined and unrefined chemithermomechanical pulp (CTMP) in order to study the role of CTMP composition and the precipitation of PCC onto the CTMP fines. The CTMP pulp, at three different refining levels, was then used for in-situ PCC precipitation and for making PCC-CTMP composite filler. The PCC-CTMP composite fillers were subsequently fractionated in order to gain a further understanding of the selectivity and precipitation efficiency of PCC onto each fraction. The effect of the different PCC-CTMP fractions on sheet properties were evaluated. The CTMP fiber was chosen because of its broad fiber size distribution and sufficiently high fines content, while primary wall parts still attached to some of the fibers.

Materials and methods

The CTMP was provided by Stora Enso (Kaukopää mill Imatra, Finland) as air dry sheets, which were disintegrated and refined using a Valley beater (SCAN-C 25:96). The Schopper Riegler freeness values (SCAN C 19:65) of the pulps were 23 (0 min refined), 42 (30 min refined) and 58° SR (60 min refined). The fiber length distributions of the CTMP materials are shown in Fig. 1. The calcium hydroxide ($Ca(OH)_2$) was prepared from calcium oxide (CaO, Honeywell reagent, purity > 96 %).

Sample preparation

PCC-CTMP preparation

The three grades of PCC-CTMP were prepared by beating the pulp to three different levels. Each grade was prepared by reacting $Ca(OH)_2$ and carbon dioxide (CO_2 (AGA, purity ≥ 99.8 %)) in the presence of CTMP fibers in a 10 l open batch reactor. The reactor height was 50.6 cm and inner diameter 16.2 cm. The reactor was equipped with a gas outlet at the bottom and a stirrer with three impellers, 8.4 cm Roushton which was the lowest and two 8.5 cm pitched blade

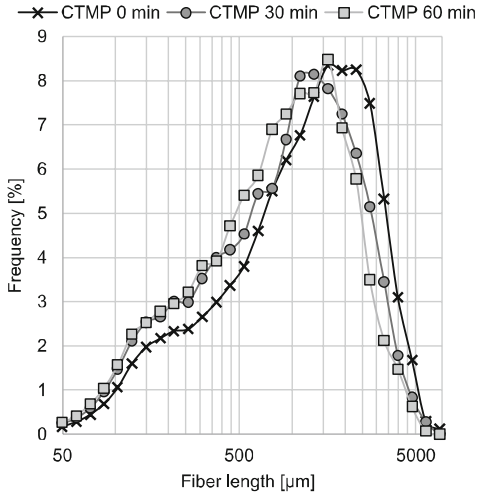

Fig. 1 Fiber length distributions of CTMP: 0 min refined (23° SR), 30 min refined (42° SR) and 60 min refiner (58° SR). The values given are weighted with respect to fiber length

impellers. The impellers were placed 16 cm distance from each other.

The batch size was 9.5 l and the fiber consistency 1.3 wt% before precipitation. For each batch, the depletion of $Ca(OH)_2$ was determined by the decrease in pH. At the beginning of the reaction, the temperature was ca. 20 °C, but it was allowed to change freely during the exothermic precipitation process. The CO_2 feed was 3 l/min and the target $Ca(OH)_2$ dose (before precipitation) was 1.0 wt%, corresponding to 50 wt% $CaCO_3$ filler (ash) content assuming 100 % conversion.

The $Ca(OH)_2$ used was prepared from CaO. Slaking was carried out for 4 h. The CaO-to-H_2O ratio used was 1:9. The initial temperature was 40 °C, but the temperature was allowed to change freely.

Pulp fractionation

The pulps (CTMPs and PCC-CTMPs) were fractionated using a Bauer-McNett classifier according to the SCAN-M 6:96 standard, with the exception of the dosed fiber weight. In case of PCC-CTMP, 20 g of solids (CTMP and PCC combined, containing approximately 10 g of CTMP), were used in the fractionation. In the case of the CTMP, the amount was equal to that used for the corresponding PCC-CTMP, i.e. close to 10 g. The wires used during fractionation were 30, 100 and 200 of the ASTM series (nominal openings 595, 149 and 75 µm, respectively) and 400 mesh wire with a measured opening of 25 µm. The fractions were labelled to indicate residuals. For example R30 refers to fraction retained by 30 mesh wire. The scheme of experiments is shown in Fig. 2.

A minimum of seven fractionations were carried out for each pulp. Five were done to collect fractions in separate vessels for further use, and two to weigh the fractions and measure their ash. To do so the fractions were collected on ashless filter paper (Macherey-Nagel MN 640 m) and dried in an oven at 105 °C prior the ash content determination. TAPPI standards T 211 om-02 and T 413 om-11 were used in conjunction to determine the ash content.

Handsheet preparation

Handsheets were prepared according to the SCAN C 26:99 standard with the exception of the drying (drum, surface temperature ca. 60 °C) and the use of an auxiliary wire (90 gsm polyester satin, thread width approximately 300 µm). The auxiliary wire was placed on the sheet mould wire and removed after wet-pressing.

Analytical procedures

Fiber analysis

The CTMPs, PCC-CTMPs and fractions were analyzed using the L&W Fiber Tester (Lorentzen and Wettre, Kista, Sweden) using a dilution of approximately 0.1 g fibers in 100 ml of water. Fiber length, fiber width, shape factor, the amount of fines and the kink index were determined and recorded as length-weighted averages.

The ash and $CaCO_3$ contents of the samples were measured according to TAPPI standards T 211 om-02 and T 413 om-11 in conjunction.

Zeta potential

The zeta potentials of the pulps and fractions were measured using the streaming potential method (Mütek SZP-06, BTG Instruments GmbH, Herrsching, German). The conductivity of the samples was increased to 0.30 ± 0.01 mS/cm with 0.1 M NaCl

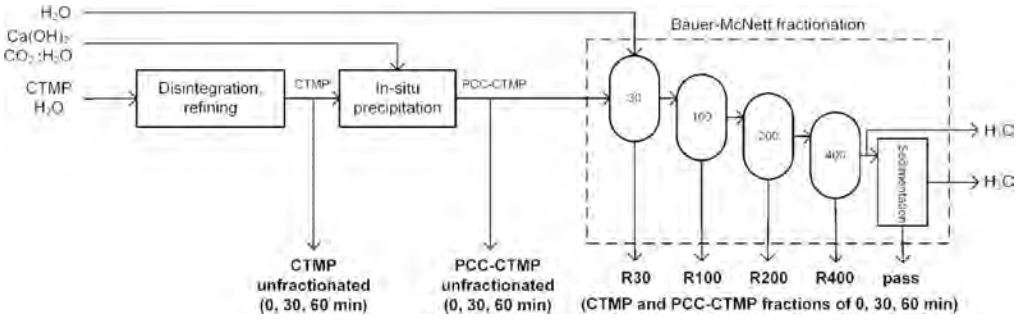

Fig. 2 Scheme of experiments. In the fractionation, the values refer to wire meshes used (ASTM series). The R30, R100, R200, and R400 fractions were collected from the wires and vessels after the fractionation. An additional sedimentation phase was added after the fractionation, and this yielded the 'pass' fraction. The bold text indicates the samples taken for further analysis

solution at least 18 h before the measurements were made.

Some of the coarsest fractions could not be measured according to the recommended procedure due to the poor water retention of the fiber cake and resulting water overflow. A filter paper (Macherey-Nagel MN 616) was therefore used, as instructed in the manual. Use of the filter paper was however found to affect the absolute zeta potential value.

Surface charge density (cationic-demand titration)

The charge density of the pulps and fractions was measured using a cationic-demand titration procedure (PCD 02, BTG Mütek GmbH and Mettler DL25, GWB for titrant dosing). Titration was done as back titration as recommended by the manufacturer, although the amount of sample was modified.

The amount of fiber slurry containing approximately 0.2 g of fiber was filtered on a polycarbonate membrane (GE Water & Process technologies, 3.0 μm) and rinsed into a decanter using deionized water to obtain a 5.0 g sample. The amount of poly(diallyldimethylammonium chloride) (PDADMAC, 1.0 mN, M = 107 000 g/mol, BTG) solution added was 20 g. Fibers were removed from the residual PDADMAC by centrifugation (6400 g). Titration was carried out using polyethene sodium sulfonate (PES-Na, 1.0 mN and M = 19 100 g/mol, BTG). After the titration, the fiber weight was determined by drying the fiber overnight at 105 °C. The results are given as averages of three or four measurements.

Scanning electron microscopy

The PCC-CTMP samples were characterized by scanning electron microscopy (SEM) using a Hitachi SU3500 equipped with a wolfram filament and backscatter electron (BSE) detector to capture micrographs of the samples. Composition (COMP) mode was used in order to obtain good contrast between PCC and the cellulosic fiber; the PCC particles or PCC rich areas therefore show lighter than areas free from PCC. The imaging was done on non-coated samples using the variable pressure (VP-SEM) mode at 60 Pa, 15 kV acceleration voltage and a working distance of 10 mm. These images are labeled with the text VP-SEM. The coated samples (sputter with an Au/Pd target) were imaged using secondary electron imaging (labeled SEM in the images), an acceleration voltage 15 kV and a working distance of 10 or 15 mm.

Handsheet testing

The handsheets were conditioned (23 °C and 50 % RH) and tested according to the SCAN standards SCAN P6:75 (grammage), SCAN P 7:96 (density and thickness), and SCAN P 38:80 (tensile index, tensile stiffness, and elastic modulus). The tensile and tensile stiffness indices were additionally calculated using a fiber-weight-based index, i.e. the ash weight was subtracted from the grammage used in the calculation. When the fiber-weight-based index is discussed, this is indicated in the text.

Brightness and opacity were measured using Elrepho (L&W) according to standards ISO 2470-1

(brightness) and ISO 9416 (light scattering coefficient (s_r), light absorption coefficient (k_r) and calculated opacity for 65 g/m^2 sheet), with the exception of measured samples (4 test pieces instead of 10).

Results

Fractionation of CTMP and PCC-CTMP

The different CTMP and PCC-CTMP furnishes were fractionated and characterized as shown in Table 1. With increasing refining, the fines content increased in both CTMP and PCC-CTMP. In the case of the PCC-CTMP, the 'pass' fraction corresponded to 40–50 % of the total dry material of the sample, which was significantly greater than for the CTMP. The 'pass' fraction was mainly PCC, as indicated by the high ash content (80–85 wt% of all the 'pass' fraction samples). Most (84–89 wt%) of the total PCC was found to pass the finest 400 mesh wire.

When the cumulative residual was determined, excluding the fraction passing the 400 mesh wire (see Fig. 3), precipitation was found to affect the distribution: the fractions of smaller fiber sizes were emphasized. This was especially obvious when the fibers were refined. This was associated mainly with the weight of PCC in the finer fiber fractions, which reduced the relative weight of the less PCC-rich fractions (see Fig. 4), and to a lesser degree with the increasing tendency of material to pass the wires.

Figure 4 shows the distribution of total ash between the PCC-CTMP fractions and the ash content in each fraction. Most of the total ash that did not pass the 400 mesh wire was found in R100 (0 min refined sample) or R200 (30 and 60 min refined samples), but the ash

Table 1 Proportions of unfractionated pulps and pulp fractions as mean values with 95% confidence intervals. The amount of $CaCO_3$ was calculated based on the 525 °C and 900 °C ash content measurements, i.e. the approximate percentage of ash that was $CaCO_3$. Values are also given for CTMP, although the samples contained no added $CaCO_3$

	CTMP			PCC-CTMP		
	0 min	30 min	60 min	0 min	30 min	60 min
Distribution in fractionation (wt%)						
R30	20.4 ± 2.6	12.2 ± 0.9	7.5 ± 0.4	8.6 ± 1.5	4.9 ± 0.5	3 ± 0.4
R100	50.4 ± 2.3	50.9 ± 2.0	50.8 ± 1.1	30.6 ± 5.6	16.3 ± 2.4	16.3 ± 3.9
R200	17.9 ± 1.3	23.2 ± 2.0	26.9 ± 1.9	14.4 ± 1.4	28.9 ± 2.1	25.7 ± 2.8
R400	4.6 ± 0.2	5.4 ± 0.2	6.3 ± 0.7	4.6 ± 0.2	6.1 ± 0.9	5.7 ± 0.6
Pass	6.7 ± 1.2	8.2 ± 0.8	8.4 ± 0.5	41.8 ± 7.1	43.9 ± 3.3	49.3 ± 1.9
Ash 525 ± 25 °C (%)						
R30	1.2 ± 0.0	1.2 ± 0.2	1.3 ± 0.1	6.4 ± 0.9	8.7 ± 1.1	7.9 ± 2.3
R100	1.1 ± 0.1	1.1 ± 0.0	1.1 ± 0.0	8.1 ± 0.9	8.5 ± 1.5	8.7 ± 3.6
R200	1.3 ± 0.1	1.2 ± 0.1	1.2 ± 0.3	15.0 ± 1.4	11.2 ± 2.1	11.4 ± 4.5
R400	1.8 ± 1.1	1.9 ± 0.4	1.7 ± 0.3	42.2 ± 3	29.4 ± 2.9	29.0 ± 7.7
Pass				89 ± 0.1	86.3 ± 0.4	84.0 ± 0.4
Not fract	1.0 ± 0.0			47.9 ± 0.7	47.3 ± 0.2	48.5 ± 0.6
Ash 900 ± 25 °C (%)						
R30	0.8 ± 0.0	0.8 ± 0.2	0.9 ± 0.1	3.8 ± 0.5	5.1 ± 0.6	4.7 ± 1.2
R100	0.8 ± 0.2	0.8 ± 0.1	0.7 ± 0.0	4.8 ± 0.5	5 ± 0.7	5.1 ± 2.1
R200	0.9 ± 0.0	0.9 ± 0.1	0.8 ± 0.2	8.6 ± 0.9	6.5 ± 1.2	6.6 ± 2.5
R400	1.4 ± 0.9	1.5 ± 0.6	1.3 ± 0.2	24 ± 0.0	17 ± 1.8	16.8 ± 4.3
Pass				50.2 ± 0.1	48.7 ± 0.1	47.4 ± 0.2
$CaCO_3$ (% of ash)						
R30	69.9	75.9	68.2	92.3	93.8	91.6
R100	66.5	66.1	70.4	94.0	94.2	92.5
R200	63.8	63.0	62.7	96.7	95.5	96.0
R400	49.3	55.2	60.4	98.1	96.3	96.0
Pass				99.1	99.0	99.3

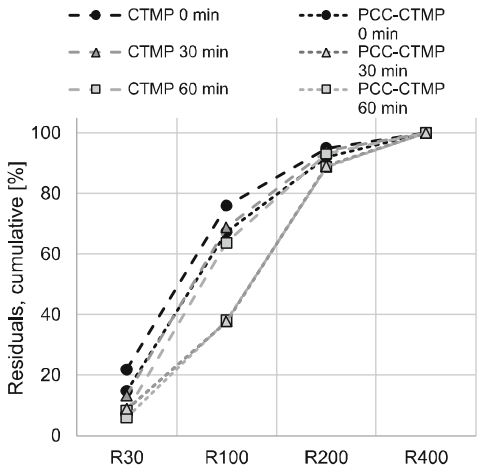

Fig. 3 Cumulative residuals on the wires, calculated by weight. The 'pass' fraction has been excluded to facilitate the comparison

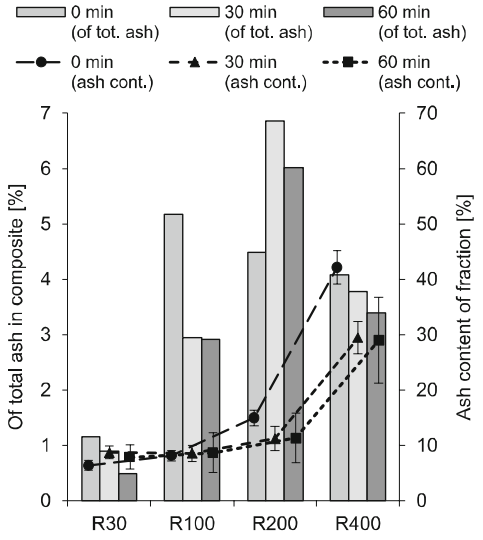

Fig. 4 Ash distribution in the fiber fractions. The bars (indicated on the left-hand ordinate, "Of tot ash in composite") show the percentage of ash in the fractions of the unrefined and refined PCC-CTMP fillers after fractionation. The lines (indicated on the right-hand ordinate, "Ash content of fraction") show the ash content in each fraction

content of the fraction increased with increasing mesh number. The ash contents of the samples refined for 30 and 60 min were essentially identical, although the 30 min sample fractions had a slightly higher percentage of total ash. This was explained by slightly better retention of ash in non-pass fractions in 30 min refined sample, and the slightly higher total ash of the 60 min refined sample.

Fiber analysis

The average fiber length, fiber width, shape factor, amount of fines and kink index are shown in Table 2. Refining of the unfractionated CTMP reduced the fiber length, fiber width and kink index, but increased the shape factor and amount of fines. Similar changes were detected for the PCC-CTMP, although the change in fiber width was negligible.

Comparison of the unfractionated CTMP and PCC-CTMP showed that the fiber length was unaffected by precipitation process of PCC. The fiber width, shape factor and amount of fines increased, but the kink index decreased. The changes caused by precipitation in width and shape factor were however very small: the maximum change detected for these values was 6.4 % increase in width.

The differences between the unfractionated PCC and PCC-CTMP were similar to those observed between the fractions. The fiber length in each fraction decreased slightly with refining, but no differences were seen between the CTMP and PCC-CTMP fractions. The main difference was in the fines content of the fractions. The CTMP fractions had more fines than the PCC-CTMP fractions, although the fines content of the unfractionated PCC-CTMP was larger than that of the CTMP.

The fiber length, fiber width and shape factor distributions of the fractions were essentially unaffected by the precipitation process, as the fines were not included in the distributions. This is illustrated in Figs. 5 and 6, which show the length and width distributions, respectively, in fractions of samples refined for 30 min.

Table 2 Physical fiber properties. Shape refers to shape factor. The amount of fines is given as a percentage of non-fines material. The values given are weighted with respect to fiber length

Sample	Length (mm)	Width (μm)	Shape (%)	Fines (%)	Kink index
CTMP					
0 min					
R30	2.65	42.8	91.2	0.6	0.19
R100	1.65	41.1	91.8	0.8	0.36
R200	1.00	36.8	91.6	11.3	0.48
R400	0.50	38.7	90.8	212.2	0.52
Not fract	1.49	39.3	90.8	10.9	0.46
30 min					
R30	2.52	44.1	93.0	0.5	0.24
R100	1.48	40.9	92.9	1.5	0.26
R200	0.95	37.1	92.4	12.2	0.33
R400	0.57	32.3	91.8	211.1	0.39
Not fract	1.26	38.2	91.0	14.5	0.33
60 min					
R30	2.40	44.1	96.6	0.4	0.10
R100	1.34	40.8	92.9	1.0	0.19
R200	0.87	37.2	92.6	11.9	0.17
R400	0.66	33.9	92.1	171.6	0.24
Not fract	1.15	38.2	91.1	15.3	0.30
0 min					
R30	2.73	43.8	92.3	0.7	0.12
R100	1.65	41.5	92.1	0.9	0.30
R200	1.06	37.8	91.8	9.3	0.38
R400	0.64	32.8	91.3	184.3	0.59
Pass	0.58	31.7	92.3	601.0	1.29
Not fract	1.50	40.4	91.1	13.7	0.38
PCC-CTMP					
30 min					
R30	2.63	45.3	93.1	0.3	0.08
R100	1.49	41.9	93.0	0.7	0.21
R200	0.94	37.8	92.6	10.0	0.31
R400	0.57	32.2	92.2	194.6	
Pass	0.77	30.6	92.6	617.6	0.50
Not fract	1.27	40.6	91.9	16.8	0.30
60 min					
R30	2.50	45.5	92.4	0.4	0.08
R100	1.33	42.0	92.9	0.8	0.21
R200	0.87	38.1	92.7	10.0	0.27
R400	0.51	31.5	91.9	270.5	
Pass	0.61	31.7	90.7	433.7	1.13
Not fract	1.12	40.3	92.2	17.0	0.25

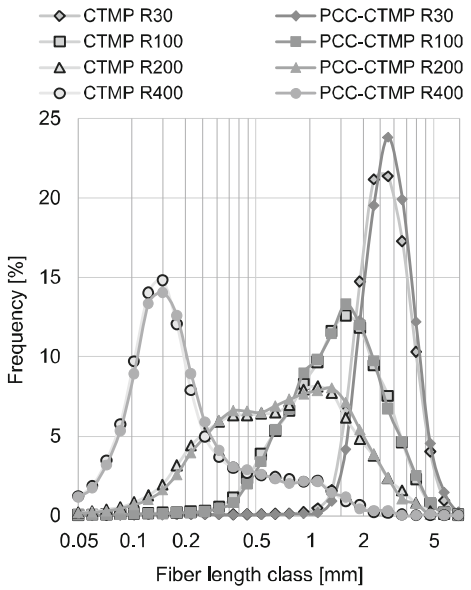

Fig. 5 Fiber length frequency distributions for CTMP and CTMP-PCC refined for 30 min. Note the logarithmic x-axis

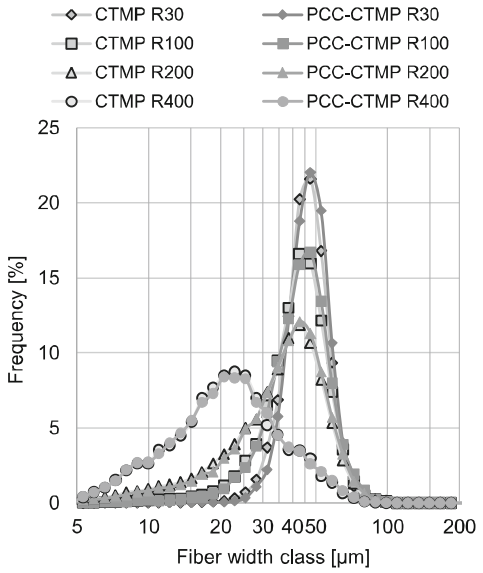

Fig. 6 Fiber width frequency distribution for CTMP and CTMP-PCC refined for 30 min. Note the logarithmic x-axis

Zeta potential and surface charge density

The zeta potential and surface charge density data are shown in Table 3; Fig. 7. Although the samples were either anionic (CTMP and most PCC-CTMP samples) or essentially non-charged (some of the PCC-CTMP samples), the unfractionated PCC-CTMPs showed positive zeta potentials. Refining of the CTMP increased the surface charge density but reduced the zeta potential, presumably due to the creation of more cellulose rich areas on the CTMP fiber surfaces (Hubbe 2006). This was observed particularly for the R30 CTMP samples. Increasing refining did not affect the surface charge of the R400 fractions in an obvious manner.

The charge development detected for CTMP is in good agreement with the literature. Sundberg and Holmbom (2004) reported that flake-like CTMP fines had a higher total charge than fibril-like fines, both of which had a total charge more than twice that of the CTMP fibers. Mosbye and Laine (2002) reported that the primary fines of mechanical pulp had a higher total charge than secondary fines, although the difference was greatly diminished by alkali treatment used to imitate the effect of bleaching. In our case the pulp was bleached.

Although the charge of PCC is commonly cationic due to an excess of positive calcium (Ca^{2+}) (Laine 2007), all fractions of PCC-CTMP, including the extremely PCC rich 'pass' fraction, had negative or essentially neutral surface charges. This may have been due to adsorbed anionic dissolved (and colloidal) material without significant incorporation of the materials into crystal as described by Jada and Verraes (2003) for a different polymer or the "cleaning effect" of the in-situ precipitation of PCC, in which dissolved (and perhaps colloidal) material is absorbed onto the PCC as reported by Matula et al. (2018).

The positive zeta potentials of unfractionated PCC-CTMP were probably an artifact caused by small, PCC-rich particles found on the 'pass' fraction of the unfractionated pulps, as they were poorly immobilized during the zeta potential measurement and were able to pass the wire and disturb the measurement. Another possible explanation was over-emphasizing of possibly cationic PCC residing on fiber surfaces of unfractionated samples due to the flow conditions and ion

Table 3 Zeta potential and surface charge mean values with 95% confidence limit. Note that R30 zeta potential absolute value was affected by the use of a filter paper

	CTMP			PCC-CTMP			Surface charge density (μekv/g)	
	Zeta potential (mv)	pH	EC (mS/cm)	Zeta potential (mV)	pH	EC (mS/cm)	CTMP	PCC-CTMP
0 min								
R30							–5.8 ± 4.3	–1.2 ± 3.9
R100							–7.1 ± 2	–3.4 ± 5.2
R200	–52.2 ± 1	7.3	0.30	–50.3 ± 2.9	8.0	0.29	–9.7 ± 0.9	–3.8 ± 3.2
R400	–29.1 ± 0.6	7.5	0.29	–26.1 ± 0.6	8.0	0.29	–46.9 ± 2.4	–41 ± 2.2
Pass								–20.2 ± 2.5
Not fract	–64.9 ± 1.6	6.5	0.30	16.8 ± 0.1	8.1	0.30	–18 ± 0.6	–26 ± 1.6
30 min								
R30	–20.4 ± 4.4	7.3	0.3				–8.3 ± 3.1	–1.9 ± 5.2
R100	–47.4 ± 1.1	7.6	0.30	–63 ± 2.3	7.9	0.29	–8.2 ± 2.1	2.1 ± 6.4
R200	–48.8 ± 2.2	7.4	0.31	–54.6 ± 1.7	7.9	0.30	–11.3 ± 3.6	–5.2 ± 3
R400	–26.8 ± 0.6	7.4	0.30	–22.8 ± 0	7.9	0.28	–47.3 ± 1.7	–42.1 ± 1.2
Pass								–31.1 ± 4.1
Not fract	–55 ± 1.6	6.3	0.3	14.2 ± 1.7	8.5		–21.2 ± 2.7	–20.5 ± 1.2
60 min								
R30	–13.6 ± 1.1	7.7	0.29				–10.7 ± 4.2	–10.9 ± 4.3
R100	–47.3 ± 1.4	7.5	0.31	–60.8 ± 1.2	8.0	0.30	–12.1 ± 0.5	–9.7 ± 1.5
R200	–51.8 ± 1.6	7.5	0.30	–32.1 ± 0.8	8.0	0.30	–10.8 ± 2.7	–16.6 ± 1.7
R400	–26.8 ± 9.5	7.4	0.30	–23.7 ± 0.4		0.29	–45.9 ± 5.5	–57.6 ± 1.1
Pass								–38.2 ± 1.6
Not fract	–44.6 ± 1.7	6.7	0.30	12.4 ± 0.5	8.5	0.30	–27.8 ± 0.4	–15.5 ± 3.4

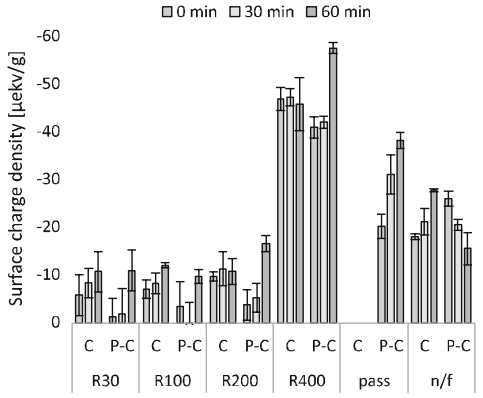

Fig. 7 Surface charge densities of the samples. C refers to CTMP and P-C to PCC-CTMP. The error bars represent 95 % confidence values. n/f = not fractionated

flux. In addition, the streaming potential method used in this study is affected by fiber pad compression (Hubbe 2006), and the fiber pad compression was visibly dependent on the fraction measured, which may explain why the zeta potential was closer to zero for R30 and R400 than for R100 and R200.

Scanning electron microscopy

Scanning electron microscopy of the fractionated PCC-CTMP samples further confirmed that the ash content increased with decreasing fiber size, see Fig. 8. The PCC was in the form of typically nano-sized roundish particles and their aggregates or clusters. No variation in PCC morphology or primary particle size was detected between the different fiber fractions, but the larger amount of PCC in the fines fraction suggested that the PCC nanoparticle aggregate size perhaps increased.

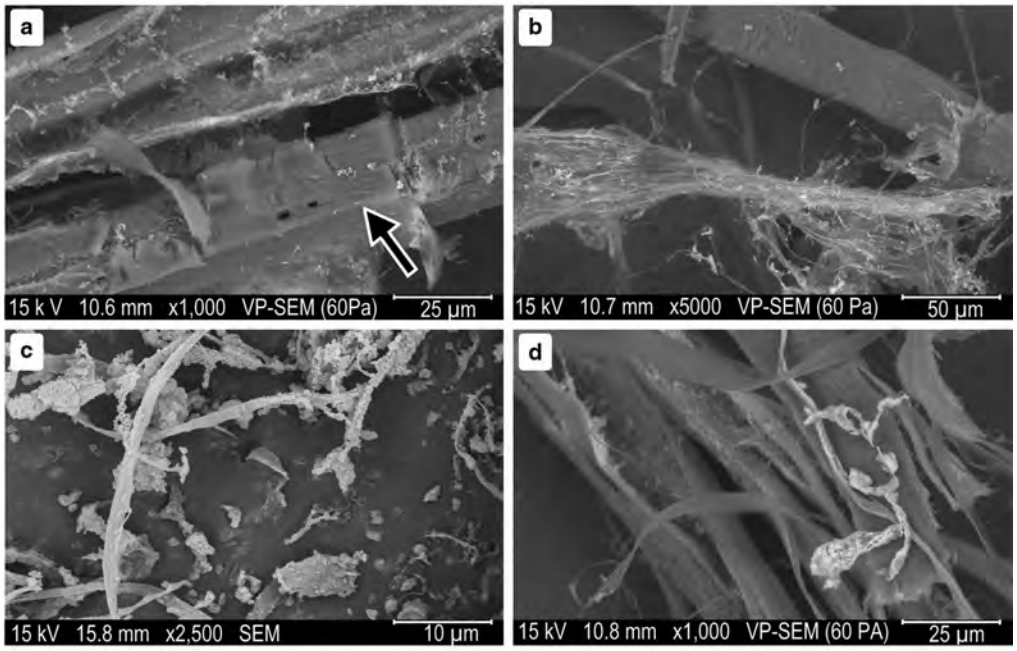

Fig. 8 SEM micrographs of fractionated PCC-CTMP samples. **a** (30 min R200): a band of outer fiber layers essentially free from PCC (indicated with the arrow), surrounded by more PCC rich areas. **b** (0 min R200): heavily fibrillated fiber with high content of PCC and a more intact fiber with substantially no PCC. **c** (0 min 'pass' fraction): fibrils and fines extremely rich in PCC. Image **d** (60 min R200): split or cleaved fiber with PCC deposited in lumen and outer layer essentially free from PCC

The PCC was located mainly on fiber regions where the outer layer of the fibers had been removed (Fig. 8a) or where the fiber surface was damaged or subjected to fibrillation (Fig. 8b). The tendency of the PCC to attach to fibrils or to damaged regions of the fiber was clearly evident in the fractionated samples with the highest amount of fines, i.e. the R400 and in 'pass' fractions (Fig. 8c). Split fibers had enriched PCC deposits in the lumen, while the outer surface appeared to be essentially free from PCC (Fig. 8d). This type of finding was usually seen in R100 and R200, but occasionally also in R30.

When the fractions of PCC-CTMP were compared with the unfractionated PCC-CTMP (Fig. 9), it was evident that a larger portion of the fibers were substantially free from PCC in the fractionated pulps than in the unfractionated sample. Some of this difference could be explained by the hypothesis that the fines in the unfractionated pulp were attached or otherwise located on larger fibers (thus appearing a part of them), and these objects containing more PCC were removed during fractioning. The surfaces of the larger CTMP fibers were however also affected by fractionation: some of the PCC residing on the fiber surface was removed during fractionation.

Handsheet properties

Physical properties

The physical properties of the handhseets are shown in Table 4 and in Figs. 10, 11, 12 and 13. The sheets had an average grammage of 68.6 g/m^2 (standard deviation 5.8 g/m^2). The ash content of the sheets was assumed to be close to that of the pulp or fraction used in sheet preparation (Table 1), since the auxiliary wire improved mechanical retention.

The density of PCC-CTMP handsheets from unfractionated pulps was higher than that of CTMP handsheets free from PCC. The difference in density

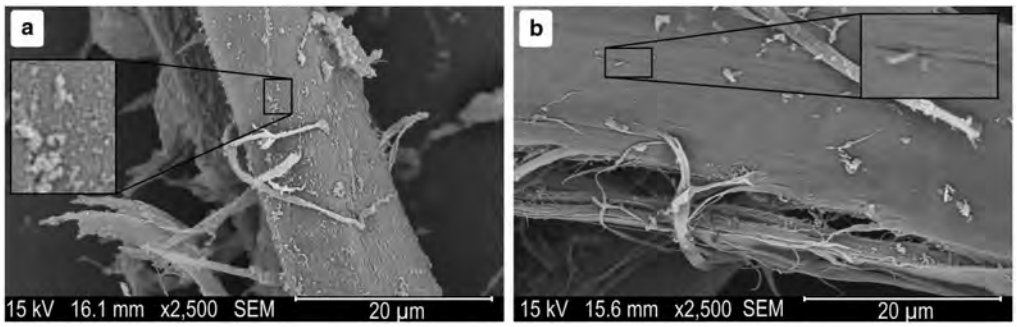

Fig. 9 Unfractionated pulp (**a**) and fractionated pulp (**b**) R30. Both images were taken on PCC-CTMP refined for 60 min

was 16, 14 and 7 % for samples refined for 0, 30 and 60 min, respectively. The handsheet strength increased with decreasing fiber size and increasing pulp refining for both CTMP and PCC-CTMP. The coarse, stiff fibers, as in R30, are known to give high bulk and a highly porous sheet, but poorer bonding than the more flexible and conformable finer fibers (Retulainen et al. 1998). This result was, therefore, expected.

A more relevant comparison between CTMP and PCC-CTMP sheets reveals the effect of the PCC. The increase in density of the PCC-CTMP fraction sheets with increasing refining level was not as pronounced as that of the CTMP sheets. PCC-CTMP sheets from the 60 min refined pulp fractions had lower density than the corresponding CTMP sheets. This was associated with the debonding effect of nanosized particles and agglomerates of PCC on the fiber. The debonding effect is supported by the tensile index and tensile stiffness index results.

There was a good linear correlation between tensile index, elastic modulus, tensile stiffness and density for both CTMP and PCC-CTMP sheets made of fractions (Fig. 14). The slopes of the regression lines differed greatly for CTMP and PCC-CTMP sheets in the case of tensile index versus density (0.130 and 0.061, respectively) and tensile stiffness index versus density (0.015 and 0.010, respectively). The difference in slope was significantly less for elastic modulus versus density (0.0075 and 0.0062, respectively).

When the fiber-weight-based indices were calculated, the tensile index values of the fractionated PCC-CTMP and the corresponding CTMP sheets were similar, although the tensile index of the PCC-CTMP sheets was lower than that of the CTMP sheets. Similarly, fiber-weight-based tensile stiffness index for PCC-CTMP was only slightly lower for R100 and R200. PCC-CTMP R400 sheets instead had a clearly higher tensile stiffness index than the corresponding CTMP R400 sheets.

Optical properties

Both the brightness (Fig. 15) and the opacity (Fig. 16) of the PCC-CTMP handsheets were greater than those of the CTMP sheets when unfractionated pulps were used. This was not, however, the case for the individual fractions. The opacity of all the fractions increased when PCC was added, but the brightness decreased for fractions R30, R100 and R200 sheets, and increased for R400 sheets.

The scattering coefficient (s_r) and absorption coefficient (k_r) (Table 5), showed that the PCC-CTMP fraction sheets had, on average, a slightly higher s_r and k_r than the CTMP sheets, except for the R400 fraction sheets. In other words, although the light scattering improved, the change in the opacity of the fractions was due to an increase in light absorption rather than due to an increase in light scattering. The increase in opacity and brightness of the unfractionated PCC-CTMP sheets over those of the unfractionated CTMP

Table 4 Physical properties of the handsheets. n/f = not fractionated pulp. n/d = not detected (in this case due to poor sheet strength). For the ash contents of the pulps, see Table 1.

	Grammage (g/m^2)		Thickness (μm)		Density [kg/m^3]		Tensile index [Nm/g]		Elastic modulus [MPa]		Tensile stiffness index [kNm/g]	
	CTMP	PCC-CTMP	CTMP	PCC-CTMP	CTMP	PCC-CTMP	CTMP	PCC-CTMP	CTMP	PCC-CTMP	CTMP	PCC-CTMP
0 min												
R30	73.0	69.5	382 ± 80	359 ± 26	192	194	n/d	n/d	n/d	n/d	n/d	n/d
R100	69.0	67.5	337 ± 36	333 ± 22	205	202	n/d	n/d	n/d	n/d	n/d	n/d
R200	68.0	68.0	254 ± 8	253 ± 12	267	268	8.1 ± 0.6	6.4 ± 0.5	0.38 ± 0.02	0.31 ± 0.02	1.4 ± 0.03	1.15 ± 0.10
R400	52.0	81.0	134 ± 16	179 ± 19	387	454	24.7 ± 1.6	11.8 ± 0.4	1.34 ± 0.04	1 ± 0.03	3.48 ± 0.11	2.21 ± 0.08
Pass		67.5	74 ± 7	74 ± 7		914						
n/f	67.0	68.0	275 ± 18	241 ± 30	243	282	10.7 ± 0.9	n/d	0.44 ± 0.03	n/d	1.81 ± 0.14	n/d
30 min												
R30	69.0	67.0	390 ± 28	366 ± 18	177	183	n/d	n/d	n/d	n/d	n/d	n/d
R100	71.0	67.0	329 ± 30	305 ± 31	216	220	5.5 ± 0.6	4.3 ± 0.1	0.2 ± 0.02	0.16 ± 0.02	0.91 ± 0.11	0.73 ± 0.03
R200	69.0	65.0	251 ± 12	250 ± 29	274	260	10.3 ± 0.4	7.7 ± 0.6	0.49 ± 0.02	0.39 ± 0.02	1.8 ± 0.06	1.49 ± 0.09
R400	73.0	81.5	171 ± 10	166 ± 15	427	492	29.5 ± 1.5	21.5 ± 1.1	1.61 ± 0.04	1.76 ± 0.08	3.77 ± 0.10	3.57 ± 0.17
Pass		67.5		68 ± 0		991						
n/f	65.5	65.0	249 ± 22	216 ± 17	263	300	18.9 ± 0.7	n/d	0.74 ± 0.04	n/d	2.81 ± 0.15	n/d
60 min												
R30	75.0	68.5	327 ± 50	321 ± 17	229	213	5.4 ± 0.3	5.7 ± 0.5	0.21 ± 0.01	0.21 ± 0.01	0.92 ± 0.05	0.96 ± 0.08
R100	70.5	66.5	286 ± 21	284 ± 22	246	234	7.1 ± 0.6	5.5 ± 0.4	0.33 ± 0.02	0.24 ± 0.01	1.34 ± 0.07	1.04 ± 0.06
R200	67.0	66.5	224 ± 14	237 ± 18	298	280	12 ± 1.4	8.2 ± 0.5	0.66 ± 0.05	0.46 ± 0.02	2.21 ± 0.17	1.65 ± 0.06
R400	61.0	79.0	139 ± 9	154 ± 13	441	512	34.7 ± 1.7	23 ± 0.7	1.92 ± 0.03	2.04 ± 0.05	4.36 ± 0.07	3.97 ± 0.09
Pass		69.0		68 ± 0		1043						
n/f	66.5	62.5	196 ± 11	172 ± 8	339	363	20.9 ± 2.5	n/d	1.08 ± 0.08	n/d	3.2 ± 0.24	n/d

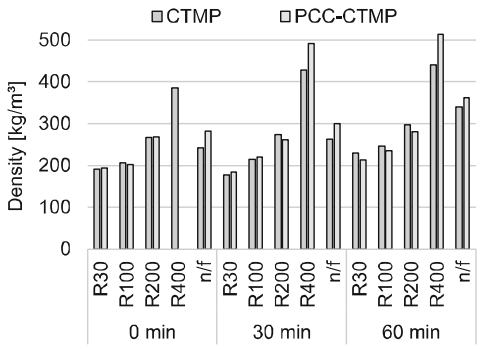

Fig. 10 Densities of the CTMP and PCC-CTMP sheets. n/f = not fractionated

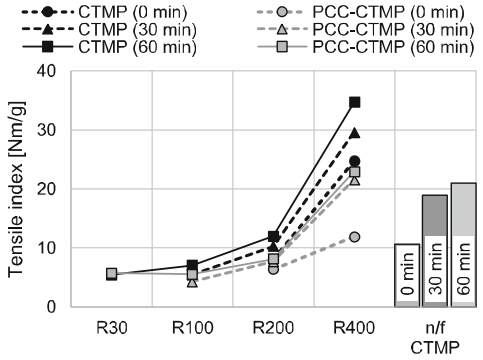

Fig. 11 Tensile index of CTMP and PCC-CTMP sheets. n/f = not fractionated. The tensile indexes of unfractionated PCC-CTMP sheets were below the test limit

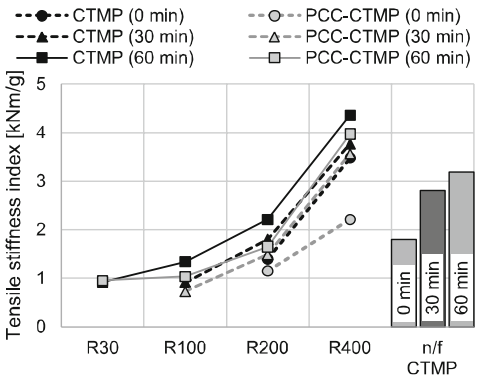

Fig. 12 Tensile stiffness indexes of the CTMP and PCC-CTMP sheets. The category n/f refers to the sheets made using unfractionated pulp. Tensile stiffness indexes of unfractionated PCC-CTMP sheets were below test limit

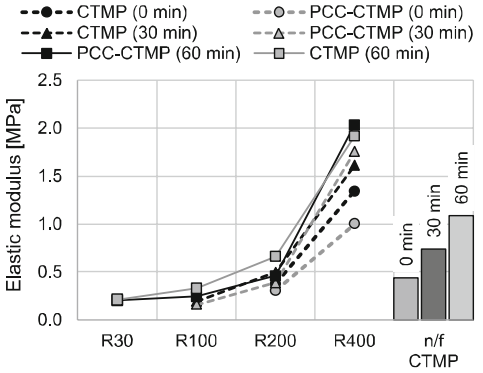

Fig. 13 Elastic moduli of the CTMP and PCC-CTMP sheets. n/f = not fractionated. The elastic moduli of unfractionated PCC-CTMP sheets were below the test limit

sheets was therefore mainly due to the presence of the mineral-rich 'pass' fraction.

Discussion

Effect of CTMP refining on the in-situ precipitation of calcium carbonate

The current work confirms that mechanical refining changes the precipitation efficiency and thus the composition and properties of the PCC-fiber composite. The CTMP has a large particle size distribution in which fines have physical and chemical properties different from those of the coarse fraction. Refining introduces changes, including fiber damage and removal of the fiber layer and the formation of debris.

Calcium carbonate precipitation onto the fibers can be affected by refining. PCC was found to be more prone to attach to the fiber parts where the outer layer (*P*1) had been removed or damaged, and SEM images showed that a prolonged refining and formation of higher content of split fibers means that PCC can be found on the inner lumen wall, despite the fact that the outer layers of CTMP fibers (primary wall and

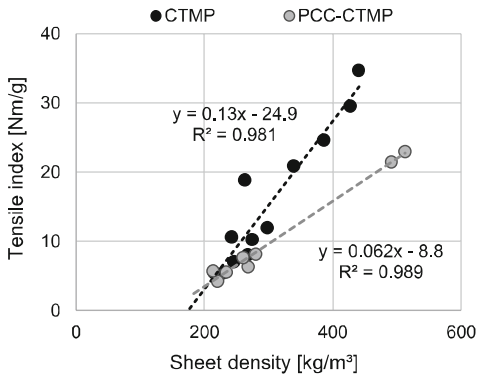

Fig. 14 Tensile index versus sheet density of fractionated sheets. The lines show the linear regression

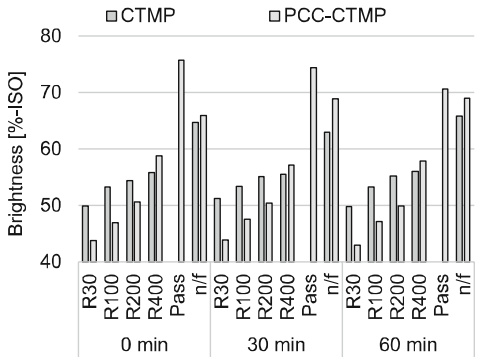

Fig. 15 Brightness (R457C) of the handsheets prepared using fractions of CTMP and CTMP-PCC. n/f indicates sheets made using unfractionated pulp

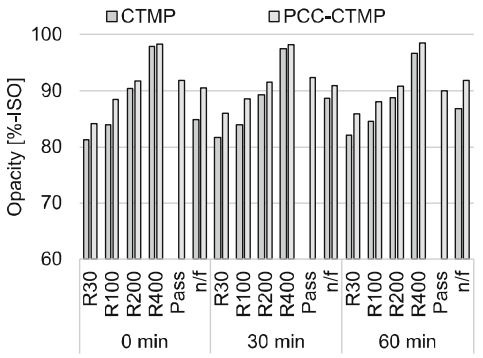

Fig. 16 Opacity of the handsheets prepared using fractions of CTMP and CTMP-PCC. n/f indicates sheets made using unfractionated pulp

secondary wall *S*1) are known to be richer in charged species (such as lignin) than the inner layers of the fibers, which in turn are richer in less charged cellulose (Hubbe 2006). The study showed an approximately linear correlation between the ash content of the PCC-CTMP fractions and the anionic surface charge density of the corresponding CTMP fraction (R^2 of liner fit was 0.849, see Fig. 17).

Assuming that the metal-binding ability of the functional groups correlates with their charge, this is partly in conflict with the hypothesis that the functional metal-binding groups steer the precipitation onto the fibers. The situation is however more complex. The dominating interaction is stated to be the interaction with Ca^{2+} and the partial negative charge of the hydroxyl group (due to polarization) (Dalas et al. 2000), but the hydroxyl groups on the fibers require alkaline conditions to ionize (Sjostrom 1989) and contribute to the fiber surface charge. The fiber charge at neutral pH range is commonly attributed to carboxyl groups found e.g. in hemicelluloses instead of cellulose (Laine 2007; Sjostrom 1989), and $CaCO_3$ has been reported to precipitate onto surfaces via an ACC precursor that attaches onto the surface containing carboxyl groups (Stephens et al. 2011).

Lignin is known to form complexes with metals (Schmidt 2010) and has been reported to have a high affinity towards Ca^{2+} (Torre et al. 1992). The mechanism of metal uptake of lignin is however not well understood (Guo et al. 2008; Suhas et al. 2007). It has been linked with proton displacement (Christ et al. 2002; Guo et al. 2008) and carboxylic and phenolic sites, of which phenolic groups are thought to be dominant (Guo et al. 2008). The hydroxyl groups of cellulose may undergo metal-ion facilitated deprotonation especially at high pH (Al-Sogair et al. 2011), whereas it has been reported that lignin exhibits the opposite behavior, i.e. a decreasing deprotonation with increasing pH (Christ et al. 2002). This could explain why cellulose was "more effective than its charge" in initiating PCC precipitation under the conditions used in our work, especially if the charges are compared at neutral pH.

Another possible reason for the increase in ash content with increasing beating and increasing surface

Table 5 Optical properties of CTMP and PCC-CTMP handsheets

	R457C	s_r (m^2/kg)	k_r (m^2/kg)	Opacity (YC/2)
CTMP				
0 min				
R30	50.0	22.42	1.92	81.3
R100	53.3	27.11	1.82	84.0
R200	54.4	37.63	2.34	90.4
R400	55.7	69.69	4.18	97.9
Not fract	64.7	35.71	1.09	84.8
30 min				
R30	51.2	23.22	1.86	81.6
R100	53.3	26.85	1.84	83.9
R200	55.1	35.51	2.18	89.2
R400	55.5	64.78	4.01	97.5
Not fract	63.0	40.94	1.49	88.7
60 min				
R30	49.8	23.24	1.98	82.1
R100	53.2	27.54	1.90	84.6
R200	55.2	34.80	2.10	88.7
R400	56.1	59.83	3.60	96.7
Not fract	65.8	39.54	1.17	86.8
PCC-CTMP				
0 min				
R30	43.8	22.47	2.63	84.2
R100	46.9	28.95	2.81	88.4
R200	50.7	36.91	2.92	91.7
R400	58.8	78.23	4.13	98.3
Pass	75.7	60.70	1.11	91.8
Not fract	65.8	47.86	1.48	90.6
30 min				
R30	43.9	24.15	2.86	86.1
R100	47.5	29.28	2.79	88.5
R200	50.4	36.39	2.94	91.5
R400	57.1	74.73	4.37	98.3
Pass	74.5	60.25	1.29	92.4
Not fract	68.9	52.03	1.33	91.0
60 min				
R30	43.0	23.51	2.95	85.9
R100	47.1	28.35	2.78	88.1
R200	50.0	34.68	2.86	90.8
R400	57.9	79.36	4.51	98.5
Pass	70.7	47.24	1.39	90.1
Not fract	69.0	54.70	1.41	91.8

charge density was the increase in surface area and fiber damage (resulting in high energy sites). It can be argued that the surface created in refining has, for the most part, a charge similar to that of pre-existing surface because the newly created surface has a chemical composition similar to that of the pre-

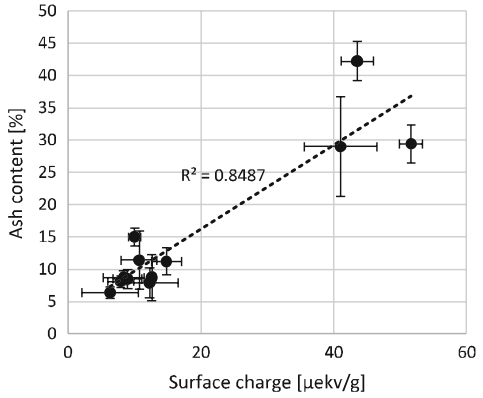

Fig. 17 Ash content of PCC-CTMP fractions plotted against the surface charge of the corresponding CTMP fraction. The error bars represent 95 % confidence values

existing surface. In this case the surface charge would be indicative of an approximately proportional increase in surface area, and the observed correlation with the surface charge density could indicate a correlation with surface area. The changes in the surface area alone do not, however, explain why PCC appeared to discriminate against the areas with intact primary wall, and it does not explain the obvious difference in fiber coverage by PCC between fines and larger fibers.

It is tempting to think that the correlation between ash content and surface charge supports a precipitation mechanism similar to that described by Subramanian (2008), i.e. that the precursor of PCC aggregates on the cellulosic particles due to electrostatic interactions, and that it adheres and subsequently crystallizes as $CaCO_3$. The precursor was expected to be cationic due to an excess of Ca^{2+} in compared to the CO_3^{2-} during precipitation. The "charge neutralization by $CaCO_3$ precursor" concept may be partially supported by the data, as the PCC-CTMP R30 and R100 fractions refined for 0 and 30 min had essentially no anionic surface charge and that of R200 was also extremely low. On the other hand, the highly anionic surface charge of R400 and the 'pass' fraction, although the 'pass' fraction had a high mineral content, do not fully support the simple "charge neutralization by $CaCO_3$ precursor" mechanism.

The surface charge of a pulp commonly depends on the production process (Laine 2007). Therefore, the relationship between the surface charge or the surface concentration of a functional groups and precipitated filler could be useful for controlling the formation of PCC-fiber composite material, if such a correlation were universally established. It was shown that the fiber surface and morphology plays a role in PCC precipitation, and that this affects the homogeneity of the PCC-fiber composite, although the precipitation was carried out in a simplified system free from many susbstances, such as cationic polymers and inorganic salts such as sulphates at present in paper mill waters (Laine 2007). Some of these substances may be designed to alter fiber surfaces (such as cationic polymers) and some, for example sulphonates (Tang et al. 2012), may affect the precipitation of PCC. While the concentration of a single substance in PCC-fiber composite preparation may be below the concentration it alone would significantly affect the precipitation and steering of particles onto the fiber, the net effect of different substances is difficult to predict.

Papermaking potential of PCC-CTMP: influence on fiber bonding and optical properties

As the fiber morphology remained essentially the same, the differences between the CTMP and PCC-CTMP sheets were associated with the presence of the mineral. The information regarding the role of different fractions may help to explain why the same precipitation process on different pulps may result in differences in the relative development of optical and strength properties, as was reported by Kumar et al. (2009) to happen.

The physical and optical properties of the CTMP and PCC-CTMP sheets made using the fractionated pulps suggested that the enrichment of PCC onto the desired fractions of the pulp (or onto the desired parts of the fiber) is important when tailoring the PCC-fiber composite. The differences observed between CTMP and CTMP-PCC sheets were primarily associated with differences in surface characteristics, i.e. mainly in light scattering but also in debonding as indicated by the tensile strength and density development of the sheets. The presence of a salt such as sodium or calcium chloride has been associated with changes in fiber swelling and tensile index (Fält and Wågberg 2003), but it is not known whether the PCC precipitation can alter fiber swelling. Another factor

affecting the bonding was that the PCC was precipitated in (split fiber) lumens and perhaps inside the fibrillated structures of the more well-fibrillated CTMP, which is expected to stiffen the fibers, to make them less conformable and less collapsible (Kumar et al. 2011). Such factors are desirable when high bulk is required, but they tend to have a negative effect on bonding.

There was significantly less debonding with the separate fractions than with the unfractionated PCC-CTMP. The large-fiber fractions retained their strength properties better than the small-fiber fractions. A comparison of the fiber-weight-based indices for PCC-CTMP and CTMP sheets showed only a slight decrease on strength for most fractions, and the tensile stiffness index of R400 even increased although filler is known to disturb the formation of a fiber network (Hubbe and Gill 2016). The conserved strength could depend on the distribution of PCC in the sheets (different perhaps to that of traditionally filled sheets, as reported by Silenius (2002)), or due to differences in segment activation compared with a typical sheet. The results suggest, however, that the fines fractions may be capable of containing a considerable amount of PCC without losing their bonding potential to a proportional degree.

Based on the SEM micrographs, most the PCC present was expected to form a PCC-CTMP composite, i.e. the yield of CTMP and $Ca(OH)_2$ to PCC-CTMP was considered to be high. This suggests excellent retention during sheet-making, but this may not be so since the fines easily passed wires during fractionation.

Fines were expected to grow in size due to attachment of PCC. This may partially explain why the fines content increased during precipitation of PCC onto CTMP (i.e. they were better detected by the fiber analyzer), but the increase in size does not explain the increased tendency for the fines to pass the wires. We suggest that the loss of fines during fractionation was due to the precipitated PCC that reduced the tendency of the fines to attach onto other particles. Such result has been reported by Klungness et al. (1996): In their pilot trial, when using a PCC-fiber composite the total first pass retention was negatively affected, though first-pass retention of filler increased.

The PCC attached onto the fines appeared to prevent the fines from forming a gel-like, water-removal-resisting structure, which was observed on the 400 mesh wire when the CTMP was fractionated. Reduced interparticle interactions can explain the increase in fines content during precipitation of PCC and the loss of fines during fractionation. This is in good agreement with the report that water removal from a MNFC-containing furnish is increased when PCC-fiber composite is created on the MNFC (Rantanen et al. 2015), although the increase in the amount of mobile fines is expected to decrease the water removal from the sheet (Hubbe and Heitmann 2007). Since the PCC was found to be attached mainly onto the fines, which increases the light scattering of mechanical pulp (Leskelä 1998), the increase in s_r was probably also low for the fines fraction.

Therefore, assuming that PCC is enriched on the fibrils of externally fibrillated fibers similarly than it attaches onto fines and damaged CTMP fibers, a carefully executed refining of the pulp prior to precipitation phase could be beneficial for pulp intended for PCC-fiber composite preparation. By controlling external fibrillation it could be possible to tailor PCC-fiber composites, for example by steering the precipitation onto larger fiber fractions by the use of external fibrillation. The use of selected fractions in pulp blends could also be of interest, although fractionation as such may not be the most alluring industrial approach.

Conclusions

Fractionation of the PCC-CTMP composite showed that the ash content increased with decreasing fraction size. The PCC was attached well onto the fiber, as shown by its tendency to remain in the samples and by SEM micrographs in case of the 'pass' fraction.

The reason for the preferred precipitation onto fines is unclear, but a correlation was found between the anionic surface change density of the CTMP fraction and the ash content of the PCC-CTMP fraction. SEM micrograph data suggests that the PCC prefers to precipitate to the areas typically associated a lower charge than the primary wall. This may, however, be explained by chemical changes such as metal-ion facilitated deprotonation in cellulose due the higher pH. The correlation is therefore thought to support the suggestion that the interparticle (fiber-ACC) interactions, perhaps partially originating from cationic-

anionic interactions, steer the ACC onto the cellulosic fibers, onto which it subsequently precipitates as PCC.

The PCC-CTMP handsheets based on the coarser fiber fractions were more prone for brightness loss, probably due to a combined effect alkali yellowing and less enhanced light scattering due to lower PCC content, whereas sheets comprising higher content of the fine fractions provided positive effects especially on light scattering. The fines also contained significant amount of PCC without proportional loss in fiber-weight based tensile index, suggesting that the substrate fiber properties can greatly affect the PCC-fiber composite and its effects on paper. These findings demonstrate the importance of controlling the substrate fiber properties e.g. by ensuring that the pulp contains the different fiber fractions in desirable proportion, or by favorable external fibrillation of larger fibers. The findings also suggest that careful, target-oriented refining of the fiber is an important pre-treatment when attempting to control the properties of PCC-fiber composite material.

Acknowledgments Stora Enso Oyj is acknowledged for financial support of the project. Dr Anthony Bristow is thanked for linguistic revision of the work.

Funding Open access funding provided by LUT University (previously Lappeenranta University of Technology (LUT)). This research did not receive any specific grant from funding agencies in the public, commercial, or not-for-profit sectors.

Declarations

Conflict of interest The authors declare that they have no conflict of interest.

References

Al-Sogair F, Operschall BP, Sigel A, Sigel H, Schnabl J, Sigel RKO (2011) Probing the metal-ion-binding strength of the hydroxyl group. Chem Rev 111:4964–5003. https://doi.org/10.1021/cr100415s

Christ RH, Martin JR, Christ DR (2002) Heavy metal uptake by lignin: comparison of biotic ligand models with an ion exchange process. Environ Sci Technol 36:1485–1491. https://doi.org/10.1021/es011136f

Ciobanu M, Bobu E, Ciolacu F (2010) In-situ cellulose fibres loading with calcium carbonate precipitated by different methods. Cellul Chem Technol 44(9):379–387

Dalas E, Klepetsanis PG, Koutsoukos PG (2000) Calcium carbonate deposition on cellulose. J Colloid Interf Sci 224:56–62. https://doi.org/10.1006/jcis.1999.6670

Fält S, Wågberg L (2003) Influence of electrolytes on the swelling and strength of kraft-liner pulps. Nord Pulp Pap Res J 18(1):69–73. https://doi.org/10.3183/npprj-2003-18-01-p069-073

Fortuna ME, Harja M, Bucur D, Cimpeanu SM (2013) Obtaining and utilizing cellulose fibers with in-situ loading as an additive for printing paper. Materials 6:4532–4544. https://doi.org/10.3390/ma6104532

Guo X, Zhang S, Shan X (2008) Adsorption of metal ions on lignin. J Hazard Mater 151:134–142.

Heinemann S, Vehniäinen A, The character and properties of mechanical pulps, in 'Papermaking chemistry' 2nd ed, Papermaking science and technology vol. nbsp;5, Lönnberg B. (ed), 2009, p. and nbsp;458–514

Hubbe MA (2006) Sensing the electrokinetic potential of cellulosic fiber surfaces. BioResources 1(1):116–119

Hubbe MA, Gill RA (2016) Fillers for papermaking: a review of their properties, usage practices, and their mechanistic role,. BioResources 11(1):2886–2963

Hubbe MA, Heitmann JA (2007) Review of factors affecting the release of water from cellulosic fibers during paper manufacture. BioResources 2(3):500–533

Jada A, Verraes A (2003) Preparation and microelectrophoresis characterisation of calcium carbonate particles in the presence of anionic polyelectrolyte. Colloid Surf A 2019:7–15. https://doi.org/10.1016/S0927-7757(03)00010-4

Klungness JH, Sykes MS, Tan F, Abubakr S, Eisenwasser JD (1996) Effect of fiber loading on paper properties. Tappi J 79(3):297–301. https://doi.org/10.1177/1687814016664258

Klungness J, Ahmed A, Ross-Sutherla N, AbuBakr S (2000) Lightweight, high-opacity paper by fiber loading: filler comparison. Nord Pulp Pap Res J 15(5):345–350. https://doi.org/10.3183/npprj-2000-15-05-p345-350

Krogerus B (2007) Papermaking additives. In: Alén R (ed) Papermaking chemistry, 2nd edn. Gummerus Oy, Jyväskylä, pp 56–121

Kumar P, Gautam S, Kumar V, Singh S (2009) Enhancement of optical properties of bagasse pulp by in-situ filler precipitation. BioResources 4(4):1635–1646

Kumar P, Negi YS, Singh SP (2011) Filler loading in the lumen or/and cell wall of fibers -a literature review. BioResources 6(3):526–3546

Laine J (2007) General aspects of papermaking chemistry. In: Alén R (ed) Papermaking chemistry, 2nd edn. Gummerus oy, Jyväskylä, pp 28–53

Lakshminarayanan R, Valiyaveettil S, Luan Loy G (2003) Selective nucleation of calcium carbonate polymorphs: role of surface functionalization and poly(vinyl alcohol) additive. Cryst Growth Des 3(6):953–958. https://doi.org/10.1021/cg034022j

Leskelä M (1998) Optical properties. In: Niskanen K (ed) Paper physics. Gummerus Oy, Jyväskylä, pp 117–137

Matula J, Räsänen J, Tahkola K (2018) In-line PCC technology cleans up circulation water from dissolved materials, metals and bio based microorganisms resulting to clean process and high runnability. In: PaperCon 2018. Charlotte, North Carolina, April 15–18

Mohamadzadeh-Saghavaz K, Resalati H, Ghasemian A (2014) Cellulose-precipitated calcium carbonate composites and their effect on paper properties. Chem pap 68(6):774–778. https://doi.org/10.2478/s11696-013-0513-7

Mosbye J, Laine J (2002) The charge and chemical composition of fines in mechanical pulp. Nord Pulp Pap Res J 17(3):352–356. https://doi.org/10.3183/npprj-2002-17-03-p352-356

Odabas N, Henniges U, Potthast A, Rosenau T (2016) Cellulosic fines: properties and effects. Prog Mater Sci 83:574–594. https://doi.org/10.1016/j.pmatsci.2016.07.006

Park Y, Rawat P, Ford E (2017) Role of Polymerized Micelles on the Calcium Carbonate Mineralization of Nanofibers. Ind Eng Chem Res 56:8241–8250. https://doi.org/10.1021/acs.iecr.7b00902

Rantanen J (2016) The manufacturing potential of micro and nanofibrillated cellulose composite papers Ph.D. Dissertation (Tech.), Aalto University

Rantanen J, Dimic-Misic K, Kuusisto J, Maloney TC (2015) The effect of micro and nanofibrillated cellulose water uptake on high filler content composite paper properties and furnish dewatering. Cellulose 22:4003–4015. https://doi.org/10.1007/s10570-015-0777-x

Retulainen E, Niskanen K, Nilsen N (1998) Fibers and bonds. In: Niskanen K (ed) Paper physics. Gummerus Oy, Jyväskylä. pp 55–83

Schmidt JA (2010) Electronic spectroscopy of lignins. In: Heither C, Dimmel DR, Schmidt JA (eds) Lignin and lignans: advances in chemistry. CRC Press, Miami, pp 49–102

Seo BS, Ahn JH, Lee HL (2017) Upgrading waste paper by in-situ calcium carbonate formation. J Clean Prod 155(1):212–217. https://doi.org/10.1016/j.jclepro.2016.09.003

Shen J, Song Z, Qian X, Liu W (2009) Modification of papermaking grade fillers: a brief review. BioResources 4(3):1190–1209

Silenius P (2002) Improving the combinations of critical properties and process parameters of printing and writing papers and paperboards by new paper-filling methods. Dissertation PhD (Tech.), Helsinki University of Technology

Sjostrom E (1989) The origin of charge on cellulosic fibers, Nord. Pulp Paper Res J 4(2):90–93. https://doi.org/10.3183/npprj-1989-04-02-p090-093

Stephens CJ, Kimy Y-Y, Evans SD, Meldrum FC, Christenson HK (2011) Early stages of crystallization of calcium carbonate revealed in picoliter droplets. J Am Chem Soc 133:5210–5213. https://doi.org/10.1021/ja200309m

Stoica-Guzun A, Stroescu M, Jinga S, Jipa I, Dobre T, Dobre L (2012) Ultrasound influence upon calcium carbonate precipitation on bacterial cellulose membranes. Ultrason Sonochem 19:909–915. https://doi.org/10.1016/j.ultsonch.2011.12.002

Subramanian R (2008) Engineering fine paper by utilising the structural elements of the raw materials. Ph.D. Dissertation (Tech.), Helsinki University of Technology

Suhas, Carrott PJM, Ribeiro Carrott MML (2007) Lignin – from natural adsorbent to activated carbon: a review. Bioresource Technol 98:2301–2312. https://doi.org/10.1016/j.biortech.2006.08.008

Sundberg A, Holmbom B (2004) Fines in spruce TMP, BTMP and CTMP - chemical composition and sorption of mannans, Nord. Pulp Pap Res J 19(2):176–182. https://doi.org/10.3183/npprj-2004-19-02-p176-182

Tang Y, Zhang F, Cao Z, Jing W, Chen Y (2012) Crystallization of CaCO3 in the presence of sulfate and additives: experimental and molecular dynamics simulation studies. J Colloid Interf Sci 337(1):430–437. https://doi.org/10.1016/j.jcis.2012.02.069

Torre M, Rodrigues AR, Saura-Calixto F (1992) Study of the interactions of calcium Ions with lignin, cellulose, and pectin. J Aric Food Chem 40:1762–1766. https://doi.org/10.1021/jf00022a007

Publication III

Laukala, T., Ovaska, S.-S., Kerttula, N., and Backfolk, K.

Three-dimensional thermomechanical converting of CTMP substrates: Effect of bio-based strengthening agents and new mineral filling concept

Reprinted with permission from
Cellulose
Vol. 28(15), pp. 9751–9768, 2021

The final publication is available at Springer via
http://dx.doi.org/10.1007/s10570-021-04139-4

Cellulose
https://doi.org/10.1007/s10570-021-04139-4

ORIGINAL RESEARCH

Three-dimensional thermomechanical converting of CTMP substrates: effect of bio-based strengthening agents and new mineral filling concept

Teija Laukala · Sami-Seppo Ovaska · Ninja Kerttula · Kaj Backfolk

Received: 2 January 2021 / Accepted: 10 August 2021

Abstract The effects of bio-based strengthening agents and mineral filling procedure on the 3D elongation of chemi-thermomechanical pulp (CTMP) handsheets with and without mineral (PCC) filling have been investigated. The 3D elongation was measured using a press-forming machine equipped with a special converting tool. The strength of the handsheets was altered using either cationic starch or microfibrillated cellulose. Precipitated calcium carbonate (PCC) was added to the furnish either as a slurry or by precipitation of nano-sized PCC onto and into the CTMP fibre. The 3D elongation of unfilled sheets was increased by the dry-strengthening agents, but no evidence on the theorised positive effect of mineral fill on 3D elongation was seen in either filling method. The performance of the strengthening agent depended on whether the PCC was as slurry or as a precipitated PCC-CTMP. The starch was more effective with PCC-CTMP than when the PCC was added directly as a slurry to the furnish, whereas the opposite was observed with microfibrillated cellulose. The 3D elongation correlated positively with the tensile strength, bursting strength, tensile stiffness, elastic modulus and bending stiffness, even when the sheet composition was varied, but neither the strengthening agent nor the method of PCC addition affected the 3D elongation beyond what was expectable based on the tensile strength of the sheets. Finally, mechanisms affecting the properties that correlated with the 3D elongation are discussed.

Keywords 3D elongation · Press forming · PCC · CTMP · Composite filler

Introduction

Wood-fibre-based packaging materials offer a more sustainable alternative to fossil-based thermoplastic materials, but their use is hampered in many applications by their limited formability. Complex 3D shapes cannot be produced from 3D blanks or web substrates and the production of sealable trays and similar items faces difficulties due to the formation of wrinkles, cracks, holes or uneven rims. Recently, both the forming process (Groche et al. 2012; Leminen et al. 2015; Tanninen et al. 2015) and the paperboard substrate has gained interest with particular emphasis

Supplementary Information The online version contains supplementary material available at https://doi.org/10.1007/s10570-021-04139-4.

T. Laukala (✉) · N. Kerttula
Packaging Technology of LUT School of Energy Systems, Lappeenranta-Lahti University of Technology, P.O. Box 20, 53850 Lappeenranta, Finland
e-mail: teija.laukala@lut.fi

S.-S. Ovaska · K. Backfolk
Stora Enso Oyj, Research Center Imatra, 55800 Imatra, Finland

Published online: 25 August 2021

on its formability, the "ability of paper to be formed into 3D shapes without defects in appearance and functionality" as defined by Vishtal (2015). The mechanical properties that govern the formability of the substrate differ between the sliding blank and fixed blank processes, the latter of which emphasises extendable behaviour of the substrate (Vishtal 2015; Östlund 2017).

The extendable behaviour of paper and board is determined by the single fibre properties, fibre bonds, web structure, and any residual (drying) stresses (Östlund 2017). The relationship between the extensibility in 3D and the physical properties of board is however somewhat unclear, especially if post-treatments known to improve extensibility and their effect on the properties are considered. This, alongside related apparent contradictions connected to possible pre-treatments, is illustrated in Table 1 on behalf of some of the properties measured from paperboard on routine.

Laukala et al. (2019) reported that the characteristics of fracture in press-forming (fixed blank mode) depended on the pulp type used and they found that with CTMP pulp, fracture typically occurred in areas with a locally high fine content, while regions beneath the surface fines that contained longer fibres were found to be relatively intact. Such a failure and rupture of the surface has been linked to the tensile failure of bonds (Page 1969; Seth 2005). Individual CTMP fibres are bulky, stiff and strong but they are known to have poorer bonding than kraft fibres. The characteristic behaviour of the bulky and stiff CTMP fibres supports the hypothesis that sheet failure in 3D may be especially due to weak interfibre bonding. Although CTMP has a lower extensibility than kraft pulp (Laukala et al. 2019), CTMP offers the bulk and stiffness needed in many packaging applications, and has environmental benefits (such as a higher yield and chlorine-free bleaching) over kraft pulp, while simultaneously being less prone to taste- and smell-related issues than mechanical pulps. These factors make CTMP-based boards interesting for 3D formation, especially if ways can be found to enhance the extensibility.

The relationship between the failure of fibres and the failure of bonds has been discussed by many authors, including Page (1969), who wrote: "as the point of failure is approached, more bonds fail in the rupture region and the remaining fibres take more of the sheet load, until the fibres lying in the direction of loading reach their rupture strain", and Retulainen (1996), who presented two formulae for tensile

Table 1 Pre-treatments and some physical properties measured on routine, and their mentioned correlation with the 3D extensibility. All the 3D extensibility results reported were obtained using fixed blank mode type of stretching, except those marked with an asterisk (*) were given in a more general context

Property or pre-treatment	Effect on 3D extensibility	Link to other properties affecting 3D extensibility
Elastic modulus	High elastic modulus said to be detrimental*[1] Positive correlation observed experimentally[2]	
Bending stiffness	Negative correlation observed experimentally[2]	Linked with elastic modulus, high elastic modulus increases bending stiffness[3]
Tensile strength	Typically, positive correlation reported[4]; higher extensibility in the cross direction than the machine direction[5]	Lower tensile index in the cross direction than the machine direction[5]
Compaction treatment, spraying with selected polymer(s)	Positive correlation observed experimentally[4]	Decreasing tensile stiffness[4], compaction decreases tensile strength[5,6]
Increased moisture and temperature (in thermoforming)	Positive correlation reported*[1]	Reduction in elastic modulus[7]
Deformation and microcompression of fibres	Improvement in extensibility[4]	Decreased elastic modulus[8,9,10]

[1]Kajanto (2003), [2]Laukala et al. (2019), [3]Kajanto (1998), [4]Vishtal (2015), [5] Vishtal and Retulainen (2014a, b), [6]Ihrman and Öhrn (1965), [7]Salmén (1993), [8] Page et al. (1979), [9]Page and Seth (1980a), and [10]Page and Seth (1980b)

strength: one for sheets with poor bonding and thus few fibre breaks, and another for sheets in which a more significant amount of fibre breaks also take place. These formulae suggest that tensile strength can be increased by increasing the fibre width and fibre length, the amount of fibres on a fracture line, the specific bond strength and relative bonded area and, if a significant amount of fibre breaks take place, the single fibre's strength.

Within the paper industry, the dry strength is commonly improved by beating the pulp and by using dry-strengthening agents. To prepare a substrate with good (3D) elongation, beating is of great importance since it promotes internal and external fibrillation and leads to an increase in fines content, which improves strength properties (Koskenhely 2008). Microcompressions and deformations that reduce straightness, the presence of which have been associated with increased 3D elongation (Vishtal 2015), may also be created (Koskenhely 2008). A side-effect of beating, however, is a reduction in bulk (Koskenhely 2008), which may not be desired. The literature proposes techniques for the bulk preservation of (chemi)thermomechanical pulps, for example, by the microfibrillated cellulose (MFC) addition (Jahangir and Olson, 2020). It was shown that replacement of low consistency refining by the addition of MFC resulted in greater mechanical strength and a higher bulk. In combination with recent improvements in MFC production and fibre engineering, MFC is thus an interesting candidate as an agent strengthening fibre-based, bulky, 3D-formable materials.

Alongside the strengthening agents, another type of material often added to papermaking are mineral fillers, such as calcium carbonate either as ground or precipitated (GCC or PCC, respectively), clay, calcium sulfate or even titanium dioxide (Hubbe and Gill 2016). The mineral fillers differ both chemically and physically, and the different fillers can be used to alter and fine-tune the end-product properties, but also to reduce costs, or both (Hubbe 2004; Koivunen et al. 2009; Hubbe and Gill 2016). The typical motivation for filler use is to increase brightness and opacity, but also to control the pore size and friction of the paper (Shen et al. 2009; Hubbe and Gill 2016). Although the fillers also bring in negative effects, such as losses in sheet strength properties due to debonding (Hubbe and Gill 2016; Krogerus 2007), some of the effects, such as those related to altered friction, may be of interest in the context of 3D forming. In general, a low friction coefficient is beneficial for 3D forming (Östlund 2017), and the friction coefficient between metal and the substrate have been reported to correlate with formability in the fixed blank process (Vishtal 2015). In deep drawing, the friction affects runnability and process reliability (Lenske et al. 2017).

The use of fillers has also been suggested to improve thermal conductivity of the sheets, which may facilitate plasticization of the sheet in the thermoforming press (Kajanto 2003). In some cases, a synergy between the mineral filler and a dry-strengthening agents may result in a significant improvement of the paper strength (Lindström et al. 2005). Cationic starch is reported to have such an effect (Lindström et al. 2005), and numerous methods to improve calcium carbonate filler by starch-modification have been reported (He et al. 2016; Kuusisto and Maloney 2016; Li et al. 2016).

The purpose of this study was to further clarify the role of strengthening agents and mineral fillers in 3D formable structures made of CTMP sheets with controlled and confirmed composition in respect to the fibres, strengthening aids and fillers, but different physical properties. The relationship between the physical properties and the 3D elongation was studied, with an emphasis on the role of strengthening agents as bonding enhancers, and dosing strategies for adding the filler. The dosage of cationic starch or MFC was varied, and the PCC filler was added either by adding the PCC as a slurry or by using a novel filler-fibre composite (PCC-CTMP prepared using in-situ precipitation of PCC). The PCC mineral was thus either synthetised in a batch process and added to the furnish, or in the presence of CTMP to prepare a composite filler-denoted PCC-CTMP, where a large proportion of the nano-PCC particles nucleated and grew onto and into the CTMP fibres.

Materials and methods

A hardwood (birch) CTMP was provided as dry sheets by Stora Enso Kaukopää mill (Imatra, Finland). The microfibrillated cellulose was a wood-based grade (Celish KY100S, Daicel FineChem Ltd., Japan) obtained in a high solids content (ca. 25 wt-%) material, which was diluted to 1 wt-% solids under

high shear mixing conditions using a Diaf dissolver mixer.

Calcium oxide, CaO, (Honeywell, purity ≥ 95%) and CO_2 gas (AGA, purity ≥ 99.8%) were used to precipitate calcium carbonate. The cationic starch used was Raisamyl 50021 (Chemigate, cationised potato starch with degree of substitution 0.035). The starch was mixed in 60 °C water, which was heated to 95–98 °C and cooked for 30 min while stirring. The cooked starch was stored in a closed vessel in an oven at 65 °C and used within 24 h of cooking.

Sample preparation

The sample preparation is shown diagrammatically in Fig. 1, and the precipitation steps and handsheet preparation is further described from 2.1.1. to 2.1.3. For clarity, pulp mixtures and handsheets are referred to on the basis of their composition as indicated in Table 2.

The CTMP was prepared by disintegration of CTMP pulp sheets with a Valley beater according to the ISO 5264–1 standard. After the disintegration, a CTMP pulp deficient in fines was prepared by applying a washing procedure because it has been reported that PCC preferentially precipitates on the fine fibre surfaces (Silenius 2002). Ca. 8 L of CTMP pulp from the beater (consistency ca. 15.7 g/l) was placed on a vessel equipped with 200 mesh metal wire. Water and fines were allowed to drain under gravity through the wire while stirring, and tap water was added to maintain its furnish volume. Each of the eight batches was washed using ca. 16 L of water for each batch. After the fines removal, the batches were mixed together to homogenise the material before use.

PCC-CTMP composite filler precipitation

The PCC-CTMP was prepared by reaction of $Ca(OH)_2$ and CO_2 to precipitate calcium carbonate in the presence of CTMP fibres in a 10 L, open-batch reactor. The reactor was equipped with a stirrer and a gas outlet at the bottom. The fibre consistency was 1.3 wt-%. The depletion of $Ca(OH)_2$ was determined by the decrease in pH. The temperature at the beginning of the exothermic reaction was ca. 20 °C and the reaction was allowed to proceed without any further temperature control. A total of three batches were prepared and mixed together to provide a homogeneous material.

The $Ca(OH)_2$ used was prepared from calcium oxide by slaking in water with a $CaO:H_2O$ ratio of 1:9 for four hours. The initial temperature was 40 °C. The $Ca(OH)_2$ slurry obtained was filtered through a metal wire (63 µm openings) to remove large aggregates before use.

PCC precipitation

The PCC filler used was a laboratory-prepared grade free from chemical additives such as dispersing agents. The PCC was synthetised from $Ca(OH)_2$ and CO_2 as described above, but a higher reaction temperature was used, 77 ± 3 °C, to control the particle morphology, and the batch size was 2000 g (before precipitation). The reactor was equipped with a stirrer and a heating or cooling jacket for temperature control. The $Ca(OH)_2$ concentration in the batch was 22 wt-% (prior to precipitation). After the precipitation, the PCC was allowed to rest in an open container overnight to allow any excess CO_2 to leave the sample. The PCC was then stored on a rotating table to avoid sedimentation. The PCC obtained was spikey, i.e., an agglomerated cigar-shaped particles. An example can be seen in Fig.

Handsheet preparation

Handsheets were prepared according to the ISO 5269–1:2005 standard with the exceptions of

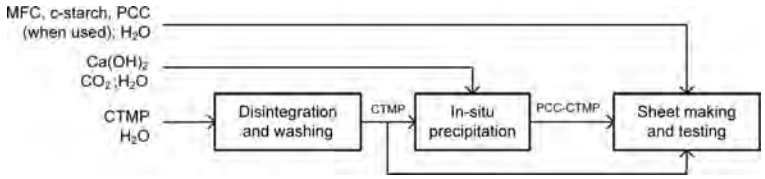

Fig. 1 Schematic diagram of the experiments

Table 2 Nomenclature of samples

Sample identifier	Description
CTMP	CTMP without added filler or strengthening agents
PCC-CTMP	PCC-CTMP composite prepared via in-situ precipitation
PCC	The PCC filler, $CaCO_3$ precipitated in laboratory
CTMP&PCC	CTMP with PCC filler, the mineral added as a slurry. No strengthening agents used
CTMP&PCC(CS)	CTMP with PCC filler added as a slurry plus cationic starch as a strengthening agent
CTMP&PCC(MFC)	CTMP with PCC filler added as a slurry. Microfibrillated cellulose as a strengthening agent
CTMP&PCC-CTMP	PCC-CTMP filled CTMP sheet, or pulp mixture. No strengthening agents used
CTMP&PCC-CTMP(CS)	PCC-CTMP filled CTMP sheet, or pulp mixture. Cationic starch as a strengthening agent
CTMP&PCC-CTMP(MFC)	PCC-CTMP filled CTMP sheet, or pulp mixture. Microfibrillated cellulose as a strengthening agent

grammage (190 gsm) and drying, done using a drying drum (Lorentzen and Wettre) with a surface temperature of ca. 60 °C to allow shrinkage. The sheets prepared and their compositions are presented in Table 3.

The sheet composition was controlled gravimetrically. CTMP and PCC-CTMP (when used) were mixed in pre-determined ratios, and MFC and PCC were added to the pulp mixture until the targeted sheet weight was reached. Starch was added assuming 100% retention.

Methods of analysis

Fibre analysis

The samples were MFC, PCC-CTMP, PCC and the pulp mixtures used in handsheet preparation were analysed using the L&W Fiber Tester (Lorentzen and Wettre, Kista, Sweden)diluted using approximately 0.1 g fibres to obtain 100 ml of fibre suspension. The fibre length, fibre width, shape factor, amount of fines, mean kink angle, kinks per mm, kinks per fibre and kink index were then recorded. The results are length-weighted.

Handsheet testing

The handsheets were tested according to the ISO 534 (density, thickness and bulk), ISO 5636–3 (Bendtsen porosity), ISO 8791–2 (Bendtsen roughness), ISO 287 (moisture content 50% RH and 80% RH), ISO 1924–3 (tensile strength, tensile stiffness, and elastic modulus), ISO 1974 (tearing resistance), ISO 2759 (bursting strength) and ISO 536 (grammage) standards. SCAN-P 92 was used for formation and specific formation, and bending stiffness (5°) was measured using DIN 53121. The measurements were made at 23 °C and 50% RH using conditioned sheets. The amount of starch in the handsheets was measured using the Tappi standard T 419 om-04.

Scanning electron microscopy

FE-SEM imaging was conducted on cross section samples using an FEI Nova NanoSEM 450 field emission scanning electron microscope (FE-SEM) equipped with a Schottky-type emitter. The microscope was operated in a low vacuum mode using a Gaseous Analytical Detector (GAD) and a field-free final lens mode. The detected signal consisted of backscattered electrons (BSE). The chamber pressure was set to 70 Pa using water vapor from a built-in reservoir. The working distance was set to 5.0 mm and the acceleration voltage to 5.0 kV. Some images were obtained by mapping and stitching individual FE-SEM images with in-built automated image acquisition software, FEI MAPS 2.0.

Prior to FE-SEM imaging, the cross-section samples were prepared using a broad ion beam (BIB) cross section cutter (Hitachi IM4000) with a beam current of 120 μA, 3 kV acceleration voltage, 1.5 kV discharge voltage and 400 μA discharge current. The argon (Ar) gas flow was 0.08 ml/min and Ar ions hit the wire side first. A cover glass was placed between the sample and the mask.

Table 3 The handsheets designations and their compositions. The ash, starch and moisture contents were measured using the handsheets, but the MFC content is given as the targeted, gravimetrically controlled dose

Ident	Sheet type	Ash content, 525 ± 25 °C [%]	MFC, targeted dose [%]	Starch [%]	Moisture, 50% rh [%]	Moisture, 80% rh [%]
1	CTMP	0.7	–	–	7.8	12.0
2	CTMP&PCC–CTMP	3.8	–	–	7.4	12.3
3	CTMP&PCC–CTMP	12.3	–	–	6.8	11.1
4	CTMP&PCC–CTMP	15.4	–	–	6.4	10.9
5	CTMP&PCC(MFC)	8.8	3.6	–	6.7	11.6
6	CTMP&PCC(MFC)	25.0	3.6	–	5.9	9.5
7	CTMP&PCC(CS)	8.5	–	1.0	7.5	11.8
8	CTMP&PCC(CS)	14.1	–	1.0	6.9	10.6
9	CTMP(MFC)	0.7	1.6	–	8.2	11.1
10	CTMP(MFC)	0.7	4.8	–	7.6	11.9
11	CTMP(MFC)	9.0	1.6	–	7.4	11.6
12	CTMP&PCC–CTMP(MFC)	8.6	4.8	–	7.3	11.1
13	CTMP&PCC–CTMP(MFC)	15.3	1.6	–	6.4	11.1
14	CTMP&PCC–CTMP(MFC)	16.7	4.8	–	6.6	11.0
15	CTMP(CS)	0.7	–	0.8	7.9	12.4
16	CTMP(CS)	0.7	–	0.9	7.8	12.5
17	CTMP&PCC–CTMP(CS)	7.7	–	0.7	7.3	12.0
18	CTMP&PCC–CTMP(CS)	7.6	–	1.0	7.3	12.5
19	CTMP&PCC–CTMP(CS)	17.7	–	0.8	6.5	10.6
20	CTMP&PCC–CTMP(CS)	15.8	–	1.2	6.9	11.1

Press-forming trials

To determine the 3D elongation of the sheets, samples were press-formed using the LUT Packaging Line using a MiniMould tool (Fig. 2) developed to test the formability of experimental materials such as handsheets. The method involves press-forming of the substrate using a fixed blank mode, with an unheated male tool and a heated female tool. Female tool temperatures of 120 and 160 °C were used. Before forming, the sheets were conditioned at 23 °C and 80% RH. The conditioning was chosen based on a previous suggestion (moisture level of the formed sheet approximately 9–11%) by Tanninen et al. (2017a). 3D elongation of a material was determined to be the maximum forming depth without ruptures detected visually. The equipment and methods are described in more detail by Tanninen et al. (2017b).

The 3D elongation is given as the average of the measured elongation at the two temperatures, as the 3D elongation rarely differed between the different temperatures.

Results

Fibre characterization

Results of the fibre characterisation are shown in Fig. 3. The tabulated values are available in Online Resource 1. The CTMP showed long (1.57 mm) and wide (41.4 µm) fibres. The fines content after washing

Fig. 2 Press-forming tool set: (1) the male mould, (2) the female mould, (3) the rim tool and (4) the heating unit

was only 10.2%, and the fibres were quite straight with a shape factor of 89.5%.

When the PCC-CTMP was prepared, the shape factor, the fibre width and the amount of fines were slightly increased, whereas the fibre length and the kinkiness slightly decreased. The most significant change was the increase in fines content, which was associated primarily with an increase in the size of the fine particle fraction due to the precipitation of PCC on CTMP fines, bringing the smaller fines to a size large enough to be detected by the fibre analyser.

It has been suggested that the PCC precipitates primarily on the cellulosic fines because the surface area of fines is much greater than that of the larger fibres (Silenius 2002). PCC attached to the surfaces of larger fibres should also increase the fibre width, and a small increase (0.3 μm) was observed. The increase was in good agreement with the mineral layer thickness (ca. 150 nm) in the SEM images (Fig. 8), although the detected change was smaller than the sensitivity of the fibre analyser indicated by the manufacturer.

The fibre analyser had a limited capacity to recognise small fibre fractions and fillers, but samples of the PCC filler and MFC were measured to observe how the materials were detected. The PCC was poorly detected, and the MFC was seen as short and thin fibres with a low shape factor. The amount of fines was high, 110% related to the amount of fibres with a length greater than 0.2 mm. The mean kink angle, kink index and kinks/mm were higher than those of CTMP or PCC-CTMP, but the number of kinks/fibre was lower.

When samples of the pulp mixture were taken during handsheet preparation, the fibre properties were found to follow the furnish composition in a logical manner. For example, when MFC was added to the mixture, the fibre width and fibre length decreased slightly and the fines content increased.

Sheet composition and properties

The handsheets and their compositions are listed in Table 3, and the physical properties of the handsheets are given in Table 4. The effects of the reinforcing agents and of increasing ash content are summarised in Table 5. The data plots are available in the Online Resource 1. The trends observed in the handsheet properties were in general as expected, i.e. mineral filler decreased strength and bulk, and the strengthening agents increased strength but reduced bulk. Some exceptions and differences were, however, observed between CTMP&PCC and CTMP&PCC-CTMP sheets, and between the strengthening agents.

With increasing ash content, the CTMP&PCC-CTMP(CS) showed a slight increase in tensile stiffness and elastic modulus, but a negative effect on bulk and strength. The difference in strength properties between CTMP&PCC-CTMP(CS) and CTMP&PCC(CS) sheets was not explained by the presence of starch, as the CTMP&PCC(CS) sheets had 1.0% starch and the CTMP&PCC-CTMP(CS) contained from 0.7 to 1.2% starch. Starch was therefore more effective as a strengthening agent for CTMP&PCC-CTMP than for CTMP&PCC. The situation was the opposite when MFC was used as a strengthening agent. At a given ash content, CTMP&PCC-CTMP(MFC) had a lower strength than CTMP&PCC(MFC).

The observed difference in strength was attributed to the decreased bonding of MFC due to a loss of PCC-free surface area in both PCC-CTMP and MFC (see Fig. 8c and d), but also to a synergy between the starch and PCC-CTMP. These factors are discussed in more detail later.

The strengthening agents affected the specific formation of the sheets in a negative manner, but when PCC-CTMP was used instead of PCC, the negative effect was less obvious, and the specific formation was improved by an increase in ash content. The difference was not due to a difference in starch retention, since this was similar with both dosing strategies.

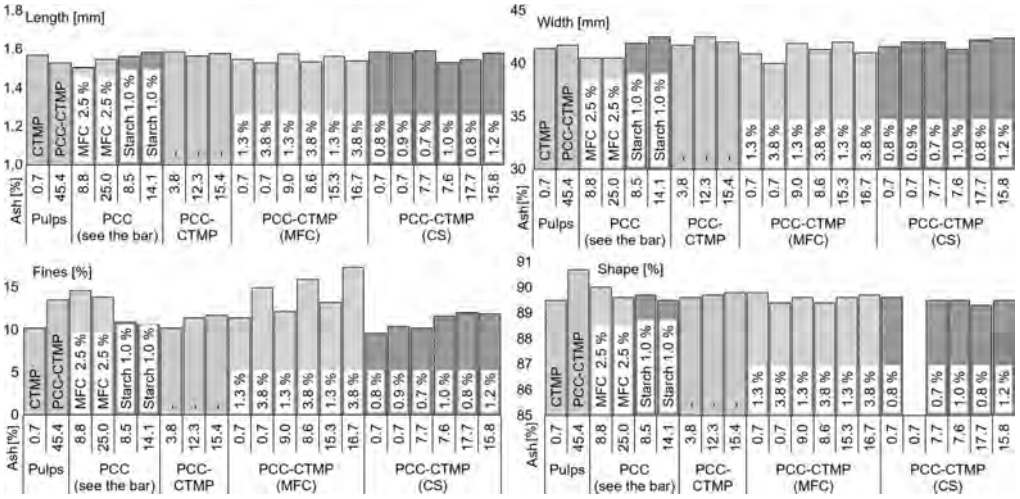

Fig. 3 Fibre characteristics of CTMP, PCC-CTMP and the mixtures used to make the handsheets. The x-axis indicates ash content of the sheet obtained using the material and the filler type, i.e. whether PCC or PCC-CTMP was used. The amount of reinforcing agent (or the pulp type) is indicated inside each bar. The amount of starch was measured after the sheets had been prepared, whereas the MFC amount is the targeted amount

The use of cationic starch appeared to increase the bulk of CTMP&PCC(CS) and CTMP&PCC-CTMP(CS) sheets in comparison to that of the CTMP and CTMP&PCC-CTMP sheets. This was probably due to the rougher sheet surface, as the thickness was measured using a single sheet. The roughness values exceeded the equipment maximum, but a greater roughness was supported by the poorer formation and cross-section SEM images (Fig. 7), which suggested that the fibres were packed more densely. The sheets were thinner when the starch was used, despite the similar grammage. The bulk was decreased with the addition of MFC.

3D elongation tests and the relationship between 3D elongation and sheet properties

According to Vishtal (2015), sheet extensibility and tensile strength govern formability (i.e. depth of shape) in the case of fixed blank forming. In the present case, sheet extensibility was measured as 3D elongation using a fixed blank mode. In the Mini-Mould system used, the 3D elongation indicated by the maximum depth without rupture is known to correspond to the 3D elongation defined based on the surface area increase of the elongating part of the substrate during forming. A more detailed description of the 3D elongation is given by Tanninen et al. (2017b).

In the present case, the reference CTMP sheets had a 3D elongation of 2 mm, which in the system used corresponded to a value of 0.5%. For comparison, the system has previously yielded a 3D elongation of 2% for the 190 g/m^2 commercial three-ply board used to prepare pressed trays, and 1.2% for CTMP sheets with a fines content of 11.7% (Laukala et al. 2019). The 3D elongation results for the handsheets are shown in Fig. 4 and tabulated in Table 4.

Neither dosing method of filler or strengthening aid was found to be superior for enhancing the 3D elongation. Their effect on sheet 3D elongation is described in 3.3.1 Effect of the strengthening agents and ash content. Correlation was found, however, for the 3D elongation with a set of physical properties of the sheets: a positive correlation between 3D elongation and bending stiffness, elastic modulus, tensile strength and stiffness and bursting strength within each series, with the exception of the elastic modulus and tensile stiffness in the case of CTMP&PCC-CTMP(CS). The correlations, described under 3.3.23D elongation: comparison of all the sheets, remained when no respect was paid to the sheet

Table 4 Physical properties of the handsheets

	Grammage [g/m^2]	Thickness [μm]	Bulk [cm^3/g]	Porosity* [ml/min]	Bending stiffness (5°) index [Nm^7/kg^3]	Specific formation [g$^{0.5}$/m]	Tensile index [Nm/g]	Tensile stiffness index [kNm/g]	E-modulus [MPa]	Bursting index [Pa·m^2/g]	3D elongation [%]
1	206	760	3.70	> 8820	1.49	1.17	8.1	1.35	364	311	0.50
2	205	708	3.46	~ 8700	1.19	0.94	6.2	1.21	351	215	0.50
3	208	694	3.33	~ 8700	0.49	0.85	2.4	0.55	165	106	0.30
4	204	653	3.20	~ 8300	0.53	0.78	2.4	0.55	172	123	0.40
5	201	656	3.27	6000	1.07	1.05	8.7	1.39	426	304	0.50
6	209	608	2.91	4600	0.57	1.2	5	0.92	316	124	0.50
7	188	661	3.52	~ 8800	1.45	1.5	9.3	1.65	468	362	0.50
8	176	578	3.28	~ 8600	1.28	1.42	8.2	1.59	483	301	0.50
9	208	726	3.49	~ 7800	1.50	1.15	9.9	1.61	462	370	0.65
10	202	679	3.35	5500	1.48	1.1	13	1.98	591	543	0.75
11	210	717	3.41	~ 8200	0.79	0.86	4.1	0.86	252	114	0.30
12	208	658	3.16	5000	0.92	0.89	7.5	1.49	473	255	0.50
13	206	652	3.17	7000	0.66	0.78	3.3	0.77	243	121	0.30
14	207	603	2.92	3900	0.71	0.85	5.1	1.14	391	184	0.50
15	206	796	3.86	> 8820	1.63	1.1	12	1.73	447	476	0.75
16	207	807	3.91	> 8820	1.83	1.18	12	1.81	463	460	0.75
17	200	702	3.52	> 8820	1.60	1.08	11	1.87	532	425	0.50
18	201	710	3.53	> 8820	1.67	0.97	11	1.92	543	467	0.50
19	210	632	3.01	~ 8300	1.20	1	9.6	1.91	635	357	0.50
20	205.3	656	3.2	6700	1.24	1.08	9.4	2.09	654	385	0.75

* Some of the measured values exceeded the equipment range. In these cases, the equipment maximum was used when calculating the mean. The values with such results are indicated with a tilde (~). When all the measured values exceeded the equipment maximum, this is indicated with a chevron (>)

Table 5 Qualitative summary of the effects of the dry strengthening agents on the sheet properties with increasing ash content by ash type. Effect of the strengthening agents is given in comparison with the strengthening-agent-free PCC-CTMP series

	Filling method	Effect of increasing ash and effect of MFC	Effect of increasing ash and effect of cationic Starch
Bending stiffness	PCC slurry	Filler decreased bending stiffness. The loss of bending stiffness was slightly alleviated by the MFC	Filler decreased bending stiffness. The loss slightly alleviated by the starch
	PCC-CTMP	See PCC slurry	Filler decreased bending stiffness. The loss alleviated by the starch more than in the case of traditional dosing
Elastic modulus	PCC slurry	Filler decreased elastic modulus. Loss alleviated by the MFC	Effect of filler negligible, increase in elastic modulus due to the starch
	PCC-CTMP	See PCC slurry	Filler increased elastic modulus, which was further increased by the starch
Tensile stiffness	PCC slurry	Filler decreased tensile stiffness. Loss slightly alleviated by the MFC	Filler decreased tensile stiffness. Loss alleviated by the starch
	PCC-CTMP	See PCC slurry	Filler increased tensile stiffness, which was further increased by the starch
Tensile strength	PCC slurry	Filler decreased tensile strength. Loss alleviated by the MFC	Filler decreased tensile strength. Loss was alleviated by the starch, but to a lesser degree than in the case of PCC-CTMP
	PCC-CTMP	Filler decreased tensile strength. Loss was alleviated by the MFC, but to a lesser degree than in the case of traditional dosing	Filler decreased tensile strength. Tensile strength greatly improved by the starch
Bursting strength	PCC slurry	Filler decreased bursting strength. Loss alleviated by the MFC	Filler decreased bursting strength. The loss alleviated by the starch
	PCC-CTMP	See PCC slurry	Filler decreased bursting strength. The loss greatly alleviated by the starch
Formation	PCC slurry	Filler increased formation, MFC use increased formation	Decrease of formation with increasing ash, but great increase of formation by the starch
	PCC-CTMP	Filler decreased formation, but an increase of formation took place when MFC was used	Decrease of formation with increasing ash, but an increase of formation when the starch was used
Bulk	PCC slurry	Decrease of bulk with increasing filler and MFC	Decrease of bulk with increasing ash and by the starch
	PCC-CTMP	See PCC slurry	See PCC slurry

composition. The properties found to correlate with the 3D elongation also correlate themselves. This is further discussed under 4.2 3D elongation and the load-elongation curve. The other physical properties measured were not found to show a significant correlation with the 3D elongation, and no evidence on the effect of filling or strengthening aids, e.g., via altered friction of thermal conductivity was observed, beyond that of their effect on the physical properties of the sheets.

Effect of the strengthening agents and ash content

The strengthening agents increased the 3D elongation when no mineral filler was used. With increasing ash content, CTMP&PCC, CTMP&PCC(CS) and CTMP&PCC(MFC) sheets showed the same 3D elongation behaviour as the CTMP sheet, although the chemical compositions and strength properties of the sheets were altered due to the filler and use of the strengthening agent. Even when the ash content reached 25%, the 3D elongation of CTMP&PCC(MFC), 25 kg_{MFC}/t, was not less than that of the CTMP sheets. This appeared to be due

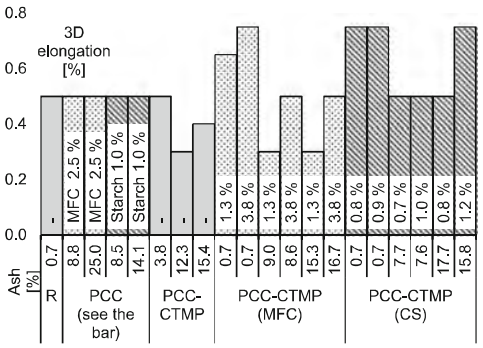

Fig. 4 Summary of the 3D elongation results. The x-axis shows the dosing method of the PCC (i.e. whether PCC was added as a slurry or as PCC-CTMP), the bonding agent used, and the handsheet ash content (525 ± 25 °C). The amount of bonding agent is indicated inside each bar. Reference (*R*) was the CTMP sheet with neither the mineral filler nor the binder

primarily to the ability of the MFC to maintain the strength properties of the CTMP&PCC(MFC) sheets. The tensile strength was similar to that of the CTMP&PCC-CTMP(MFC) sheet with 16.7% ash and 38 kg_{MFC}/t, and the 3D elongation of the sheets was mainly explained by their strength properties (see: 3.3.2 3D elongation: comparison of all the sheets).

Filling the sheet with PCC-CTMP without a strengthening agent decreased the 3D elongation of the sheets, see Fig. 4, but either MFC or starch restored the 3D elongation when a sufficiently large dose was used. However, when the sheets were filled with PCC-CTMP, the starch (12 kg/t and 15.8% ash) increased the 3D elongation above that of the reference, whereas MFC appeared detrimental for 3D elongation when the dose was low, as CTMP&PCC-CTMP(MFC) with 1.3 wt-% MFC gave a lower 3D elongation than the CTMP&PCC-CTMP with a similar ash content. Starch was more effective for improving or maintaining the 3D elongation of the sheets than the MFC, especially when the filler was PCC-CTMP.

3D elongation: comparison of all the sheets

The 3D elongation is plotted against the tensile stiffness and the tensile strength in Figs. 5 and 6, respectively. A positive trend is evident in both cases, but the R^2 values are low, possibly due to the limited resolution of the 3D elongation measurements, or perhaps variations in the properties.

There was no significant correlation between 3D elongation and ash content, but there was a negative correlation between ash content and bending stiffness probably due to the decrease in sheet thickness with increasing ash content. The lack of correlation between the ash content and the other properties was probably affected by the fact that the strengthening agents were able to compensate for the strength loss caused by the filler.

Scanning electron microscopy

SEM micrographs of cross-cut samples (Figs. 7 and 8) showed the differences between the samples depending on sample composition. The most obvious changes were between sheets filled with PCC or PCC-CTMP, which was evident based on the filler morphology, and the CTMP sheet, which did not contain PCC. In addition, a change in sample thicknesses was detected although the grammages were similar, especially when cationic starch was used, both for CTMP&PCC(CS), in Fig. 7d, and CTMP&PCC-CTMP(CS), in Fig. 7e.

Figure 7 shows the two-sidedness of the non-formed sheets and particularly that the fillers were concentrated on the wire side, especially when the PCC filler was used (Fig. 7d). In the case of PCC-CTMP (Fig. 7b, c and e), the PCC was more strongly attached on the fibres prior to the forming of the sheet,

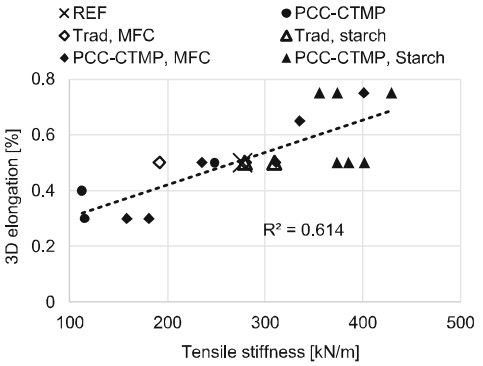

Fig. 5 The correlation of 3D elongation and tensile stiffness. Note that the resolution of 3D elongation results at the range of the measurements was 0.25%. The results were given as an average after measuring in two forming temperatures

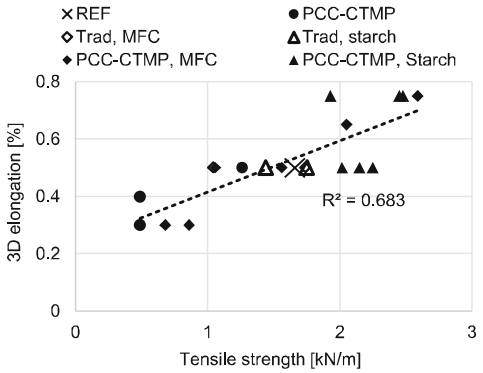

Fig. 6 The correlation of 3D elongation and tensile strength. Note that the resolution of 3D elongation results at the range of the measurements was 0.25%. The results were given as an average after measuring at two different forming temperatures

and the mineral was also found inside the fibre lumens, where aggregates of nano-sized particles formed an uneven coating on the inner fibre surface, as shown in Fig. 8c. An example of a fibre with a more heavily filled lumen is shown in Fig. 8c

A small amount of loose fibrils were seen in the CTMP reference (Fig. 7a), but the amount increased when PCC-CTMP was added to the furnish (Fig. 7b). A comparison between covered and not covered fibrillary material is shown in Fig. 8 (the close-ups). When the sheets were filled with PCC (Figs. 7d and 8b), the mineral was seen to attach onto the fibrils, but much of the area of fibres and fibrils remained PCC-free, and use of starch decreased the amount of loose fibrils (Fig. 7d, it close-up and e). The micrographs suggest that the MFC was dispersed quite well, as no obvious MFC flocs are seen in the micrographs. Another detail of PCC-CTMP filled sheets was that when the starch was used as a strengthening agent, the PCC appeared to form bridges between fibres. An example of this is shown in Fig. 9.

Discussion

Despite the sheets being filled using two different dosing strategies, and the use of a strengthening aid, no evidence of the effect of filling or strengthening aids beyond that of their effect on the physical properties of the sheets was observed. The findings are discussed from two perspectives. First, the effects of sheet composition on their physical properties is covered under 4.1 Effect of mineral phase on sheet physical properties. Then, under 4.2 3D elongation and load-elongation curve, the discussion focuses on the 3D elongation and the physical properties for which the correlations were found. The relationships and origins of the properties are used to discuss the finding that the correlation for 3D elongation and the elastic modulus and/or tensile stiffness was positive for the CTMP despite the high elastic modulus usually being viewed as detrimental (Kajanto 2003).

Effect of mineral phase on sheet physical properties

The differences in fibre morphology between the PCC-CTMP and CTMP pulps were insignificant and unlikely to explain the differences in sheet properties. The physical and chemical conditions of PCC-CTMP preparation were relatively mild, and a chemical change sufficient to significantly contribute to the physical properties was deemed unlikely. The differences in physical properties between the CTMP&PCC and CTMP&PCC-CTMP sheets were attributed to distribution of the mineral phase, resulting in disruption of the sheet bonding and possible interaction with the strengthening agent.

The PCC filler was of a high-bulking type known to reduce sheet strength due to the loss of inter-fibre bonding (Hubbe 2004), whereas the PCC-CTMP had a more even distribution of PCC on fibre surfaces and a large PCC surface area. The mineral in the PCC-CTMP was expected to prevent direct contact between the cellulosic fibres and to reduce inter-fibre bonding. Such a loss of strength is known to take place when filler particles are small (Hubbe 2004), and the lower strength in the case of CTMP&PCC-CTMP suggested that this was the case. The loss of strength remained when the amount of ash was subtracted from the grammage used in the calculation of the various indexes (fibre-weight based).

The ineffectivity of MFC as a strengthening agent was partially linked to its only moderate ability to increase the dry strength of mechanical pulp sheets (Kajanto and Kosonen 2012), but this does not explain why the MFC appeared to be more beneficial for PCC than PCC-CTMP-filled sheets, while the situation was the opposite with starch. The loose fibrils seen in the

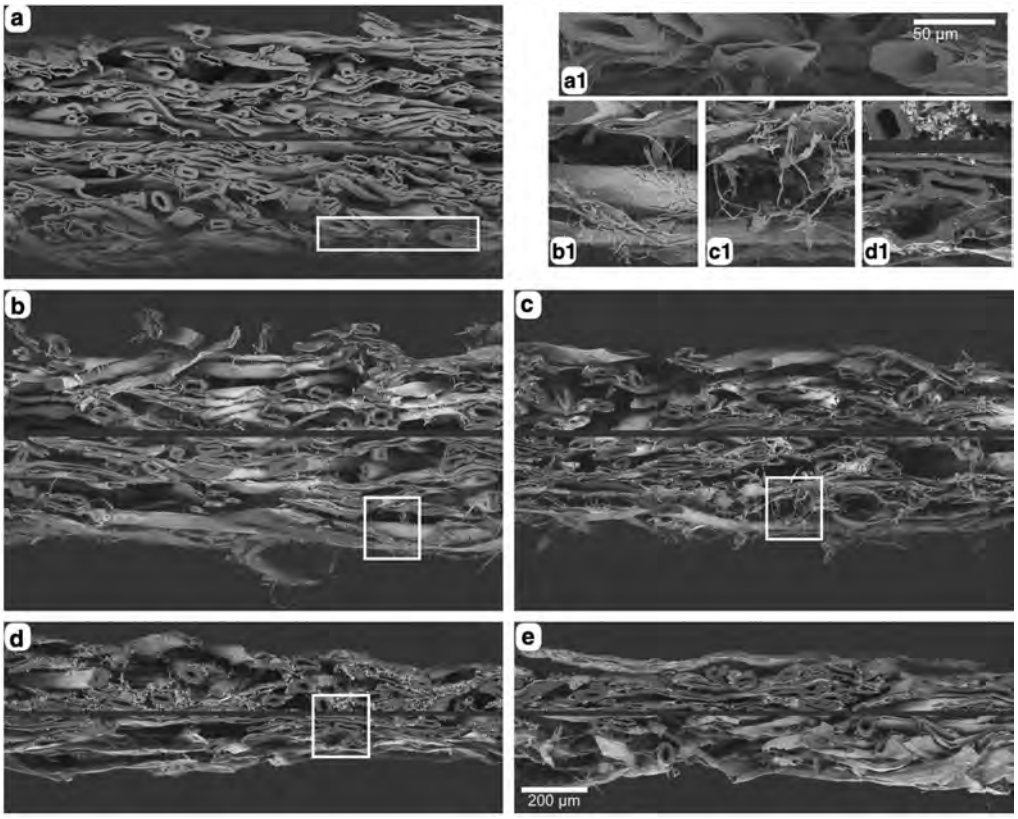

Fig. 7 SEM micrographs of the cross-section of samples: **a** CTMP: reference sample, **b** CTMP&PCC-CTMP, without a strengthening agent, **c** CTMP&PCC-CTMP(MFC), 13 kg_{MFC}/t **d** CTMP&PCC(CS), 12 kg_{CS}/t, and **e** CTMP&PCC-CTMP(CS), 10 kg_{CS}/t. The ash contents of the filled sheets were ca. 15%. The 200 µm scale bar applies to the micrographs marked with letters only, and the 50 µm scale bar applies all close-ups (indicated with letter and a number). The grey bars in the middle represent the bulk of the sheet; the thickness corresponding 320 µm was removed from each micrograph. The wire side is facing upwards

SEM images (Fig. 7c) suggest that bonding of MFC was poor when PCC-CTMP was used, which was the probable reason for its poor performance. The PCC appeared to reside on the MFC fibrils, even though the MFC was added to the furnish after the PCC precipitation.

This, combined with the lack of CTMP fibres free from PCC in the samples filled using PCC-CTMP, suggests that the free PCC had an affinity for fibrous surfaces. This may have been due to a charge in the particles. Korhonen and Laine (2014) reported for the flocculation of cationic PCC and nanocellulose without any retention aid, but in our case, the charge was not investigated. The loss of mineral-free surface area was, however, also associated with the poor bonding of the cellulosic species in the MFC-reinforced sheets.

According to the literature, the higher the filler content of the sheet, the higher the strength improvement that can be achieved using cationic starch (Lindström and Florén 1987; Lindström et al. 2005). The improvement is often explained by hydrogen-bonding of the starch to the filler surface, or within the filler structure, and ability of the filler to bond with the fibres (He et al. 2016; Li et al. 2016). This may have taken place, but the magnitude of the improvement was surprising because the CTMP&PCC-CTMP(CS)

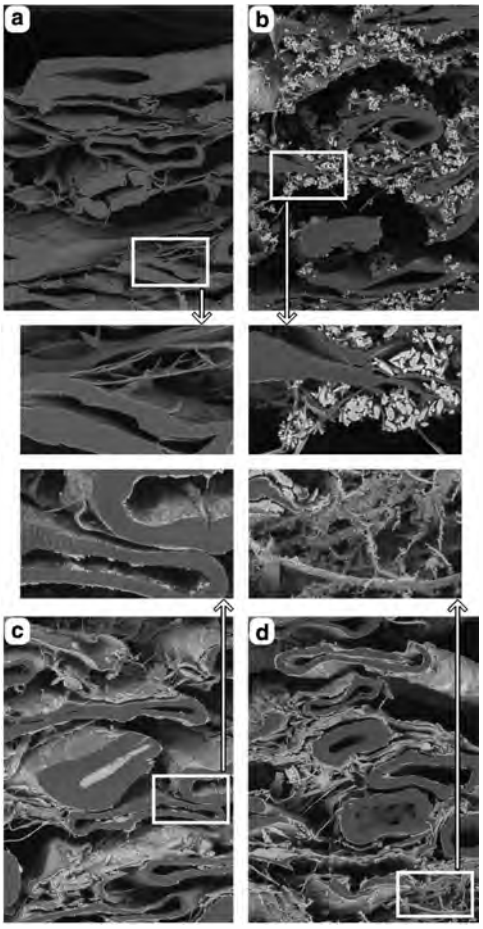

Fig. 8 SEM micrographs of the samples: **a** CTMP: reference sample **b** CTMP&PCC(CS)starch,12 kg_{CS}/t **c** CTMP&PCC-CTMP without a strengthening agent **d** CTMP&PCC-CTMP(MFC), 13 kg_{MFC}/t. The ash contents of filled sheets were ca. 15%. The 25 µm scale bar applies to all micrographs marked with letters, and the 5 µm scale bar applies to the close-ups. The wire side is facing upwards

sheets were significantly stronger than the CTMP&PCC(CS) sheets, and some of the properties improved with increasing ash content, although the amount of starch was the same. This suggests that the mineral played a more active role in creating sheet strength, perhaps because aggregates of nano-PCC attached to CTMP fines were able to function as bond-forming material between the fibres, due to the starch

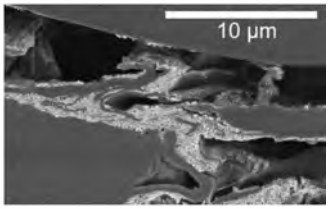

Fig. 9 A bridge of PCC and perhaps cellulosic fines between two CTMP fines in CTMP&PCC-CTMP(CS), 12 kg_{CS}/t. The ash content was 15.8%

on the mineral surfaces. In the traditionally filled sheets, the surface area of PCC was smaller (based on the SEM micrographs), and the load-bearing ability of the looser aggregates was less. The SEM micrographs of the CTMP&PCC-CTMP(CS) sheets (Fig. 9) support the hypothesis that PCC-rich, bridge-like areas exist between the fibres, although it is not clear from the images whether these structures are able to bear any load.

3D elongation and load-elongation curve

Elastic modulus, tensile stiffness and bending stiffness

Many of the strength properties found to correlate with extensibility are defined in a manner that they share a physical component, ratio of applied tensile force and elongation ($\Delta F/\Delta\delta$). Elastic modulus, reported to correlate with 3D elongation, is defined as "tensile stiffness divided by thickness" under the standard ISO 1924–3. The same standard ISO 1924–3 defines tensile stiffness as "maximum slope of the curve obtained when tensile force per unit width is plotted versus strain", and that it can be calculated using the equation

$$E^b = \frac{\Delta F}{\Delta\delta} \cdot \frac{l}{b} \quad (1)$$

where F is force, δ elongation, l is the initial length and b the initial width of the test piece. Also, bending stiffness is linked with the $\Delta F/\Delta\delta$ due to its link with elastic modulus (prediction with $S_b = \int E(z)z^2\,dz$ (Kajanto 1998)).

Since the applied pressure in forming alters the sample thickness and thus elastic modulus, and the load is borne by the solid components in the sheets (Page et al. 1979), it could be better to calculate the

specific modulus of elasticity, E/ρ, for attempting to predict the 3D elongation.

$$\frac{E}{\rho} = \frac{\frac{\Delta F}{\Delta \delta} \cdot \frac{l}{bt}}{\rho} = \frac{\Delta F}{\Delta \delta} \cdot \frac{l}{bw} \tag{2}$$

in which ρ is the initial density of the test piece and w is the grammage of the sheet. In our data, the coefficient of determination R^2 for 3D elongation versus specific modulus of elasticity was higher than that for 3D elongation versus elastic modulus (0.59 and 0.50, respectively). When the tensile stiffness was correlated with the 3D elongation, the R^2 value for the relationship between 3D elongation and tensile stiffness, shown in Fig. 5, was 0.61.

The R^2 value for the relationship between 3D elongation and bending stiffness was 0.52. For non-layered sheets, the bending stiffness can be calculated using

$$S_b = Ed^3/12 \tag{3}$$

(Kajanto 1998), and the calculated values were found to be in good agreement with the measured values. Both the elastic modulus and the bending stiffness thus depended on the ratio $\Delta F/\Delta\delta$ and sheet thickness. Although this study did not show a good correlation between 3D elongation and bending stiffness, its role should be further clarified using layered sheets with a controlled structure and composition in order better to distinguish bending stiffness and the $\Delta F/\Delta\delta$ ratio based on tensile stretching.

Tensile strength and bursting strength

When the coefficient of determination, R^2, for 3D elongation versus a correlating property (tensile stiffness, elastic modulus, bending stiffness, tensile strength or bursting strength) was determined, the highest R^2 value (0.68) was for 3D elongation versus tensile strength, followed by R^2 value 3D elongation versus bursting strength (0.67).

Bursting strength correlated well with the tensile strength (R^2 value of tensile strength versus bursting strength was 0.96). The correlation between tensile strength and bursting strength is typical because they are affected by the same fibre properties (Wistara and Young 1999), and bursting strength can be calculated using the product of tensile strength and square root of sheet stretch (Seth 2005). The correlation and burst test geometry that resembles fixed blank forming geometry make the bursting strength a property of interest when searching for correlations between 3D elongation and a results of standardised laboratory tests. A method with similarity to the standard bursting strength test, pneumatic bulge test (PBG), has also been developed and applied to characterise stretching (Huttel et al. 2011; Groche et al. 2012).

The positive correlation between 3D elongation and tensile strength is explained by improved distribution of tensile stress in the sheet, and the improved utilisation of fibre straining potential (Vishtal 2015). Retulainen (1996) suggests that with a given set of fibres at a given grammage, the tensile strength can be altered by changing the bonding. The tensile strength can also be affected by the fibre network structure and therefore by, e.g., restrained drying, but in our CTMP sheets, it can be assumed that tensile strength depended mainly on the bonding.

Tensile stiffness and tensile strength in assessing 3D elongation

In the context of 2D stretching, Seth (2005) introduced the concept of the stretch-potential of fibres and explained that in order to realise the potential, sufficient bonding is required, and this was confirmed by Kouko et al. (2020). We suggest that in the context of 3D elongation, the observed results may also be explained in the same manner. Tensile strength in many cases is probably indicative of the bonding and stress distribution within the sheet, while the role of the "$\Delta F/\Delta\delta$ dependent" parameters, i.e. elastic modulus, tensile stiffness, and perhaps bending stiffness, is probably more complex.

We suggest that in bulky and somewhat poorly bonded sheets, such as the CTMP sheets, the 3D elongation is strongly dominated by the bonding, which explains the strong correlation between 3D elongation and tensile strength. The elastic modulus, tensile stiffness and perhaps bending stiffness probably show a positive correlation with 3D elongation because the specific elastic modulus increases with increasing bonding until it reaches a plateau, unless the fibre elasticity is simultaneously affected (Seth and Page 1981).

In more strongly bonded sheets, we expect to see a weaker correlation between tensile stress and 3D elongation, as the increase in sheet bonding allows a

greater realisation of the elongation potential of the fibres and of the fibre web structure. Simultaneously a negative correlation between tensile stiffness and 3D elongation is expected, due to an unrestrained sheet drying and the presence of microcompressions and crimps in the fibres (Vishtal 2015), which increases the extensibility in press forming while negatively affecting the tensile stiffness (Vishtal 2015) and specific elastic modulus (Page and Seth 1980b).

This hypothesis is in agreement with the work of Page et al. (1979), who described two mechanisms that affect the specific elastic modulus, improved stress-distribution resulting from an increase in bonding (controlling the elastic modulus of the less bonded sheets), and by the elastic properties of fibres (affected, for example, by the presence of crimps and stresses in the fibres), which control the plateau level of specific elastic modulus.

This would explain why the heat and moisture during the press-formation generally improve the extensibility, despite the decreasing elastic modulus and the observed correlation between the 3D elongation and elastic modulus being the opposite. The plasticisation of the fibre polymers caused by heat and moisture affects fibres in a manner that improves their stretch potential under given bonding, although the bond strength is also affected by the moisture content (Salmén 1993). Therefore, it is expected that if the moisture content is increased further, the 3D elongation is reduced when the negative effects on sheet bonding exceed the positive effects on plasticisation. Tanninen et al. (2017a) have reported a decrease in formability with high moisture contents, and Salmén (1993) describes the softening of wood polymers with heat and moisture, especially the decrease in elastic modulus and the loosening of bonds due to the presence of moisture.

To summarise, we suggest that the correlation between 3D elongation and tensile strength (and thus burst strength) results from increased bonding of the sheet, while the correlation between 3D elongation and tensile stiffness, elastic modulus and, perhaps, bending stiffness is more complex originating at the fibre and sheet level, the dominating factor in the generation of sheet elongation depending on whether the bonding allows the elongation potential of the fibre to be realised. This stresses the importance of understanding the origin of each property correlating with the 3D elongation.

Conclusions

In this work, we studied the 3D elongation and strength of CTMP-based sheets filled with PCC added as a slurry to the furnish or precipitated onto the fibre surfaces often as nano-sized particles. MFC or cationic starch were added as dry-strengthening agents. The 3D elongation correlated positively with the tensile strength and bursting strength (affected by the same fibre properties, and tensile strength often being associated with the bond strength), and with tensile stiffness, elastic modulus and bending stiffness, all of which are related to the ratio of applied tensile force and elongation ($\Delta F/\Delta\delta$) in a tensile test via the formulae of paper physics. No significant correlations were observed with the 3D elongation and other measured physical properties of the sheets. Despite the use of the two morphologically different PCC fillers and the two chemically different strengthening aids, no evidence on the effect of filling or strengthening aids on 3D elongation were observed beyond those related to the strength properties, despite their hypothesised effects on friction and thermal conductivity of the sheet and thus, the possibility for improved plasticisation.

The method of mineral filling affected the effectiveness of the strengthening agents: MFC performed poorly on PCC-CTMP filled sheets, but cationic starch performed better on PCC-CTMP and some strength properties increased with increasing ash content even at a constant level of adsorbed starch. The difference was attributed to a decrease in mineral-free surface area of the fibre and a resulting loss of bonding (MFC) and of the active role of the mineral in sheet bonding (cationic starch). However, no obvious correlation between 3D elongation and ash content took place, despite the theorised benefits of presence of filler in forming.

Acknowledgments Stora Enso Oyj is acknowledged for financial support of the project. Dr. Anthony Bristow is thanked for linguistic revision of the manuscript. Mr. Antti Pesonen and Dr. Panu Tanninen are thanked for their help in running the press-forming trials. The staff of Stora Enso Research Centre Imatra is gratefully acknowledged for participation in assessing the physical properties of the handsheets.

Funding Open access funding provided by LUT University (previously Lappeenranta University of Technology (LUT)).

References

Groche P, Huttel D, Post P-P, Schabel S (2012) Experimental and numerical investigation of the hydroforming behavior of paperboard. Prod Eng Res Devel 6:229–236. https://doi.org/10.1007/s11740-012-0365-y

He M, Cho B-U, Won JM (2016) Effect of precipitated calcium carbonate-Cellulose nanofibrils composite filler on paper properties. Carbohyd Polym 136:820–825. https://doi.org/10.1016/j.carbpol.2015.09.069

Hubbe, M.A, Filler Particle Shape vs. Paper Properties–A Review, TAPPI 2004 Spring Tech Conference, Altlanta, Paper 7–3

Hubbe MA, Gill RA (2016) Fillers for papermaking: a review of their properties, usage practices, and their mechanistic role. BioRes 11(1):2886–2963

Huttel D, Post P, Schabel S, Groche P (2011) The stress strain behaviour of paperboard in tensile and bulge tests. In Proceedings of the 10th International Conference on Technology of Plasticity, ICTP 2011 (G. Hirt, Tekkaya E.A, eds.), Aachen, Germany, pp 811–816, 2011.

Ihrman C.B, Öhrn, O.E (1965) Extensible paper by the double-roll compacting process. In Consolidation of the Paper Web. Trans. 3rd Fund. Res. Symp. (F. Bolam, ed.), pp 410–434, Cambridge, U.K., 1965.

Jahangir ES, Olson JA (2020) Low consistency refined lignocellulose microfibre: an MFC alternative for high bulk, tear and tensile mechanical pulp papers. Cellulose 2020(27):2803–2816. https://doi.org/10.1007/s10570-019-02956-2

Kajanto I (1998) Fibers and bond. In: Niskanen K (ed) Papermaking science and technology vol. 16, Paper physics, Fapet Oy, Jyväskylä, pp. 193-221

Kajanto I (2003) Paper physicist's point of view to moulding of paperboard trays. In Annual traystorming seminar, Düsseldorf Germany

Kajanto I, Kosonen M (2012) The potential use of micro- and nano-fibrillated cellulose as a reinforcing element in paper. J-FOR 2(6):42–48

Koivunen K, Niskanen I, Peiponen K-E, Paulapuro H (2009) Novel nanostructured PCC fillers. J Mater Sci 44:477–482. https://doi.org/10.1007/s10853-008-3095-y

Korhonen J, Laine J (2014) Flocculation and retention of fillers with nanocelluloses. Nord Pulp Pap Res j 29(1):119–128. https://doi.org/10.3183/npprj-2014-29-01-p119-128

Koskenhely K (2008) Refining of chemical pulp fibers. In: Paulapuro H (ed) Papermaking science and technology vol. 8, Papermaking Part 1: Stock Preparation and Wet End, Papet Oy, Jyväskylä, pp. 94-139

Kouko J, Turpeinen T, Kulachenko A, Hirn U, Retulainen E (2020) Understanding extensibility of paper: role of fiber elongation and fiber bonding. Tappi J 19(3):125–135

Krogerus B (2007) Papermaking additives. In: Alén R (ed) Papermaking science and technology vol. 4, 2nd ed., Fapet Oy, Jyväskylä, pp. 56–126

Kuusisto J, Maloney TC (2016) Preparation and characterization of corn starch–calcium carbonate hybrid pigments. Ind Crop Prod 83:294–300. https://doi.org/10.1016/j.indcrop.2016.01.026

Laukala T, Ovaska S, Tanninen P, Pesonen A, Jordan J, Backfolk K (2019) Influence of pulp type on the three-dimensional thermomechanical convertibility of paperboard. Cellulose 26:3455–3471. https://doi.org/10.1007/s10570-019-02294-3

Leminen V, Tanninen P, Lindell H, Varis J (2015) Effect of Blank Holding Force on the Gas Tightness of Paperboard Trays Manufactured by the Press Forming Process. BioRes 10(2):2235–2243. https://doi.org/10.15376/biores.10.2.2235-2243

Li T, Fan J, Chen W, Shu J, Qian X, Wei H, Wang Q, Shen J (2016) Coaggregation of mineral filler particles and starch granules as a basis for improving filler-fiber interaction in paper production. Carbohyd Polym 149:20–27. https://doi.org/10.1016/j.carbpol.2016.04.082

Lenske A, Müller T, Penter L, Schneider M, Hauptmann M, Majschak JP (2017) Evaluating the factors influencing the friction behavior of paperboard during the deep drawing process. BioRes 12(4):8340–8358

Lindström T, Florén T (1987) The effect of filler particle size and the dry-strengthening effect of cationic starch wet-end addition. Nord Pulp Pap Res j 2(4):142–145. https://doi.org/10.3183/npprj-1987-02-04-p142-145

Lindström T, Wågberg L, Larsson T (2005) On the nature of joint strength in paper - A review of dry and wet strength resins in paper manufacturing. In: Advances in Paper Science and Technology, Trans. of the XIIIth Fund. Res. Symp. Cambridge (S.J. I'Anson, ed.), pp 457–562, FRC, Manchester, 2018. https://doi.org/10.15376/frc.2005.1.457

Ostlund S (2017) Three-dimensional deformation and damage mechanisms in forming of advanced structures in paper. In: Advances in Pulp and Paper Research, Oxford 2017, Trans. of the XVIth Fund. Res. Symp. Oxford, 2017, (W. Batchelor and D. Söderberg, eds), pp 489–594, FRC, Manchester, 2018.

Page DH (1969) A theory for the tensile strength of paper. Tappi J 52(4):674–681

Page DH, Seth RS (1980a) The elastic modulus of paper II. The importance of fiber modulus, bonding and fiber length. Tappi J 63(6):113–116

Page DH, Seth RS (1980b) The elastic modulus of paper III The effects of dislocations, microcompressions, curl, crimps and kinks. Tappi J 63(10):100–102

Page DH, Seth RS, De Grace JH (1979) The elastic modulus of paper I. The Controlling Mechanisms. Tappi J 62(9):99–102

Retulainen E (1996) Fibre properties as control variables in papermakin? Part 1. Fibre properties of key importance in the network. Pap Puu 78(4):187–194

Salmén L (1993) Responses of paper properties to changes in moisture content and temperature. In: Products of Papermaking, Trans. of the Xth Fund. Res. Symp. Oxford, 1993, (C.F. Baker, ed.), pp 369–430, FRC, Manchester, 2018.

Shen J, Song Z, Qian X, Liu W (2009) Modification of papermaking grade fillers: a brief review. BioRes 4(3):1190–1209

Seth RS (2005) Understanding sheet extensibility. Pulp Pap-Canada 106(2):33–38

Seth, R.S., Page D.H. (1981) The stress strain curve of paper, In: J Brander (ed) The Role of Fundamental Research in Paper Making, Trans. VIIth Fund. Res. Symp. Cambridge, pp 421–452.

Silenius P (2002) Improving the combinations of critical properties and process parameters of printing and writing papers and paperboards by new paper-filling methods. Dissertation, Helsinki University of Technology

Tanninen P, Leminen V, Eskelinen H, Lindell H, Varis J (2015) Controlling the Folding of the Blank in Paperboard Tray Press Forming. BioRes 10(3):5191–5202. https://doi.org/10.15376/biores.10.3.5191-5202

Tanninen P, Matthews S, Ovaska S-S, Varis J, Backfolk K (2017a) A novel technique for the evaluation of paperboard performance in press-forming. J Mater Process Technol 240:284–292. https://doi.org/10.1016/j.jmatprotec.2016.10.002

Tanninen P, Ovaska S-S, Matthews S, Mielonen K, Backfolk K (2017b) Utilization of production-scale machine in experimental fiber material convertibility test using a novel press forming tool set. BioRes 12(1):3030–3042

Vishtal A (2015) Formability of paper and its improvement. Dissertation, Tampere University of Technology

Vishtal A, Retulainen E (2014a) An approach for improved 3D formability of paper. IPW 12:46–50

Vishtal A, Retulainen E (2014b) Boosting the extensibility potential of fibre networks: a review. BioRes 9(4):7951–8001. https://doi.org/10.15376/biores.9.4.7951-8001

Wistara N, Young RA (1999) Properties and treatments of pulps from recycled paper. Part I. Physical and chemical properties of pulps. Cellulose 6:291–324. https://doi.org/10.1023/A:1009221125962

ACTA UNIVERSITATIS LAPPEENRANTAENSIS

951. SOBOLEVA, EKATERINA. Microscopy investigation of the surface of some modern magnetic materials. 2021. Diss.

952. MOHAMMADI ASL, REZA. Improved state observers and robust controllers for non-linear systems with special emphasis on robotic manipulators and electro-hydraulic servo systems. 2021. Diss.

953. VIANNA NETO, MÁRCIO RIBEIRO. Synthesis and optimization of Kraft process evaporator plants. 2021. Diss.

954. MUJKIC, ZLATAN. Sustainable development and optimization of supply chains. 2021. Diss.

955. LYYTIKÄINEN, JOHANNA. Interaction and barrier properties of nanocellulose and hydrophobically modified ethyl(hydroxyethyl)cellulose films and coatings. 2021. Diss.

956. NGUYEN, HOANG SI HUY. Model based design of reactor-separator processes for the production of oligosaccharides with a controlled degree of polymerization. 2021. Diss.

957. IMMONEN, HEIKKI. Application of object-process methodology in the study of entrepreneurship programs in higher education. 2021. Diss.

958. KÄRKKÄINEN, HANNU. Analysis of theory and methodology used in determination of electric motor drive system losses and efficiency. 2021. Diss.

959. KIM, HEESOO. Effects of unbalanced magnetic pull on rotordynamics of electric machines. 2021. Diss.

960. MALYSHEVA, JULIA. Faster than real-time simulation of fluid power-driven mechatronic machines. 2021. Diss.

961. SIEVINEN, HANNA. Role of the board of directors in the strategic renewal of later-generation family firms. 2021. Diss.

962. MENDOZA MARTINEZ, CLARA. Assessment of agro-forest and industrial residues potential as an alternative energy source. 2021. Diss.

963. OYEWO, AYOBAMI SOLOMON. Transition towards decarbonised power systems for sub-Saharan Africa by 2050. 2021. Diss.

964. LAHIKAINEN, KATJA. The emergence of a university-based entrepreneurship ecosystem. 2021. Diss.

965. ZHANG, TAO. Intelligent algorithms of a redundant robot system in a future fusion reactor. 2021. Diss.

966. YANCHUKOVICH, ALEXEI. Screening the critical locations of a fatigue-loaded welded structure using the energy-based approach. 2021. Diss.

967. PETROW, HENRI. Simulation and characterization of a front-end ASIC for gaseous muon detectors. 2021. Diss.

968. DONOGHUE, ILKKA. The role of Smart Connected Product-Service Systems in creating sustainable business ecosystems. 2021. Diss.

969. PIKKARAINEN, ARI. Development of learning methodology of additive manufacturing for mechanical engineering students in higher education. 2021. Diss.

970. HOFFER GARCÉS, ALVARO ERNESTO. Submersible permanent-magnet synchronous machine with a stainless core and unequal teeth widths. 2021. Diss.

971. PENTTILÄ, SAKARI. Utilizing an artificial neural network to feedback-control gas metal arc welding process parameters. 2021. Diss.

972. KESSE, MARTIN APPIAH. Artificial intelligence : a modern approach to increasing productivity and improving weld quality in TIG welding. 2021. Diss.

973. MUSONA, JACKSON. Sustainable entrepreneurial processes in bottom-of-the-pyramid settings. 2021. Diss.

974. NYAMEKYE, PATRICIA. Life cycle cost-driven design for additive manufacturing: the frontier to sustainable manufacturing in laser-based powder bed fusion. 2021. Diss.

975. SALWIN, MARIUSZ. Design of Product-Service Systems in printing industry. 2021. Diss.

976. YU, XINXIN. Contact modelling in multibody applications. 2021. Diss.

977. EL WALI, MOHAMMAD. Sustainability of phosphorus supply chain – circular economy approach. 2021. Diss.

978. PEÑALBA-AGUIRREZABALAGA, CARMELA. Marketing-specific intellectual capital: Conceptualisation, measurement and performance. 2021. Diss.

979. TOTH, ILONA. Thriving in modern knowledge work: Personal resources and challenging job demands as drivers for engagement at work. 2021. Diss.

980. UZHEGOVA, MARIA. Responsible business practices in internationalized SMEs. 2021. Diss.

981. JAISWAL, SURAJ. Coupling multibody dynamics and hydraulic actuators for indirect Kalman filtering and real-time simulation. 2021. Diss.

982. CLAUDELIN, ANNA. Climate change mitigation potential of Finnish households through consumption changes. 2021. Diss.

983. BOZORGMEHRI, BABAK. Finite element formulations for nonlinear beam problems based on the absolute nodal coordinate formulation. 2021. Diss.

984. BOGDANOV, DMITRII. Transition towards optimal renewable energy systems for sustainable development. 2021. Diss.

985. SALTAN, ANDREY. Revealing the state of software-as-a-service pricing. 2021. Diss.

986. FÖHR, JARNO. Raw material supply and its influence on profitability and life-cycle assessment of torrefied pellet production in Finland – Experiences from pilot-scale production. 2021. Diss.

987. MORTAZAVI, SINA. Mechanisms for fostering inclusive innovation at the base of the pyramid for community empowerment - Empirical evidence from the public and private sector. 2021. Diss.

988. CAMPOSANO, JOSÉ CARLOS. Integrating information systems across organizations in the construction industry. 2021. Diss.

ISBN 978-952-335-732-7
ISBN 978-952-335-733-4 (PDF)
ISSN-L 1456-4491
ISSN 1456-4491
Lappeenranta 2021